Biocompatible carbon nanotube/β-titanium alloy composite materials

Nataliia Stepina

Corpus Christi College

A thesis submitted for the degree of

Doctor of Philosophy in Material Science

University of Oxford

Michaelmas Term 2015

Abstract

Biocompatible carbon nanotube/β-titanium alloy composite materials

Nataliia Stepina

Corpus Christi College

Submitted for the degree of Doctor of Philosophy, Michaelmas Term 2015

The thesis describes a study of the modifications of orthopaedic Ti-based substrates using nanomaterials, and the evaluation of their biocompatibility for further use as implant material, with the aim to develop new, biocompatible β-Ti/CNT composite materials. Traditionally, CNTs require the presence of a transition metal catalyst such as Fe, Ni, Co, for successful growth. Different aspects of a catalyst-assisted CVD MWCNTs growth on various Ti-based substrates including bulk, thin films and 3D porous scaffolds, have been investigated. Low concentrations of catalyst were deposited using spin coating on titanium substrates of various forms and shapes. A strong influence of the surface topography was observed. In contrast, no effect of the elemental composition of the substrate could be detected.

To evaluate the biocompatibility of the newly created materials, cell culture studies using fetal human osteoblasts (fHobs) were performed. It was shown that β-Ti/MWCNTs samples possess good initial osteoblast attachment, but no long-term osteoblast activity. Hence the biocompatibility of isolated (*i.e.* without a Ti substrate) MWCNTs was studied, using MWCNT carpets and various types of MWCNTs buckypapers. All the samples revealed very low cell activity. While β-Ti/MWCNTs samples did not exhibit good biocompatibility, alternative β-Ti/TiC samples were synthesized with a simple CVD method and revealed good osteoblast response with increased mineralization. Moreover, good corrosion resistance and mechanical properties of β-Ti/TiC samples have been reported.

Finally, successful method for non-catalytic CVD MWCNTs growth on Ti substrates was developed for the first time, thereby excluding potentially toxic catalysts from the implant material. CVD was performed with acetylene precursor on bulk titanium substrates etched with Piranha solution, which generated an appropriate surface to foster MWCNTs growth. A combination of the change in the surface roughness, improved hydrophilicity, and elemental composition of the surface as a result of the Piranha etching is likely to be responsible for the successful formation of MWCNTs.

Acknowledgements

This thesis became possible with the help of many people to whom I am very grateful.

Firstly, I would like to thank my supervisor Prof. Nicole Grobert for giving me the opportunity to study for my DPhil, her guidance and help over the last four years. I am also very thankful to Dr. Lavina Snoek for her priceless scientific contributions, her language advice, and encouragement during the thesis writing.

Within the Materials Department, there are a lot of people to whom I would like to express my gratitude. To all *Nanomaterials by Design* group members, in particular to Madhuri, Jude, Jonathan, Vitaly, and Laura for their scientific advice and personal encouragement. To the *Oxford Materials Electron Microscopy and Microanalysis* group, especially Gabriela Chapman and Dr. Gareth Hughes for electron microscopy training and advice. I am also grateful to Dr. Alison Crossley, Dr. Phil Holdway, Dr. Colin Johnston and Dr. Chris Salter from *Oxford Materials Characterisation Services (OMCS)* for help with training and sample characterisation.

This thesis was a part of a *BioTiNet Marie Curie Initial Training Network*[*] funded by the *European Commission's Seventh Framework Programme,* and I am grateful for all the project meetings, training and financial support provided by the network. I would like to acknowledge the following collaborators within the *BioTiNet*, who hosted me during my secondments and provided scientific help. IFW Dresden: Dr. Vyacheslav Khavrus, Dr. Leonhard, Prof. Mariana Calin; University of Cambridge: Dr. Roger Brooks and Dr. Konstantin Edi Tenase; UAB Barcelona: Prof. Maria Dolores Baró, Prof. Jordi Sort, Dr. Eva Pellicer; University of Ioannina: Dr. Christina Lekka. I would also like to thank all *BioTiNet* fellows for their support and our unforgettable time together.

Also, this thesis would not be possible without the encouragement of my previous supervisors, Prof. George Broza and especially Prof. Volodymyr Donchak, who was sure that I would do a DPhil even before I could imagine it.

Additional thanks go to Corpus Christi College, Oxford, for being an essential and enjoyable part of my postgraduate studies and especially to Ms. Rachel Pearson and Dr. Liz Fisher.

Of course, I am also grateful to my friends in Oxford who offered help during this long time. To Assia, for her sofa and coffees together. To Helen, for warm talks over the almond tea. To Rebecca, for her encouragement and help with my English. To Madhuri and Jude for their overall support and help.

Last but not least I would like to thank my family. To my Mom and Dad, Aunt Natasha, Sasha, and Françoise for their love and support. Special thanks go to my dear Pierre for being always by my side, believing in me in every moment of this long way and his love that gave me strength this work.

[*] Under grant agreement no. 264635.

Preface

The work reported in this thesis was carried out by the author in the Department of Materials, University of Oxford, between October 2011 and January 2016, under the supervision of Prof. Nicole Grobert.

No part of this thesis has been previously submitted for a degree at this or any other university. A list of references has been given at the end of the thesis. Some of the work described in this thesis has been presented at conferences listed below:

2nd BioTiNet Workshop, Leuven, Mar. 2012: Oral Presentation 'Progress report Oct 2011 - March 2012. Carbon nanotube/β-Ti alloy composite materials.'

NanoteC12, Brighton, Sep. 2012: Poster Presentation 'Biocompatible carbon nanotube/β-Ti composite materials'

1st year viva, Oxford, May 2012: Oral Presentation 'Biocompatible carbon nanotube/β-Ti composite materials'

BioTiNet Summer School, Barcelona, June 2012: Oral Presentation 'Progress report March – June 2012. Biocompatible carbon nanotube/β-Ti alloy composite materials.'

Mid-term Review Meeting, Corfu, Sep. 2012: Oral Presentation 'Mid-term Report. Biocompatible carbon nanotube/β-Ti alloy composite materials.'

3rd BioTiNet Workshop, Cambridge, Jan. 2013: Oral Presentation 'Progress report Sep – Dec 2012. Biocompatible carbon nanotube/β-Ti alloy composite materials'

2nd year DPhil talk, Oxford, Feb. 2013: Oral Presentation 'Biocompatible carbon nanotube/β-Ti composite materials'

4th BioTiNet Workshop, Neuchatel, June 2013: Oral Presentation 'Progress report Jan – June 2013. Carbon nanotube growth on Ti-based films.'

4th BioTiNet Workshop, Neuchatel, June 2013: Poster Presentation 'Carbon nanotube growth on Ti-based films'

3rd year poster competition, Oxford, Feb. 2014: Poster Presentation 'Carbon nanotube growth on Ti-based films'

BioTiNet Winter School, Vienna, Feb. 2014: Oral Presentation 'Progress report June 2013 – Feb 2014. Carbon nanotubes, Strong biocompatible CNT/β-Ti Alloy Composite Materials'

Final BioTiNet Conference, Dresden, Nov. 2014: Oral Presentation 'Final Report. Biocompatible Carbon Nanotube/β-Ti alloy Composite Materials/Surface'

List of abbreviations

CNTs	Carbon nanotubes
SWCNTs	Single-wall carbon nanotubes
DWCNTs	Double-wall carbon nanotubes
MWCNTs	Multi-wall carbon nanotubes
N-MWCNTs	Nitrogen-doped multi-wall carbon nanotubes
Si-MWCNTs	Silicon-doped multi-wall carbon nanotubes
CNFs	Carbon nanofibers
CVD	Chemical vapour deposition
CCVD	Catalytic chemical vapour deposition
AACVD	Aerosol-assisted chemical vapour deposition
PECVD	Plasma-enhanced chemical vapour deposition
PVD	Physical vapour deposition
SEM	Scanning electron microscopy
TEM	Transmission electron microscopy
TGA	Thermogravimetric analysis
XRD	X-ray diffraction
EDX	Energy-dispersive X-ray spectroscopy
FIB	Focus ion beam
AFM	Atomic force microscopy
XPS	X-ray Photoelectron Spectroscopy
PLD	Pulsed laser deposition
PIII	Plasma immersion ion implantation
LFM	Lateral force microscopy
SLM	Selective laser melting
TOF-SIMS	Time-of-flight secondary ion mass spectroscopy
Ti	Titanium
CoCr	Cobalt-chromium
HA	Hydroxyapatite
BP	Buckypaper
TiC	Titanium carbide
SiC	Silicon carbide
HBSS	Hank’s balance salt solution
OCP	Open-circuit potential
DMF	Dimethylformiade
PTFE	Polytetrafluoroethylene
DMEM	Dulbecco’s modified Engle medium
FBS	Foetal bone serum
fHobs	Foetal osteoblast cells

Contents

Chapter 1. Introduction and Literature Review

1.1. Background

At present, one of the most significant human health problems is musculoskeletal disorder. It affects hundreds of millions of patients all over the world, and it is one of the main factors that causes pain and disability[1–3]. Additionally, it creates quantifiable effects on societies and economies in general; for example, it costs the USA circa 254 billion dollars. In developed countries, bone and joint diseases account for half of all chronic conditions in people over 50 years old. Furthermore, musculoskeletal disorders are predicted to increase dramatically by 2020, as the number of persons aged over 50 will probably double in number. Moreover, the number of young people that suffers from these problems will increase as well, and a contributing factor is a high number of road accidents[1]. A survey conducted by Exponet Inc. in Philadelphia, Pennsylvania, predicted that the annual hospital charges in the USA will increase by 340 % for primary total hip replacement surgery and by 450 % for primary knee replacement surgery between 2005 and 2015 (Figure 1.1)[4].

In recent years, not only replacement surgeries but also revision surgeries have increased. Due to the limited implant lifetime, a revision surgery is necessary after 10-15 years. There are several reasons for such short life of implants: loosening of the implant; infection of the implant; breakage or wearing out of the implant; and damage to the bone surrounding the implant[5,6]. Implant loosening is the most common problem with hip and knee replacements. During replacement surgery, the implant is tightly fitted to the bone in order to prevent implant loosening. Loose implants result in pain and loss of motion. Loosing occurs due to the wear of the implant, which can lead to the release of debris

from the implant into surrounding tissue, which in turn can result in bone resorption, poor osseointegration and biocompatibility of the implant to the bone tissues. In such case, revision surgery is required. Recently, hospital charges for total hip revision arthroplasty are also expected to increase up to 290 % and to 450 % (Figure 1.2) for knee revision arthroplasty[4]. Unfortunately, revision surgeries are not only expensive and very painful, but also have low rates of success.

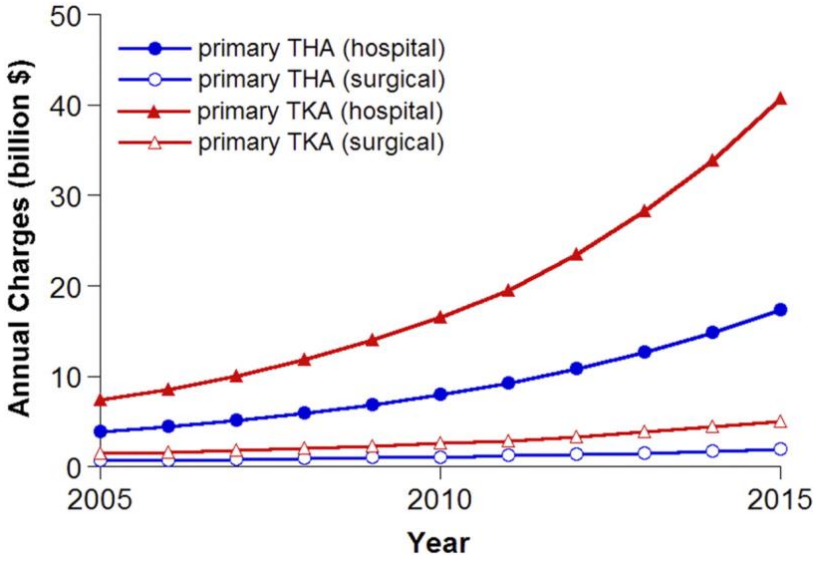

Figure 1.1. *Predicted increase in annual charges for primary implant surgeries, including primary total hip arthroplasty (THA) and primary total knee arthroplasty (TKA)*[4].

In order to address issues of bone resorption and in order to reduce the number of implant surgeries, improved artificial biomaterials are being developed. Thus, the development of new implant materials akin to bone tissue is crucial in order to increase the lifetime of implants. The structure of bone, which mainly consists of nanoscale organic calcium and phosphate crystals and collagen fibers (Figure 1.3), should be kept in mind when designing new biomaterials as explained further in Section 1.1.1.

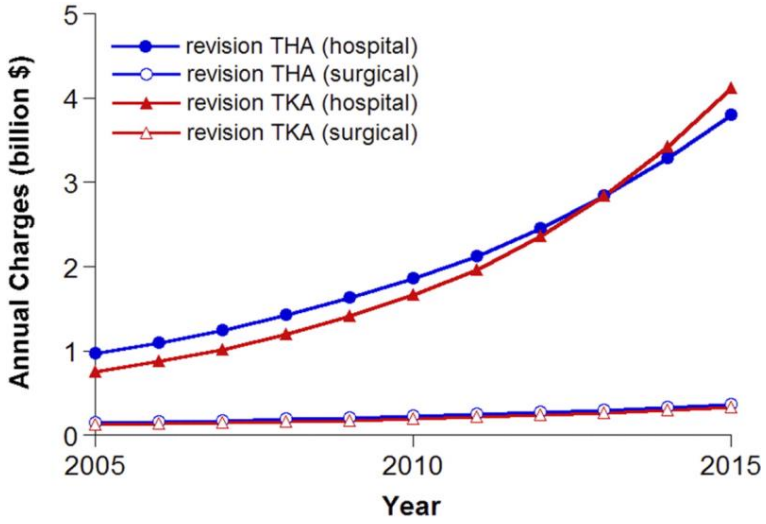

Figure 1.2. *Predicted increase in annual charges for implant revision surgeries, including revision total hip arthroplasty (THA) and revision total knee arthroplasty (TKA)*[4].

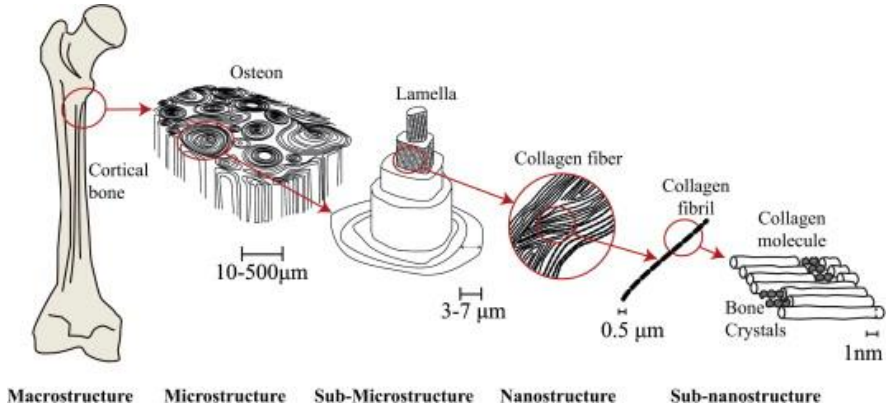

Figure 1.3. *Schematic representation of the hierarchical structure of cortical bone from the macrostructure, microstructure, sub-microstructure to the nanostructure and sub-nanostructure*[7].

1.1.1. Implants biomaterials

The biomaterials market is growing rapidly. In 2012, it reached 44.0 billion dollars worldwide, and it is expected to reach 88.4 billion dollars by 2017[8]. Orthopedic biomaterials are a significant part of this market.

For any biomaterial, including orthopedic biomaterials, certain requirements have to be fulfilled. As early as 1998, Breme and Biehl formulated the main principal requirements for biomaterials[9]. Those conditions include (a) biofunctionality (e.g. mechanical properties: Young's modulus and fatigue strength), (b) corrosion resistance, (c) appropriate tissue response (e.g. bone ingrowth for bone implants), (d) biological safety, (e) processability, and (f) availability.

Orthopedic biomaterials can be of two main types: scaffolds or implants (together with their accessories). Scaffolds are usually made of biodegradable polymers and their composites. Implants can be made of various materials such as (a) polymers (nylon, silicon, rubber, polyester, etc.), (b) ceramics (aluminum oxide, calcium phosphates), (c) composites (carbon-carbon, wire or fiber reinforced bone cement), and (d) metals (stainless steel, CoCr alloys, Ti and its alloys).

Metallic implant biomaterials are very common nowadays due to their good mechanical, thermal, and electrical properties. They can replace both hard and soft tissues.

Metals for hard tissue replacement are mainly used as artificial hip and knee implants (Figure 1.4), bone plates, dental implants[10].

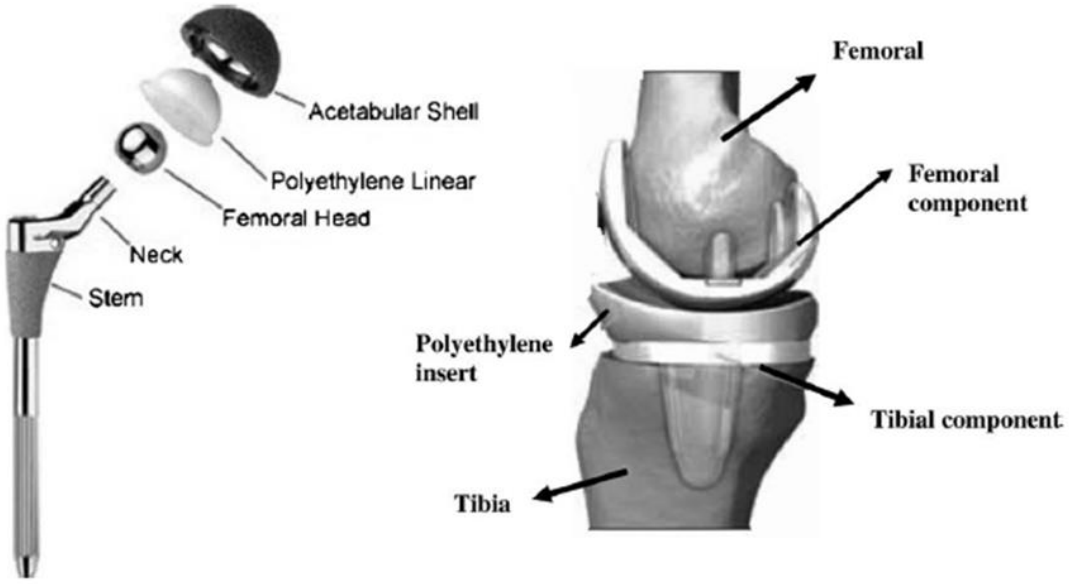

Figure 1.4. *Metal are widely used to produce various parts of total hip and knee replacement implants*[1].

Stainless steel was the first metal used for artificial implants. SUS 316L stainless steel is the only steel suitable for the medical application. However, even 316L steel, with a carbon content of only 0.03 %, can still corrode in the human body and has poor wear resistance. Moreover, it could be allergenic due to the presence of Ni in it[10,11]. Therefore, Ni-free stainless steels, which would not possess adverse reactions, have been developed using new fabrication methods. Nowadays, stainless steel is used only for temporary implants.

After steel, cobalt-chromium alloys became widely used for implants due to their high corrosion resistance. However, it was found that similar to stainless steel, they corrode inside the human body and release toxic Cr and Co particles[1].

The first attempt to use Ti as implant material was in 1930 when it was found that it was suitable for cat femurs. Interestingly, only 20 years later, in the 1950s-60s, implants based on titanium alloys were already extensively used in England, while in the USA, they only

became common in the 1970s[1]. Additionally, Ti was found to be the only 3d transition metal that has no negative influence on biological systems[3]. Ti fulfills all main requirements for orthopedic biomaterials presented earlier.

Titanium is a silver-grey transition metal with a melting temperature of 1675 °C. It has two crystalline states[12]:

1) α-phase with hexagonal close-packed (h.c.p) crystal structure,

2) β-phase with body-centered cubic (b.c.c) structure.

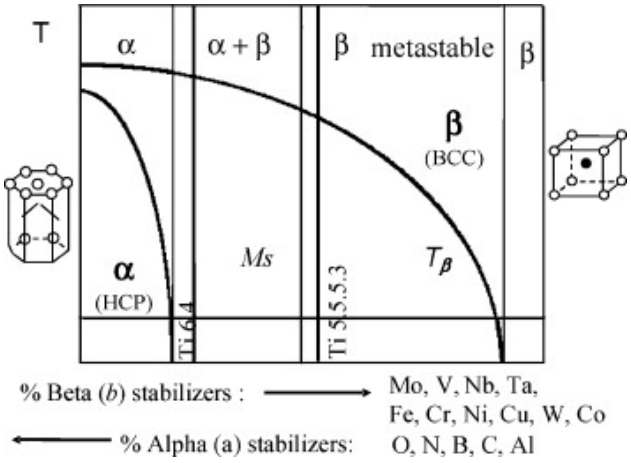

Figure 1.5. *Phase diagram of the titanium alloys showing the influence of additional elements in Ti alloys which could either stabilize α- or β-phase in alloys*[13].

Ti undergoes an allotropic transformation at 882 °C, which is called 'beta transus temperature.' It plays a critical role in manufacturing Ti alloys[14]. Additional elements in Ti alloys could be either α- or β-phase stabilizers, and this is taken into account while preparing Ti alloys (Figure 1.5). By adding different alloy elements, the phase transformation temperature can be controlled: α-stabilizers raise the transformation temperature and β-stabilizers lower it. The most common α-stabilizers are C, Al, O, and N, whereas Zr, Sn, and Si are neutral elements that neither raise nor lower the transformation temperature. β-stabilizers can be two types: those that form the β-

isomorphous system: Nb, Mo, V, Ta; and those that form the β-eutectoid system: Cu, Co, Mn, Cr, Fe and Ni. β-eutectoid elements form intermetallic components while β-isomorphous do not[14].

Ti and its alloys are usually used for replacing hard tissue, which includes artificial hip and knee implants, dental implants, and other dental products. However, Ti can also be used to fix soft tissues such as blood vessels[1]. The reason for this is their high biocompatibility that can help to avoid an allergic reaction, especially if the immune system is weak[15].

Recently, Ti alloys have also found an application in the field of healthcare goods. They are used for sports wheelchairs, e.g. basketball or racing chairs.

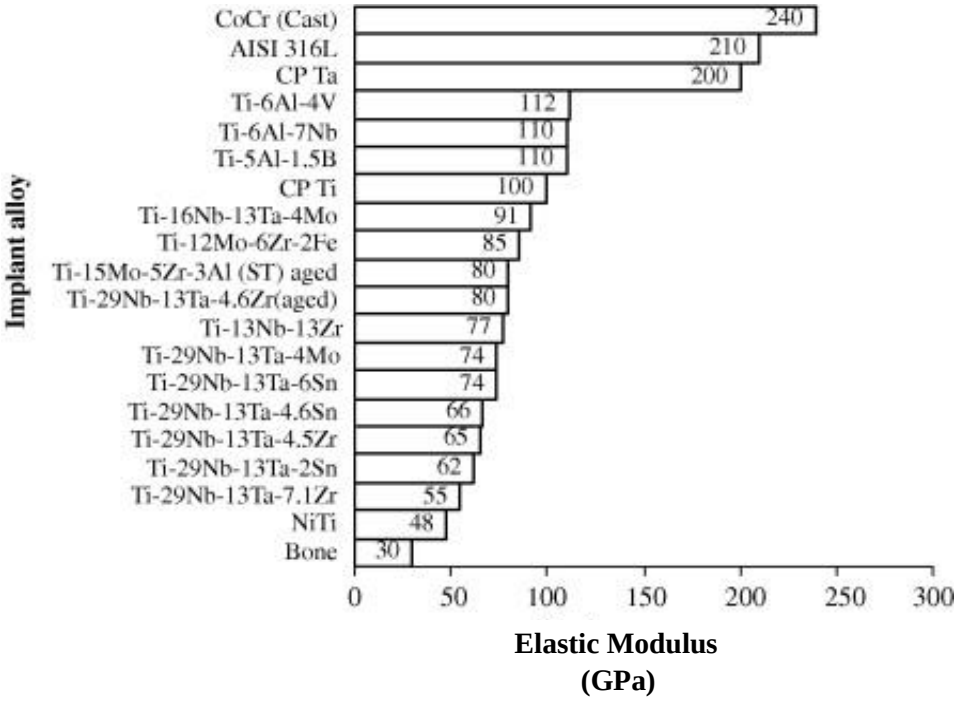

Figure 1.6. *Comparison of the elastic modulus of various metal biomedical alloys used as orthopedic biomaterials*[1].

The advantages of titanium as orthopedic biomaterials compared to other metals include its low elastic modulus (110 - 55 GPa) (Figure 1.6), excellent biocompatibility and

corrosion resistance, low density and good fracture strength and light weight[11,16–18]. For implants manufacturing, pure Ti, α-Ti, α+β, and β-Ti alloys can be used. Pure Ti and Ti-6Al-4V were initially made for the aerospace industry but later used as biomaterials, while β-Ti alloys were specially designed for biomedical applications[3]. Pure Ti (α phase) and Ti-6Al-4V (α+β) are currently primarily used. Nevertheless, Al and V can cause allergies, be mutagenic, and cytotoxic. Therefore, β-alloys are preferable due to the absence of toxic elements, better resistance to fatigue and lower elastic modulus[3,19], which is crucial for long-term implants in order to prevent stress shielding and implant loosening. Chemical elements such as Nb, Ta and Zr were found to have no toxic and no allergic response and are thus considered the safest alloying elements for Ti-based alloys[15].

The composition of β-alloys and the β-transition temperature are responsible for the stability of the alloy. It was also found that the β-stabilizers such as Nb and Ta can decrease the elastic modulus of the alloys; however, the elastic modulus increases in conjunction with the increase of β-stabilizer[20]. The stability of the β-phase has similar behaviour[21].

Due to the fact that the b.c.c. β phase is ductile, β-Ti alloys exhibit excellent cold workability. This property allows the possibility to increase the strength of β-Ti alloys and simultaneously keep the elastic modulus low[22]. As an example, the relationship between tensile strength, elastic modulus, and cold work ratio of 29Nb-13Ta-4.6Zr is shown in Figure 1.7[15].

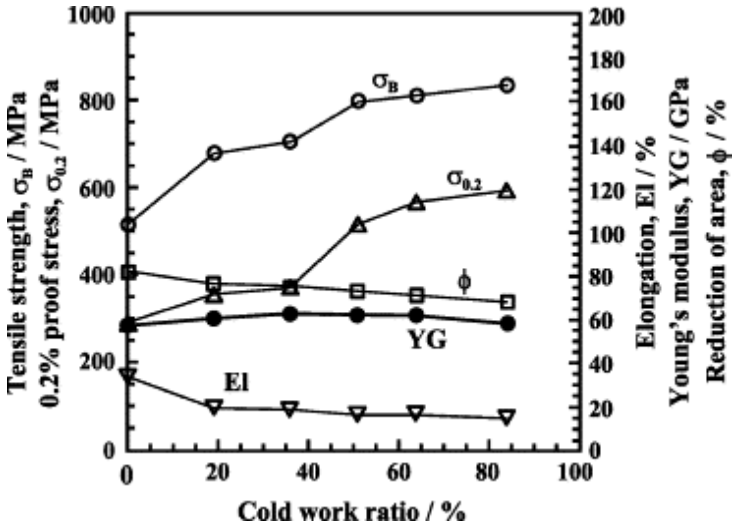

Figure 1.7. *Tensile properties and elastic modulus of Ti–29Nb–13Ta–4.6Zr as a function of cold work ratio; σ_B: tensile strength, $\sigma_{0.2}$: 0.2 % proof stress, El: elongation, YG: Young's modulus, ϕ: reduction of area*[15].

It is also worth mentioning that the TiO_2 layer on titanium, present due to oxidation processes, improves the biocompatibility of implants. Even if this oxide layer is damaged, it is immediately reformed. The surface of the implants is capable of binding with water and has a small negative charge due to the O- and OH- ions once it is implanted. This charge provides a corrosion resistance to the implant and, therefore, enhances bonding with the cells and proteins. Furthermore, a significant number of experiments conducted in the last 50 years showed that the biocompatibility of Ti itself is attributed to its oxide layer[21]. However, the thickness and structure of the oxide layer are vital. If the titanium oxide layer is too thick, the biocompatibility could decrease.

Despite the advantages of metallic biomaterials, in general, and Ti, in particular, several issues remain. Metals exhibit higher fracture toughness and stiffness than bone and, therefore, lead to bone resorption and implant loosening[23,24]. This mismatch is called 'stress shielding effect' [24,25]. Thus, the goal is to create a biomaterial that combines high strength with low elastic modulus, *i.e.*, as close to the properties of bone as possible. Their

modulus of elasticity is the lowest among all metallic materials without compromising its high strength[26,10].

Another problem is bone-implant integration. It is crucial for the implant and the surrounding bone tissue to be well connected in order to minimize the risk of implant loosening. As a result, to ensure the long-term performance of the implant, the degree of osseointegration should be as high as possible.

Osseointegration is a complex process of new bone formation as well as bone healing. After implant surgery, a number of biological reactions occur. It begins with water and protein adsorption on the surface of the implant and then the growth of new bone cells, which is not always successful since the growth of new bone depends on the surface topography, chemistry, roughness, and surface energy[27].

In order to improve the degree of osseointegration and create a bioactive implant material, various physical and chemical modifications of Ti surfaces could be performed[10], which will be discussed in the following section.

1.2. Surface modification of titanium alloys

The problem of the limited lifetime of surgical implants can be addressed to a certain extent by appropriate surface coatings that mimic the structure of the bone and which can initiate the bone growth. A number of techniques have been investigated in order to enhance wear and corrosion resistance[1]. For example, ion implantation[28] and plasma spray coating[29] can be used in conjunction with thermochemical treatments including nitriding, carburization, and borizing[1] to improve corrosion resistance. Titanium nitride coating was shown to improve wear resistance and fosters biocompatibility. Hydroxyapatite and oxide coatings, thermal treatment, and the development of porous surfaces and nanostructured surfaces are also currently used to improve the implant - bone interaction and osseointegration[1].

Surface topography of the implant has a critical influence on the cell-implant interaction[30,31]. In the past, researchers believed that the microstructure of the implant had a great influence on implant behaviour, and this was the area of intensive investigations. However, according to the detailed analysis of *in vivo* cell behaviour studies, it was concluded that the nanostructured topography has a stronger influence on protein and collagen formation than the microstructure of the implant[30,32,33]. Therefore, more attention should be paid to the nanostructure of an implant material in order to improve its properties.

The bone itself is a typical example of a nanocomposite, and Christenson *et al.* reported nanostructured coatings have a high potential for orthopedic biomaterials[27]. There is evidence that biomaterials with nanostructured surfaces are biologically privileged[34,35] because the surface area to volume ratio of nanostructured biomaterials is much higher. The reason for this is the presence of more atoms and crystal grains, leading to appropriate

surface energies necessary for protein absorption. Moreover, the total absorption of proteins is much higher on the nanometer-size grain materials due to the higher number of atoms and crystal grains[27]. Therefore, these investigations demonstrate a positive effect of the nanostructured coating. Nanometric features on the surface of metal and Ti implants should be further investigated in order to find the most suitable ones.

There are different methods for modifying Ti surfaces using nanostructures. This Chapter focuses on two main techniques. The first method uses Ti nanotopography, and the second one uses carbon nanostructures for the surface modification of Ti.

1.2.1. Modification of Ti surfaces with Ti nanotopography

There are several studies regarding the modification of Ti surfaces using nanomaterials with a size similar to the size of osteoblast cells (20-40 nm). A review by Balasundaram *et al.* shows the possibility of nanostructured materials to have similar dimensions to natural bone, and initiate and improve bone formation[36]. Previous studies showed[37–39] that biocompatibility of the Ti surface with Ti nanostructures is higher than that for conventional Ti. The presence of Ti nanostructures resulted in increased absorption, promoted cell attachment, and cell proliferation. Nanostructured Ti surfaces are generally fabricated by a) anodisation; b) chemical etching; c) electron-beam evaporation[40].

Webster *et al.* found that the reason for better cell growth on nanostructured Ti is the increase of particle boundaries at the surface due to the smaller particle size of the nanomaterial, as the osteoblast formation can be seen exactly on the particle boundaries[37]. This study not only offered for the first time the explanation that nanostructured Ti surfaces are suitable for osteoblast adhesion due to their higher surface area, but also

confirmed this theory experimentally. It provided the impetus for further investigations in the area of nanostructured metals and Ti in particular.

Another study by Ward and Webster also demonstrated the increase of osteoblast formation on nanostructured metals[38]. Powders of Ti, Ti6Al4V, and CoCrMo with different particle sizes were analyzed. Cell studies were conducted in three 'generations' with a growth period of 21 days each. The evidence of increased formation of calcium and phosphorous containing minerals on nanostructured powders in comparison with conventional powders was reported[38]. As a result, this work confirmed the advantages of using nanophase titanium and it brought the field one step closer to improving the performance of orthopedic implants.

A few years later, Rani *et al.* demonstrated the possibility of forming various nanostructures on the surface of Ti using wet chemical processes[41]. A wide range of structures, such as nanoflowers, nanoleaves, nanoneedles, nanorods, mesoporous nanoscrolls, and octahedral bipyramids were fabricated. It was shown that the morphology of nanostructures depended on the temperature, reaction time, composition and concentration of the reaction medium. All Ti nanostructures showed no toxic effect on osteoblast cells. Moreover, protein absorption increased on such surfaces — thus, nanotopography has a positive impact on osteoblast function[41]. In contrast to other studies, which mainly focused on one type of nanostructures, this study reported the synthesis of a broad range of nanostructures on Ti that could be well controlled. It inferred that it might be beneficial to pay more attention to unique Ti nanostructures that can have a significant influence on orthopedic implant application. Nevertheless, even when taking into account the large numbers of newly reported structures, extended investigations of each type of structures should be carried out.

In continuation of the previously described work in 2012, another study by Rani *et al.* has been reported. *In vitro* cellular response and *in vivo* osseointegration of Ti nanostructures were analyzed in greater details[30]. Ti nanoscaffolds, nanoleaves, and nanoneedles were produced by a hydrothermal process (Figure 1.8). Rani *et al.* showed that not all nanostructures have the same biological response. Nanoleaf morphology showed the highest protein formation during the *in vitro* tests. *In vivo* tests were performed using commercially pure Ti screws modified with nanotopography as described earlier. Ti screws with nanoleaf morphology showed the highest percentage of bone-implant contact and no inflammatory response[30]. The advantage of this study is that during both *in vitro* and *in vivo* studies, nanoleaf structures showed the best results, showing that they are a good alternative to other Ti nanotopography.

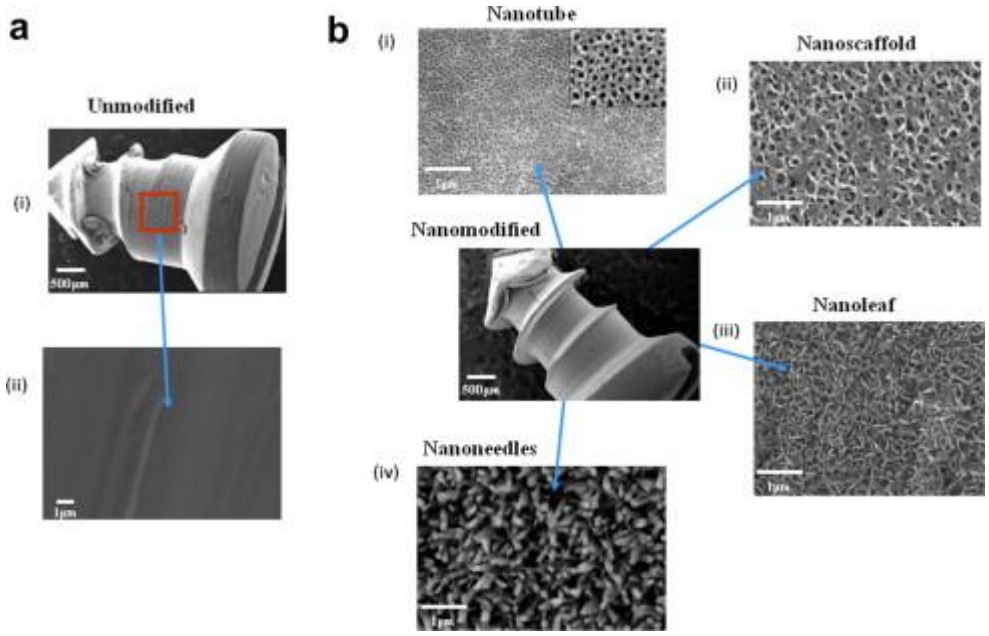

Figure 1.8. *Representative SEM images of (a) nanopolished Ti screw: (i) low magnification image and (ii) featureless surface morphology of nanopolished Ti. (b) Nanostructural features generated on surface modified Ti screws: (i) nanotubes, (ii) nanoscaffold, (iii) nanoleaf and (iv) nanoneedles*[30].

Since 1998, a considerable number of papers on titanium dioxide and titanates have been produced. Due to its properties, TiO_2 can be used for various applications: self-cleaning, solar energy, gas sensing and, of course, biomedicine[42]. It was demonstrated that TiO_2 nanotubes positively influence bone-implant interaction. The TiO_2 nanolayer improves corrosion resistance, increases cell adhesion and enhanced bone growth[43–49]. There are three main techniques for TiO_2 nanotubes fabrication: a) thermal synthesis; b) hydrothermal methods, and c) electrochemical anodisation. Electrochemical anodisation is the most popular technique for TiO_2 nanotubes growth. It allows to control easily the size of the pores, and to form uniform structures with good conformability[46]. TiO_2 nanotubes are formed on the natural self-forming oxide layer of Ti. In electrochemical anodisation, the cathode is graphite or platinum and Ti acts as the anode (Figure 1.9). The electrodes are dipped into the electrolyte solution and then the voltage is applied for a certain period. Electrolytes with organic compounds such as glycerol and ethylene glycol are preferable in the case of biomaterials. They improve the adherence between bone tissue and implant. The hydrofluoric solution is a long-time known and commonly used electrolyte, but nowadays there is a number of different electrolytes that are used for Ti anodisation. Another important parameter for TiO_2 nanotube growth is the time of anodisation. There are no standard recipes available and research groups develop their own recipes, therefore anodisation times can range from several minutes to tens of hours. Nevertheless, the anodisation time should be long enough to allow the complete formation of the nanotube. For organic electrolytes, usually more than two hours reaction is required. The time needed for the formation of TiO_2 nanotubes varies and depends on the fluorine concentration in the electrolyte. The length of the nanotube increases with the increase of the reaction time[43]. However, it is not clear which size of TiO_2 nanotubes is preferable for improving cell formation.

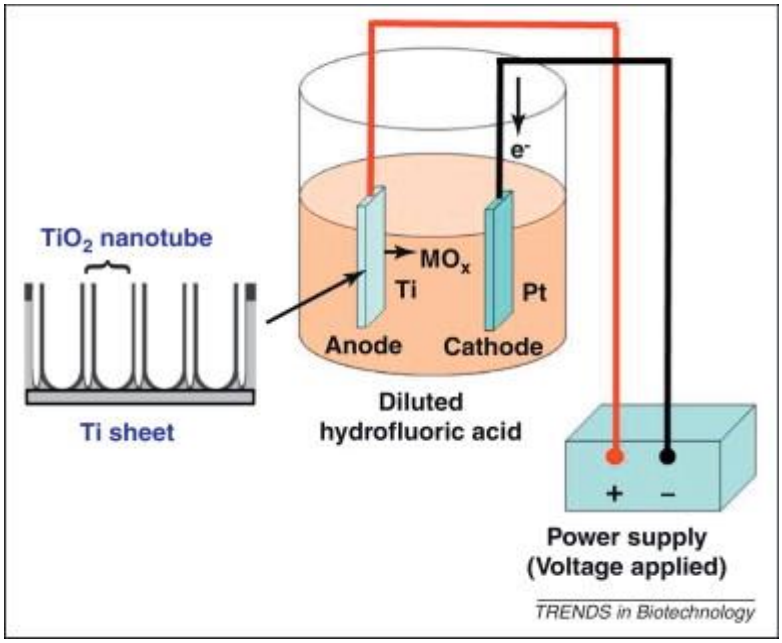

Figure 1.9. *This schematic illustrates the electrochemical anodisation process used to fabricate the titanium oxide (TiO_2) nanotube surface on titanium (Ti) metal. A Ti sheet is used as the anode, and a platinum (Pt) sheet is used as the cathode submerged in a fluoride-based electrolyte solution. The duration and magnitude of power supplied to the system determines the height and diameter of the nanotubes*[43].

1.2.2. Modification of Ti surfaces with carbon nanostructures

There are much fewer studies regarding the modification of Ti surfaces with carbon nanostructures than with Ti nanostructures. Carbon nanofibers, carbon nanotubes and titanium carbide (TiC) were reported to improve the properties of Ti implants.

The TiC layer was found to be a promising candidate to achieve excellent hardness, wear, and corrosion resistance as well as to form strong bonds between the TiC layer and substrate and have exceptional biocompatibility[50]. There are several methods commonly used to produce TiC coatings, such as pulsed laser deposition (PLD); magnetron sputtering[51]; plasma immersion ion implantation (PIII); physical vapour deposition (PVD); and, rarely, chemical vapour deposition (CVD). M. Brama *et al.* performed *in vitro* and *in vivo* experiments to compare uncoated titanium and titanium with a TiC layer produced by PLD technique. The expression of genes involved in modulation of osteogenesis and osteoblast activity was enhanced for samples with TiC layer. Also, *in vivo* studies in sheep and rabbits demonstrated greater bone density in the areas with TiC[50]. PIII method was reported to be a suitable technique to produce both TiC and TiN layers on various titanium alloys including Ti6Al4V and NiTi[52–54]. Corrosion resistance of coated surfaces increased, and new bone formation *in vivo* and *in vitro* was enhanced.

In the first study that focused on Ti with carbon nanofibers by Price *et al.*, cytocompatibility properties for use in bone prosthetic devices were investigated using an *in vitro* method[55]. A significant increase of osteoblast adhesion in comparison with conventional (micron-scale) carbon fibers was demonstrated. Nevertheless, to achieve long-term osseointegration of artificial implants, this study was not decisive enough, and further investigations were required.

Another work by Elias *et al.*[21] focused on the long-term functions of bone cells (osteoblasts) on carbon nanofibers. It is important to note that the carbon nanofibers remained unmodified for this study. It was found that osteoblasts growing on carbon nanofibers had better proliferation, generated a greater amount of alkaline phosphatase and deposited more extracellular calcium compared with carbon fibers with a diameter larger than 100 nm. Additionally, with decreasing the carbon fiber diameter, the osteoblast proliferation increased[56]. These investigations paved the way for improving existing implant materials; however, further experiments are required in order to estimate the toxicity effect of carbon fibers, before using carbon nanofibers in clinical practice. Moreover, the fact that carbon fibers with smaller diameters have a stronger influence on osteoblast formation suggests the use of carbon nanotubes, whose diameters are less than 100 nm, instead of carbon nanofibers.

Hence, carbon nanotubes are another carbon structure currently under investigation with the goal of achieving Ti implants with desirable properties. The progress regarding Ti implant improvement using carbon nanotubes is the primary focus of this work and thus is discussed in detail in the following chapters.

1.3. The use of carbon nanotubes in biomaterials

After the discovery of carbon nanotubes (CNTs) by Iijima in 1991[57], the interest in these nanostructures grew rapidly and continued to increase today. Carbon nanotubes have shown to be a promising material for biomedical applications in the following areas: drug delivery and cancer therapy; bio-sensing; biomedical imaging; bone tissue engineering[58]. Additionally, CNTs are likely to be ideal candidates for the modification of implant materials. The reason for it is the fact that CNTs match the size and shape of collagen fibers and possess suitable mechanical, chemical, and electrical properties. Moreover, CNTs appear to foster bone growth and can also be used as a mechanical reinforcement material[59].

Therefore, it is thought that CNTs can be used in two main areas of bone tissue engineering to solve the problem of long-term performance of implants: in the mechanical reinforcement of the material, and as nanostructure coating to enhance wear and corrosion resistance[60].

Carbon nanotubes on titanium

There are relatively few studies researching CNTs on Ti. Nevertheless, they have the potential to improve the biocompatibility and osseointegration of the implant to the bone tissue[61,62–67].

The key study regarding CNTs on Ti was reported by S. Sirivisoot *et al.* (2007)[67] from Brown University, USA. An improved osteoblast function on anodized Ti with CNTs was reported for the first time. In this work, commercially pure Ti was anodized for 10 min at 20V (DC) in a solution of 1.5 wt. % hydrofluoric acid to create uniform, porous TiO_2 nanotubes (50 - 60 nm diameter and 200 nm depth). Subsequently, carbon nanotubes were

grown from the TiO_2 nanotubes. The part of the samples were treated with cobaltous nitrate solution to act as a catalyst, while the other part of oxidized Ti remained untreated. CNTs were grown on both types of substrates (treated and untreated) by means of chemical vapour deposition (CVD). The pressure during the CVD process was 10 mTorr, and the synthesis temperature was 700 °C. A mixture of H_2 and C_2H_2 (40 and 160 sccm respectively) was introduced for 30 min to grow CNTs. After cell studies, an improvement in osseointegration of Ti with CNTs was observed. In particular, the increase of osseointegration was noticed in calcium deposition and alkaline phosphatase activity[67]. The results of this study are of high importance; however, it is doubtful that 'parallel' CNTs were grown from TiO_2 nanotubes without a catalyst. The only evidence of this is an SEM micrograph of a relatively poor quality (Figure 1.10). No other characterization was undertaken to confirm the presence of high-quality CNTs as described. Furthermore, it is not clear what the author means by 'parallel' and it cannot be observed from the picture provided by the paper.

There are several important studies on electrophoretic deposition of CNTs on Ti surfaces[61]. Enhanced apatite formation, as well as good cell proliferation and adhesion, were reported by Yu *et al.* In addition to this study, no separation of CNTs from Ti was observed during cell culture studies. However, the proliferation of osteoblasts was observed only on day one and day three. In order to make conclusions about the long-term performance of an implant material, cell studies are required during longer periods.

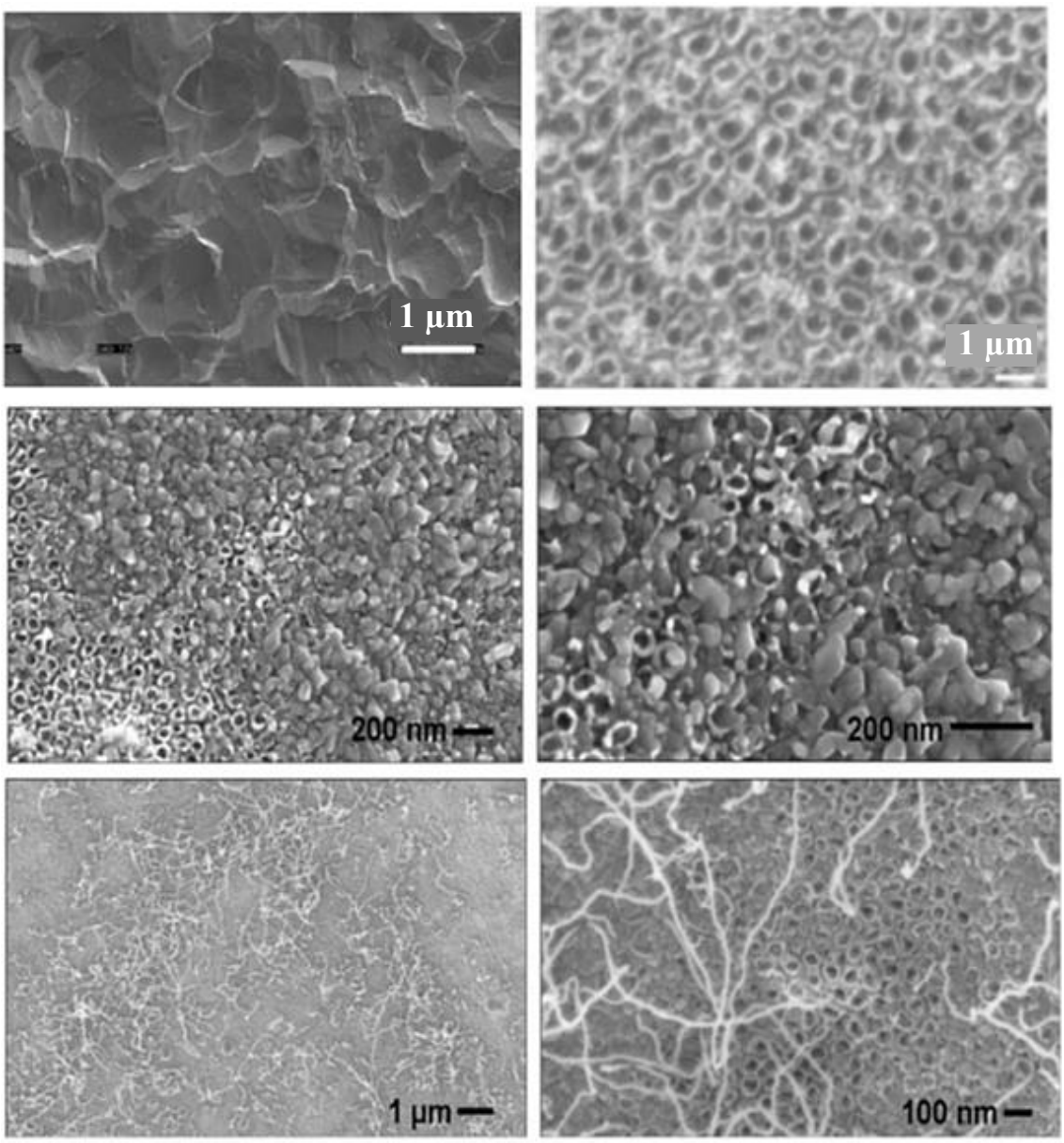

Figure 1.10. *SEM micrographs of: (a) anodized Ti; (b) anodized Ti without CNTs; (c) lower; (d) higher magnification of CNT grown from the nanotubes of anodized Ti without a Co catalyst; (e) lower and (f) higher magnification of CNTs grown from the nanotubes of anodized Ti surface with a Co catalyst*[67]*. Labaling of figures (a) and (b) was changed by the author.*

Aside of CNTs growth or deposition on Ti substrates, a number of reports regarding the synthesis of carbon nanotube reinforced hydroxyapatite composite (HA) for the coating of Ti implant were published, which lead to the development of the implant materials with greatly improved fracture toughness and wear resistance, which are summarized in

the review by D. Lahiri *et al* [68]. A positive effect of CNT-reinforced HA on biocompatibility has also been observed[68]. Nevertheless, there is a very limited amount of *in vivo* studies of CNT-reinforced HA composites implanted in the bone, and these describe only a short implantation period for up to a week[69,70]. Further investigations require more studies for longer implantation times to determine the long-term suitability of HA-CNT/Ti implants.

CNTs have potential use in the area of clinical diagnosis of orthopedic implants. MWCNTs are a suitable material for electron transport, and thus, they can be used as biosensors[62–66]. Coating of Ti electrochemical electrodes with MWCNTs leads to the increase of their active surface and direct electron transfer[66]. It was demonstrated that MWCNTs synthesized on anodized Ti substrates grown with cobalt as a catalyst improve the potential of Ti electrodes. MWCNTs-Ti electrodes showed a very high capacity and exhibit redox peaks in cyclic voltammograms[71]. However, the presence of cobalt in the implant materials should be avoided due to its toxicity. Hence, research on creating MWCNT/Ti composite without using any toxic elements should be the next step, and can open up new opportunities for *in situ* sensing of bone growth after implantation. Moreover, it may be used for further improvement in diagnostics of implants, for example, for monitoring infection processes[66].

1.4. CNT/Ti composite fabrication

In order to create CNT/Ti composites, carbon nanotubes can be deposited on the surface of titanium using two main techniques: chemical vapour deposition and electrophoretic deposition. By chemical vapour deposition, CNTs are grown on the surface of the metal, while by electrophoretic deposition a solution of previously-synthesized nanotubes is used. Both techniques will be further discussed in this section.

1.4.1. Chemical Vapour Deposition for CNT growth on Ti

There is a number of methods for producing CNTs (Figure 1.11), including arc discharge, laser ablation, chemical vapour deposition (CVD), and others[72].

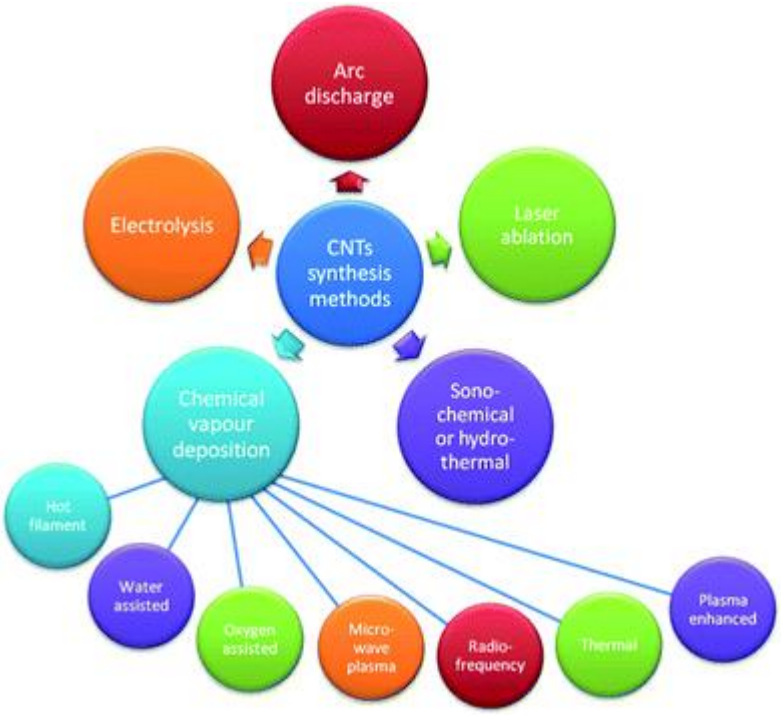

Figure 1.11. *Various methods for CNTs synthesis used to date*[72].

CVD is the most popular technique for CNTs production. It has the following advantages in comparison with other methods. It is more simple, economical, requires a relatively low temperature and ambient pressure. In CVD, different hydrocarbon (solid, liquid, gas), and different substrates can be used (powder, thin or thick films) that makes it a versatile technique for growing CNTs of various forms and purity[73].

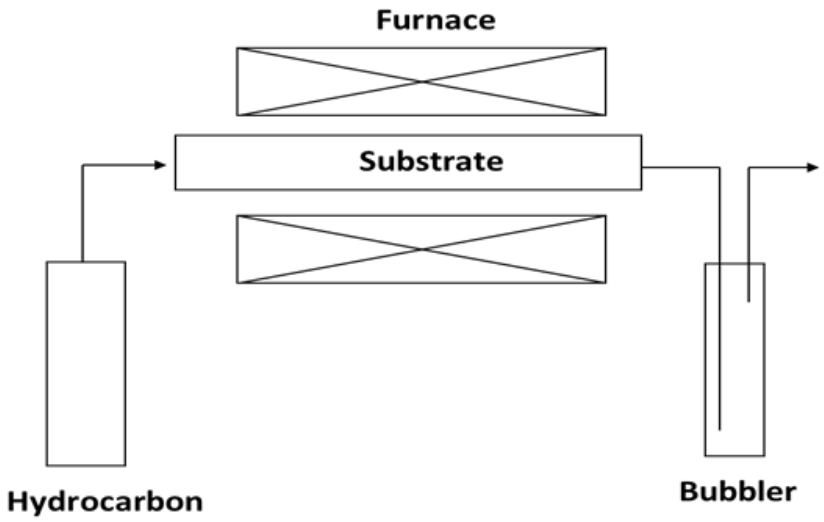

Figure 1.12. *CVD setup used in for the synthesis performed in this thesis*[72].

The schematic representation of a CVD system is shown in the Figure 1.12. The simplest set-up consists of a furnace with a quartz reactor tube placed in it, a hydrocarbon source, an exhaust gas bubbler and a control units to regulate gas flow and temperature.

The process of chemical vapour deposition involves the decomposition of a hydrocarbon by a catalyst under a thermal treatment (typically 600 - 1200 °C), in a reduced or inert atmosphere, resulting in the formation of CNTs on the catalyst.

Even though the mechanism of carbon nanotube formation is not completely clear, the traditional model of CNT growth by Baker *et al.* is widely used (Figure 1.13)[74]. It comprises two cases: tip-growth and base-growth model. The tip-growth model takes place when the interaction between catalyst and substrate is weak. The catalyst particles disconnect from the substrate and are pushed out to the top of the growing tube. The carbon nanotube grows until the top of the metal catalyst is open for hydrocarbon decomposition. The base-growth model takes place when the interaction with the substrate is strong, and catalyst particles remain at the root of the nanotube. This type of growth for CVD is common for catalyst-support powders[72,75].

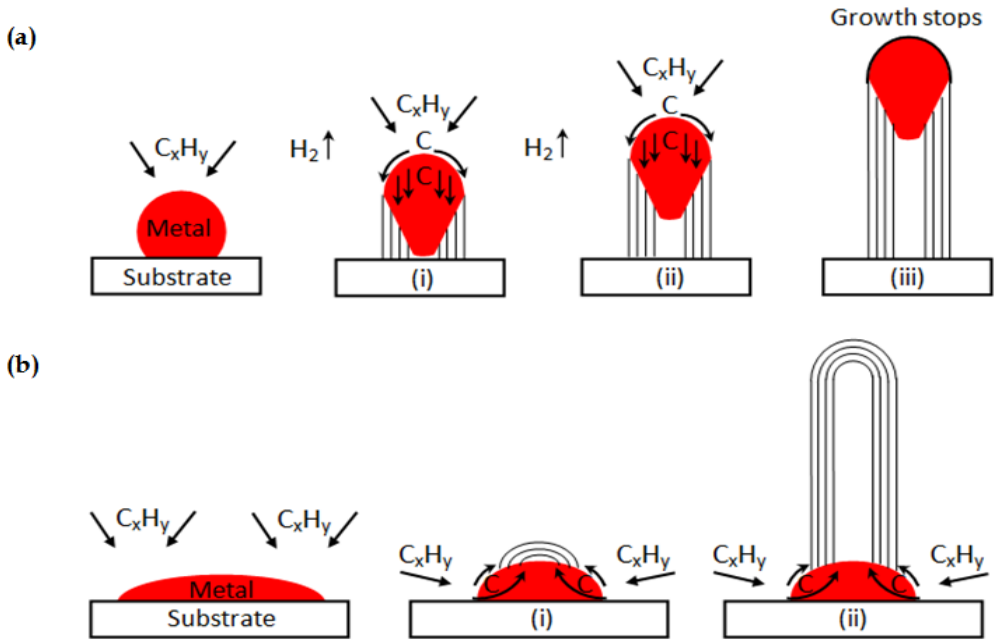

Figure 1.13. *Schematic representation of widely-accepted mechanisms of CNTs growth: (a) tip-growth model, (b) base-growth model*[75].

The size of the catalyst particles defines whether single- or multi-wall CNTs will be formed. Single-walled carbon nanotubes (SWCNTs) form from particles of a few nanometers, whilst multi-walled carbon nanotubes (MWCNTs) form from particles of a few tens of nanometers[73].

There is a number of parameters which influences CNT growth, such as precursor (hydrocarbon); catalyst; temperature; gas-flow rate; reaction time; and pressure. By varying these parameters, optimal conditions for each particular synthesis type can be found, and different types of CNTs could be grown.

Precursors for CNT growth by CVD

Acetylene, methane, ethylene, benzene, xylene, and carbon monoxide are the most common precursors for CNT growth. The morphology of CNT depends highly on the molecular structure of the precursor. Straight and hollow nanotubes are formed due to the decomposition of linear precursors such as methane; ethylene; acetylene. In contrast, the formation of spiral CNTs with possible bridges corresponds to cyclic hydrocarbons: benzene, xylene, and cyclohexane[76]. Thus, it is important to choose the appropriate precursor in order to achieve CNTs of good quality and desirable properties.

For CVD growth of carbon nanotubes on Ti substrates, methane, acetylene, and ethanol have been used as precursors[67,77,78].

Webster's group from Brown University used acetylene (C_2H_2) as a precursor for CNT growth. A mixture of 160 sccm C_2H_2 with 40 sccm H_2 was introduced for 30 minutes at 700 °C. In this case, parallel multi-walled carbon nanotubes were obtained[67]. The usage of a gas precursor provides positive results for this work, as it makes CVD syntheses simpler and potentially easier to scale up.

Takagi *et.al.* reported a possibility to grow CNT from Ti nanoparticles using both acetylene (C_2H_2) and methane (CH_4) precursors. The temperature and the gas flow rate varied for different precursors. In the case of C_2H_2, the growth temperature was 750 - 800 °C with the flow rate of 100 sccm. The CH_4 flow was 1000 sccm, and the temperature was higher – 800 - 1000 °C. The synthesis growth was from 1 to 15 minutes. SWCNTs

of different shape were obtained[78]. According to this work, it is clear that different reaction temperatures are required for different precursors.

Moreover, syntheses with ethanol as a precursor have also been reported[77]. In this case, TiO_2 nanoparticles were used as a catalyst. Two hundred sccm of H_2 was bubbled through ethanol with 1-3 % of water. Ethanol vapour was transported to the reactor which was heated to 900 °C for 10 min. Highly dense SWCNTs and MWCNTs were synthesized[77]. The problem with this method is that syntheses with ethanol could weaken the bond between Ti and CNTs due to the preferential bonding of Ti with O_2 from ethanol.

Catalysts for CVD

Traditionally, for CVD synthesis a metal catalyst is required in order to help to decompose a hydrocarbon. The most widely used catalysts are 3d transition metals such as Fe, Co, Ni[75,79]. The disadvantage of these catalysts for biomedical application is their potential toxicity. Other extensively used catalysts are solid organometallocenes such as ferrocene, cobaltocene, nickelocene. In addition to the metals already mentioned, Cu, Au, Ag, Pt, and Pd can also be used as a catalyst. In recent years, metal-free catalysts such as diamond, Al_2O_3, SiO_2, ZrO_2, and graphite have also been shown to exhibit catalytic properties. However, the process of CNT growth with metal-free catalysts is complex and requires very specific substrates, which makes it difficult to scale up[74].

Titanium has also been found to possess catalytic activity for CNT growth[77,80]. It was proven by XPS measurements that TiO_2 nanoparticles can be responsible for CNT growth. TiO_2 nanoparticles can be fabricated either by a sol-gel method or by sputtering titanium with thermal oxidation. In this case, it is easy to control diameter distribution of CNTs by varying the size of TiO_2 nanoparticles[78].

1.4.2. Electrodeposition

Electrodeposition is another method of CNTs deposition on the surface of titanium implants. Aoki *et al.* made CNT coating on Ti and investigated it *in vitro* using an electrodeposition technique. According to the electrodeposition method reported by Sano *et al.*, multiwall carbon nanotubes (MWCNTs) were deposited on Ti substrates with a diameter of 20 to 40 nm and length between 500 nm and 5μm. MWCNTs were synthesized by chemical vapour deposition. Afterwards they were dispersed in anhydrous *N, N'*- dimethylformamide (DMF) and sonicated. A voltage of 1.5 V was passed through Ti electrodes dipped into the CNT solution for 12 hours. After washing with DMF, the anode Ti substrate was used for further investigations. Human osteoblast-like cells were seeded on CNT/Ti scaffolds and examined after three days. The results showed no changes in the fibrous structure of CNTs and a good adhesion of nanotubes to the Ti surface. Moreover, in the other study by the same group, cell adhesion, and proliferation were significantly improved[81]. This work confirms that CNT coating can have a positive influence on osseointegration.

The drawback of the electrodeposition technique is that CNTs are first synthesized and only then deposited, whilst CVD is a one step process. Also, the bond between CNTs and Ti is not very strong. Therefore, CVD is the preferred technique for creating CNT/Ti composite material.

1.5. Mechanical properties

Mechanical properties should also be considered while creating CNT/β-Ti composites. Their fracture toughness, elastic modulus, hardness, and bonding strength should be investigated. Moreover, the adhesion strength of CNTs with a substrate as well as the interface is of great importance.

Bonding strength

Initially, two types of interaction between Ti and CNTs are possible[82]:

1) End contact.

In this case, covalent bonds between CNTs and metal particles take place. It is a less examined type of contact, although it is usually quite strong because the edges of nanotubes are relatively reactive in comparison with their sides, and could form stronger covalent bonds. The interaction happens between the graphitic plane of the nanotubes and d-electron of the metal forming a strong Ti-C bond.

2) Side contact.

In side contact, weak Van der Waals bonds are present that are caused by surface wetting. The contact occurs by overlapping p_z-orbitals of carbon and d-orbitals of the metal. Usually, there are no covalent bonds in the side contact. However, a re-hybridization sp^2 to sp^3 of carbon atoms within the tubes occurs locally when the adhesion of the metal is strong, leading to the covalent side-bond.

The Ti-C bond is very strong. The following sequence of the binding energies E_b of metal atoms to the nanotube (or graphite) has been suggested by Zhang: Ti>Ni>Pd>Fe>Al>Au[82,83]. A strong interaction between CNT and Ti could be observed

by means of electron microscopy and photoemission spectroscopy. It is also supported by density functional calculations[84]. However, the CNT/Ti bonding is considerably weakened by the presence of oxygen, as Ti prefers to bond with oxygen atoms rather than carbon. Oxygen comes from two primary sources: the residual oxygen that is present in the chamber and from the oxidized defects of CNTs. It was found that the interaction of Ti with CNTs highly depends on the quantity of oxygen present in the initial surface layer, while a further presence of oxygen is less important. As soon as no oxygen remains Ti is able to form Ti-C bonds[84]. These studies revealed that the presence of oxygen while creating a CNT/Ti composites is critical for proper bonding between the Ti surface and the CNTs. Thus, further research to develop a system with minimum oxygen content is critical.

Fracture toughness

Human bone undergoes a significant amount of force every day. In order to prevent fractures and cracks, the fracture toughness of an implant should be very good. Fracture toughness describes the ability of a particular material with a crack to resist fracturing. The influence of CNTs on fracture toughness of titanium in a Ti/CNTs system has not been investigated yet.

Young modulus

The Young modulus of current orthopedic implant materials is much higher than that of the human cortical (compact) bone. For CoCr alloys the elastic moduli are ~ 240 GPa, for stainless steel 210 GPa, and for Ti alloys from 110 to 55 GPa, meanwhile the Young modulus for human bone is under 30 GPa. This mismatch is one of the reasons for the implant loosening described earlier. New β-Ti alloys possess the lowest elastic modulus (80-50 GPa) available at the moment, and that is one of the reasons why they are

preferable for implant application[11]. While creating CNT/Ti composites the value of their elastic modulus should be controlled according to the composition and structure, in order to avoid its unwanted increase.

Interface bonding

In order to be able to transport the beneficial properties of CNTs to the CNT/Ti composite material, the interface bonding between the implant and CNTs should be strong and well investigated. Time-of-flight secondary ion mass spectroscopy (TOF-SIMS), scanning electron microscopy (SEM) and transmission electron microscopy (TEM) are useful techniques for investigations of the bone-implant interface[85].

The structural analysis of the implant–bone interface can be analyzed using focused ion beam (FIB) for the preparation of the TEM the samples. It enables us to see the structure and composition of the sample. Time-of-flight secondary ion mass spectroscopy (TOF-SIMS) was used earlier for the overall evaluation of the interface between the bone and implants[86], and focused mainly on the inorganic components of the bone. Nowadays, TOF-SIMS can give information about both inorganic and organic parts of the bone[87]. These new investigations provide a better understanding of the interface between implant and bone.

Also, atomic force microscopy (AFM) is a commonly-used method for measuring the topography and manipulating nanomaterials[88,89]. It shows a qualitative analysis of the adhesive force. During the utilization of this technique, the sample surface is ‘probed’ with the cantilever of the AFM. In contrast to SEM and TEM, it can give three-dimensional images and requires a much easier sample preparation. Nevertheless, it does not provide any quantitative analysis. Lateral force microscopy (LFM) is a new way to measure adhesion and friction of nanomaterials[90]. By means of LFM, it is possible to

measure quantitatively the adhesive force between the CNTs and the Ti substrate. For example, in the study by Ju-Ai and Bruchan, to get the adhesive force, SWCNTs were manipulated by the AFM tip at 17 nN. At the same time, the LFM signal was recorded. The measurements were performed for welded and non-welded samples. The lateral force between SWCNT and AFM tip was found to be greater than the adhesive force of SWCNT and Ti, where Van der Waals forces are rather weak[90]. Also, it was found that welded samples possessed much higher adhesive force than non-welded ones. However, it is still difficult to obtain the critical lateral force.

Continuous and comprehensive measurements of the lateral force should be taken as the next step. In addition, it should also be investigated whether the length of the SWCNTs has an influence on the value of the adhesive force.

Moreover, new techniques to measure the intersection of the bulk sample, and not just individual nanotubes, should be developed, which would aid in improving the interaction between CNT and Ti that is crucial for long-lasting implants.

1.6. Biocompatibility

CNT/Ti composites have a high potential for orthopedic applications due to their excellent mechanical properties and ability to foster cell growth. However, each component of such a composite, as well as the composite as such, must be examined in terms of biocompatibility first before they can be used for orthopedic surgery.

There are many investigations on the biocompatibility of β-Ti and its alloying elements such as Hf, Nb and Ta both *in vitro* and *in vivo*. During *in vivo* experiments on rats both in soft and hard tissues, no inflammatory processes were observed, and after four weeks, the number of fibrous tissues had decreased[91]. Thus, Ti is already a clinically proven material, but before the use of CNT/Ti composite material in living bodies, the evaluation of its toxicity and biocompatibility by means of *in-vitro* and *in-vivo* studies are necessary.

In terms of evaluating CNTs, both their toxicity and biocompatibility should be investigated. The toxicity of CNTs is still contradictory. Following the work of Huczko *et al.*, who conducted experiments on guinea pigs in 2001, few other studies regarding the toxicity of CNTs were reported. Different research groups presented contradictory results[10,92–95]. Some studies revealed no toxic effect of carbon nanotubes[10,92,94], while others reported a cell death due to the carbon nanotubes[10,95]. Nevertheless, researchers agreed that the primary sources of CNT toxicity are transition metal catalyst particles together with impurities, defects, agglomeration and not the CNTs themselves. Furthermore, culture medium, chemicals, and pH can also influence the result of toxicity measurements[10,96,97]. According to the finding, pristine CNTs cause minimal toxicity. Moreover, chemically functionalized CNTs have not showed any toxic effects[96].

The situation concerning the biocompatibility of carbon nanotubes looks different. A significant part of investigations of CNT-based materials provided evidence for their

biocompatibility. Such studies were based on the interaction between CNT-based materials and osteoblast, fibroblast, neuron cells, as well as antibodies and cellular membranes. For implant biomaterials, a response of osteoblast cells is vital. The adhesion and the function of the bone growth of osteoblast cells were investigated[96].

Nevertheless, the number of studies on this important issue is not currently high enough to draw any accurate conclusions. Also, in order to evaluate biocompatibility of CNTs, the creation of a general protocol for carrying out experiments is essential, but this does not yet exist. Currently, each group has their criteria for examination, and their results often cannot be compared.

1.6.1. Biocompatibility of CNT/Ti composites

The evaluation of a CNT/Ti composite as a whole also consists of *in vitro* and *in vivo* biocompatibility tests. *In vitro* testing of CNTs could be of two types[97]: firstly when CNTs are dispersed in the cell culture[98–101] and secondly when CNTs are in a composition that reacts with the cell culture[102–105,106].

The biocompatibility investigation of implant materials is a complex subject, and different techniques could be used. A successfully used method for biocompatibility evaluation was reported by the group of Dr. Roger A Brooks from the Orthopedic Research Unit, University of Cambridge[107]. Within this technique, the key aspects of evaluation are cell attachment, cell growth, production, and differentiation of bone factors.

Type-1 collagen and carbonated hydroxyapatite (mineral) are the bone factors examined in their study. Cells for these experiments are human osteoblast isolated from trabecular bone from several batches and different individuals to provide reliability.

Typically, 12 samples (β-Ti/CNT composite) and 12 control discs (β-Ti) with a diameter of 10 mm are examined. First, approximately 15000/cm^2 of cells are seeded on each disc. After osteoblast attachment for three hours, samples are covered with culture medium and incubated. Following this, six samples are harvested in 24 hours to measure their cell number and alkaline phosphatase. The remaining six discs are covered with alamarBlue for 14 days or longer to assess the mineralization. The collagen production is measured for material harvested at various period. Finally, cell number and alkaline phosphates measurements are repeated at the end of the experiment. Moreover, to obtain the information about cell and matrix morphology, immunofluorescence and SEM studies could be done.

1.7. Conclusions and scope of the thesis

This chapter presented the importance of the development of new orthopedic biomaterials as well as the progress in the field of Ti implants. This thesis is focused on a development of new biocompatible CNT/Ti and carbon nanostructures/Ti composites in order to improve the performance of Ti implants. CNTs have the optimal match of size and shape to those of the bone cells, appropriate mechanical, chemical and electrical properties. Thus, they are a promising material for improving mechanical properties and biocompatibility of Ti implant materials. Studies showed that CNTs can foster cell formation. A significant increase in osteoblast proliferation and adhesion was reported that should lead to better contact between the bone and implant and consequently to the longer lifetime of the implant. Nevertheless, the biocompatibility and toxicity issues of CNTs are still under debate, and more work should be done in this area. This thesis will help to achieve this aim. Chemical vapour deposition and electrophoretic deposition are methods currently used for the manufacture of CNT/Ti composites. CVD is a versatile, controllable, relatively easy and economical technique. Moreover, it has the advantage of growing CNTs on Ti in a one-step process. CNT growth using CVD method on α-Ti and α+β-Ti alloys has been already reported by several research groups. However, experiments on β-Ti alloys, which possess lower elastic modulus, better fatigue resistance, no toxic elements and are thus preferable as implant biomaterial, have not yet been performed. Therefore, fabrication of CNT/β-Ti should be the next area of investigation.

Chapter 2. Catalytic growth of multi-wall carbon nanotubes (MWCNTs) on Ti-based thin films and bulk Ti substrates.

2.1. Background

Since the discovery of carbon nanotubes and the report by Iijima in 1991[57], the attention to these structures has been increasing. This is a result of the extraordinary properties of CNTs, including mechanical, electrical and chemical properties, which are determined by their unique structure and size[108,109]. Looking at the history of CNTs, a few important evolutionary steps can be identified. Firstly, CNTs research moved from the simple observation of a structure[57] to the production of significant quantities of CNTs[110]. The next step was a shift from the 'accidental' production to a controlled production[111]. It is only now that we are starting to improve control and up-scaling to the industrial qualities[108], and are developing applications based on CNTs[112–114]. CNTs also attracted a lot of attention in medicine[115–119]. CNTs are used as bone-resembling biomaterials[115], for drug delivery[120,121], tissue engineering[122,123], and imaging[124]. Moreover, in the past decade, a positive trend can be observed in the number of articles containing the topics 'carbon nanotubes' and 'biomaterials' from 2001 to 2013 (Figure 2.1).

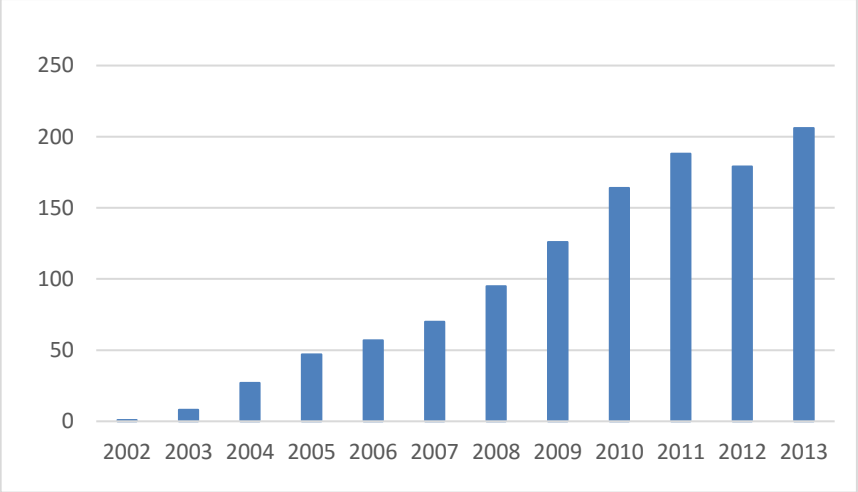

Figure 2.1. *A number of articles found in the PubMed database (http://www.ncbi.nlm.nih.gov/pubmed/) (accessed 9 February 2015), using 'carbon nanotubes' and 'biomaterials' as keywords, showing the increase in the number of articles in the recent years.*

In the field of biomaterials, improving the materials is currently of high importance, towards which CNTs are hoped to become a good candidate[59,125]. As was presented in Chapter 1 concerning implant biomaterials, nowadays metals are primarily used, amongst which titanium is the best metal for orthopaedic purpose owing to its good mechanical properties (e.g. strength, fatigue resistance), corrosion resistance, and relatively low Young's modulus (110 – 55 GPa)[1]. Ti alloys can be of several types: α-, α + β, β-alloys. Currently α-, α+β are the most commonly used the material, but β-alloys have drawn a lot of attention due to their even lower Young's modulus, high wear and fatigue resistance and absence of toxic elements[3,23,24], promising their long term use as implants due to the prevention of stress shielding and implant loosening. Taking into consideration all the advantages of β-Ti alloys, unfortunately, they are not bioactive[24], which is required for good cell ingrowth. In order to provide the material with bioactive properties, surface modification of Ti can be applied as explained in Chapter 1. For the modification of Ti, various nanostructures and in particular multi-walled carbon nanotubes (MWCNTs), are potentially good candidates[115]. Even though there are only a few studies regarding

MWCNTs growth on Ti alloys[64,65,67,126,127], MWCNTs/Ti-based composites were shown to possess good biocompatibility and improvement in bone cells proliferation and differentiation during the *in vitro* studies[64,65,67,126,127].

MWCNTs can be incorporated into biomaterials in several different ways. Ti could be coated with MWCNTs solution[128]; nanotubes could be electrodeposited[81] or grown using chemical vapour deposition (CVD) methods[67,97]. Ideally, to avoid a release of MWCNTs into the surrounding tissues and/or possible adverse reactions, they should be well connected to a substrate. During the experiments on coating technique for catalysts in this Chapter, it was observed that during the aerosol spraying of MWCNTs, the connection between the tubes and the metal is very weak due to the absence of functional groups on the MWCNTs surface. Only Van der Waals forces are responsible for the MWCNTs/substrate interaction. On the contrary, during the CVD process, CNTs are directly grown on Ti substrates, and it was observed that this enables a stronger interaction between the substrate and the CNTs. Additionally, CVD is a one-step process, while the others (coating or electrodeposition) are two-step processes in which CNTs are first synthesized and then deposited. This makes the CVD process potentially more attractive for upscaling in industry.

S. Sirivisoot *et al.* reported CNTs growth on α-Ti with a Co nitrate catalyst using the CVD technique[67]. However, it is unclear what type of nanotubes (if any) were grown by this method. There is no indication of CNTs formation except the Scanning Electron Microscopy (SEM) micrographs reproduced in Figure 2.2. Typically, a Transmission Electron Microscopy (TEM) micrograph or Raman spectrum should have been provided in order to confirm the existence of CNTs. An example is shown in Figure 2.3. It reveals CNTs growth, supported by SEM and TEM graphs and a Raman spectrum. Thus, a

reproducible, direct growth of CNTs on Ti substrates using a CVD technique would be a significant step forward.

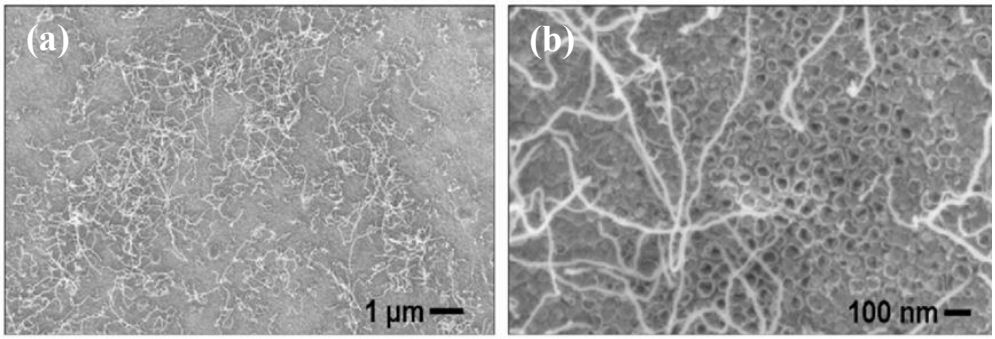

Figure 2.2. *Lower (a) and higher (b) magnification SEM micrographs showing CNTs grown on anodized Ti with a Co catalyst, as reported by S. Sirivissot et al.*[67].

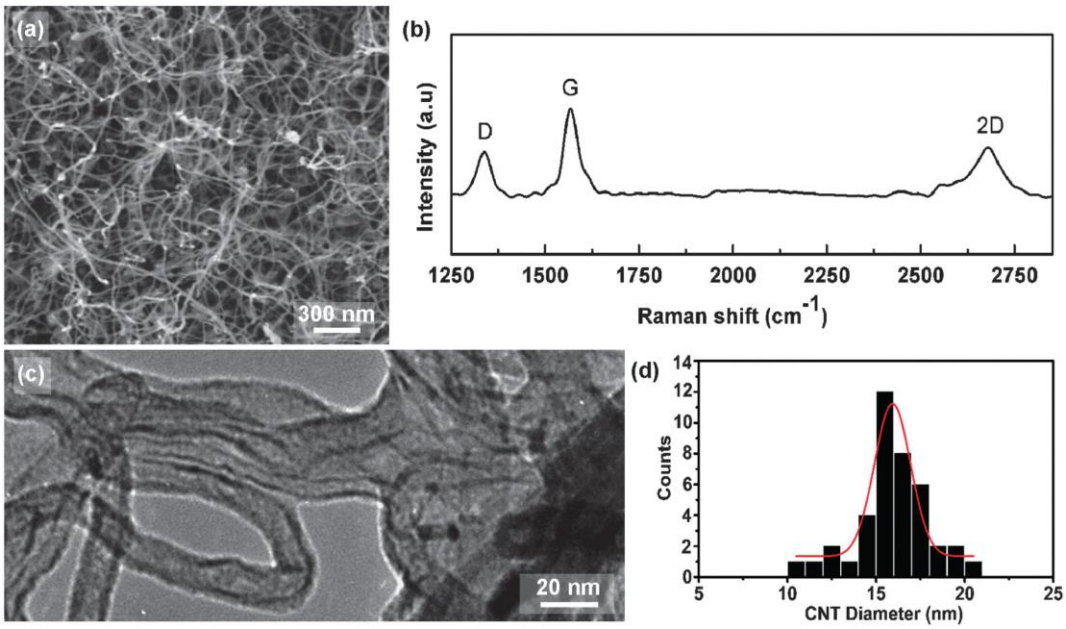

Figure 2.3. *The growth of CNTs on $SrTiO_3$ (001) substrates using supported Ni nanocrystals as catalysts. (a - c) SEM image (a), Raman spectrum (b) and TEM micrograph (c) of CNTs. (d) The diameter distribution of the nanotubes*[129].

Even though some CNTs formation on Ti was achieved[67], Ti is not a typical substrate or catalyst for CNTs growth[130], and consequently, growing CNTs on it is challenging. Until now, experiments focusing on CNTs and Ti were performed only on α-Ti and α+β substrates[67,61]. Therefore in this Chapter, β-Ti substrates are used, as well as α-Ti

substrates as a starting material, for comparison and as a reference. While growing carbon nanotubes on new types of titanium samples, it is important to take into account a number of parameters that could strongly influence the CNTs formation. These include the influence of catalyst type, concentration of catalyst, method of catalyst deposition, form of substrate (bulk or thin film), substrate composition, and the ratio of elements in the substrate alloy.

During the CVD process, the decomposition of hydrocarbons and formation of carbon nanotubes takes place in the presence of a catalyst. It is, therefore, important to choose an appropriate catalyst. The most widely used are transition metals such as Fe, Co, Ni[131]. Also, various catalyst combinations including Fe/Al_2O_3, Co/ Al_2O_3, Ni/ Al_2O_3, Fe/MnO, Co/MnO, and Ni/MnO were investigated by R. Ummethala *et al* [132]. Fe- and Co-based catalysts result in the formation of aligned MWCNTs with a smaller diameter due to a fine particle size and a favourable distribution of the respective nanoparticles on the supporting layer[132]. As we are preferably looking to grow MWCNTs of a smaller diameter (which will be comparable with the diameter of collagen fibrils, around 20 - 40 nm[60]), Fe and Co catalysts were considered in this Chapter. While growing MWCNTs for biomedical applications, the requirements of low toxicity should also be fulfilled. Toxicity of MWCNTs is often primarily associated with the presence of metal catalyst particles in the nanotubes[121]. It was reported that different metal particles possess varying degrees of potential toxicity[133]. Comparing Fe and Co particles, Fe was found to possess less potential toxicity in the human body[133]. Therefore Fe-based catalysts were chosen for this study. Since the concentration of the catalyst particles could determine the type and the diameter of CNTs[75], different concentrations of catalyst were investigated in this thesis. Results showing the influence of the catalyst are presented in Section 2.3.1.1.

Additionally, it is necessary to find an efficient way to introduce the catalyst into the system. There are several ways to deposit the catalyst onto the substrates. A common method is physical vapour deposition (PVD), although disadvantages include the need for rather complex equipment, including a vacuum environment. Moreover, this process is not easily upscale for the manufacturing of implant materials. Therefore, an alternative was sought, and several simple methods for catalyst deposition were chosen. Alternative deposition methods include drop casting, dip coating and spin coating[134], and the results of their use can be found in Section 2.3.1.1.

The influence of the substrate composition on the formation of CNTs was reported in a number of publications. Ward *et al.*[135] showed that the composition of a substrate has a strong influence on what kind of nanotubes will be formed – SWCNTs or MWCNTs. In another study, a comparison of quartz, conductive glass, porous alumina and nickel plates was conducted by Ortega-Cervantez *et al.*[136] the influence of the substrate on the type of the CNTs was observed. Not only the type of CNTs (SWCNTs or MWCNTs) is influenced by the substrates, but the diameter of the CNTs also varies on different substrates. Ortega-Cervantez *et al.* reported that MWCNTs with a diameter of 25 – 90 nm were grown on glass substrates; curled SWCNTs with a diameter 10 – 30 nm were formed on nickel, and short SWCNTs with 1.3 – 2.0 nm diameter on alumina. It was also demonstrated that the structure, quality and surface roughness of the substrate are factors that have a strong effect on the CNTs growth[136]. It has been reported that not only the composition of the substrate but also the ratio of the elements in the alloy is important for CNTs formation. D. Makris *et al.*[137] showed that Al_2O_3 pellets with different Ni content result in a different CNTs growth. No CNTs formation was observed with the low Ni content of 10 wt. %. When a higher Ni content was present, CNTs were formed, and the largest amount of nanotubes was observed with a 40 wt. % of Ni. Higher Ni content

favoured a greater conversion of precursor and, therefore, a larger growth of nanotubes[137]. Ni sites play a significant role in methane dissociation on the catalyst surface, giving rise to surface C and H atoms[137]. Therefore, Ti-based films with different compositions and elemental ratios were investigated, and results of CNTs growth are presented in Section 2.3.

CNTs were shown to grow on both bulk substrates, such as Al foils[138], and thin metal films sputtered on silicon wafers[139]. However, whether these different types of substrates influenced the formation of CNTs is not yet known. In this thesis MWCNTs growth is performed on three different types of titanium substrates: Ti-based thin films, bulk Ti-based substrates, and Ti-based scaffolds. The use of Ti-based films will reduce the cost of the material for the experiments but still allow the exploitation of the advantages of β-Ti. In addition, the CNTs growth on Ti-based films provides the possibility to work with films of different chemical composition, allowing to discover whether the composition has an influence on the formation of CNTs, and which material is the most suitable substrate. Section 2.3.1 summarises the experiments performed on Ti-based films.

A considerable attention should be also given to the metal catalyst particle location. While comparing MWCNTs growth on Si and Ti substrates with Ni and Fe catalysts, respectively, low cell viability and a low degree of cell adhesion on Ti, and good cell adhesion and viability on Si have been reported[97]. The possible explanation is that Ni particles (on Si) are enclosed by the MWCNTs, while Fe particles may be present around the MWCNTs[97]. Therefore, the interaction between the catalyst particles and the substrate is also addressed in the current Chapter. CNTs can be formed by root- or tip- growth mechanisms, which have been explained in greater detail in Chapter 1. In order to minimize possible toxic issues, a root-growth mechanism is required. To investigate the

mechanism of the CNTs formation, we look at the interface between MWCNTs and Ti-based substrates. These investigations are discussed in Section 2.3.1.2

To summarize, in order to achieve reproducible CNTs growth on titanium substrates and to understand the mechanism of nanotube formation, a systematic study was performed during which the influence of the substrate, catalyst concentration, and the time of synthesis were investigated, which is discussed in this Chapter.

2.2. Experimental Details

2.2.1. Experimental parameters for CNTs growth on Ti-based substrates

Experiments for CNTs growth on titanium substrates were performed using a chemical vapour deposition (CVD) technique. A schematic representation of a horizontal CVD system used in this thesis is shown in Figure 2.4. The CVD set-up consists of a single-zone horizontal tubular furnace (Elite Thermal Systems; 4 cm inner diameter; 60 cm long), inside which a quartz tube (Robson Scientific; 21 mm inner diameter) with titanium substrates was placed; argon, hydrogen and acetylene gas cylinders; a bubbler with acetone to capture soot and other by-products coming out of the CVD reactor as well as to prevent any potential backflow of air; and the exhaust.

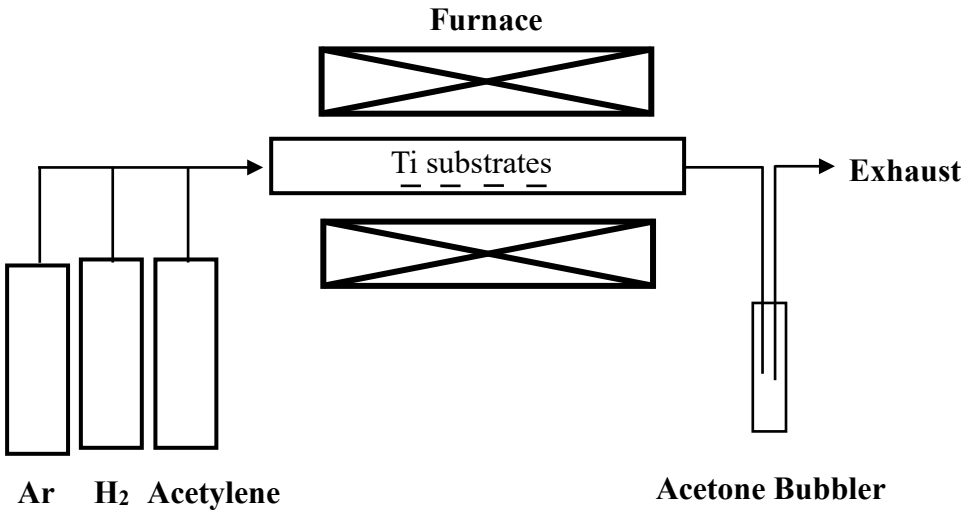

Figure 2.4. *Schematic representation of a horizontal CVD setup used for CNTs syntheses used in this thesis. It consists of gas cylinders (Ar, H_2, and Acetylene), acetone bubbler, and a single-zone tubular furnace with quartz tube inside, in which titanium substrates are placed.*

Acetylene was used as a hydrocarbon source for CNTs growth since it is a very reactive precursor and it was used for CNTs growth in other studies[67]. The furnace was heated and cooled with 200 sccm of argon as a carrier gas. After the furnace had reached the reaction temperature of 645 °C, the samples were annealed for 30 min in 45 sccm of hydrogen. Then, acetylene was introduced at a flow rate of 12 sccm, and the reaction took place. Different reaction times of 10, 15 and 20 min were applied.

All the substrates were cleaned by sonication in acetone and deionized water in turns, in order to reduce the impurities, and subsequently dried under nitrogen. After the catalyst had been deposited, the substrates were placed inside a quartz reactor tube in the furnace.

For CNTs growth on titanium substrates, two metal catalysts were chosen: a) Fe (III) nitrate; b) Fe (III) nitrate + Al nitrate (Sigma-Aldrich). They were diluted in absolute ethanol. The prepared solutions were stored in the fridge and used only for 2-3 days in order to avoid precipitation of the salt crystals. Different concentrations of catalysts were used, which include: 0.1; 0.05; 0.01; 0.005; 0.001 and 0.0005 M.

A WS-650 spin coater, Laurell Technologies (Figure 2.5) was used to deposit the catalyst onto the Ti-based samples. The catalyst solution was introduced in the middle of the sample (with a drop from a pipet) and spread quickly by the centrifugal force at high speed.

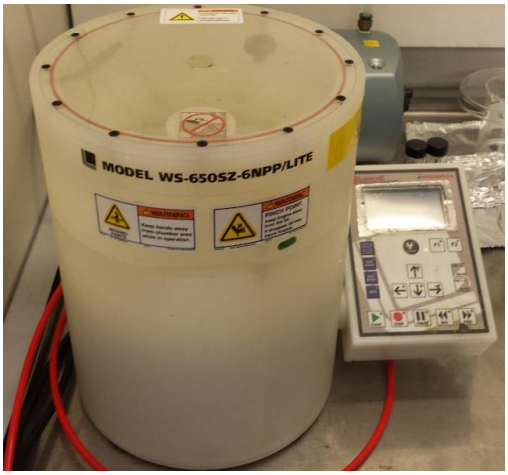

Figure 2.5. *A typical spin coater used for Fe nitrate and Fe + Al nitrate catalysts deposition on the Ti-based sample in this Chapter.*

In this Chapter, three groups of substrates were used, being Ti-based films, bulk Ti-based alloys and Ti-based scaffolds.

Ti-based thin films are listed in Table 2.1. They were produced by a custom-made magnetron sputtering deposition chamber (Figure 2.6), which was designed by BioTiNet ITN collaborator Nikolaos T. Panagiotopoulos at the University of Ioannina, Ioannina, Greece. Pure α-Ti, binary and ternary β-Ti films with different composition were deposited onto silicon substrates. The magnetron sputtering set-up consists of two sputtering guns, which are positioned at 90 degrees to each other. The substrate holder was rotated 45 degrees relative to the guns, and a DC voltage was applied to both guns. Turbo and rotary pumps were used to achieve a working pressure of 10^{-2} mbar and a base pressure of 10^{-6} mbar. For binary film growth, two different metal targets were placed in each magnetron gun. Alternatively, for ternary films, Hf foil was attached to the sputtering ring of the horizontal gun. Argon was used as a sputtering gas in the system.

Table 2.1. *The summary of Ti-based films used for CNTs growth in Section 2.3.*

Code	Sample	Type of alloy
α-Ti film	Ti film	Alpha
β-Ti film	TiNb film	Beta
β-Ti film	TiZr film	Beta
β-Ti film	TiZrHf film	Beta
β-Ti film	TiNbHf film	Beta

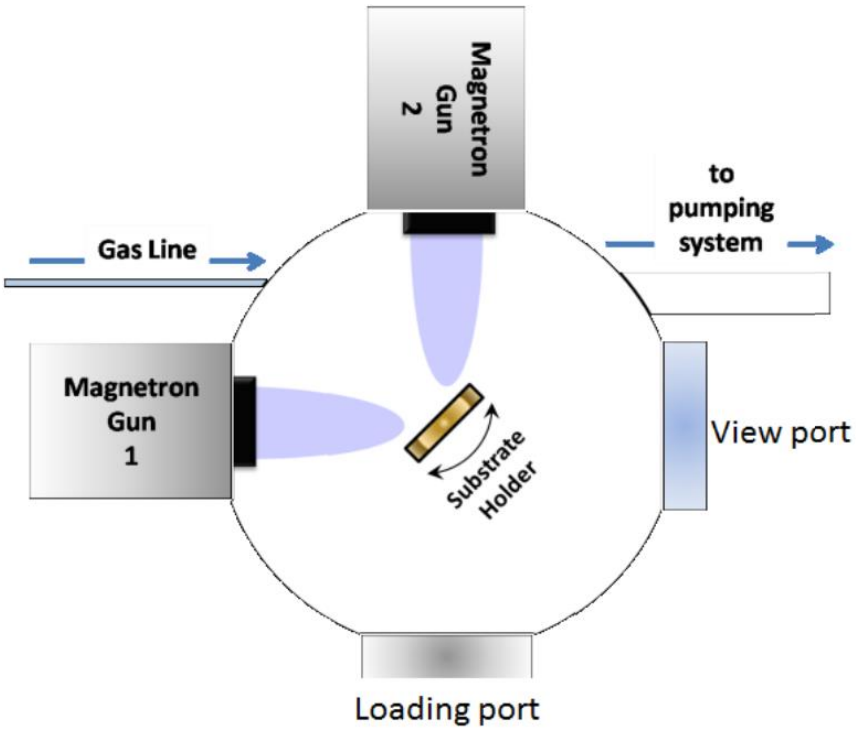

Figure 2.6. *Top view of the custom made magnetron sputtering deposition chamber with two guns positioned at 90 degrees to each other onto the Si substrates placed onto the substrate holder used for the preparation of Ti-based thin films. The design of the deposition chamber and the growth of Ti-based films was performed by Nikolaos T. Panagiotopoulos.*

Bulk Ti-based substrates were commercially produced and listed in Table 2.2. Substrates include: pure (CP) Ti foil (Alfa Aesar, 99.5 %) and TiNb rod (ATI WahChang, Ti-45Nb wt. %) with dimensions of 10 mm^2; as well as GR2 Ti (BAOJI PRO-TITANIUM METALS) and Ti-13Nb-13Zr (XI'AN CHINA) discs of 14 mm diameter.

Table 2.2. *List of bulk Ti-based samples used for the MWCNTs growth in Section 2.4.*

Code	**Sample**	**Type of alloy**
α-Ti	CP Ti foil	Alpha
β-Ti	Ti-45Nb rod	Beta
α-Ti disc	Ti disc	Alpha
β-Ti disc	TiNbZr disc	Beta

In order to modify the surface of bulk, Ti-based substrates HF treatment, and mechanical polishing were used. HF cleaning of Ti-based substrates was performed in 40 % and 8 % HF solutions. Treatment with 8 % HF was performed during various times of 1, 2, 5 and 10 min. For mechanical polishing of Ti-based substrates, three different machine polishing methods were used: 6 μm diamond paste, 100 nm silicon oxide and 20 nm silicon oxide. Also, manual mechanical polishing with SiC (1200 grit) was carried out.

Ti-based porous scaffolds of two types with 16 mm in diameter were used for CNTs growth, which are presented in Table 2.3.

Table 2.3. *Ti-based porous scaffolds used for MWCNTs growth in Section 2.5.*

Code	**Sample**	**Type of alloy**
β-Ti-1	TiNb scaffold	Beta
β-Ti-2	TiNbZr scaffold	Beta

Porous scaffolds were produced by Mathew Speirs at KU Leuven, Belgium, using selective laser melting (SLM) (Figure 2.7). During the SLM process, a layer of metal powder interacts with a laser beam, heats up and melts to form a liquid pool. Later, this metal pool cools down quickly and solidifies, and the fused material starts to form the open-structured product. After the surface area of a layer is scanned, the build platform is lowered by an amount equal to the layer thickness, *e.g.* 30 μm, and a new layer of powder is deposited[140].

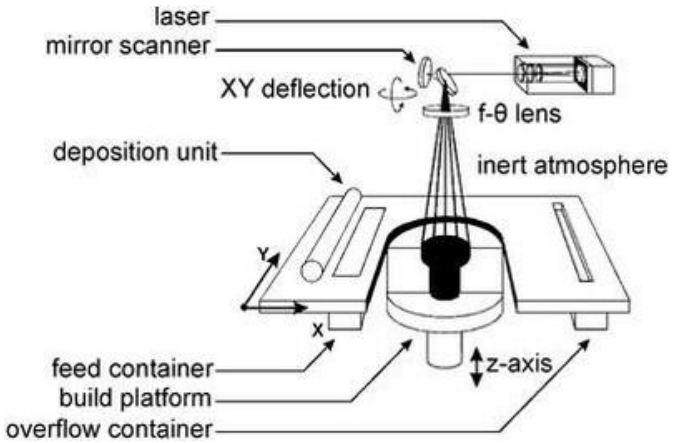

Figure 2.7. *Schematic representation of the selective laser melting (SLM) process, during which the material is build up layer by layer, while the metal powder is melted by a laser. An inert atmosphere is applied to obtain homogenous material*[140].

2.2.2. Techniques for sample analysis

Information about the surface morphology of the Ti-based substrates including whether MWCNTs were formed during the CVD synthesis was obtained using a scanning electron microscope (SEM). Information regarding the structure (aligned or not aligned), diameter, density and distribution of MWCNTs in the samples was also obtained using an SEM. In the current study, a JSM 840A SEM (operating at 10 kV), a JSM 840F SEM (operating at 5 kV), and a JSM 6500F SEM (operating at 5 kV) were used to obtain the data. The last two microscopes have field emission guns as an electron source. Samples were placed on the aluminium stubs used for imaging. As MWCNTs are electrically conductive by themselves, no further preparation was needed. Secondary electron imaging mode was used for the analysis of the samples.

Raman spectroscopy was utilized to confirm the presence of MWCNTs on Ti-based samples. All Raman investigations were performed using a JY Horiba Labram Aramis imaging confocal Raman microscope with a 532 nm frequency. Samples were placed onto the glass slides, and each measurement was repeated at least three times.

A transmission electron microscopy (TEM) technique was used to obtain high-resolution images for the investigation of the detailed internal composition and morphology of the CNTs. In order to investigate CNT/Ti composites as a whole, cross-section TEM specimens were analysed. JEOL 2000FX and JEOL 2010 transmission microscopes were used for imaging of the samples, with a typical accelerating voltage of 200 keV.

For the preparation of cross-section TEM specimens focused ion beam (FIB) milling was used, a ‘lift-out’ technique which provides very thin TEM specimens. The preparation of cross-section TEM specimens using FIB involved a number of stages (Figure 2.8). First, the region of interest was defined. Then, a thin layer of tungsten and a thicker layer of

carbon were applied in order to protect the surface of a sample during ion milling. Carbon coating ensures that the position of the nanotubes remains unchanged, enabling the real picture of MWCNTs - substrate interaction to be shown.

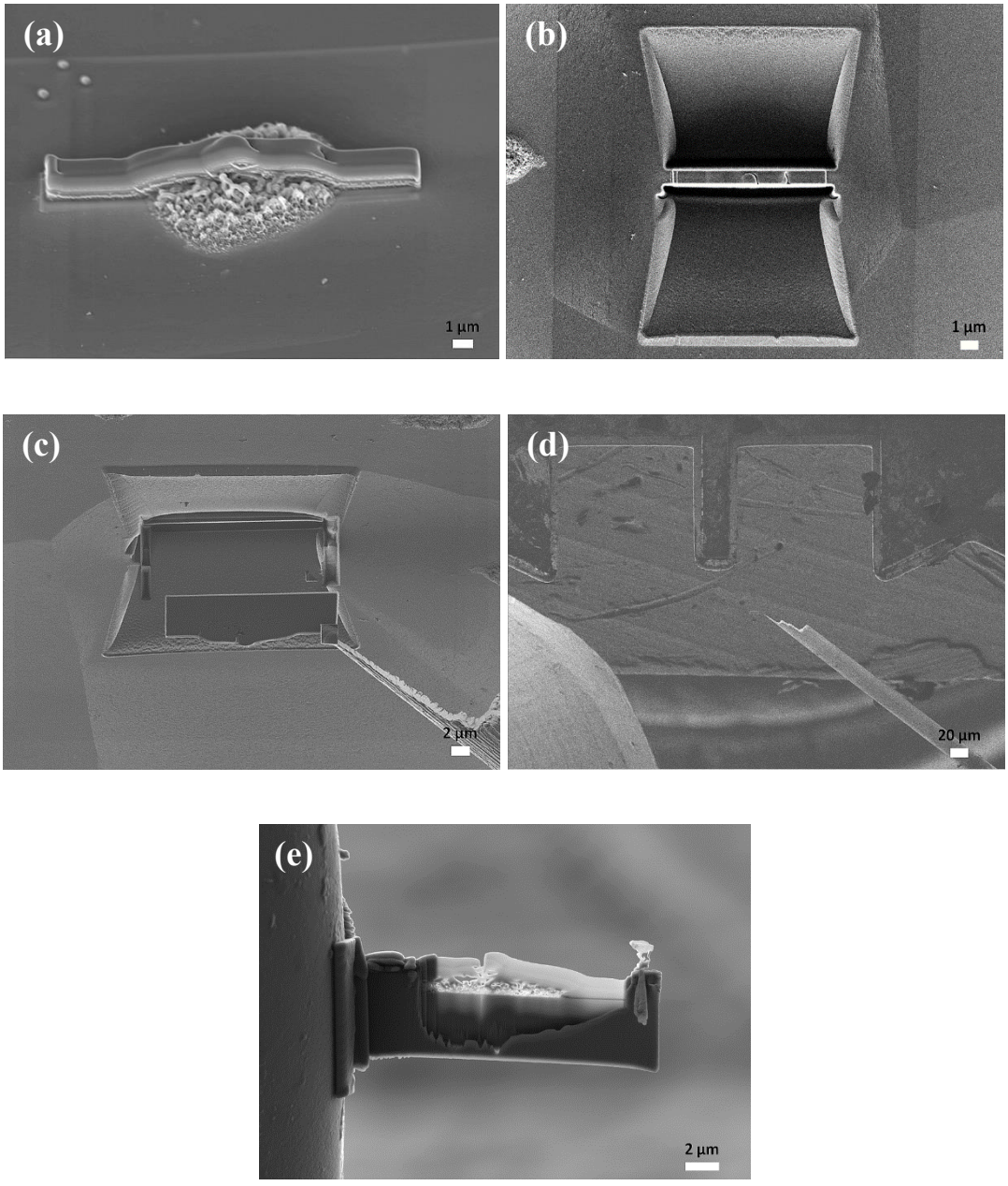

Figure 2.8. *Stages of preparing the TEM samples using a FIB instrument: a) protective coating deposition; b) cutting of trenches from both sides of the specimen; c) thinning of a specimen from both sides and its attachment to the needle; d) transfer of the specimen to the TEM grid; e) final thinning.*

After the coatings, two trenches were cut from both sides, leaving a thin wall containing the specimen. Then, the sidewalls were cut so that the specimen was only attached at the top. The specimen was then thinned from both sides. The TEM specimen was attached to the needle and transferred to the TEM grid. Finally, it underwent further thinning to achieve the desired thickness. In this work, a Zeiss NVision 40 FIB-SEM was used to look at the cross-sections of samples and for *in-situ* lift-out preparation for TEM specimens with a typical accelerating voltage of 5 keV.

Energy-Dispersive X-ray Spectroscopy (EDX) was used to identify the elemental composition of synthesized nanostructures and initial Ti-based samples. Also, the elemental composition and the presence of impurities of Ti-based samples before synthesis were detected using EDX detector inside the SEM. In addition, EDX was used to identify the elements present in a specific part of the sample, *e.g.*, to detect metal catalyst particles in CNTs. These analyses were performed using an EDX detector incorporated inside the TEM. Samples for EDX analysis were prepared as for SEM and TEM respectively. The EDX incorporated in the JEOL 840A SEM (at 20 keV), and JEOL 2010 TEM (at 200 keV) with Oxford INCA software were used for sample analyses.

Confocal optical profilometry was used to investigate the changes in the surface roughness of the substrate before and after various surface modifications such as polishing and chemical etching. Profilometry measurements were used using μscan Nanofocus, at OMCS, Oxford. UK.

2.3. Results and discussion

2.3.1. Using Ti-based thin films to study the importance of surface parameters for reproducible MWCNTs growth

2.3.1.1. Influence of catalysts and their deposition methods

SEM micrographs shown in Figure 2.9 revealed that independently of the deposition method, Fe + Al nitrate catalyst forms CNTs of smaller diameter, while Fe nitrate alone forms CNTs of larger diameter and sometimes carbon nanofibers (CNFs). A possible explanation for such behaviour is that Fe particles are dispersed between the particles of Al, which prevents the agglomeration of Fe nanoparticles into bigger clusters. When Fe nanoparticles are not separated by Al particles, they agglomerate easily at higher temperatures, and while reacting with a carbon source, nanofibers or nanotubes of a large diameter are formed[1]. As it was already mentioned, the aim of this thesis is to grow MWCNTs with a smaller diameter in order that they will be comparable with the diameter of collagen fibers. Therefore, for later experiments Fe (III) nitrate + Al nitrate catalyst was used.

To achieve reproducible and homogeneous CNTs growth, the deposition of the catalyst is critical. An ideal deposition method would be easy to use, inexpensive and allow a uniform coverage of the substrate with a catalyst. Several ways of catalyst deposition were investigated in order to satisfy these requirements including (a) drop coating, (b) dip coating, and (c) spin coating.

[1] Based on private communication with V. Khavrus, IFW, Dresden

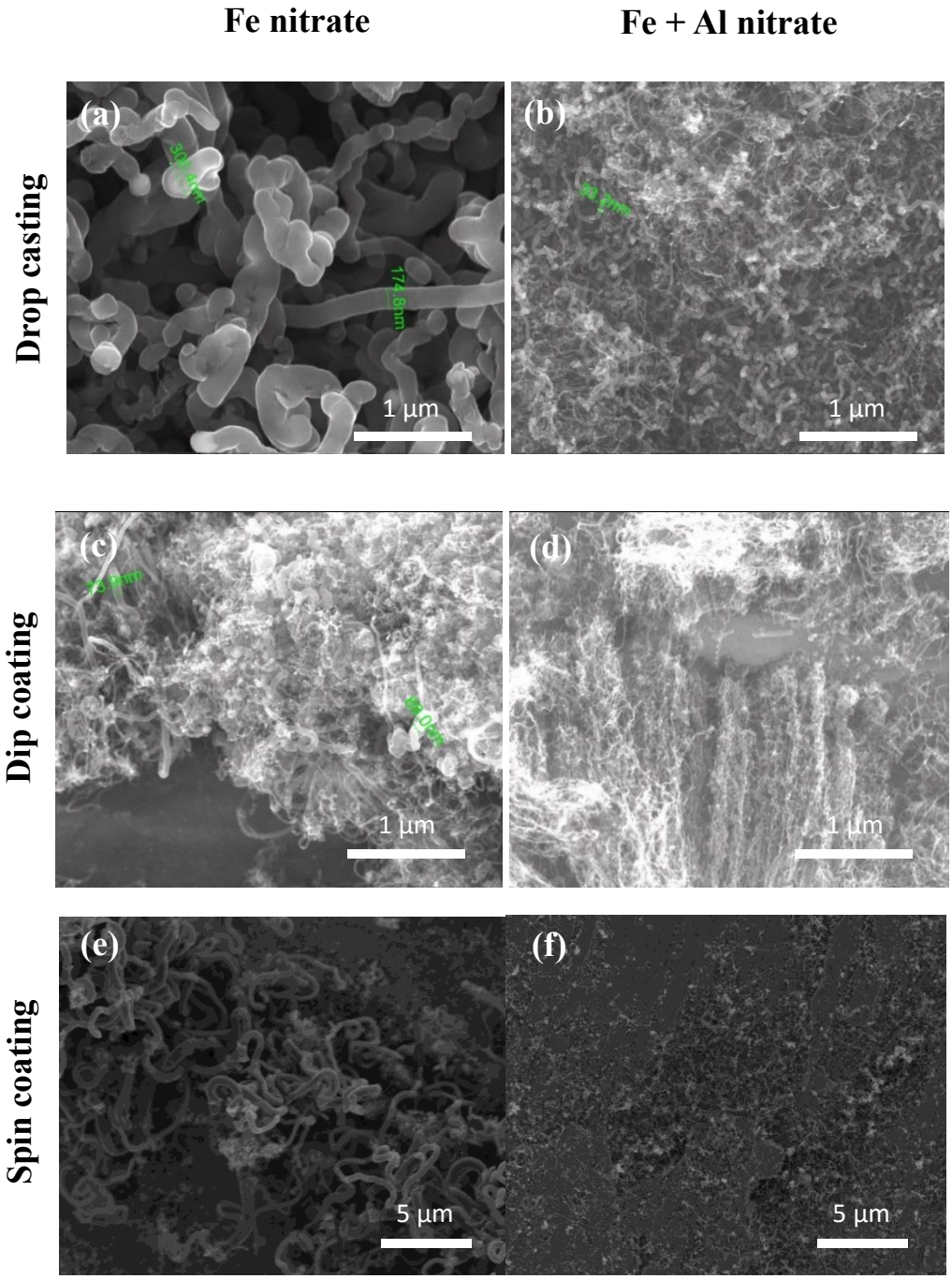

Figure 2.9. *SEM images showing MWCNTs grown with Fe (III) nitrate catalyst (left row (a), (c), (e)) and Fe + Al nitrate catalyst (right row (b), (d), (f)) using different deposition methods: (a), (b) drop casting, (c), (d) dip coating, and (e), (f) spin coating. For all deposition methods, it was found that Fe + Al nitrate catalyst forms CNTs of low diameter, while Fe nitrate results in the formation of CNTs with high diameter or CNFs.*

In Figures 2.10a, b the inhomogeneous distribution of a catalyst on Ti-based films using drop casting method was observed. High concentrations of MWCNTs are observed in some areas and no MWCNTs aggregations in other areas. The main reason of this inhomogeneity is the very small size of a sample in comparison with a drop. Previously, for samples of bigger size, the drop casting technique was used for CNTs growth on TiN, aluminum foil, steel, and other metals[138,139].

In Figures 2.10c, d, CNTs growth with dip coating method is presented. The concentration of MWCNTs is much higher in the lower part of the substrate than in the upper part. This change in the deposition of nanotubes is linked with the fact that during dip coating, the substrate is immersed in the solution and hung up by the clip. The clip is relatively big in comparison with the Ti-based samples that leads to the inhomogeneous run-off and evaporation of the catalyst. Moreover, no catalyst is deposited on the part where the substrate is attached by the clip.

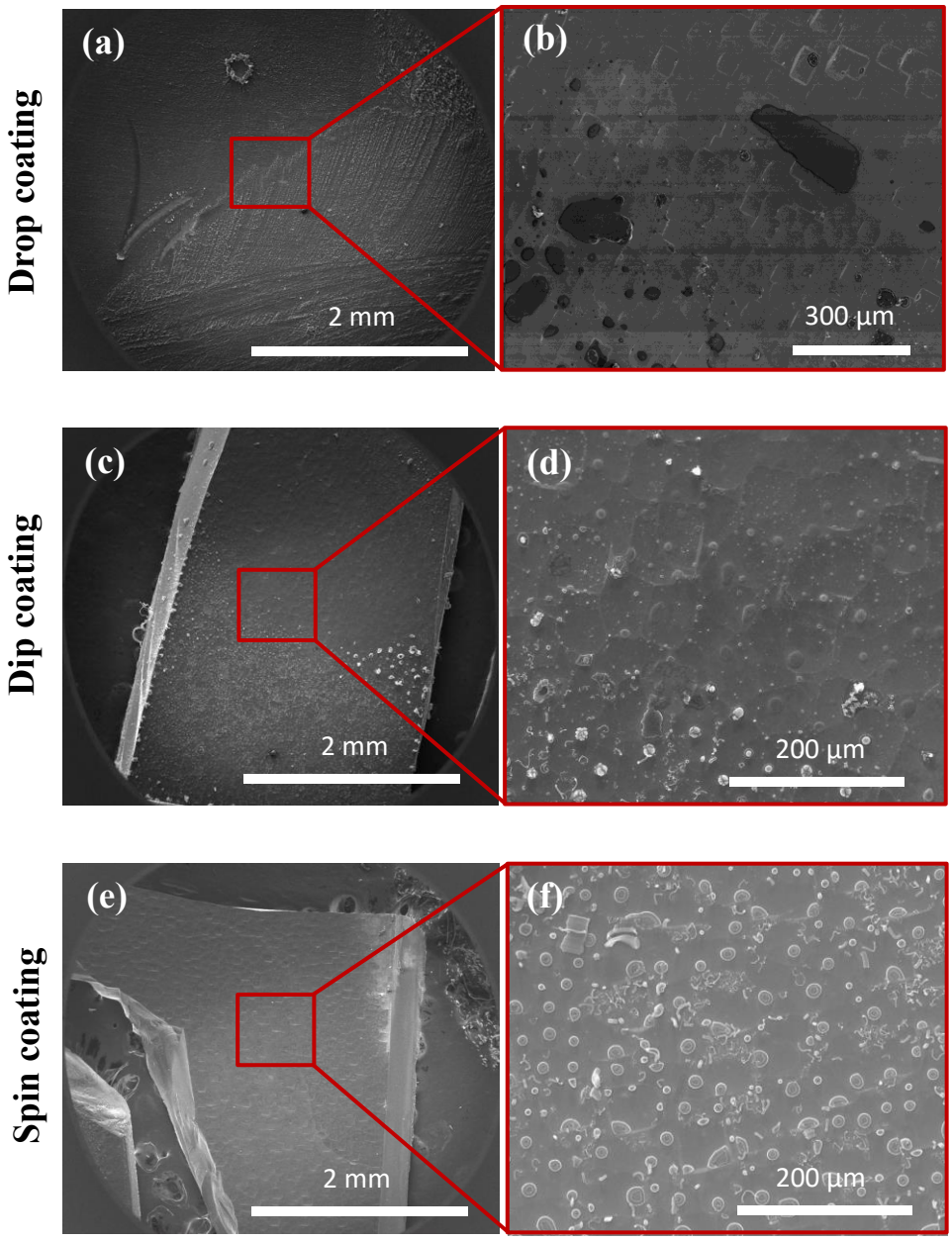

Figure 2.10. *SEM images of lower and higher magnifications showing MWCNTs grown on Ti-based films with Fe + Al nitrates catalyst deposited in different ways: (a), (b) drop casting; (c), (d) dip coating; (e), (f) spin coating. For drop casting and dip coating methods, a non-homogeneous distribution of MWCNTs across the sample was achieved. Meanwhile, spin coating resulted in a homogeneous MWCNTs growth.*

Figures 2.10d, e, shows the uniform distribution of Fe + Al nitrate catalyst on Ti-based films of various sizes and complex shapes using a spin coating. Spin coating was also proven to be an effective method for homogeneous catalyst deposition on silicon and

glass substrates[141]. It can be seen in Figure 2.10e that the MWCNTs patterns are very similar all over the sample. Therefore, spin coating was used for all further experiments presented in this Chapter.

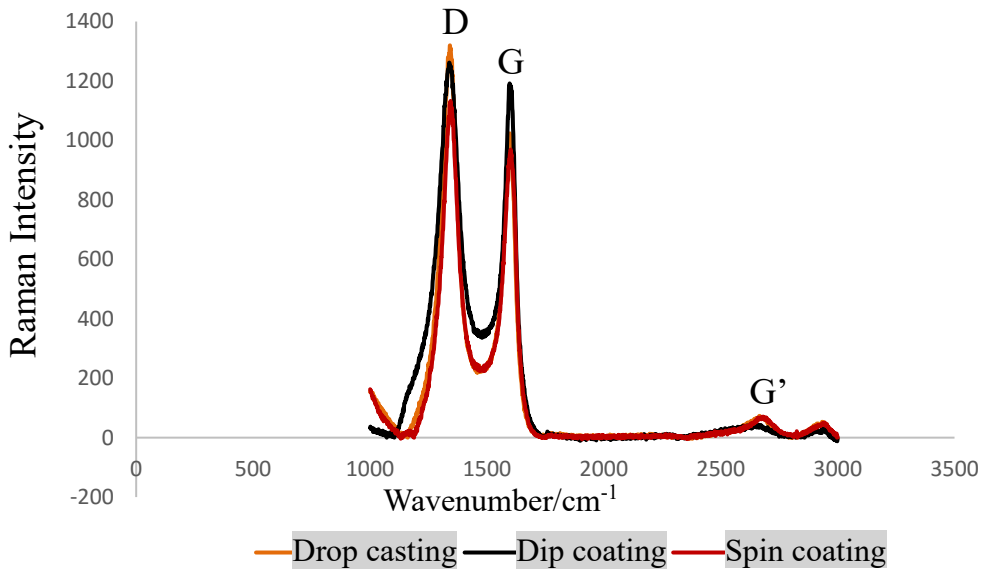

Figure 2.11. *Raman spectra's of MWCNTs grown on Ti-based films after catalyst deposition in different ways: drop casting, dip coating, and spin coating showing a very similar quality of MWCNTs grown with all the deposition techniques.*

Raman spectroscopy was used to confirm the presence of MWCNTs as well as to define their quality. In Figure 2.11, Raman graphs are presented with visible D and G-bands. The intensity ratio I_D/I_G =1.11, which shows that MWCNTs synthesized on Ti-based films are rather defective. However, for improving the implant biocompatibility, the diameter of MWCNTs, their growth mechanism and distribution over the sample are of primary importance, but not the quality of the MWCNTs.

Further in this Chapter, MWCNTs with a small diameter will be grown on Ti-based films with a Fe + Al nitrate catalyst deposited by the spin coating technique.

2.3.1.2. Influence of the catalyst concentration and reaction time on MWCNTs formation

Influence of catalyst concentration on MWCNTs growth

The growth of MWCNTs was achieved using very low concentrations of Fe + Al nitrate catalyst from 0.1 to 0.001 M. We were able to go two magnitudes lower than reported in other studies on Ti or other metals[67]. The use of such low catalyst concentrations should reduce possible toxic effects that metal nanoparticles could have on biological organisms.

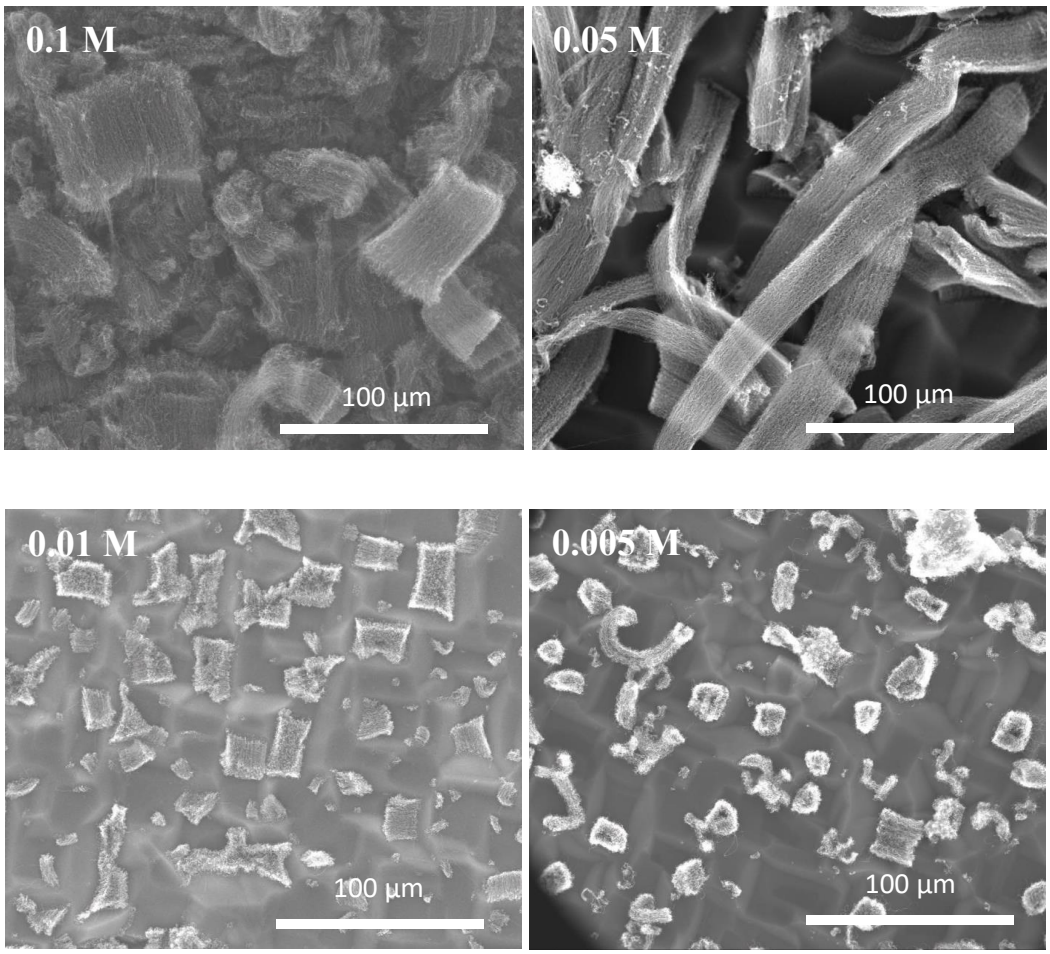

Figure 2.12. *SEM images showing the decrease in the number and density of MWCNTs patterns on α-Ti films while lowering the concentration of Fe + Al catalyst solutions from 0.1 to 0.005M with a constant time of CVD synthesis of 10 min.*

SEM micrographs of MWCNTs growth on α-Ti films are presented in Figure 2.12, showing that lower catalyst concentrations decrease the MWCNTs coverage. However, for β-Ti films, no visible relationship between the catalyst concentration and MWCNTs coverage was observed. This might be related to the topography of β-Ti films, but further experiments should be performed.

Influence of reaction time on MWCNTs growth

Together with different catalyst concentrations, different reaction times from 1 - 20 min were investigated. Reaction time is often an important factor to obtain MWCNTs growth.

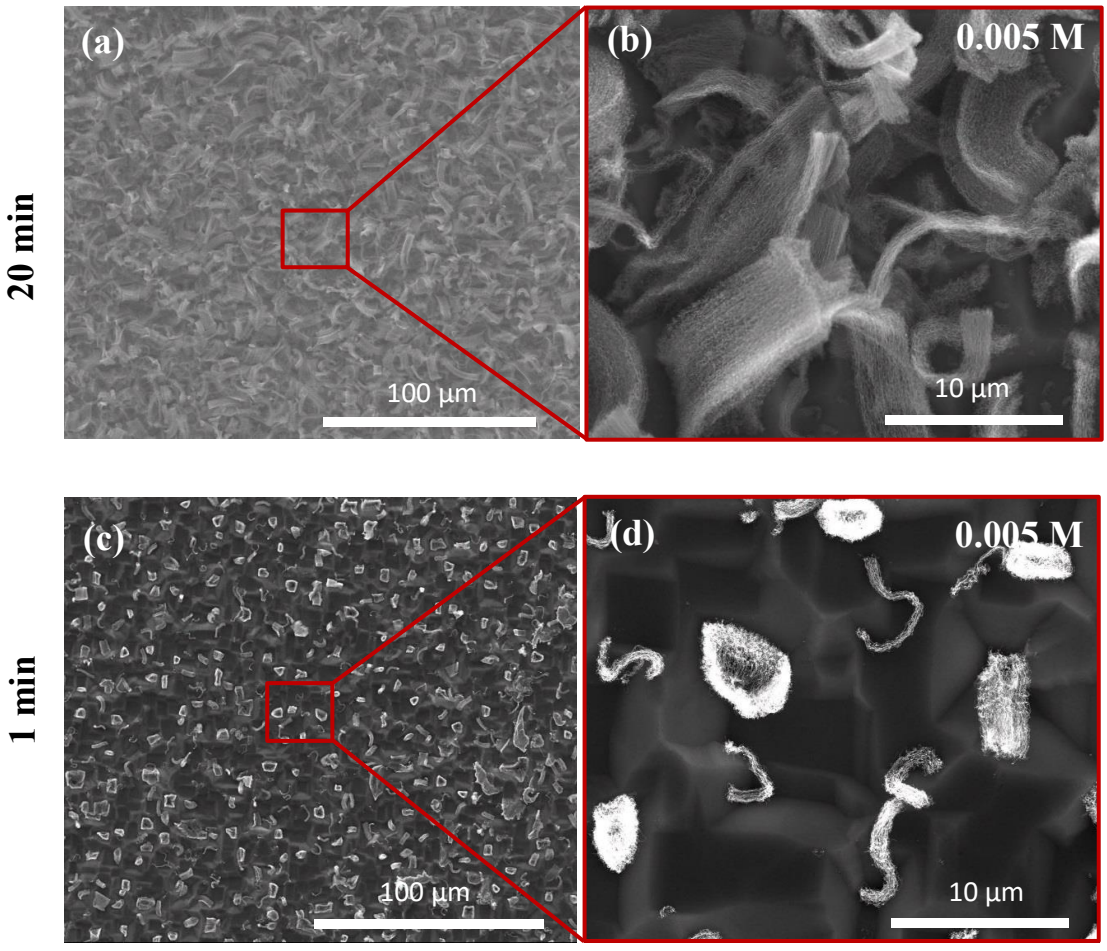

Figure 2.13. *SEM micrographs of higher and lower magnifications indicating the decrease in length and density of MWCNTs pattern growth while reducing the synthesis time from (a), (b) 20 min to (c), (d) 1 min on pure α-Ti films with 0.005 M Fe + Al nitrate catalyst.*

On pure α-Ti substrates, CNTs patterns of different length are formed by varying the time of the CNTs growth and keeping all other parameters fixed. When decreasing the reaction time from 20 min to 1 min, significantly shorter CNTs patterns are grown. In Figure 2.13a, b, long MWCNTs patterns of 15 – 20 µm, synthesized during a 20 min long experiment, are shown, while much shorter MWCNTs of 3 – 6 µm after 1 min synthesis time are presented in Figure 2.13c, d.

For β-Ti films, no significant influence of the reaction time was observed. For the experiments with low concentrations of catalyst very similar round and stick CNTs patterns were formed. This might be explained by the fact that for β-Ti films during both short and long experiments all the catalyst is used for CNTs formation, since only a small amount of catalyst aggregates on the substrate. Meanwhile, α-Ti films have deep trenches in which more catalyst aggregates and a longer experiment results in longer MWCNTs patterns

2.3.1.3. Mechanism of the CNTs growth

In order to successfully use CNTs/Ti composites as orthopedic material, it is important to understand the mechanism of CNTs formation. As mentioned earlier, CNTs are formed either by root- or tip- growth mechanism[75]. TEM analysis of CNTs/Ti cross-section specimens should be performed in order to investigate by which mechanism the nanotubes synthesized in this Chapter are formed. Therefore, appropriate TEM specimens had to be prepared. As explained in Section 2.1, conventional techniques for TEM specimens' preparation cannot be used due to the danger of destroying CNTs. Therefore, a FIB lift-out technique was utilized to prepare cross-section TEM specimens (Figure 2.14). Once the cross-section specimen was ready, TEM analysis was conducted, and a representative TEM micrograph is presented in Figure 2.14.

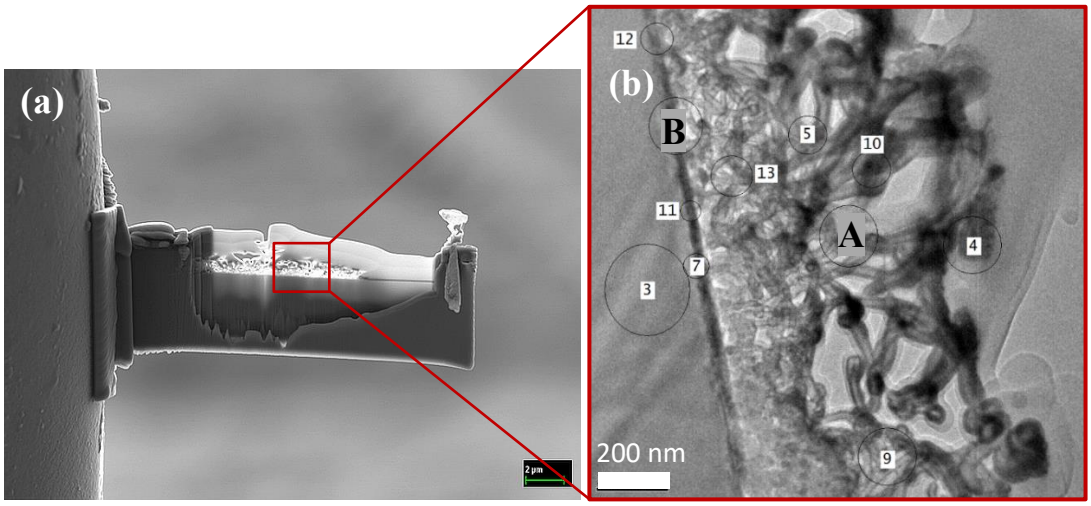

Figure 2.14. *(a) FIB cross-section of the Ti-based film with MWCNTs prepared using the FIB lift-out technique; (b) TEM image of FIB cross-section specimen showing different areas of a sample, indicated in numbers, from which the EDX spectra were taken in order to identify the location of Fe particles. Labels 'A' and 'B' corresponds to the areas from which the EDX spectra were taken that are presented in Figure 2.15.*

EDX analysis within TEM was performed in various areas of the sample, which are indicated by numbers in Figure 2.14, in order to identify the location of Fe particles. In Figure 2.14b, label 'A' indicates the part of the sample in the middle of CNTs, and label 'B' corresponds to the interface between the titanium substrates and CNTs. Those labels correspond to the areas from which the EDX spectra were taken that are presented in Figure 2.15. According to the EDX spectra, no Fe was detected in the middle of the MWCNTs or on their tips (Figure 2.15a). Fe nanoparticles were detected only at the interface between the substrate and the CNTs (Figure 2.15b) that corresponds to the root-growth mechanism of CNTs formation.

In this Section it was shown that CNTs grown by the CVD technique under the conditions described in Section 2.2.1 are formed through a root-growth mechanism, which restricts the release of catalyst particles. These findings give a perspective for its further application in biomedical and orthopaedic fields. No studies of the mechanism of CNTs formation on Ti-based substrates have previously been reported. However, root-growth was observed for nanotubes formation on Ni/Ti/Si substrates, where Ti acts as an interlayer between the Si substrate and Ni catalyst[142]. Moreover, CNTs grown on Ni substrates with TiO_2 film doped with Fe and Ni catalyst also revealed root-growth mechanism[143].

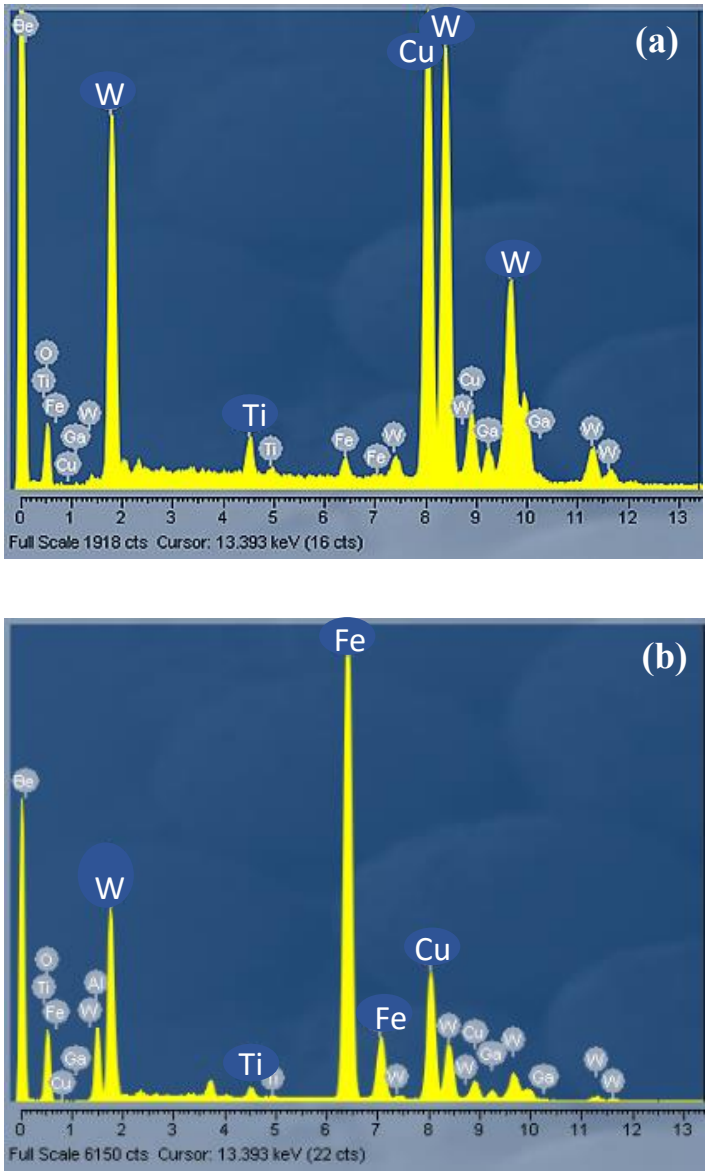

Figure 2.15. *Representative EDX spectrum taken in the TEM FIB cross-section sample of Ti-based film showing elements, which are present in the following areas of the sample: (a) in the middle of CNTs, which is marked A in Figure 2.14; (b) at the interface between substrate and CNTs, which is marked B in Figure 2.14. Fe particles are clearly present at the substrate-CNTs interface. W is detected due to the tungsten coating during TEM sample preparation. Cu is identified due to the use of copper grit for the TEM analyses.*

2.3.1.3. Influence of the substrate properties on MWCNTs formation

A systematic study of MWCNTs growth using CVD technique on Ti-based films with different topography and elemental composition was performed for the first time.

Influence of surface topography on MWCNTs growth

Ti-based films, which were used in this Chapter and listed in Table 2.1, can be divided into two groups, each revealing a characteristic surface topography. The first group, which includes commercially pure Ti films (α-Ti), reveals dips and small trenches in the substrate as can be seen in Figure 2.16a. The second group could be characterised by significantly larger, but shallower valleys, as shown in Figure 2.16c-e, and films consist of TiNb, TiZrHf, and TiNbHf alloys (β-Ti). While comparing the surface topography of the films, the surface roughness is a primary factor that needs to be investigated. The surface of α-Ti films is twice as rough as the one of the Ti-based films, with a value of 6.4 μm compared to 3.6 μm. Figures 2.16b and 2.16d show 3D surface profiles of films, from which it is also visible that the Ti-based films have lower surface roughness with shallower trenches than α-Ti films.

Depending on the topography of the films, two different carbon nanotubes patterns were observed: rectangular patterns or round and stick patterns as shown in Figure 2.17. This indicates that the topography of the substrate influences the type of MWCNTs patterns.

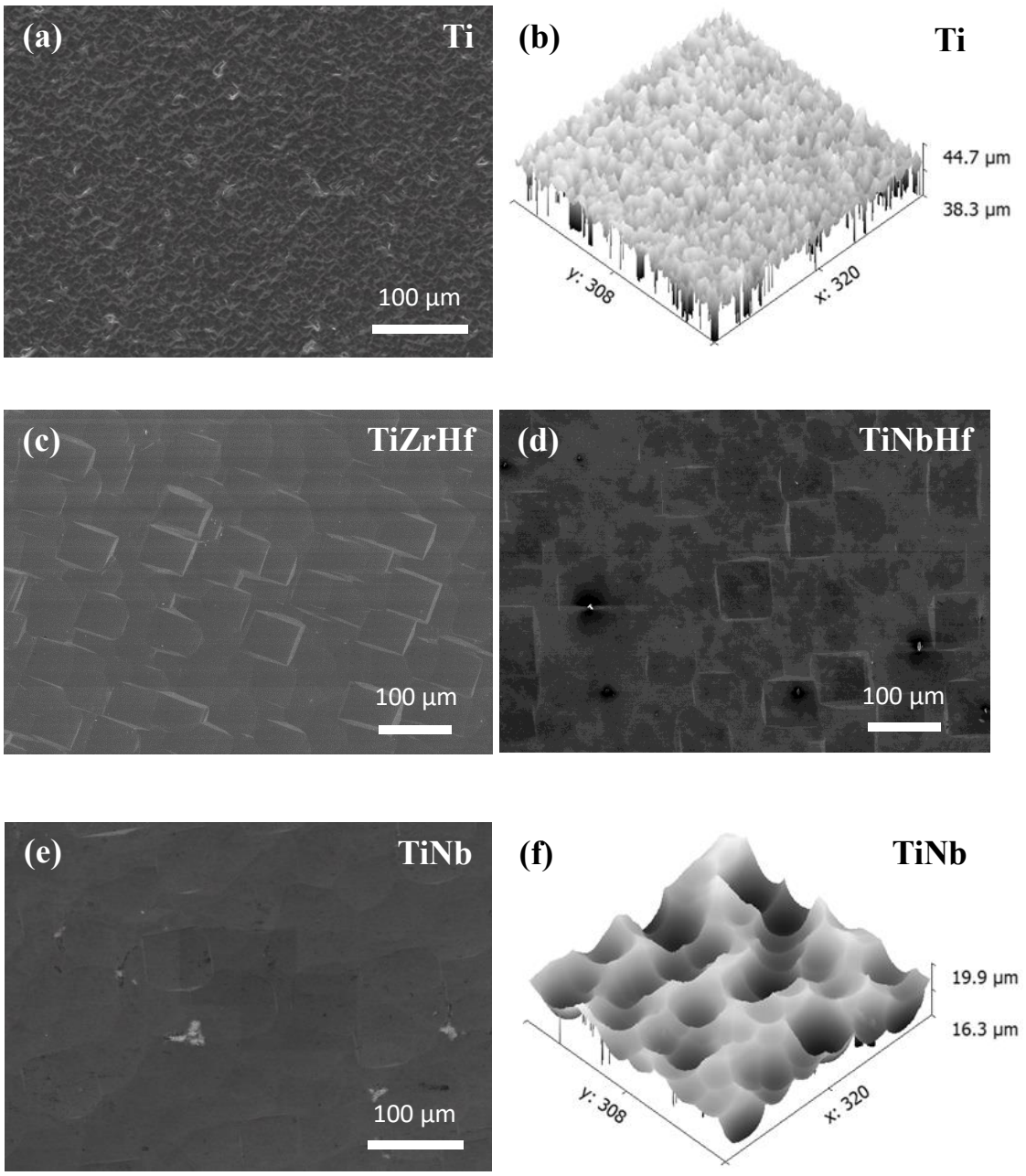

Figure 2.16. *Representative SEM micrographs showing the structure of Ti-based films: (a), Ti film (c) TiZrHf film; (d) TiNbHf film; (e) TiNb film; 3D surface roughness images of (b) Ti film, (f) TiNb film. The surface roughness of Ti film is higher than the one for the Ti-based films with smaller, deeper trenches on the surface.*

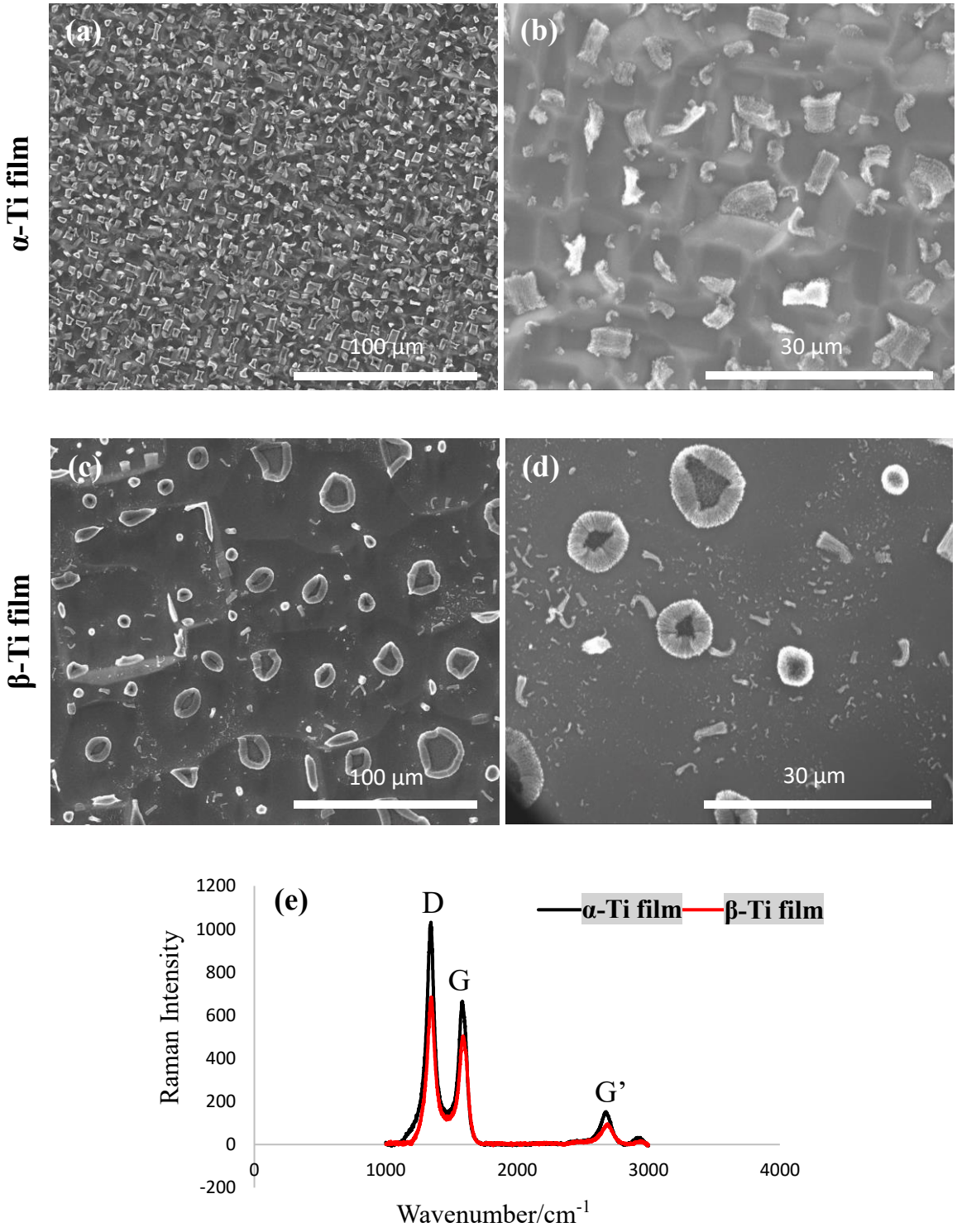

Figure 2.17. *Representative SEM micrographs of higher and lower magnification showing (a), (b) rectangular MWCNTs patterns grown on α-Ti film and (c), (d) round MWCNTs patterns grown on β-Ti films. (e) Representative Raman spectrums confirming the growth of MWCNTs on α-Ti and β-Ti films.*

Mechanism of MWCNTs pattern formation

The formation of different MWCNTs patterns could be explained by the mechanism of catalyst behaviour on the samples. Since the surface of the α-Ti film is not smooth (Figure 2.18) and has rather deep rectangular trenches, the catalyst will aggregate in the valleys after deposition. The initial rectangular valleys of α-Ti films before CVD could be seen on the SEM micrographs presented in Figure 2.18a, where they are marked with red rectangles. In Figure 2.18b, it is visible that the CNTs growth is starting in those valleys, and that the CNTs patterns take the shape of the valleys.

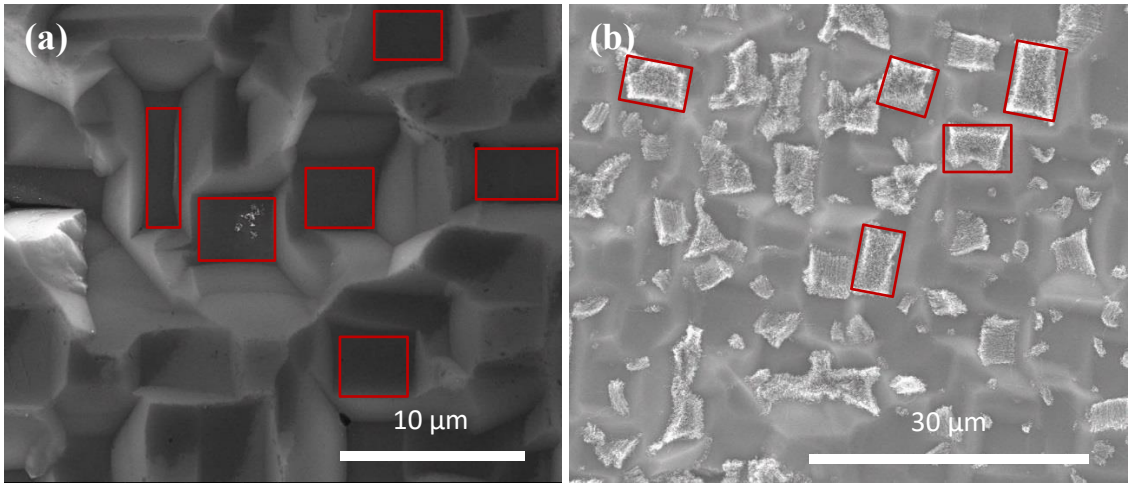

Figure 2.18. *SEM micrographs showing (a) the structure of α-Ti film with rectangular trenches (indicated in red) before the CVD experiment; (b) α-Ti film indicating the formation of MWCNTs patterns, which are localized in the rectangular trenches of the film after the CVD experiment.*

On β-Ti films, mostly stick-shaped and round MWCNTs patterns were formed (Figure 2.19a-d). The substrate topography is much smoother with shallower valleys (Figure 2.19a), compared to α-Ti films. Therefore, there are no trenches where a catalyst could accumulate and instead, the catalyst aggregated into drops all over the surface of the substrate due to the topography of the substrate (Figure 2.19a). The catalyst aggregation in drops can be linked not only to the topography of the films but also to their

hydrophobicity. For more hydrophilic surfaces the continuous film of the catalyst is formed and CNTs grow all over the substrate[144]. From these drops of catalyst, aligned MWCNTs are growing (Figure 2.19b).

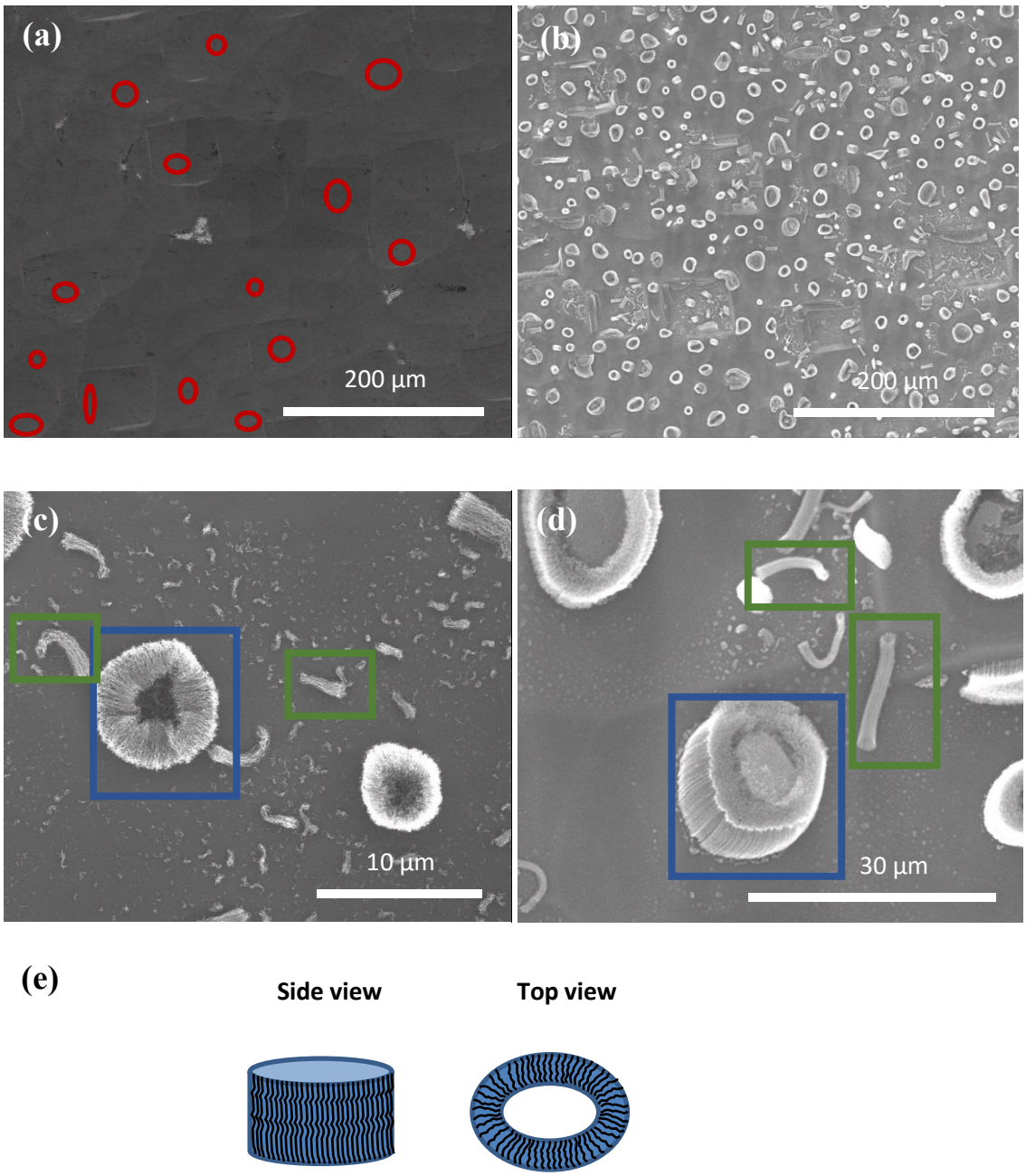

Figure 2.19. *SEM micrographs representing MWCNTs growth on β-Ti films grown with 0.01M Fe + Al nitrate catalyst for (a) 20 min, (b) 10 min. (c), (d) showing stick patterns in green frames and round patterns in blue. (e) Schematic representation of a mechanism of round, flowerlike MWCNTs pattern formation.*

When the drop is relatively small, stick patterns of aligned MWCNTs are formed as shown in Figures 2.19c, d, in green frames. If the drop is large, aligned MWCNTs start forming a stick (but a shorter one), the ends of which begin to curl together, and round (if seen from above), flower-like MWCNTs patterns are formed shown in Figure 2.19c, d, indicated in blue frames.

The efforts to incorporate the established techniques to understand the aggregation of the catalyst faced the following difficulties. The main problem was the high roughness of the initial samples, which disabled the use of such techniques as EBSD or EDX mapping, since the sample has to be much smoother for those analyses. Another idea was to prepare TEM cross-section specimens in order to identify the catalyst particles. However, since a TEM specimen is rather small (*e.g.* 15 x 5 μm), the analysis would be much localized and would not give any information about the overall sample. Therefore, further investigations to establish the exact mechanism of catalyst behaviour on Ti-based films will have to be part of future studies.

Influence of elemental composition on MWCNTs growth

By conducting CVD experiments on films with different compositions, no direct influence of the elemental composition of the type and shape of MWCNTs patterns was observed. It revealed the formation of MWCNTs patterns of the same type as for β-Ti films with a different elemental composition, which had the same surface topography. By varying the elemental ratios in the films, no influence on MWCNTs patterns was observed.

The experiments presented above showed that the surface topography and not the elemental composition of the films is influencing the formation of MWCNTs. This

conclusion can be clearly drawn by comparing β-Ti films with each other, which have the same surface topography as stated earlier. However, the topography of α-Ti films varies from that of the β-Ti films, and hence it is not possible to compare those substrates directly. In order to be able to do any comparison, additional films with the same surface topography but different elemental composition were produced. In Figure 2.20a, the initial structure of α- and β- titanium films is presented. Figures 2.20b, c and d rectangular patterns of aligned MWCNTs, which are very similar to all the films. Hence, the elemental composition is not influencing the MWCNTs formation on Ti-based thin films. Previously, CNTs were grown only on one type of Ti substrate[67] without comparing different Ti-based substrates.

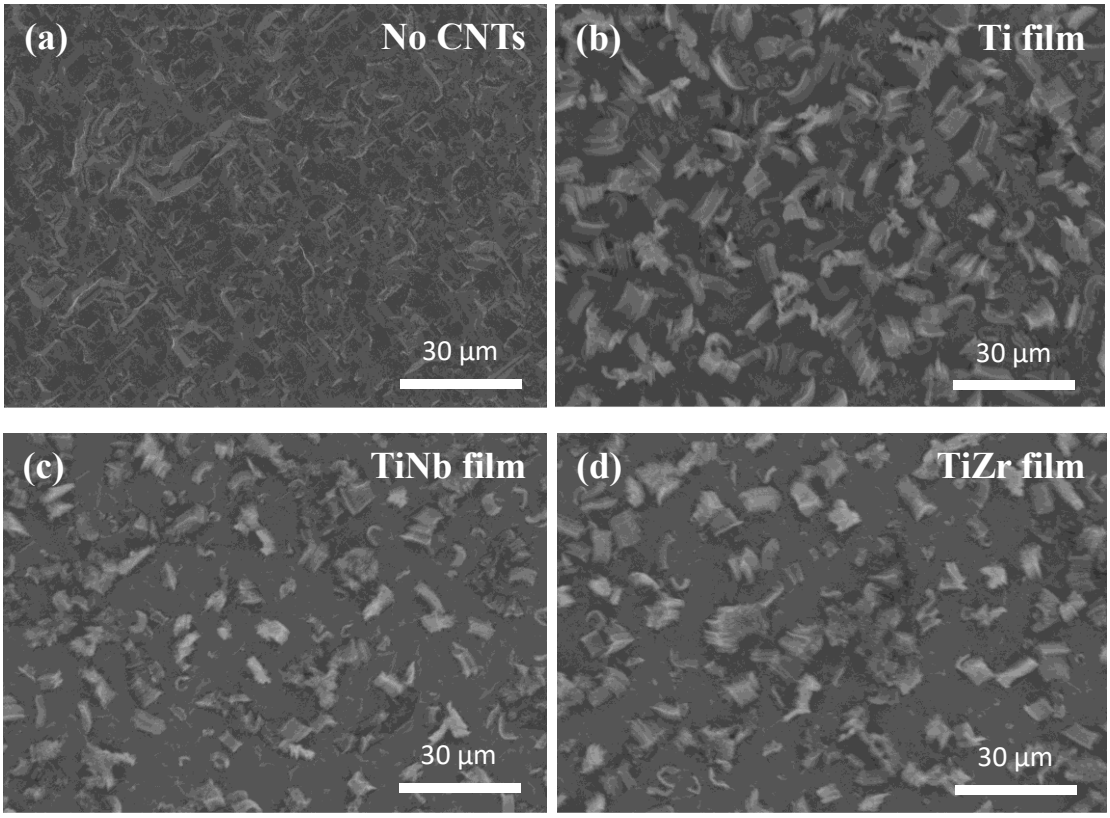

Figure 2.20. *Representative SEM micrographs showing (a) topography of α- and β- titanium film before CNTs growth; MWCNTs grown on (b) α-Ti film; (c) TiNb film; (d) TiZr film. It shows very similar MWCNTs pattern formation on films with the same surface topography but different elemental composition.*

These findings also confirmed the influence of the surface topography on the formation of MWCNTs patterns. The topography of the films shown in Figure 2.20a is similar to the one of the α-Ti film presented in Figure 2.16a. Hence, similar carbon nanotubes' formation on both films was expected, which was indeed the case.

To summarize, Section 2.3.1 showed that spin coating deposition of Fe + Al nitrate catalyst is efficient to achieve a homogenous CNTs distribution across the substrate. Even a low catalyst concentration was successful for CNTs growth. Moreover, the surface roughness of the substrate strongly influenced the CNTs formation. These results were applied to further CNTs growth on bulk Ti-based substrates and porous Ti-based scaffolds in Sections 2.3.2 and 2.3.3 respectively.

2.3.2. MWCNTs growth on bulk Ti-based samples

In Section 2.3.1 the possibility of CNTs growth on α- and β-Ti films was presented. In order to come one step closer to the creation of real CNTs/β-Ti composites, it is necessary to perform CVD experiments on more realistic substrates than Ti-based films. Bulk titanium alloys are suitable for this purpose since titanium implants are usually produced from a bulk piece of titanium.

2.3.2.1. CVD growth of MWCNTs on non-modified bulk Ti-based substrates

The first set of experiments was performed on non-modified bulk α-Ti and β-Ti substrates with low concentrations from 0.05 till 0.001 M of Fe + Al nitrate catalyst. MWCNTs synthesized on both α-Ti and β-Ti bulk substrates are shown in Figure 2.21. In Figure 2.21a, b areas of α-Ti with high and low concentrations of nanotubes respectively were observed. The same was observed for β-Ti substrates (Figures 2.21c, d). Due to the inhomogeneous distribution of MWCNTs over the substrates, no conclusions from the CVD experiments with different catalyst concentrations can be drawn. Therefore, for further evaluation of MWCNTs growth on bulk titanium, methods have to be found which achieve homogeneous, reproducible, nanotube growth.

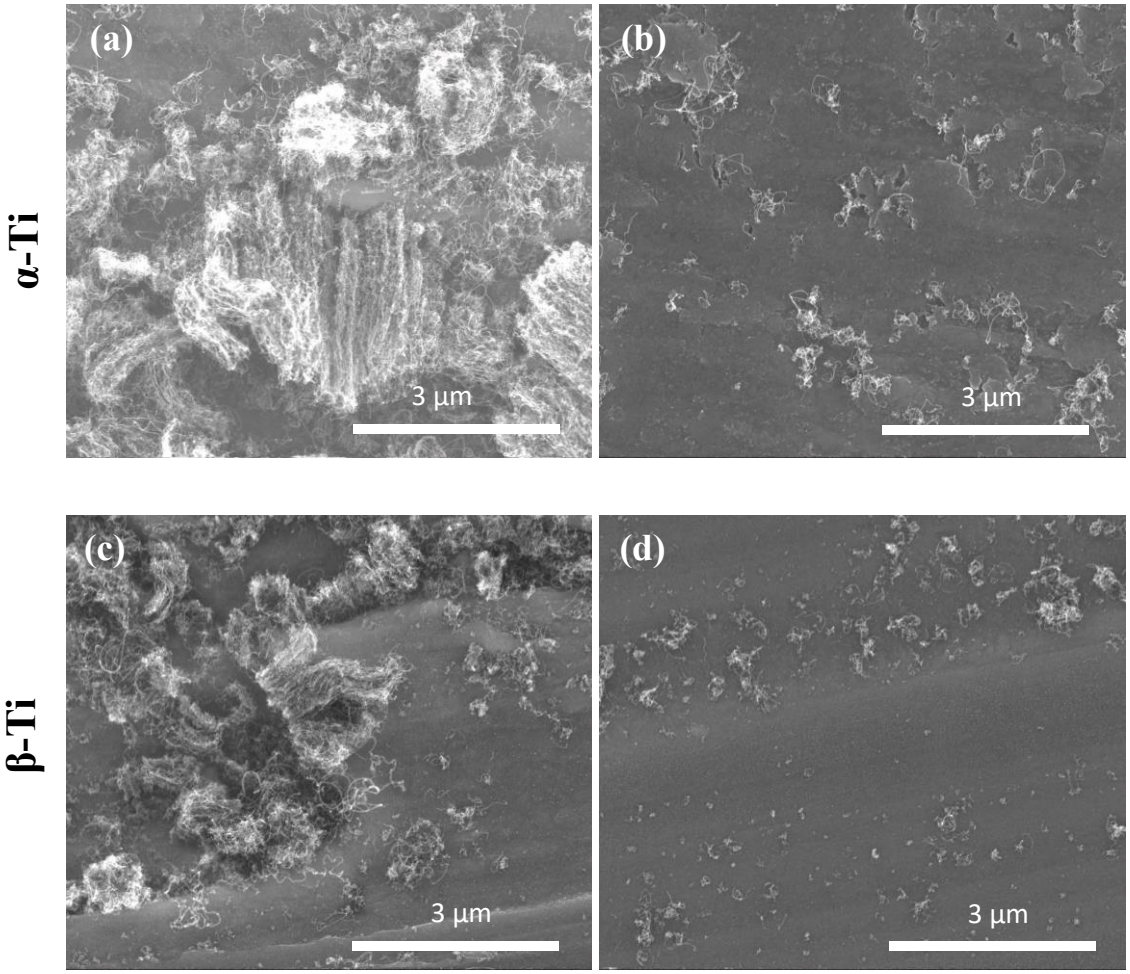

Figure 2.21. *SEM micrographs showing the inhomogeneous distribution of MWCNTs on non-modified α- and β-Ti substrates which were grown with Fe + Al nitrate catalyst. A high density of MWCNTs was observed in some areas shown in the figures (a) and (c), while very little nanotubes were deposited in another area presented in the figures (b) and (d).*

2.3.2.2. CVD growth of MWCNTs on modified bulk Ti substrates

In order to achieve homogenous CNTs distribution across the substrate, surface modifications of bulk titanium were performed. Those included HF solution treatment and mechanical polishing.

Influence of HF treatment on MWCNTs distribution

Both α-Ti and β-Ti substrates were treated with 40 % and 8 % HF solutions.

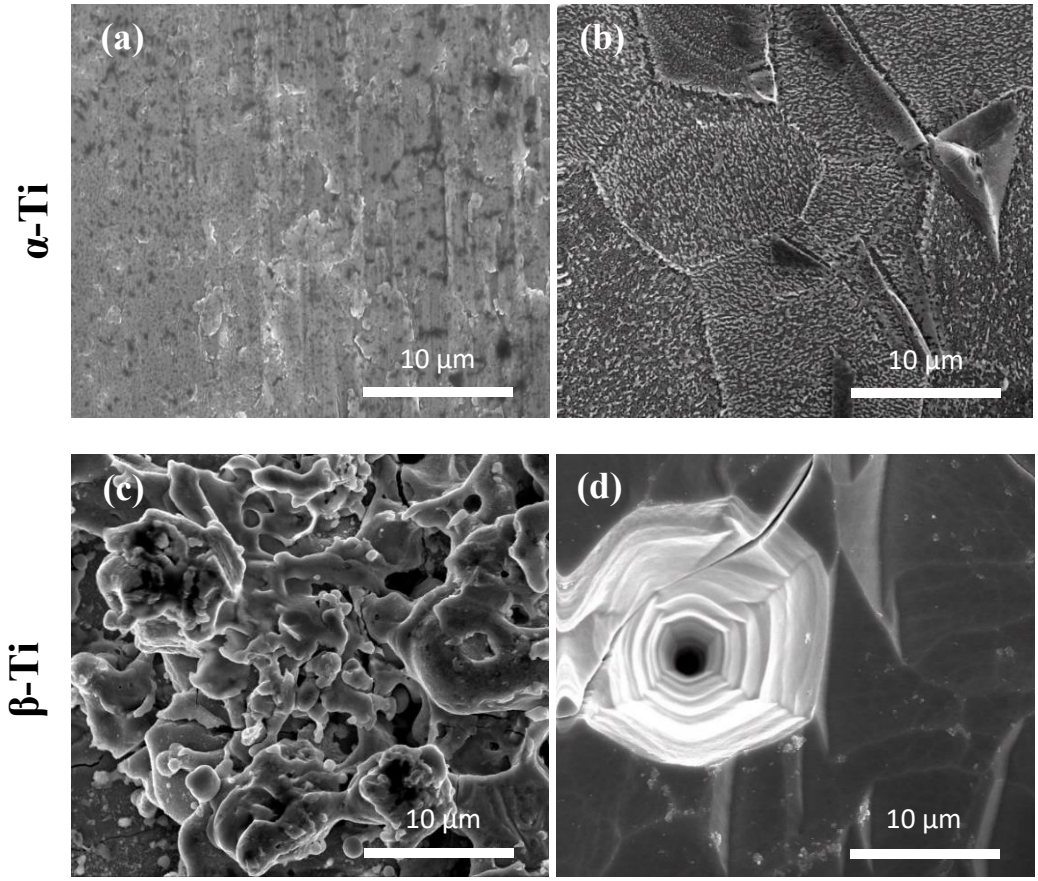

Figure 2.22. *Representative SEM micrographs showing the initial structure of non-modified (a) α-Ti and (c) β-Ti substrates; (b) α-Ti and (d) β-Ti substrates after surface cleaning treatment after 40 % HF for 1 min. The appearance of the grain boundaries was observed for both α- and β-Ti substrates, while for β-Ti substrates cracks and individual flaws also appeared.*

After the treatment, it was observed that α-Ti substrates etched quicker than β-Ti substrates. Such behaviour is associated with the more rapid reaction of HF solution with Ti rather than Nb, which is present in the β-Ti alloy. HF treatment leads to the appearance of the grain boundaries for both substrates (Figure 2.22b, d), however for β-Ti unexpected cracking of the substrate and formation of individual flaws (Figure 2.22d) was also observed. Additional experiments using different reaction times are presented in Appendix II.

In order to understand the reason for the formation of flaws on β-Ti, a close look at the reaction of HF with Ti-based alloys is necessary. HF acid treatment is a common chemical etching method of titanium and its alloys. As seen from Table 2.2, the composition of the bulk β-Ti substrate is TiNb. Therefore, it is necessary to look at the reaction of Ti and Nb elements with HF solution. HF quickly reacts with Ti and the titanium oxide layer, and forms titanium fluorides and hydrogen, as shown in Equation (1) [29]. Meanwhile, Nb is more resistant to the HF solution than Ti and similarly forms niobium fluoride and hydrogen, according to Equation (2).

$$Ti + 3HF = TiF_3 + 3/2\ H_2 \qquad (1)$$

$$2Nb + 10HF = 2NbF_5 + 5H_2 \qquad (2)$$

According to the literature[145], HF treatment on neither Ti nor Nb can lead to the formation of the severe flaws shown in Figure 2.22d. A possible explanation for these flaws can be the presence of impurities, since it was reported[145] that in Nb-containing alloys HF attacks preferentially at the places of impurities, which do not have such strong, passive films as the Nb oxide film, Nb_2O_5. Indeed, EDX spectra presented in Figure 2.23 reveal no additional elements for α-Ti, whereas for β-Ti Zn and Cu were detected. Zn and Cu

contaminations originated from the cutting of β-Ti with the electrical discharge machine (EDM).

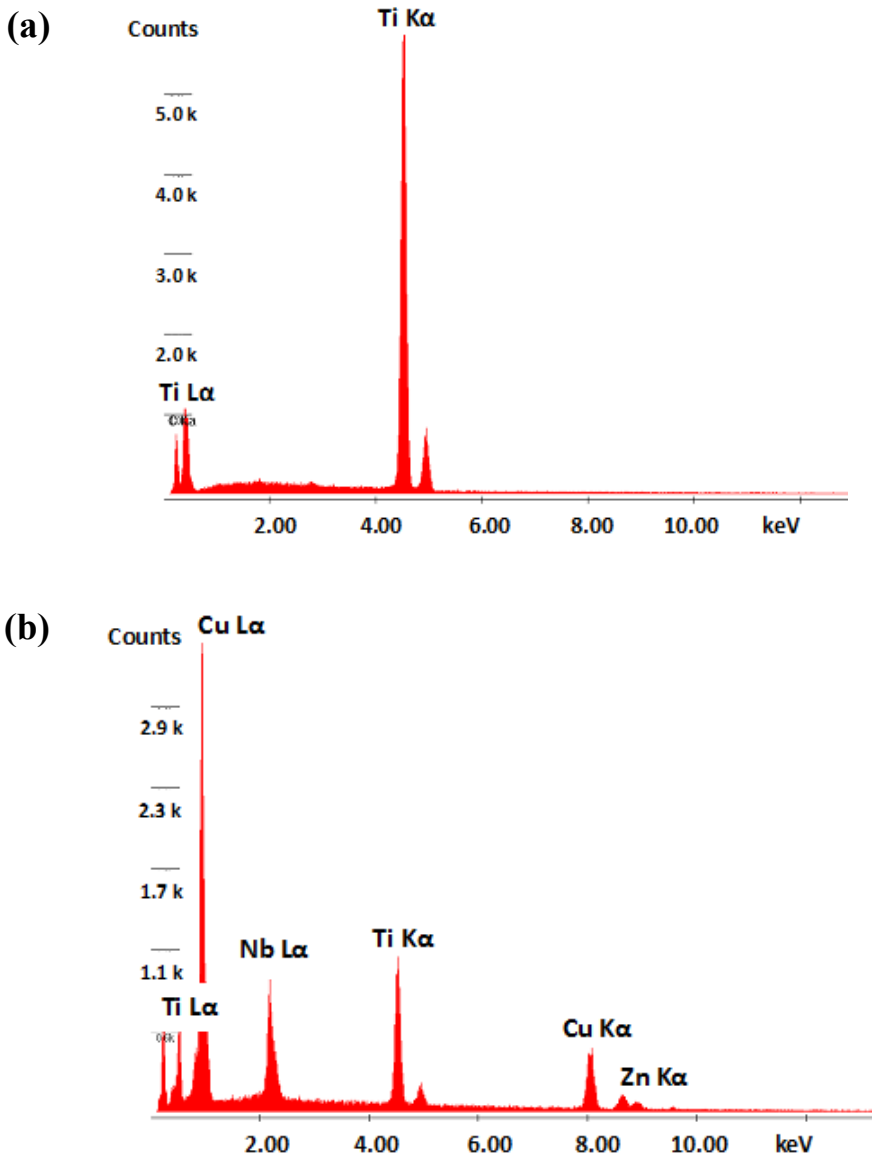

Figure 2.23. *EDX spectra of (a) α-Ti substrate indicating the presence of Ti, and (b) β-Ti substrate showing the presence of Ti and Nb, together with Cu and Zn contaminations from the cutting procedure.*

CVD experiments performed on HF-treated bulk titanium substrates did not result in a homogeneous distribution of CNTs. Further details can be found in Appendix II. Therefore, the next studies focused on other modifications of titanium surface.

Influence of mechanical polishing on MWCNTs distribution

Mechanical polishing was also used for modifying the surface of α-Ti and β-Ti substrates. During both manual and machine polishing of rectangular titanium substrates, it was extremely challenging to achieve a homogeneously polished surface as the substrates were not completely flat. Often the corners of the substrates were completely ripped off, as can be seen in Figure 2.24. In order to avoid this problem, Ti-based substrates of a different geometry had to be sourced, and α-Ti and β-Ti discs were used for further experiments.

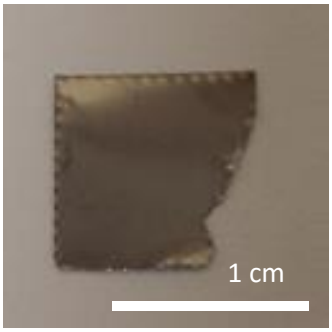

Figure 2.24. *Picture of an early α-Ti substrate with ripped-off edges after machine polishing.*

Machine polishing of α-Ti discs with 6 μm diamond paste gave more or less homogeneous surface, however, the polishing of β-Ti discs was much more difficult due to the presence of the alloying element. Therefore, simple manual polishing was investigated, and polishing with 1200 SiC grit was sufficient to obtain appropriate surfaces for carbon nanotube growth on both α-Ti and β-Ti discs.

Further CVD experiments were performed only on polished β-Ti discs, since the aim of the thesis is to produce β-Ti/CNT composite materials; α-Ti is not the focus of this thesis and was used just for reference. Low concentrations of Fe + Al nitrate catalyst similarly to the experiments on unmodified substrates were used for CNTs growth. A very low catalyst concentration of 0.001 M was not sufficient for the synthesis of MWCNTs. By

increasing the catalyst concentration up to 0.01 and 0.05 M, satisfactory MWCNTs growth was achieved. Depending on the temperature of the furnace at which the substrates were inserted into the reactor, different formation of MWCNTs was observed.

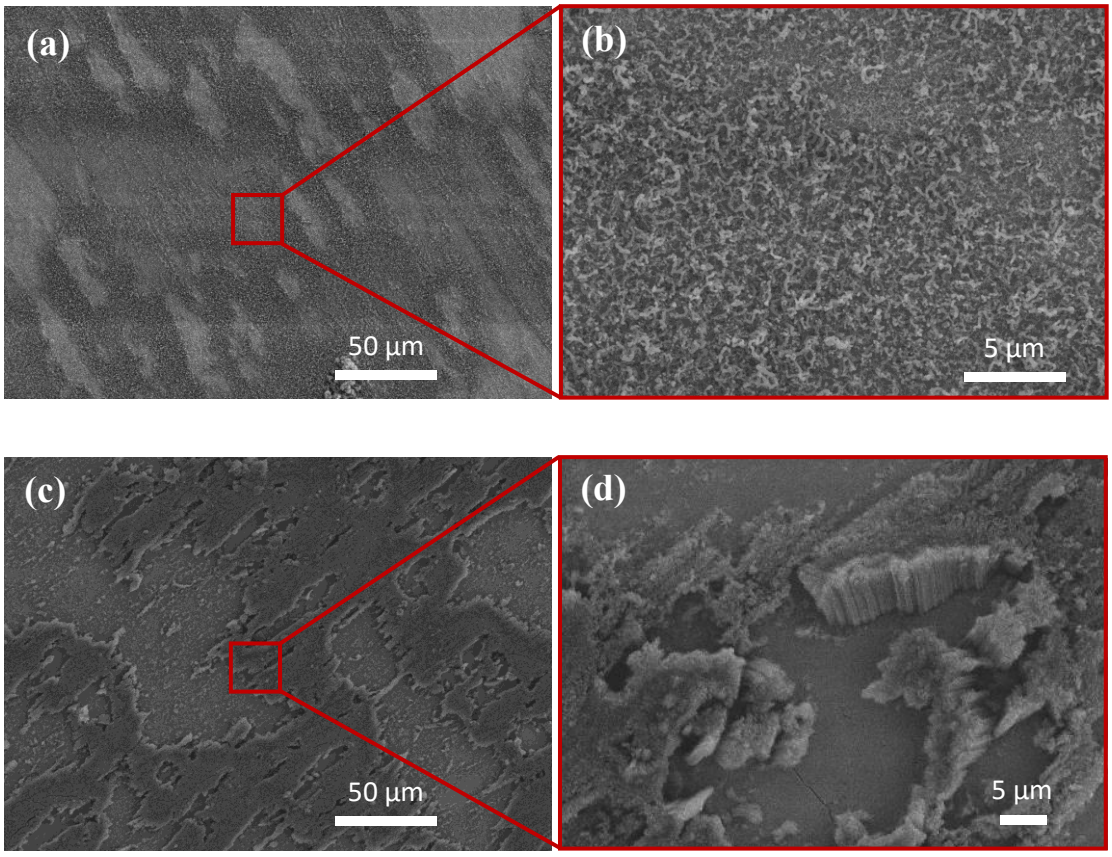

Figure 2.25. *Representative SEM micrographs of lower and higher magnifications of polished β-Ti discs with 0.05M Fe + Al nitrate catalyst after the CVD revealing (a), (b) entangled MWCNTs growth when substrates were inserted inside the CVD furnace at room temperature (22 °C); (c), (d) aligned MWCNTs growth when substrates were moved inside the furnace at ~ 400 °C.*

When substrates were inserted in the furnace at room temperature (22 °C), entangled MWCNTs were formed, while when substrates were moved inside the furnace at ~ 400°C, aligned MWCNTs carpets were observed. The reason of different MWCNT growth is most likely to be linked the pyrolysis of acetylene precursor since the temperature has an influence upon the gas phase composition[146]. When the substrate is inserted inside the CVD furnace at elevated temperature (400 °C), the pyrolysis of acetylene starts much

quicker than when it is inserted at a room temperature. Thus, a greater amount of acetylene undergoes pyrolysis, and MWCNTs carpets are formed. It is also possible that the entangled MWCNTs that shown in Figure 2.25a, b, are actually very short MWCNTs carpets.

To summarize, this section reported the possibility of MWCNTs growth on bulk β-Ti substrates. A simple mechanical polishing combined with low catalyst concentrations (0.01 and 0.05 M of Fe + Al nitrate catalyst) were necessary for MWCNTs deposition all across the β-Ti substrates.

2.3.3 MWCNTs growth on Ti-based porous scaffolds

In this Section the possibility of CVD synthesis on porous Ti-based scaffolds was investigated. Scaffolds are porous material structures which assist in the healing of large bone defects. These structures are capable of supporting three-dimensional tissue formation. Experiments performed in Sections 2.3.1 and 2.3.2 provided the information regarding the influence of the substrate composition, the catalyst and its concentration, and how to improve MWCNTs growth. In order to extend the application of CNTs from the improvement of titanium implants to that of scaffolds, which are also widely used in orthopaedic surgery, preliminary experiments were performed on porous structures, to identify the applicability of the earlier developed methods of CNTs growth.

Two β-Ti scaffolds, TiNb and TiNbZr (Table 2.3), were chosen for the investigations in this Section. SEM micrographs presented in Figure 2.26 reveal the structures of the titanium scaffolds. Due to the 3D structure of the scaffolds, the deposition of the catalyst might be more difficult than on the flat Ti-based films and bulk substrates, and higher concentrations of the catalyst may be required. Nevertheless, initial experiments with the

same low concentration of Fe + Al nitrate catalyst of 0.01 and 0.05 M as for bulk titanium were performed. SEM micrographs presented in Figure 2.27 showed that such concentrations are also sufficient for inducing carbon nanotube growth on Ti-based porous scaffolds.

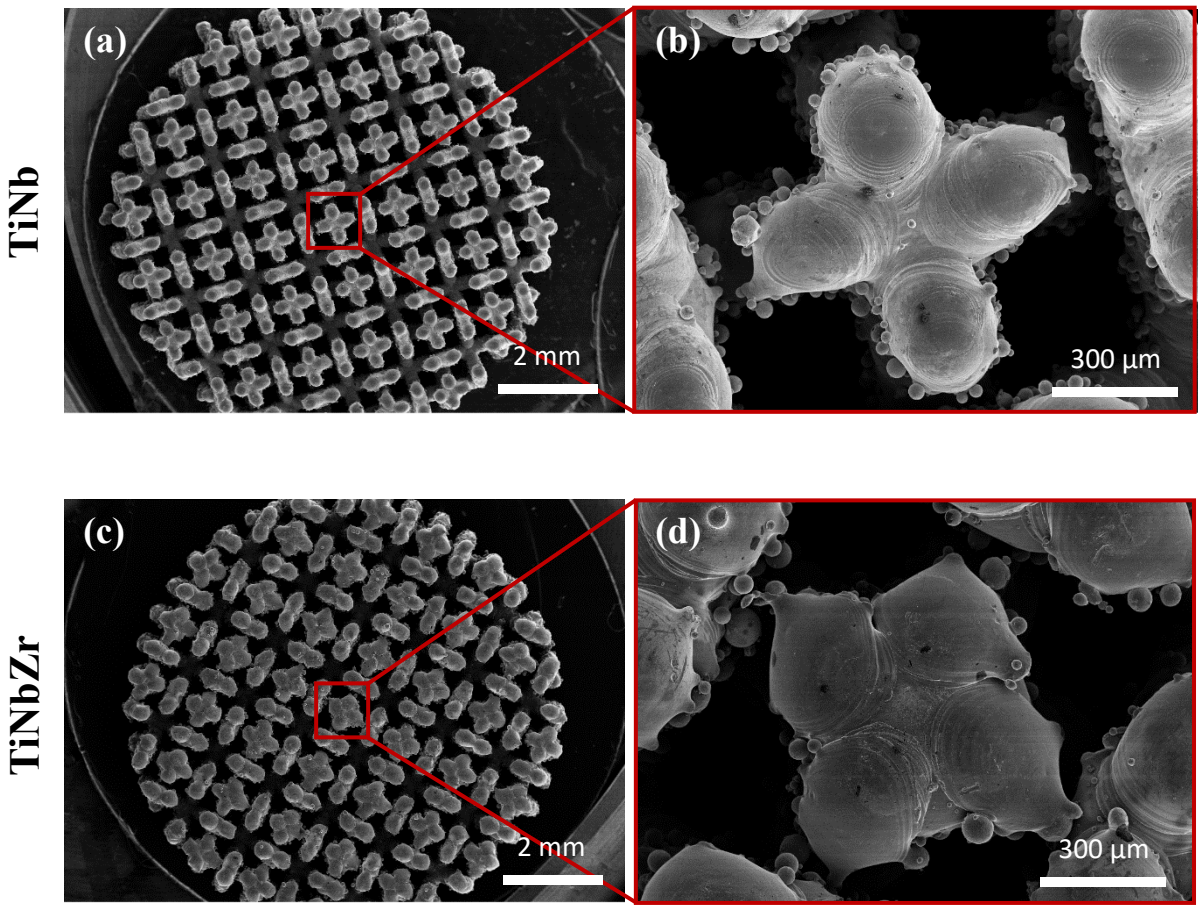

Figure 2.26. *SEM micrographs at lower (a) and higher (b) magnification of a TiNb scaffold; lower (c) and higher (d) magnification of the TiNbZr scaffold, showing the initial structure of the scaffolds prepared by selective laser melting technique without any cracks on their surface.*

A relation between the concentration of the catalyst and MWCNTs coverage was observed for both type of samples: when using a concentration of 0.01 M catalyst, the scaffold became very slightly covered with nanotubes, while a much larger part of the scaffold was covered when using 0.05 M catalyst, which is shown in Figure 2.27.

Additionally, after the CVD experiments noticeable cracks on both Ti-based scaffolds were observed (Figure 2.27a, c).

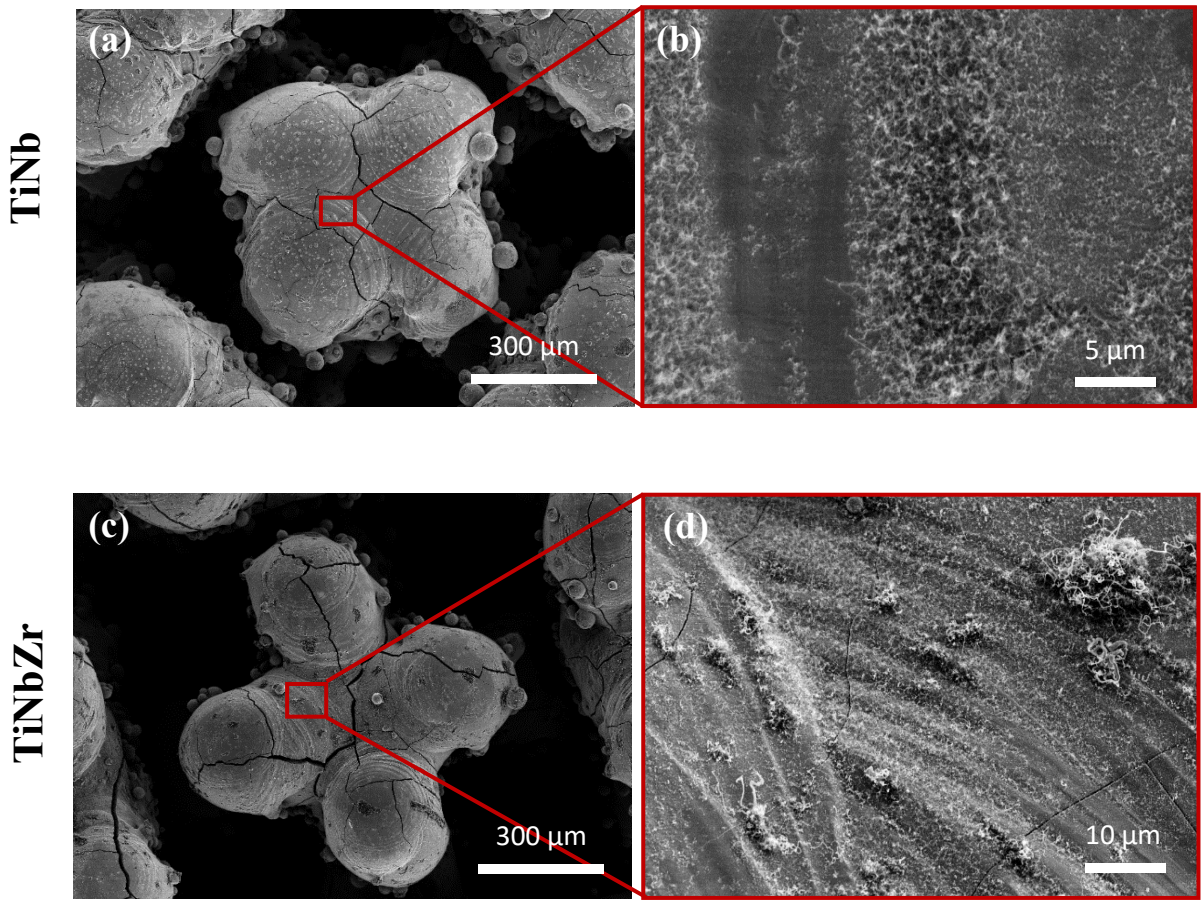

Figure 2.27. *SEM micrographs at lower (a) and higher (b) magnification of a TiNb scaffold; lower (c) and higher (d) magnification of a TiNbZr scaffold after CVD with 0.05 M of Fe + Al nitrate catalyst showing the localization of MWCNTs grown on the scaffolds together with the cracks, which occur after the CVD.*

According to these preliminary results, MWCNTs were successfully grown on two different compositions of β-Ti porous scaffolds, under the same synthesis conditions as for bulk substrates: MWCNTs were deposited all over the surface of the 3D scaffolds using a low Fe + Al nitrate catalyst concentration of 0.05 M.

2.4. Conclusions

This Chapter described how to grow CNTs on β-Ti substrates for their further use as an orthopaedic material. From the results presented in Section 2.3, several conclusions can be drawn.

Spin coating appeared to be the most efficient method of catalyst deposition on the large variety of titanium substrates investigated in this Chapter, including Ti-based films, bulk substrates, and porous scaffolds, allowing a homogeneous growth of CNTs. Substrates of different shape and sizes can be treated, which was shown by successfully depositing a Fe + Al nitrate catalyst onto very small films with uneven shape, as well as onto the much bigger disc substrates. Spin coating was much more efficient than drop casting and dip coating methods. These findings agree with other studies that reported a successful catalyst deposition on the other substrates (*e.g.* Si)[141,147]. This was achieved due to the fact that while rotating at a high speed, the catalyst solution is spreading very quickly due to the centrifugal force and evaporates at the same time, which gives rather uniform thin films on the substrate. It was previously reported that depending on the rotation speed and the amount of catalyst, it is possible to vary the thickness of the deposited catalyst[148,149], but these further tests were beyond the scope of this Chapter.

It was reported by Ward *et al.*[135] and Ortega-Cervantez *et al.*[136] that the composition of the substrate has an influence on what kind of nanotubes are formed as well as on their diameter, length, and shape. The investigation of Al_2O_3 pallets with various Ni content by Makris *et al.*[137] showed that the elemental ration also has an influence on CNTs formation. Therefore, it was anticipated that the substrate elemental composition and the ratio of the elements of Ti-based films would have an influence on the CNTs formation. However, the influence of various alloying elements in the titanium alloys on the growth of CNTs,

which had not been investigated before was not observed to influence the CNTs formation. This is likely to be linked with the fact that the alloying elements Nb, Zr, and Hf do not know to possess any catalytic activity. Meanwhile, the surface topography was observed to have a significant influence, since different patterns of MWCNTs were formed. Similarly, the surface topography was found to be the governing factor for the growth of CNTs and their alignment on Al foils reported by V. Khavrus *et al.*[150]. According to these findings, it can be concluded that when selecting materials for CNTs growth, foremost attention should be paid to the surface topography of the implant, and the composition can be optimised by considering *e.g.* mechanical properties and corrosion resistance. Recently, a number of new β-Ti alloys have been developed, and having a non-selective surface modification method gives it a great, all round, advantage.

It is important to perform the experiments on material which will be as close as possible to the one used as orthopaedic implants. The CVD growth of MWCNTs on bulk titanium substrates was reported in this thesis. In other studies, CVD syntheses were reported only on anodized titanium substrates[67]. Moreover, in the earlier reported studies only α- or α+β titanium alloys were used, while β-Ti alloys, which possess the advantages of low Young's modulus, the absence of toxic elements were used in this Chapter. Two types of MWCNTs were grown on β-Ti alloys: entangled MWCNTs and aligned MWCNTs. The difference in nanotube formation was governed by the temperature at which the substrates were inserted in the furnace and related with the degree of acetylene pyrolysis. Entangled nanotubes were formed when the substrates were inserted in the furnace at room temperature (24 °C), while aligned CNTs were observed at 400 °C. The influence of the temperature on CNTs growth has been investigated in the previous studies[151,152], however the attention was drawn only to the temperature of the synthesis themselves and not on the temperature at which the substrate was introduced into the furnace.

CNTs growth on Ti-based scaffolds was also reported for the first time. The successful growth of MWCNTs on substrates with various shapes and 3D structures, including porous scaffolds, using the same experimental conditions, allows its applications to go beyond orthopaedic implants into the field of bone repair. This is also important since implants can have complex shapes and 3D topography on their surface. It is still necessary to optimise the MWCNT growth methods on the scaffolds, since cracks were observed after the syntheses. Therefore, only preliminary experiments were conducted, and further investigations are necessary.

Since the final goal of this thesis was to create implant materials with improved biocompatibility, bulk β-Ti substrates, coated with MWCNTs synthesized in Section 2.3.3 were further used to perform cell culture experiments. The bone cell's (osteoblast's) responses need to be evaluated in order to see whether MWCNTs indeed lead to the improvement of osteoblast attachment and growth. The results of the cell culture studies will be described in detail in Chapter 3.

Chapter 3. Biocompatibility evaluation of β-Ti/MWCNTs substrates

3.1. Introduction

In Chapter 2 bulk β-Ti/MWCNTs samples were identified as the most promising material for biological investigations, in combination with the deliberate use of a low concentration of catalyst and the resulting partial CNT coverage of the surface metal. The use of such samples allows the growth of bone cells (osteoblasts), not only on the surface of CNTs but also on the titanium itself, enabling a proper connection of the cells with the implant material. A schematic representation of titanium/MWCNTs/osteoblasts interaction is presented in Figure 3.1.

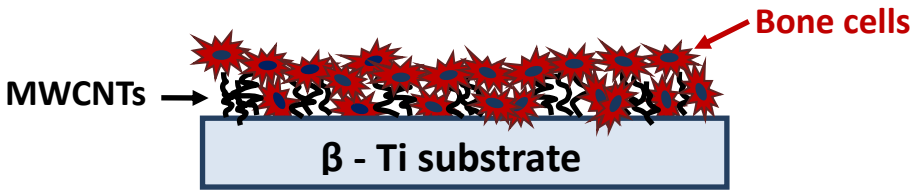

Figure 3.1. *Schematic representation of β-Ti/MWCNTs/osteoblasts interaction showing β-Ti with MWCNTs grown on it in the way that it allows osteoblasts to connect with the underlying titanium itself.*

For an orthopaedic material to be biocompatible, it has to promote cell growth, not to cause cell rejection and to be non-toxic. The biocompatibility of β-Ti alloys has already been proven in a number of publications[153–155]. However, the biocompatibility and toxicity of CNTs are currently still under debate, which is explained in Chapter 1. Previous cell culture studies of Ti alloys with CNTs were limited and not consistent[67,156].

The investigation of TiAlV samples with MWCNTs/HA nanocomposite films with 0.5 – 1 wt. % of carbon nanotubes shows normal cell adhesion[156]. Additionally, S. Sirivisoot *et al.* showed a slight improvement in the osteoblast growth on anodized titanium with CVD-grown CNTs[67]. However, in another study[97], only a small degree of cell adhesion on MWCNTs grown on Ti substrates was observed compared with MWCNTs grown on Si. The possible explanation is that Ni particles (used to grow MWCNTs on Si) were enclosed by the MWCNTs, while Fe particles were likely to be present around the carbon nanotubes. Taking this into account, significant attention should be given to the metal catalyst particle location. Therefore, the β-Ti/MWCNTs samples with Fe particles encapsulated on the surface of Ti and nanotubes that were synthesized in Chapter 2, were examined in order to enable better osteoblast cells adhesion. The biocompatibility studies of CNTs are still contradictive[10,92–95]. One of the reasons is that CNTs can be prepared by various techniques and can be of different kinds. These differences will influence the biocompatibility of CNTs. Therefore, it is important to investigate different types of CNTs.

For successful biological investigations, it is important to choose an appropriate protocol for cell culture studies. No standard protocols have yet been decided on, and different laboratories follow their own protocols that differ significantly with regards to cell type and the source from which they are isolated, to even the cell culture medium composition. For example, in a study by I. Rajzer *et al.* human osteoblast-like MG-63 cells were used and seeded in the dwell plates with a density of 50000 cells/well with 1.5 ml of Dulbecco's Modified Eagle Medium supplemented with 10 % of fetal bovine serum and gentamicin (40 lg/ml) in each dwell[157]. Meanwhile, human osteoblastic line hFOB in 1:1 mixture of Ham's F12 medium and Dulbecco's modified Eagle's medium with $2.5*10^{-3}$ mol/l^{-1} L-glutamine and 0.3 mg/ml G418 with 10 % of foetal bovine serum was used by

J.Chlopek *et at.*[101]. These differences make it difficult to compare the results from various studies. Therefore, it is of great importance to develop an appropriate protocol and to conduct all the studies under the same conditions.

The choice of the cells for cell culture studies is by all means the most important parameter in the protocol. Some of the widely used cells for the evaluation of biocompatibility are osteoblasts, fibroblasts, endothelial cells, muscle cells, bone marrow cell, and stem cells[31]. Depending on the intended application different cell types can be used. For orthopaedic applications, osteoblast cells are of primary use. This can be adult human osteoblast (aHob) or human foetal osteoblast (fHob) cells. Adult osteoblast cells possess disadvantages such as short life span and variation due to the age and gender of the donor. Hence, it is challenging to perform a study with only one batch of aHob cells and to expect consistent results. A single batch of foetal osteoblasts, on the other hand, provides the possibility to perform the complete assessment, due to their high proliferation rate. Malheiro[158] conducted an extensive comparison of fHob cells, which were used in this thesis, showing that the differentiation of fHobs is very similar to that of aHobs. It also highlights the advantages of the fHob cells, such as larger alkaline phosphatase (ALP) enzymatic activity, faster growth rate, and earlier start of their mineralization. Additionally, fHob cells possess no batch-to-batch variability. Because of all these benefits, fHob cells were chosen for the experiments performed in Chapter 3. The whole protocol chosen for the biological investigations in this Chapter is described in Section 3.2.

Chapter 3 summarizes the findings of cell culture studies on two types of samples. Section 3.2 describes the material used for cell culture studies as well as the protocol for the experiments. The evaluation of the biocompatibility of β-Ti/MWCNTs samples is discussed in Section 3.3. In order to draw further conclusions on the role of MWCNTs in

the osteoblast response, additional cell culture studies of isolated, different types of MWCNTs were performed and presented in Section 3.4. For all the samples short-term and long-term adhesion of osteoblasts were investigated.

3.2. Experimental

The β-Ti/MWCNTs samples produced in Chapter 2, including β-Ti + entangled MWCNTs and β-Ti + aligned MWCNTs, were used for the cell culture studies. Tissue plastic and β-Ti were used as reference materials. Tissue plastic was used to make sure that cell culture studies were performed correctly, and β-Ti was used to evaluate the influence of MWCNTs in the β-Ti/MWCNTs samples on the biocompatibility. All samples were produced in the form of discs with a diameter of 16 mm. More details regarding samples preparation can be found in Section 2.3.1.

Cell culture experiments were conducted at the Orthopaedic Research Unit, University of Cambridge, UK, in collaboration with Dr. Roger Brooks and Dr. Konstantin Edi Tenase as part of a secondment within the BioTiNet project. The procedure for the experiments is presented in Figure 3.2 and explained in more detail below.

Substrate Sterilization

Substrates were placed into clean Petri dishes, closed with a lid, covered with foil and sealed using dry heat indicator tape. Substrates were left in the sterilizing oven (Schwabach, Germany) for two hours at 200 °C. After that, the samples in the Petri dishes were transferred to a laminar flow cabinet (Figure 3.2), where, after cooling down, the experiments took place. The laminar flow cabinet was used to avoid contamination by bacteria, yeast, fungi, mycoplasma, and viruses. Additionally, the following aseptic techniques such as antibacterial soap, disinfectants (70 % ethanol, *etc*), 95 % ethanol, laboratory coats, latex gloves, and disposable containers were utilized for cell culture studies. All items were sterilized or disposed of after single use.

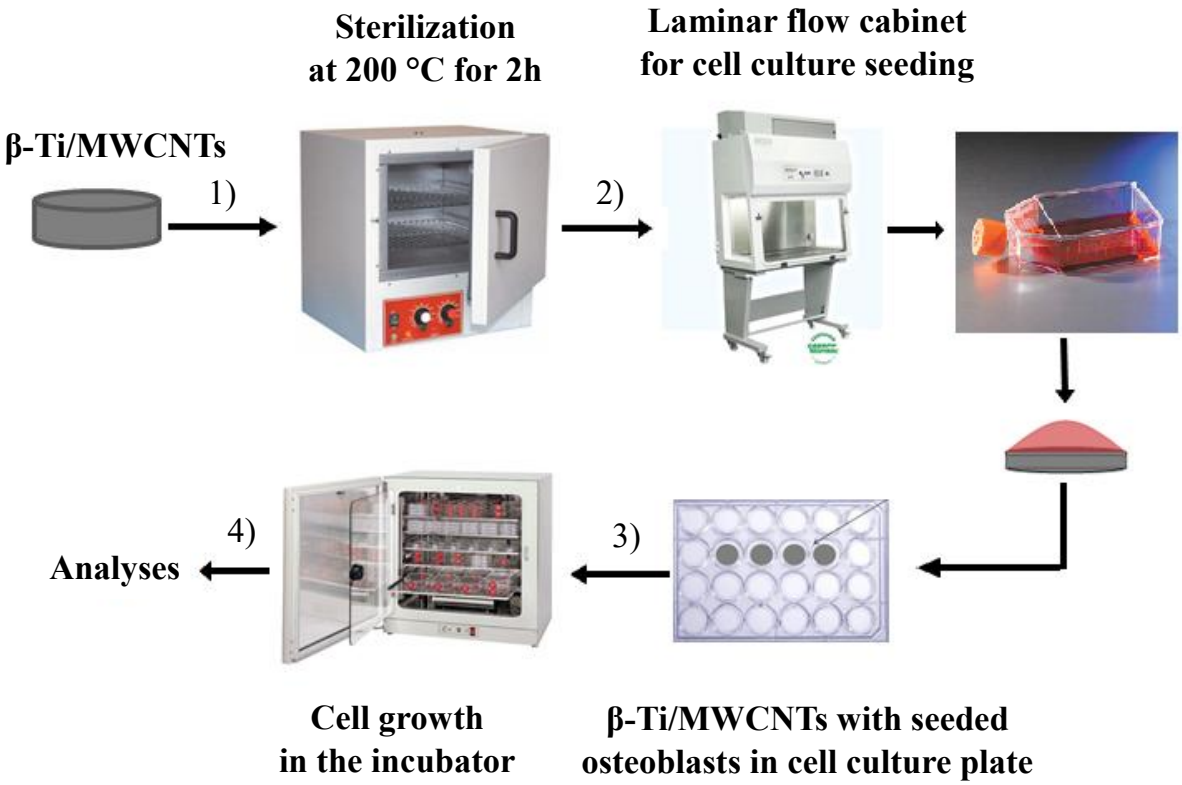

Figure 3.2. *Schematic representation of the cell culture studies protocol, which includes the following steps. 1) Sample sterilization in the oven at 200 °C for 2 hours. 2) Cell culture seeding, which takes place in the laminar flow cabinet, into the cell culture plate. 3) Cell growth in the incubator. 4) Sample analyses for the evaluation of biocompatibility.*

Cell culture seeding and incubating

All experiments were performed with P5 or P6 foetal osteoblast cells (fHobs). These were obtained from the European Collection of Cell Cultures and stored frozen in liquid nitrogen. After defrosting they were cultured in Dulbecco's modified Eagle medium (DMEM) with 10 % foetal bone serum (FSB), 1 % penicillin-streptomycin (10000 units/mL penicillin and 10 mg/mL streptomycin), and 30 mg/mL vitamin C.

The β-Ti/MWCNTs substrates were placed into culture plates, and the fHob cells were seeded at a density of 5000 cells/cm^2. Samples were randomly allocated for the experiment. Afterwards, culture plates were centrifuged for 10 min at 300 m/s^2. Substrates were transformed to another cell culture plate, and complete culture medium

was added to each sample. Samples were placed in the incubator under stable conditions for cell culture (5 % CO_2, 95 % humidity and 37 ^{0}C). Plates were kept in the incubator for the whole time of the experiments, except when the medium was changed or experiments were performed.

Analytical techniques

Fluorescence microscopy

Fluorescence microscopy is widely used in cell biology to identify cells and their components with a high degree of specificity. The image is generated by the irradiation of the specimen with light of a certain wavelength that is absorbed by the fluorophores present in the sample. The light is then separated from the much weaker emitted fluorescence through the use of a spectral emission filter, and recorded in order to see only the contributions of fluorescing cells.

AlamarBlue assay

Metabolic activity was investigated using alamarBlue® assay (AbDSerotec). The working principle of the assay is that the living cells naturally reduce the resazurin to the resorufin by the metabolic activity of the cells (Figure 3.3). Resazurin is a nonfluorescent blue dye which, upon entering a living cell, transforms into the red colour resorufin due to the reduced environment inside the viable cells. Alive cells perform the reduction of the dye all the time and by this, the viability is quantified. The intensity of the fluorescence produced is proportional to the number of the living cells. Damaged cells have lower innate metabolic activity and thus generate a proportionally lower signal than healthy cells. Nonviable cells do not have the reduced environment, and the process does not occur.

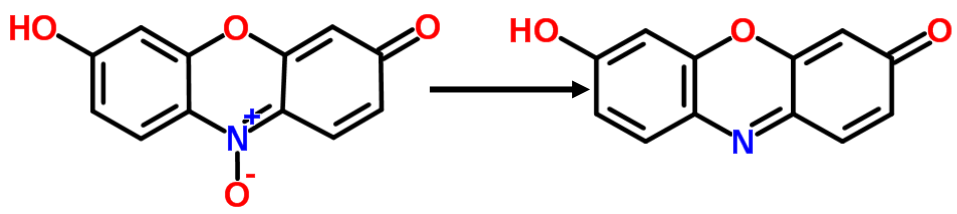

Resazurin **Resorufin**

Figure 3.3. *The process of chemical reduction of the alamarBlue assay from resazurin to resorufin.*

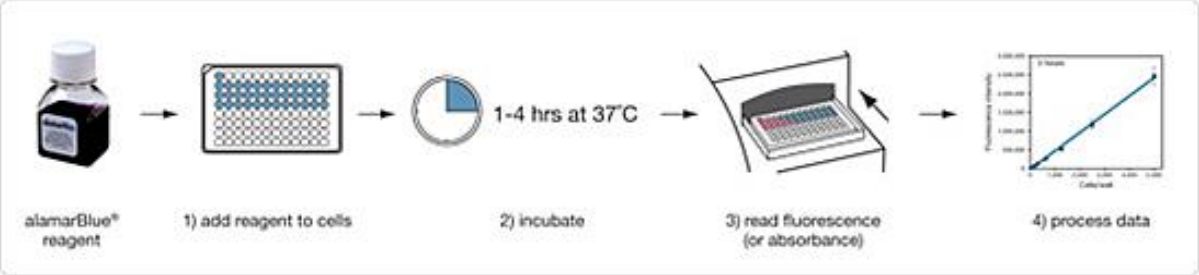

Figure 3.4. *Schematic representation of the process of alamarBlue assay activity. AlamarBlue reagent is added to the 96-well plate and incubated at 37 °C when the reduction of resazurin to resorufin takes place. Then the plate is read by the spectrophotometer, and the results are exported and visualized by plotting the cell activity graph*[159].

The assessment was performed following the protocol of the manufacturer, which is schematically presented in Figure 3.4. Part of the culture medium was removed from each sample and replaced with 10 % (v/v) of the alamarBlue® solution. Then it was incubated for 3 hours at 37 °C. After that, 100 µL of the medium from each sample was collected in triplicate and injected into the 96-well plate to be read on the fluorescence plate reader FLUOstar Optima (BMG Labtech, Offenburg, Germany) at 530 nm excitation, 590 nm emission wavelength (Figure 3.5).

Figure 3.5. *FLUOstar OPTIMA fluorescence microplate reader for the evaluation of the metabolic activity of osteoblast cells, using alamarBlue® assay*[160].

3.3. Results and discussion of cell culture studies on β-Ti/MWCNTs samples

Osteoblast cells are round before they attach to a substrate, whereas after attaching they spread out and start to elongate, making connections with the substrate. The initial attachment of fHob's cells on β-Ti samples was determined using fluorescence microscopy. In Figure 3.6 fluorescence images of β-Ti, β-Ti + entangled MWCNTs and β-Ti + aligned MWCNTs samples are presented. Due to the transparency of the tissue plastic, it was not possible to visualize osteoblast cells of tissue plastic samples with fluorescence microscopy without fixing the cells. For all the samples, including β-Ti/MWCNTs and reference materials, good initial attachment after 24 hours was observed. This indicated that the β-Ti/MWCNT samples were not highly toxic, and cells were able to attach and start to grow successfully.

In the left column in Figures 3.6a, c, e, whole fHob cells are imaged, and the cells are shown in red. It was observed that osteoblasts on a β-Ti substrate (Figure 3.6a) are better visible than on β-Ti with MWCNTs (Figure 3.6c, e). It is likely to be due to the black background of the MWCNTs, which made the visualization of the cells more difficult. Additionally, the roughness of β-Ti with MWCNTs samples could also prevent proper imaging since the cells can overlap. Therefore, in order to reduce the possibility of overlapping the cell nuclei, which are much smaller, were imaged, and these are shown in blue in the right column in Figures 3.6b, d, f. Micrographs showing whole osteoblasts and their nuclei were acquired from the same area of the sample.

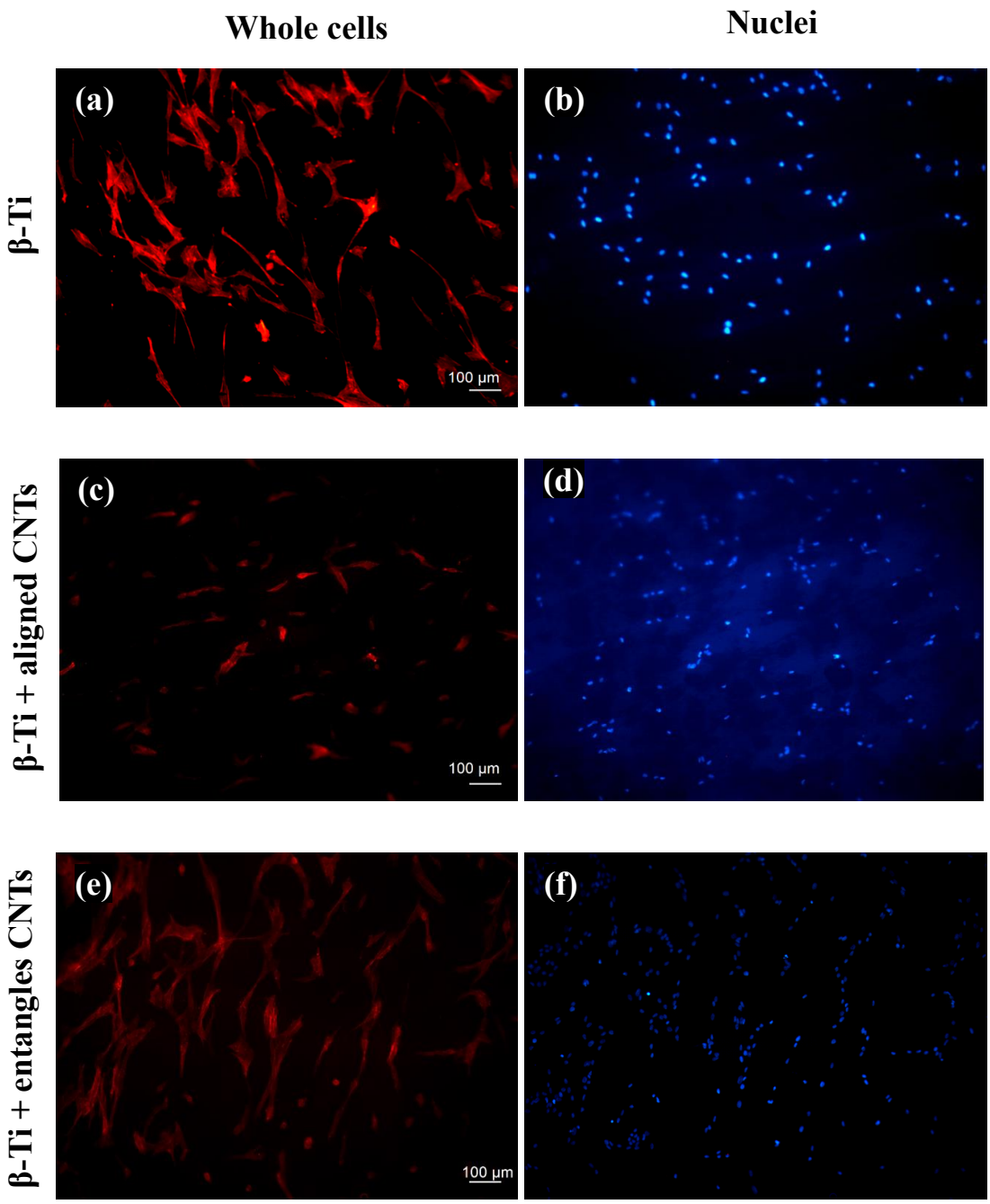

Figure 3.6. *Representative fluorescence micrographs illustrating the viability of fHob's cells after initial attachment on (a), (b) β-Ti; (c), (d) β-Ti + aligned MWCNTs; (e), (f) β-Ti + entangled MWCNTs. The whole fHob's cells are shown in red, and nuclei of the same area of the sample are shown in blue. A slight increase in cell number for β-Ti + entangled MWCNTs were observed, while for β-Ti + aligned MWCNTs the number of cells is very similar to β-Ti without carbon nanotubes.*

The combination of both micrographs can provide more representative information about the initial MWCNTs attachment. By looking at the number of nuclei on β-Ti, it is clear that there is no decrease in the cell number on β-Ti with MWCNTs, which is contradicting the study by A. Przekora *et al.*, which reported a slight decrease in osteoblast attachment after 24 hours[161]. Moreover, there is a small increase in the cell number for β-Ti with aligned MWCNTs and even bigger for β-Ti with entangled MWCNTs.

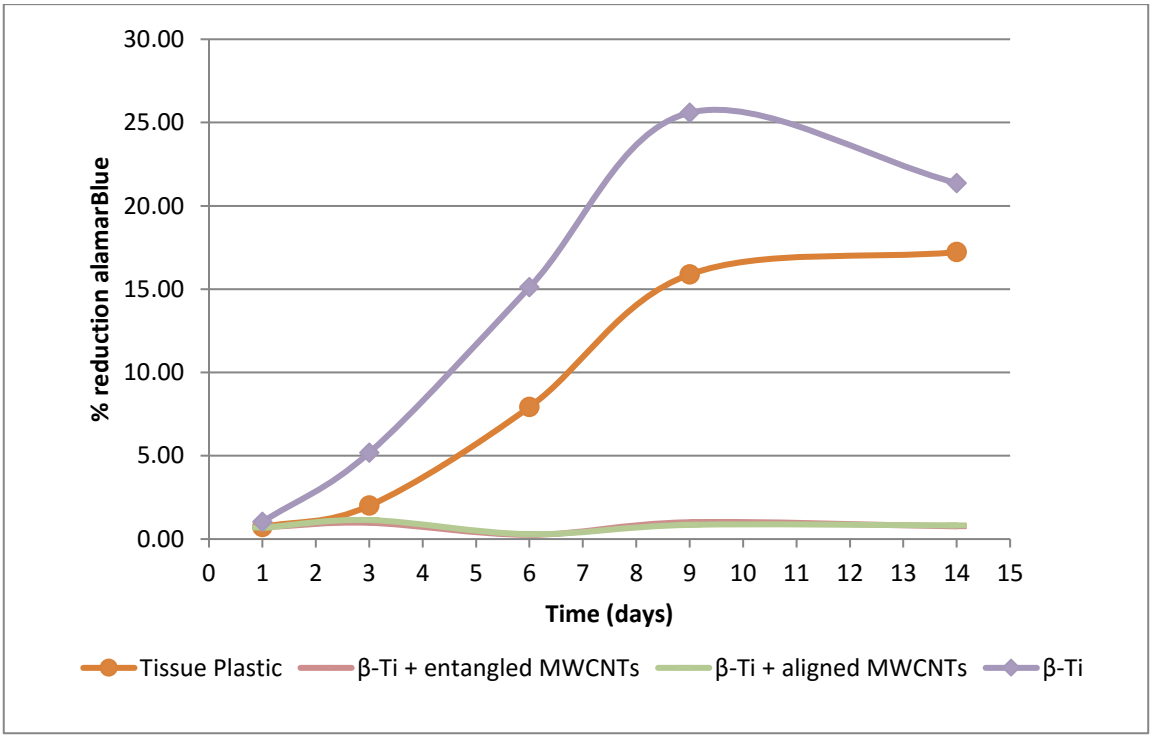

Figure 3.7. *Metabolic activity of fHob's seeded onto Tissue plastic; β-Ti +entangled MWCNTs; β-Ti + aligned MWCNTs; and β-Ti at different time points up to 14 days. A typical metabolic activity was observed for Tissue plastic and β-Ti samples, however, no metabolic activity was detected for β-Ti with both entangled and aligned MWCNTs (overlapping curves).*

To evaluate the long-term performance of osteoblast cells, the metabolic activity and cell proliferation was determined using alamarBlue assay. A culture medium was harvested from three replicas on day 1, 3, 6, 9, and 14. Figure 3.7 shows the relation between reduction of alamarBlue and culturing time. The higher the percentage of the alamarBlue

reduction, the greater the metabolic activity of cells on the corresponding material has been. Reference materials in this study, including tissue plastic and β-Ti, showed a typical metabolic activity with the region of the increase of metabolic activity during the lag phase, its further increase during the log phase and the decrease of metabolic activity. That indicates that the cell culture was grown successfully. A high activity was observed for β-Ti, which proves that β-Ti has a good biocompatibility. However, almost no metabolic activity on β-Ti samples with MWCNTs was observed. Therefore, β-Ti/MWCNTs samples were shown to be inappropriate material for successful osteoblast cells growth. In order to draw further conclusions, it is important to understand why the β-Ti/MWCNTs samples were not biocompatible. It is well known the biocompatibility of titanium is good and therefore, the β-Ti should be excluded from the experiment in order to understand solely the interaction between the osteoblast cells and carbon nanotubes, and whether only MWCNTs are responsible for the bad long-term cell growth. This is the subject of the next section, 3.4.

3.4. Cell culture studies on isolated MWCNTs

3.4.1. Introduction and methodology

In order to explain and understand the poor biocompatibility of the β-Ti/MWCNTs samples reported in Section 3.3, cell culture studies on isolated MWCNTs were performed.

For this thesis pristine (non-modified) MWCNTs, and Si- and N-doped MWCNTs were used. The reason for this was to see whether the doping could help to improve biocompatibility. These types of tubes can be synthesized directly on Ti substrates during (catalyst-assisted) CVD, which is a primary requirement for this thesis. In addition, these sorts of doping do not possess any potential toxicity. A comparison of different types of CNTs could provide a better understanding of the carbon nano-family, with regards to their interaction with bone tissue.

According to the literature[162,163], comparable cell culture experiments are usually performed using MWCNTs dispersed in the solution. For this study, such a model is not similar enough to the real implant situation where CNTs are not dispersed but connected to each other and the titanium substrate. In order to mimic the arrangement of carbon nanotubes in β-Ti/MWCNTs samples in the most realistic manner, MWCNT buckypaper (BP) and MWCNT carpets were used. α-Ti, tissue plastic and carbon paper were used as reference materials.

MWCNT carpets

MWCNTs carpets were prepared by aerosol assisted chemical vapour deposition (AACVD) by Dr. S. Meysami. Figure 3.8b, d show aligned MWCNT carpets, which resemble the arrangement of MWCNTs on a β-Ti substrate.

MWCNT Buckypaper

The arrangement of carbon nanotubes in buckypaper is presented in Figure 3.8a, c, and it resembles the arrangement of CNTs in the β-Ti + entangled MWCNTs samples. There are only a few works addressing the biocompatibility of BPs[164] and no data regarding the osteoblasts response is available. For the other cell types, contradictory results have been reported. Investigations with cancer cells showed decreased proliferation on BPs, however, there was no decrease in human arterial smooth muscle cells and human dermal fibroblasts when these were grown on BP[164].

All MWCNTs were synthesized by AACVD in the Nanomaterials by Design Group, Materials Department, University of Oxford, by Benoit Grosjean and Dr. Seyyed Shayan Meysami. Buckypapers from different types of MWCNTs were prepared by Benoit Grosjean and Karwei So. The BP samples were produced as discs with a diameter of 10 mm.

Buckypaper (BP) is a thin sheet made from an aggregated carbon nanotubes (Figure 3.8). The first single walled carbon nanotubes (SWCNTs) BP was reported in 1998 by J. Liu *et al.*[165], and was made by filtering carbon nanotube solution through a membrane. Initially, BP was produced from SWCNTs, as they have superior thermal, mechanical, and electrical properties. However, SWCNTs are delicate to handle and expensive for commercial use. Therefore, BPs from DWCNTs, MWCNTs, and mixed nanotubes were produced. Kim *et al.*[166] reported the fabrication of DWCNTs BP.

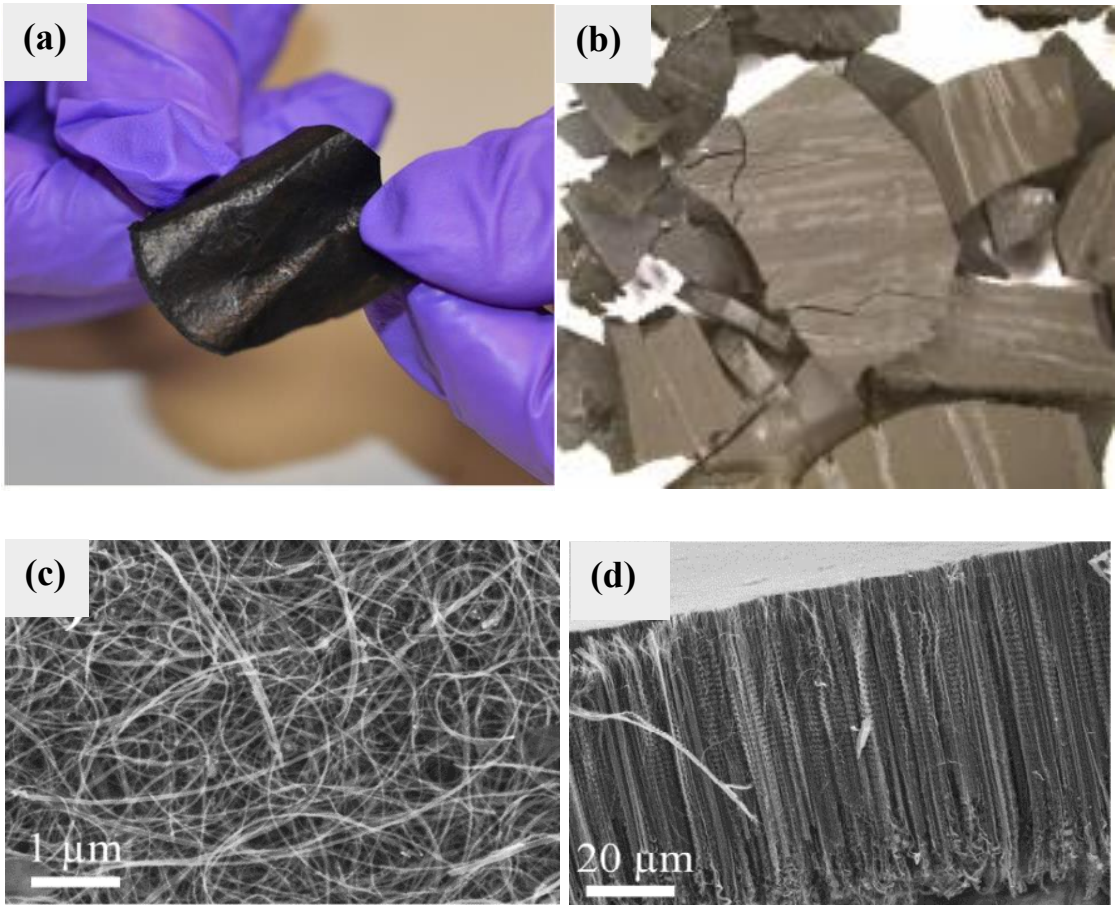

Figure 3.8. *Images showing (a) buckypaper (BP); (b) MWCNTs carpets; Representative SEM micrographs of the (c) random arrangement of the carbon nanotube is MWCNTs BP, (d) aligned arrangement of carbon nanotubes in MWCNT carpets. Samples and micrographs (a), (c), (d) were produced by B.Grosjean. and (b) by Dr. S. Meysami*[167].

Additionally, BPs from different types of MWCNTs can be produced. By using MWCNTs with the different structure the properties of BP can be tuned, including their biological response. It was reported that functionalized or purified CNTs show better biocompatibility than pristine CNTs, primarily due to the reduction of the catalyst particles and defects[168,169].

The procedure of BP preparation is briefly described below. First, the filtration of dispersed CNTs in an appropriate solvent (ethanol or water) and surfactant took place. The filtration set-up consists of a 1 L vacuum resistant flask with a vacuum pump

connected to it and a Sartorius® 'Glass vacuum filtration holder' for a 47 mm membrane filter with a glass filter support (See Figure 3.9) placed on the top of the flask. The Whatman® (PC membrane or polytetrafluoroethylene (PTFE) membrane) filter with 1 μm pore size was wetted with the solvent used for the CNTs dispersion, and then the CNT solution itself was poured on. While more and more CNTs were deposited on the membrane, the filtration slowed down. In order to eliminate the surfactant from the deposit, the following procedure was used. A solvent consisting of 50 to 100 mL ethanol was rinsed, followed by 50 to 100 mL water for SDBS; 200 mL isopropanol (IPA, Sigma-Aldrich®, 99.5 %) as reported in the literature[170]; 100 mL water for GA was poured on. Finally, filters with samples were dried under vacuum for several minutes. Then the samples were peeled off the filters and dried at room temperature in a vacuum oven.

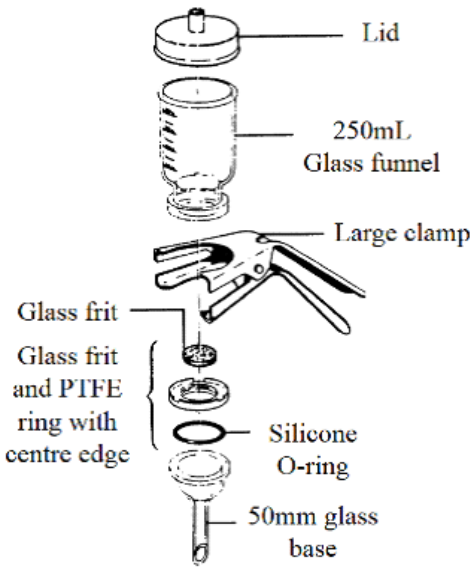

Figure 3.9. *A filtration set-up used for the production of buckypapers employed in this thesis. It consists of Sartorius® 50 mm filter holder, silicon O-ring, glass frit, clamp, 250 ml glass funnel, and a lid. The figure was adapted from Sartorius® catalogue by B. Grosjean.*

3.4.2. Results and discussion of cell culture studies on isolated MWCNTs

The initial attachment of fHob cells was observed for all the substrates but was difficult to image. It is likely to be due to the porous structure of the samples. For buckypaper samples, it was possible to image only the cell's nuclei, the typical image of which is shown in Figure 3.10a. On carbon paper, which was used for comparison, it was possible to see the osteoblasts more clearly (Figure 3.10b, c), since the density of the sample was higher than the one using BP. Nevertheless, not all the cells were detected due to the layered structure of carbon paper, where only the cells in the upper layers were possible to be visualized.

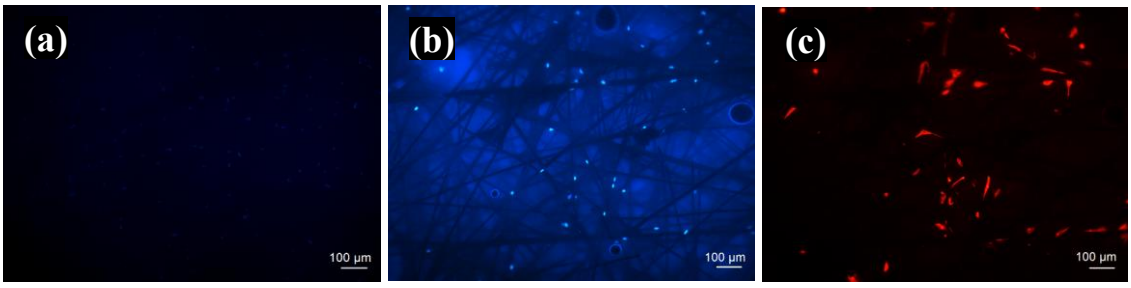

Figure 3.10. *Representative fluorescence micrographs illustrating the viability of fHob's cells after initial attachment to (a) buckypaper and (b), (c) carbon paper. The nuclei of osteoblasts are shown as blue spots in figures (a) and (b) and the whole cells are presented in red in figure (c).*

Figure 3.11 shows the metabolic activity curves (as % reduction alamarBlue) of fHob's on MWCNTs samples and reference materials during 14 days. Tissues plastic and α-Ti showed good typical metabolic activity, which is very similar to the activity curves obtained in Section 3.3 for reference materials. For entangled MWCNTs BP and aligned MWCNTs carpets there is a slight increase in the metabolic activity over time, however,

it is very low. Nevertheless, their metabolic activity is higher than for the corresponding β-Ti/MWCNTs samples.

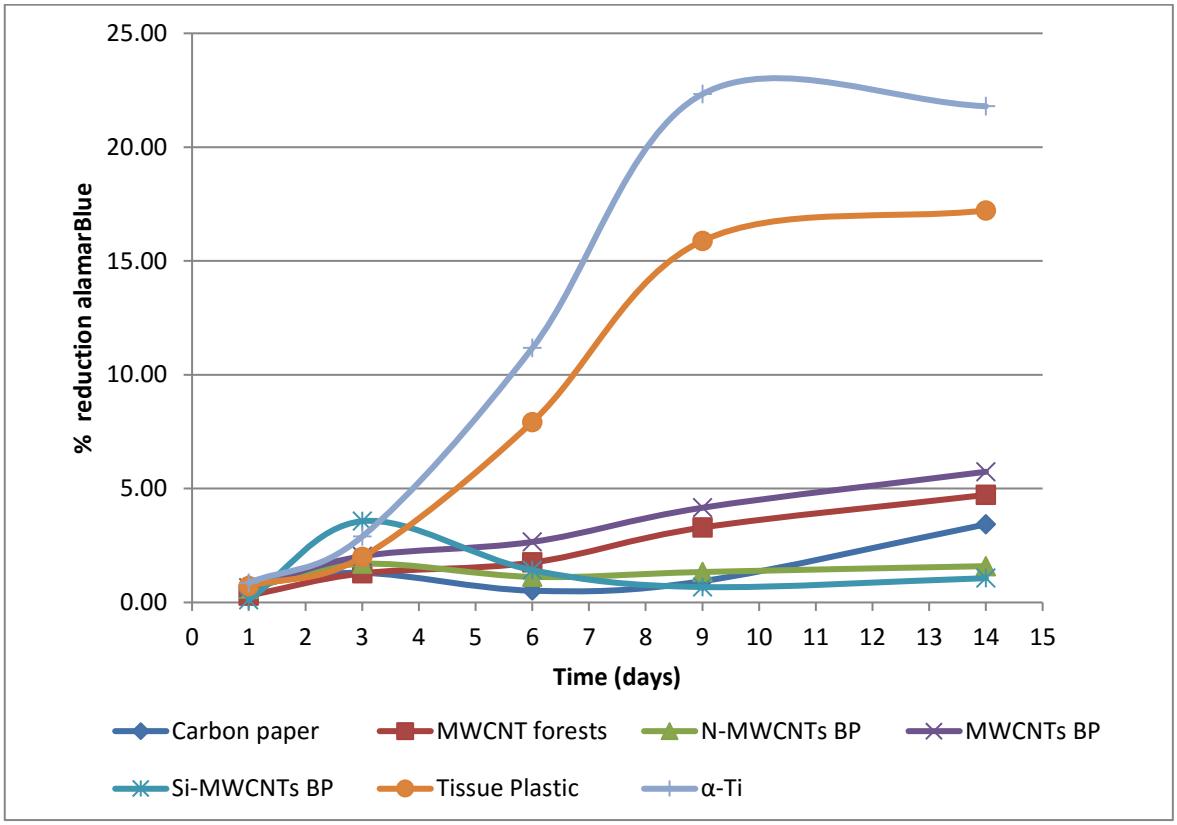

Figure 3.11. *Metabolic activity curves of fHob's seeded onto carbon paper; MWCNTs forests; N-MWCNTs BP; MWCNTs BP; Si-MWCNTs + MWCNTs BP; Tissue plastic; and α-Ti (α-Ti) at different time points up to 14 days. α-Ti and Tissue plastic samples showed typical metabolic activity, while for the rest of the samples very low activity was observed.*

Doped BPs showed a different behaviour. Cells on N-MWCNTs BP showed almost no activity. Meanwhile, the Si-MWCNTs BP activity curve showed a slight increase after day 3, but then a decrease until day 14 when it reach almost to the same value as N-MWCNTs BP. Metabolic activity of carbon paper also slightly increased on day 3, similar to all the other samples, and then decreased. Table 3.1 shows the comparison of the metabolic activity of different MWCNTs samples and reference materials. It can be concluded from the table, that all MWCNTs samples have very low metabolic activity. While comparing samples with each other, entangled MWCNTs BP and aligned

MWCNTs carpets have a slightly higher activity than others. This indicates that these types of tubes are better candidates for the creation of β-Ti/CNTs composites.

Table 3.1. *Comparative results of metabolic activity of osteoblast cells on various MWCNTs substrates and reference materials.*

	MWCNTs forests	MWCNTs BP	N-MWCNTs BP	Si-MWCNTs BP	Carbon Paper	Tissue plastic	α-Ti
Metabolic activity at day 14, %	5	6	1	1	3	17	22

It worth mentioning that the handling of MWCNTs buckypaper and MWCNTs carpets is difficult. The first challenge is the hydrophobicity of the samples, due to which they tend to float on the surface of the culture medium. A drop method of cell seeding and a culture plate with the same diameter as samples (10 mm) were used. Nevertheless, MWCNTs samples are rather fragile, and there is a risk of damaging samples during the insertion into the culture plate. Therefore, the development of new improved methods of sample handling would be beneficial.

3.5. Conclusions

The evaluation of the biocompatibility of β-Ti/MWCNTs samples, both with aligned and entangled MWCNTs, consisted of the investigation of the initial attachment and long-term activity of osteoblast cells. Both types of β-Ti/MWCNTs substrates investigated in this Chapter showed good initial osteoblast attachment. A slight increase in the cell number for β-Ti with aligned MWCNTs and even larger for β-Ti with entangled MWCNTs after 24 hours was observed.

No comparative studies on MWCNTs grown on β-Ti substrates have been performed by other research groups, but S. Sirivisoot *et al.*[67] studied the attachment of osteoblast cells on α-Ti, anodized α-Ti and anodized α-Ti/MWCNTs. The initial attachment on anodized α-Ti/MWCNTs showed a slightly decreased in comparison with samples without nanotubes. Long-term osteoblasts' function was not observed, which was demonstrated by a near-zero metabolic activity of the cells on β-Ti/MWCNTs samples. In contrary, N. Aoki *et al.*[81] reported *in vitro* improvement of Ti with electrodeposited CNTs. However, their metabolic activity was evaluated after three days, which is quite a short period and does not fully represent the long-term activity. Another study by S. Sirivisoot *et al.*[67] showed that the osteoblast activities on day 7 and day 14 were comparable, and the activity on day 21 showed an increase. This improvement might have been connected with the anodized TiO_2 tubes, and the changes that occurred after the CVD since the improvement of osteoblast activity on titanium TiO_2 tubes compared with pure Ti has already been reported[171].

The observed, overall bad osteoblast cell response on β-Ti/MWCNTs samples is likely to be associated with the presence of MWCNTs. This can be concluded from the additional experiments performed on MWCNTs without titanium. Various types of MWCNTs

buckypaper (conventional, N- and Si-doped) and MWCNTs carpets were analysed and showed very low long-term cell activity. Some variation in behaviour between different MWCNTs samples was observed, but they were not significant.

A number of studies by other groups complement the obtained results, and report cell death due to the presence of carbon nanotubes[10,95]. The earlier hypothesis made in this Chapter whether doping of nanotubes would improve their biocompatibility was not supported by the cell culture studies conducted in this Chapter.

As mentioned in Chapter 1, there is no clear answer as to what can trigger the toxicity or bad cell response. One of the reasons for the bad cell response shown in this Chapter could be related to the growth of conventional, non-modified MWCNTs with their impurities, defects, and agglomeration. A number of studies show that the modified and purified MWCNTs possess no toxic effects[96,161]. Nevertheless, there are some contradicting studies, which show that purified SWCNTs and oxidized MWCNTs are more toxic than pristine nanotubes[172]. To incorporate MWCNTs in future orthopaedic material it is important to achieve a very good connection between the substrate and the nanotubes, and MWCNTs need to be directly grown on the titanium substrates. Therefore, by performing any purification (removing catalyst particles) or functionalization of MWCNTs is not ideal, since the connection between the substrate and the nanotubes would not be good. A second reason could be the presence of a potentially toxic metal catalyst. As was stated in Chapter 2, for the growth of carbon nanotubes in β-Ti/MWCNTs composites, a very low concentration of 0.05 M catalyst was used, and also, catalyst particles were detected on the interface between the nanotubes and the titanium. Since the influence of the catalyst particles on the toxicity of CNTs has not been investigated in detail yet, it might still have an influence on the response of the cells, even

though the study by S. Sirivisoot *et al.*[67] with higher concentration of catalyst for MWCNTs growth (5M cobaltous nitrate) showed no adverse reactions.

Additionally, a high hydrophobicity of examined samples has an influence on the osteoblast response. For a good cell adhesion on the biomaterials, hydrophilic surfaces are preferred. It was shown that the poor cell response and toxicity of purified SWCNTs might be associated with the hydrophobicity of the samples. Nevertheless, it was shown that the toxicity of oxidized MWCNTs also increased in with comparison with pristine ones, even though the oxidation makes the samples more hydrophilic[172]. Hence, it is difficult to relate directly the hydrophobicity of the samples to the osteoblast response.

On the other hand, an increased osteoblast activity on carbon fibers[56] and diamond-like carbon[173] and TiC[50] has been reported. Hence, there is potential biocompatibility for some specific carbon structures. TiC is a promising material to be incorporated into β-Ti substrates, not only due to the increase of their biocompatibility but also their mechanical and corrosion properties, which are critical for the successful and long-term performance of the implant materials. Further investigations of TiC growth on β-Ti substrates and their biological evaluation will, therefore, be discussed in Chapter 4.

Chapter 4. CVD growth of TiC on Ti-based substrates

4.1. Background

As mentioned in Chapter 1, CNTs are not the only structures, which were reported to improve the performance of titanium implants. Carbide hard coatings of various transition metals are often used for the improvement of the wear resistance of implant materials[53]. Since the material discussed in this thesis will be tested for biological applications, it is preferable not to introduce any external metals into the system, thus avoiding any possible toxic effects. The substrates utilized in this thesis are titanium alloys, and that is why a titanium carbide (TiC) coating was investigated in this Chapter.

There is a number of publications reporting on the formation of TiC layer on titanium alloys. Until now only α- and α + β Ti alloys have been investigated[1-4]. In this Chapter, the possibility to obtain a TiC coating on β-Ti substrates was explored. Usually, such methods as magnetron sputtering[174,175], pulsed laser deposition (PLD)[50], plasma immersion in implantation and deposition (PIII&D)c, or plasma CVD[51] are used for the synthesis of TiC. However, more simple techniques like physical vapour deposition (PVD) and chemical vapour deposition (CVD) are also known to be used to deposit thin layers of carbides on other metal surfaces[53].

The method of TiC synthesis using atmospheric pressure CVD on β-Ti substrates is presented and discussed in Section 4.3.1, opening new perspectives on its use in biomaterials. Atmospheric pressure CVD (from now on called CVD) has several advantages over other methods. It is quicker, cheaper and easier to scale up the process.

The mechanical properties and corrosion resistance of titanium substrates with TiC need to be investigated since it is important to know how TiC influences the Young's modulus, hardness and corrosion properties, and whether they are still appropriate to be used as biomaterials. The zeta potential is also an important property of charged solid/liquid interfaces and an indicator for the actual surface charge of a solid in contact with an electrolyte. The electrical charge on the surface of the material is considered to be one of the main physical factors involved in the biological evolution of the tissues around the implant. Krajewski *et al.*[176] showed that the surface charge properties influence the protein absorption. The zeta potential can be determined by measuring the streaming potential and streaming current. Further details regarding the evaluation of those parameters are discussed in Section 4.3.2.

TiC layers have been shown to promote bone growth and improve the biocompatibility of Ti implants. Studies reported the increase of osteoblasts proliferation, adhesion and differentiation on Ti surfaces with a TiC layer[50]. The *in vitro* studies of titanium coated with a TiC layer produced by the PLD showed the improved osteoblast activity and after *in vivo* studies the bone density was enhanced[50]. It is also of high importance to evaluate the biological response of the Ti-based samples with CVD-grown TiC. Details of the evaluation of the biocompatibility of the Ti-based samples with TiC are presented in Section 4.3.3.

4.2. Experimental Details

The experiments of TiC growth were performed on both α- and β-Ti substrates (Table 4.1). α-Ti foil (Alfa Aesar, 99.5 %) and β-Ti rod (ATI WahChang, Ti-45Nb wt. %) substrates were cut into 10 mm^2 squares with the thickness of 0.1 and 0.5 mm respectively. All substrates were cleaned by sonication in acetone and deionized water in turns, as with the substrates in previous chapters. While TiNb (β-Ti) was the main investigated material, CP Ti (α-Ti) was used as a reference. Cleaned substrates were placed in a quartz reactor tube, which was positioned inside the CVD furnace.

Table 4.1. *Titanium substrates used for TiC growth in Chapter 4.*

Code	**Substrate**	**Form of alloy**
α-Ti	CP Ti foil	Alpha
β-Ti	Ti-45Nb rod	Beta

Syntheses were performed in an atmosphere of 200 sccm Ar as a carrier gas. The furnace was heated up to the reaction temperature (between 950 to 1100 °C) and then substrates were annealed with 100 sccm of H_2 for 30 min. Later, in addition to the hydrogen, 5 sccm of methane (carbon precursor) was added for another 30 min. Finally, the furnace was cooled down under 200 sccm of Ar. When cold, all the gases were switched off, and the substrates were removed.

A Zeiss NVision 40 FIB-SEM was used to perform the cross-sections of samples in order to identify the thickness of the TiC layer with a typical accelerating voltage of 5 keV.

Corrosion studies were performed in collaboration with Dr. Eva Pellicer at the Universitat Autònoma de Barcelona, Bellaterra, Spain using an electrochemical method using PGSTAT120 Autolab potentiostat/galvanostat (Eco Chemie). An electrochemical corrosion cell with a three-electrode configuration was used: reference, counter and working electrodes. As a reference electrode, an Ag/AgCl electrode filled with 3 M KCl inner solution and 1 M NaCl outer solution was used. The counter electrode had a platinum foil attached to it. The investigated sample was attached to the working electrode. Naturally-aerated simulated physiological Hank's balance salt solution (HBSS)[**], a group of salts rich in bicarbonate ions, was used as a buffer solution. The physiological pH of 7.0 – 7.4 and temperature of 37.5 °C were maintained during the measurements. The cell was cleaned with a solution of HNO_3 in H_2O, and several times with Millipore water. Samples were cleaned by rinsing with acetone and Millipore water. The sample to be investigated was attached to the working electrode and isolated with insulating tape. The size of the area exposed to the corrosion experiment was measured before the experiment. Each sample was left for 30 min in the solution to stabilise. The corrosion current density (j_{corr}) was obtained from the Tafel extrapolation method[177]. The surface roughness was evaluated using confocal profilometry with a Gaussian filter (0.25 mm) at the Universitat Autònoma de Barcelona, Bellaterra, Spain.

Zeta potential measurements were performed by Dr. Thomas Luxbacher at the Anton Paar Company, using a SurPASS Adjustable Gap Cell (Figure 4.1). For measuring the streaming potential and the streaming, the current samples were attached to the sample holder using double-sided adhesive tape. The distance between the sample surfaces in the

---

[**] HBSS composition: 8.0 g dm^{-3} NaCl + 0.4 g dm^{-3} KCl + 0.04788 g dm^{-3} Na_2HPO4 + 0.06 g dm^{-3} KH_2PO4 + 0.185 g dm^{-3} $CaCl_2 \cdot 2\ H_2O$ + 0.09767 g dm^{-3} $MgSO_4$ + 0.35 g dm^{-3} $NaHCO_3$ + 1.0 g dm^{-3} D-glucose.

Adjustable Gap Cell was 100 μm. The background electrolyte was a 0.001 M/l KCl solution.

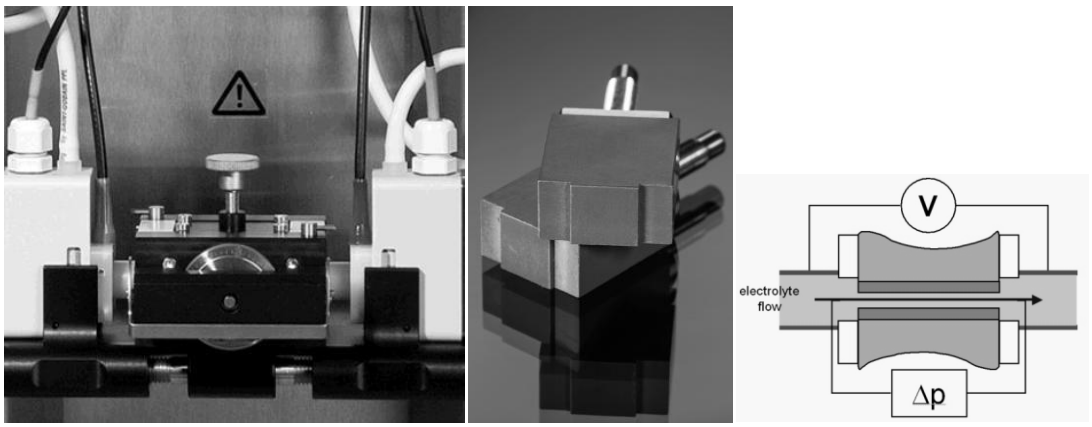

Figure 4.1. *An adjustable Gap Cell mounted between electrodes (left), the sample holder for square plates, and measuring principle (right)*[178].

The zeta potential can be defined in different ways[178]. It can be calculated from streaming current measurements according to the following equation:

$$\zeta = \frac{dlstr}{d\Delta p} * \frac{\eta}{\varepsilon 0 * \varepsilon} * \frac{L}{A}, \quad (1)$$

where dlstr/dΔp – streaming current coefficient (slope of streaming current vs. differential pressure), η – electrolyte viscosity, ε – dielectric coefficient of water, ε_0 – vacuum permittivity. L/A – length L and cross section A of the slit channel (the rectangular gap between planar samples).

Also, it can be calculated from the streaming potential according to the following equation:

$$\zeta = \frac{dUstr}{d\Delta p} * \frac{\eta}{\varepsilon * \varepsilon} * K, \quad (2)$$

where dUstr/dΔp – streaming potential coefficient (slope of streaming potential vs. differential pressure), K – electrolyte conductivity.

4.3. Results

4.3.1. Synthesis and first characterization of a TiC layer on Ti-based alloys

This Section reports on TiC synthesis using the CVD technique on α-Ti and β-Ti substrates, and their preliminary characterisation. In Figure 4.2 SEM micrographs of α-Ti samples after CVD are shown. It is visible that the whole sample is homogeneously covered with rough structures, which consist of Ti and C according to the EDX measurements (Figure 4.3).

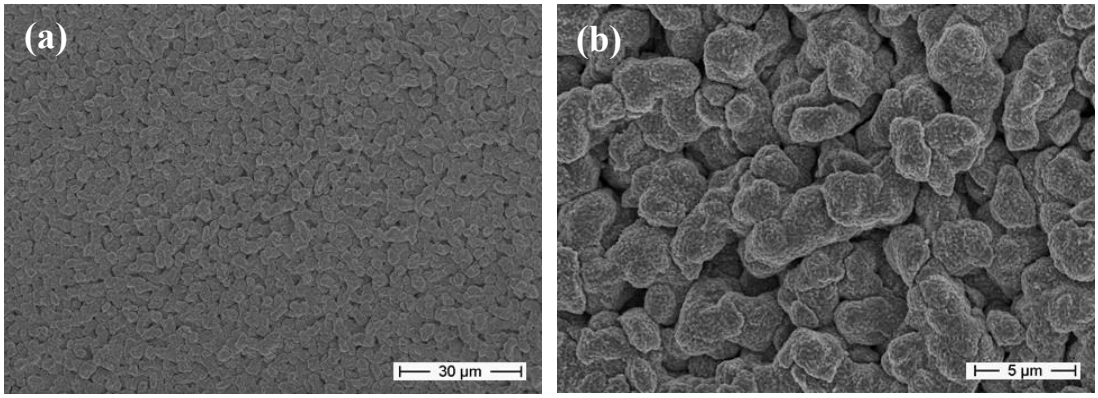

Figure 4.2. *SEM micrograph of α-Ti substrates after CVD at 1100 °C and 30 min reaction time, showing the formation of a homogenous TiC surface layer (determined via EDX and XRD).*

Figure 4.4 displays the XRD trace from TiC on Ti along with the pattern for TiC. The blue lines represent the real peak positions for TiC phase and do not quite fit the observed peaks. The purple lines represent the peak positions after they have been shifted and a fit to the observed peaks is now very good. This shift might be explained by a change in the composition which generally course a change in lattice parameter.

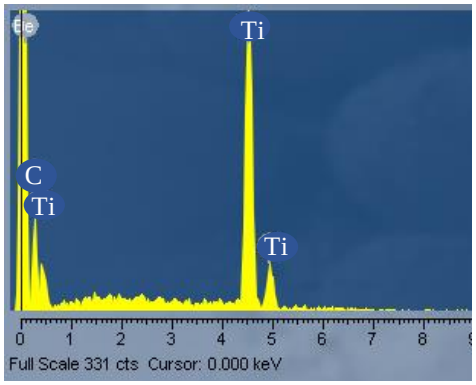

Figure 4.3. *EDX spectrum recorded from a α-Ti sample after the CVD indicating the dominant presence of titanium and carbon elements.*

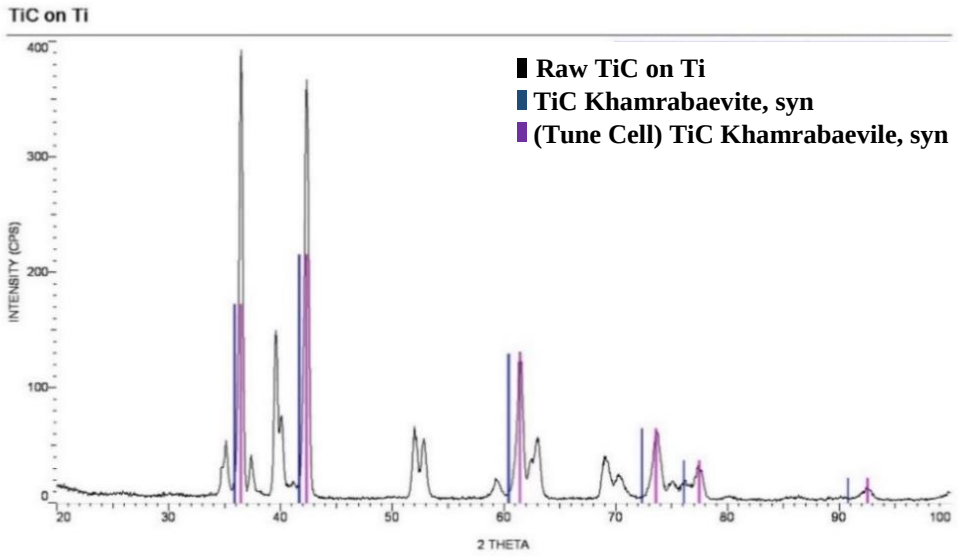

Figure 4.4. *XRD spectrum of α-Ti/TiC sample presented in black, showing the peaks of TiC peaks in blue and shifted TiC peaks in purple, which show a very good fit and indicate the presence of TiC layer on the sample with Cu cathode.*

Figure 4.5 shows micrographs of β-Ti substrates after the CVD. Very similar structures to the one on α-Ti were observed all over the sample. EDX spectra (Figure 4.6) identified the Ti and Nb elements in β-Ti substrates, which correspond to the composition of the substrate[***], as well as C.

[***] Ti-45Nb at. %

XRD measurements of the same sample are presented in Figure 4.7. This plot shows the shifted TiC pattern in blue which matches the main peaks well. The remaining peaks appear to match β-Ti, shown in red, and possibly an oxide phase in purple, although this fit is not totally convincing since not all the peaks of titanium oxide correspond to the peaks in the spectrum presented in Figure 4.7.

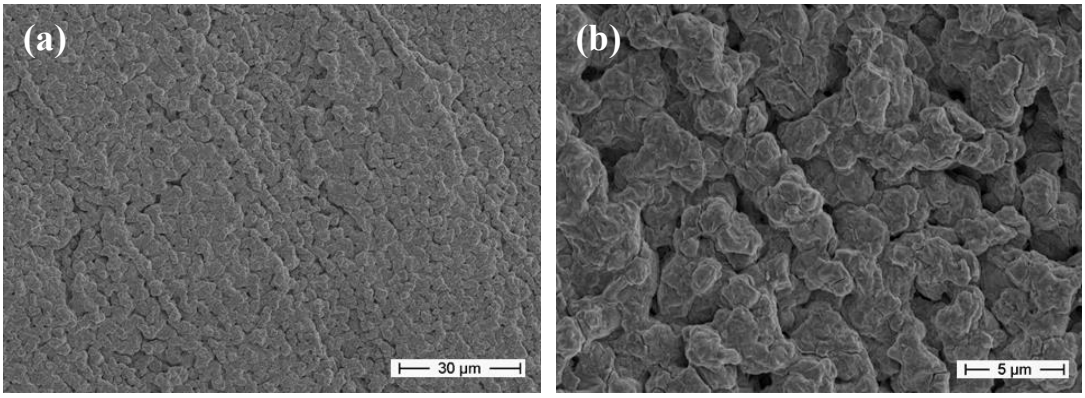

Figure 4.5. *SEM micrographs of β-Ti substrates after the CVD at 1100 °C and 30 min reaction time showing the formation of a TiC layer.*

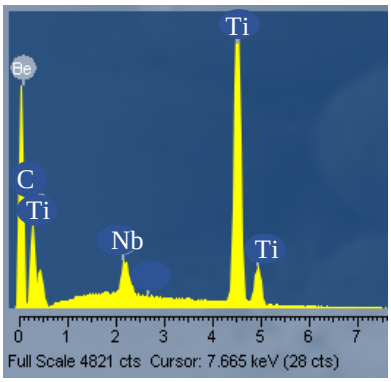

Figure 4.6. *EDX spectrum recorded from the β-Ti sample after the CVD indicating the presence of titanium and carbon elements.*

In order to improve the properties of titanium, not only the presence of a TiC layer but also the thickness of the layer is important. J. Yi *et al*. reported that the TiC layer with a thickness of 2-3 µm is sufficient to improve the biocompatibility of titanium. Another

study reported the necessity of at least a 3 μm thick TiC layer[51]. Hence, these values can be used as a guideline for a minimal thickness of TiC.

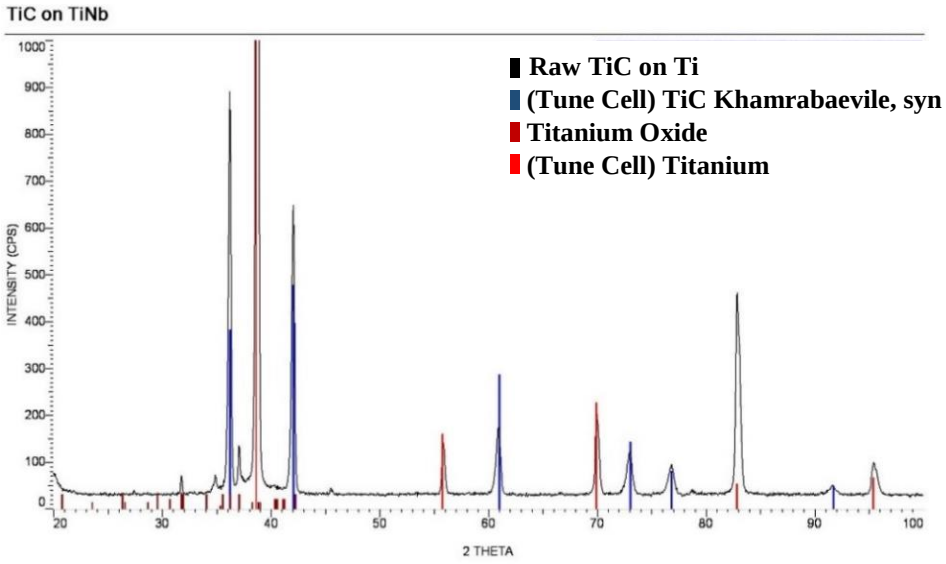

Figure 4.7. *XRD spectrum of β-Ti/TiC sample indicating the peaks of TiC presented in blue, the red peaks of titanium itself, and possible titanium oxide phase features indicated in purple with Cu cathode.*

FIB-machined cross sections were created in order to identify the thickness of the TiC layer. SEM images, shown in Figure 4.8, revealed that the thickness of the TiC layer for both α-Ti and β-Ti samples is around 6-7 μm that is sufficient for the improvement of the biocompatibility.

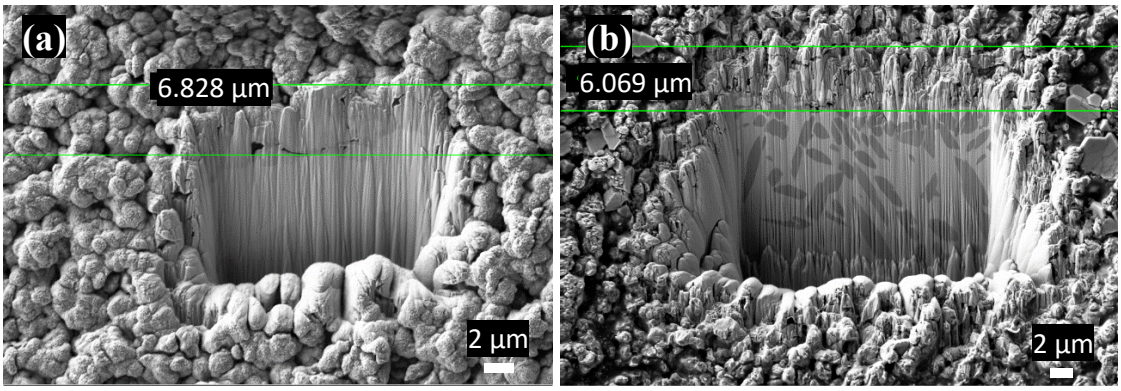

Figure 4.8. *Cross section of (a) α-Ti/TiC and (b) β-Ti/TiC samples, generated using FIB milling.*

It was found that the reaction temperature during the CVD has a strong influence on the formation of TiC layer. Figure 4.9 compares experiments performed at various temperatures. There is clearly no formation of a TiC layer at 900 °C (Figure 4.9a). At 950 °C, the first stage of TiC formation was observed (Figure 4.9b), but the layer is not fully developed across the sample. At 1000 °C and higher, the full formation of a TiC layer was observed (Figures 4.9c, d).

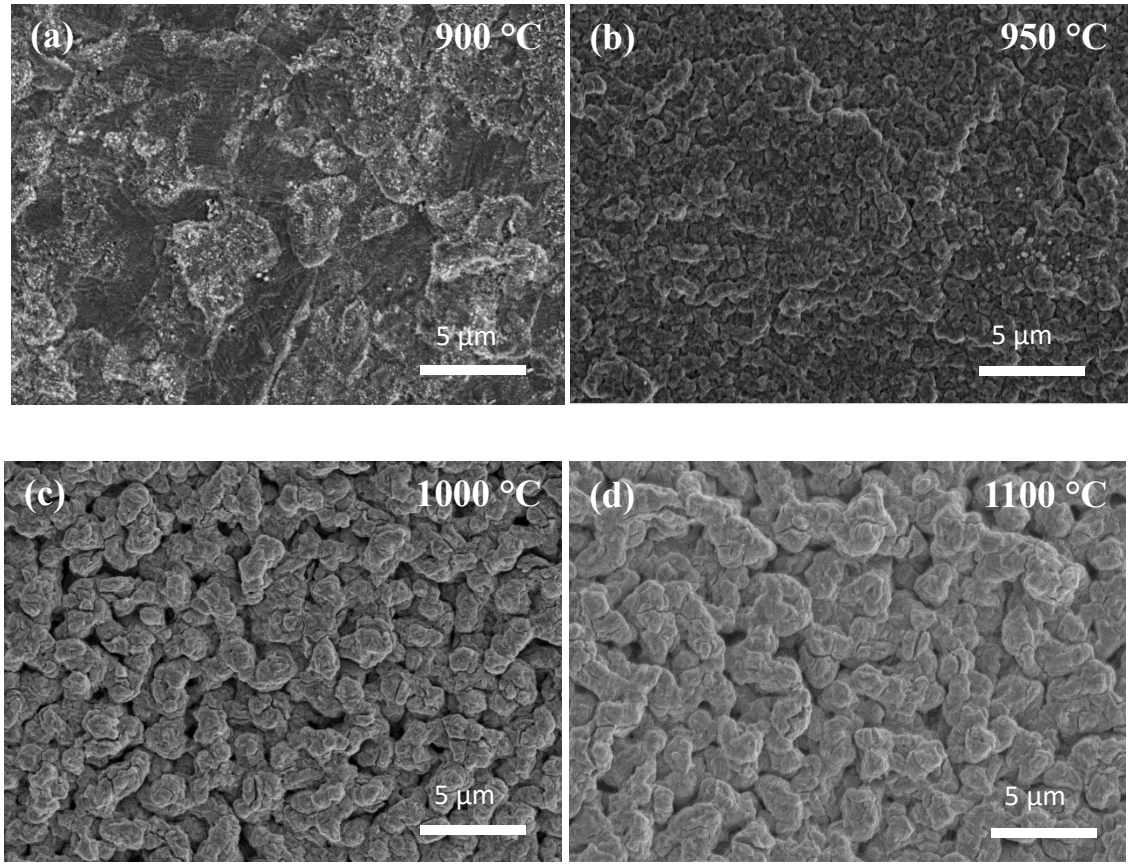

Figure 4.9. *Representative SEM images, showing titanium substrates after the CVD synthesis at different temperatures, revealing: (a) no TiC formation at 900 °C; (b) beginning of the formation of TiC at 950 °C; (c), (d) fully developed TiC layer at 1000 and 1100 °C respectively.*

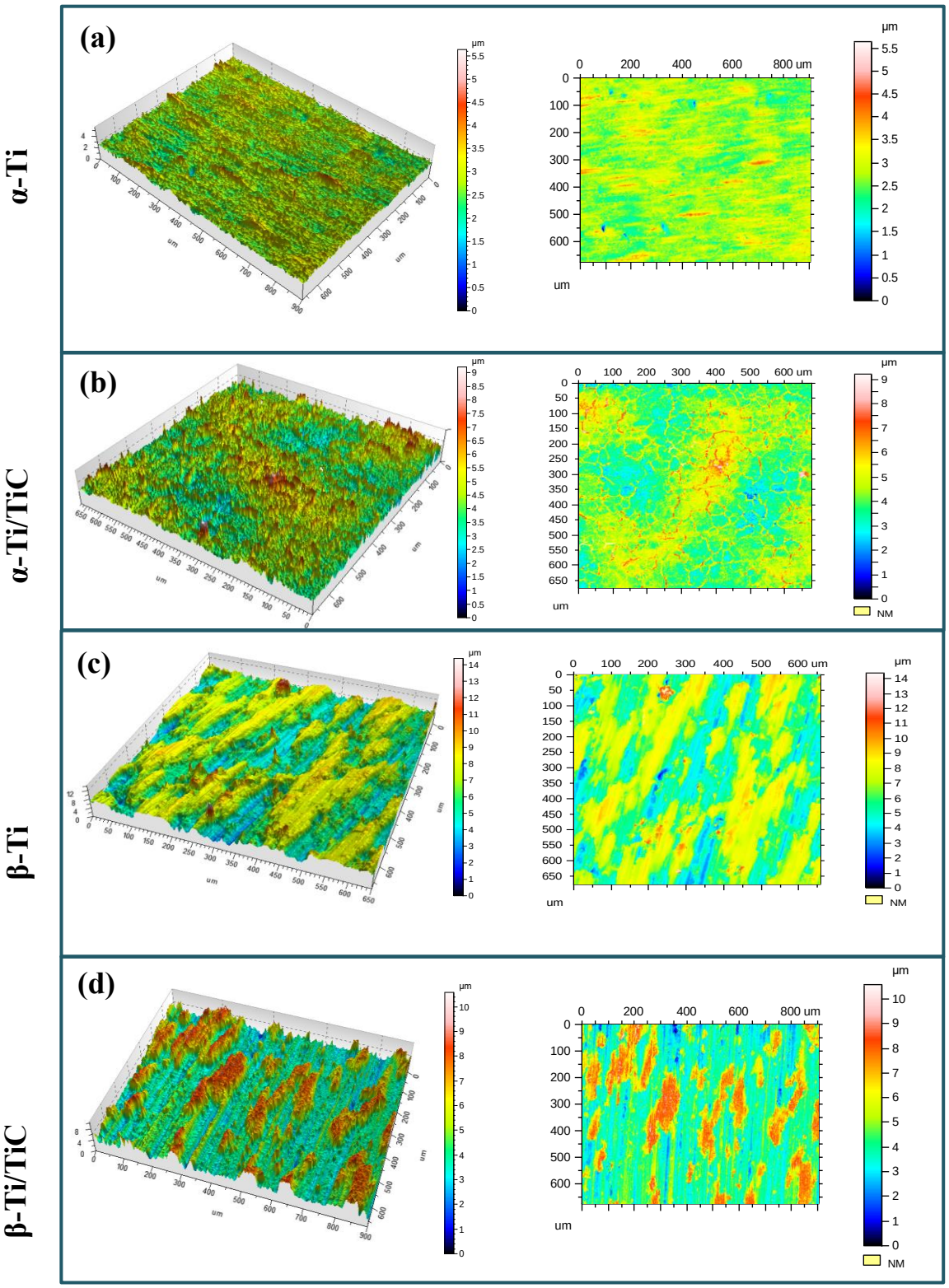

Figure 4.10. *Representation of the surface roughness of (a) α-Ti substrate before the CVD; (b) β-Ti substrate before the CVD; (c) α-Ti/TiC sample; (b) β-Ti/TiC sample, showing the increase in the surface roughness for both α- and β-Ti after the synthesis of TiC layer.*

It is known that the surface roughness has a strong influence on the biological properties of implants[179,180,55]. Enhanced osteoblast cell differentiation[179] and prolifferation[55] on rough vs. smooth titanium surfaces have been reported. Figure 4.10 shows the roughness profiles of α-Ti and β-Ti samples with and without a TiC layer. It was found that the surface of α-Ti samples with a TiC layer became twice rougher (Table 4.2). In contrast, the roughness of β-Ti with and without carbide is of the same order of magnitude (Table 4.2). Therefore, for β-Ti samples, the differences in the properties (*e.g.* corrosion resistance, biocompatibility) during further testing would not be associated with the differences in the surface roughness of samples.

Table 4.2. *Comparison of the values of the surface roughness of α-Ti and β-Ti substrates with and without TiC layer.*

	α-Ti	**α-Ti/TiC**	**β-Ti**	**β-Ti/TiC**
R_a, µm	0.209	0.481	1.038	1.008
Std Deviation	0.031	0.066	0.192	0.186

TiC was successfully synthesized on both α-Ti and β-Ti substrates and has a potential to improve their corrosion resistance, mechanical and biological properties. Therefore, further studies were centred on the evaluation of these parameters.

4.3.2. Evaluation of the Ti/TiC samples

Before moving to the biological evaluation of the TiC layer, it is important to satisfy other requirements for implant materials such as their mechanical stability and good corrosion resistance. It is well known that α-Ti and β-Ti have low Young moduli and excellent corrosion resistance. However, modifying the surface of the metal could potentially change the mechanical and corrosion behaviour. Additionally, as mentioned in the Introduction, titanium alloy implants tend to oxidize with time in the physiological environment and reduce corrosion resistance. Therefore, mechanical and corrosion properties of samples with a TiC layer should be analysed and ideally have better properties, in particular, better corrosion resistance.

Corrosion resistance

In order to evaluate the corrosion resistance of the samples, electrochemical corrosion tests were performed. Figure 4.11 illustrates the polarization curves on a logarithmic scale (Tafel plots) for α-Ti/TiC and β-Ti/TiC samples in comparison with titanium samples without a TiC layer. All the anodic polarization curves showed the same trend, typical for a passive character. Ti samples with and without TiC (Figure 4.11a) show the same trend and only β-Ti substrates have a sharp peak (Figure 4.11c). The polarization curves of α-Ti/TiC and β-Ti/TiC samples are shifted towards the anodic region, qualitatively suggesting a slight improvement in the corrosion resistance. The values of the corrosion potentials (Ecorr) and the corrosion current densities (Jcorr), are listed in Table 4.3.

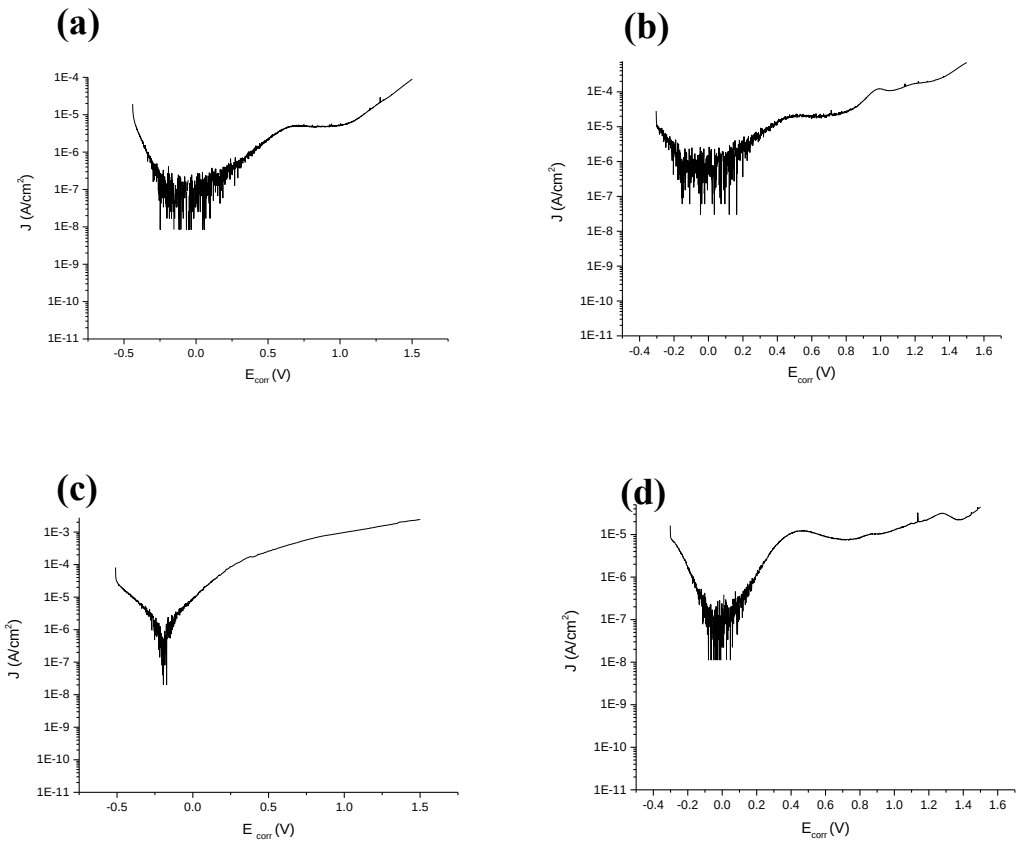

Figure 4.11. *Potentiodynamic polarization curves in Hank's solution at 37.5 °C of (a) samples α-Ti, (b) α-Ti/TiC, (c) β-Ti, (d) β-Ti/TiC samples, showing similar trend for all the samples. α-Ti/TiC and β-Ti/TiC samples are shifted towards the anodic region that indicates a slight improvement in the corrosion resistance after coating with TiC.*

Table 4.3. *Values of corrosion potential (Ecorr) and corrosion current density (Jcorr) of α-Ti/TiC and β-Ti/TiC samples compared with uncoated α-Ti and β-Ti substrates showing a slight increase of corrosion potential for α-Ti/TiC β-Ti/TiC samples in comparison with uncoated samples.*

Sample	Ecorr (V)	Jcorr (A/cm2)
α-Ti uncoated	-0.067	8.48×10^{-8}
α-Ti/TiC	0.034	3.05×10^{-8}
β-Ti uncoated	-0.194	2.03×10^{-8}
β-Ti/TiC	-0.018	1.13×10^{-8}

Zeta potential measurements of β-Ti and β-Ti/TiC samples

Since β-Ti/TiC samples showed improved corrosion resistance and lower Young's modulus in comparison with other samples their properties were analysed further. Bare β-Ti was used as a reference material. Figure 4.12 shows the comparison of the zeta potential for β-Ti and β-Ti/TiC samples, calculated using streaming current measurements with equation (1) and streaming (apparent) potential with equation (2). At the native pH 6 in 0.001 mol/1, KCl solution, both β-Ti and β-Ti/TiC samples were found to be negatively charged.

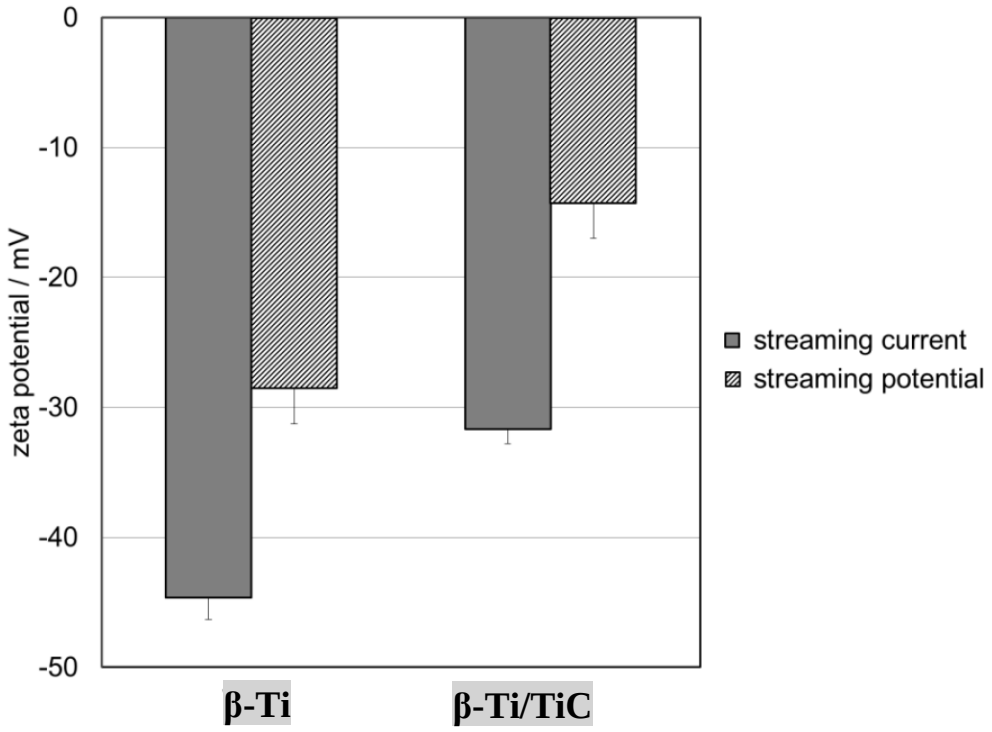

Figure 4.12. *Comparison of the zeta potential obtained from the streaming current and streaming potential measurements for β-Ti and β-Ti/TiC at pH 6 showing the negative zeta potential values for both samples and revealing the difference in the valued calculated by streaming current and streaming potential*[178].

A significant difference was observed for zeta potential measurements calculated from the streaming current Eq.1 and streaming potential Eq.2. This difference can be explained

by the fact that zeta potential values obtained through the streaming potential are related to the electrolyte conductivity and the conductivity of the material. Assuming that the conductivity of titanium is zero, zeta potential values calculated by both methods are identical. However, metals are conductive, and their conductivity needs to be added to the conductivity of the electrolyte solution, which causes the difference in values. In Figure 4.12 it is shown that β-Ti ζ = -44.7 ± 1.7 mV and for TiC/β-Ti ζ = -31.7 ± 1.1 mV. While calculating the zeta potential from the streaming potential, an even greater difference was observed for β-Ti ζ = -28.5 ± 2.7 mV and TiC/β-Ti ζ = -14.3 ± 2.7 mV. This effect has a higher influence for β-Ti/TiC (45 %) than β-Ti (64 %) samples, which can be explained from the additional conductance from the surface layer.

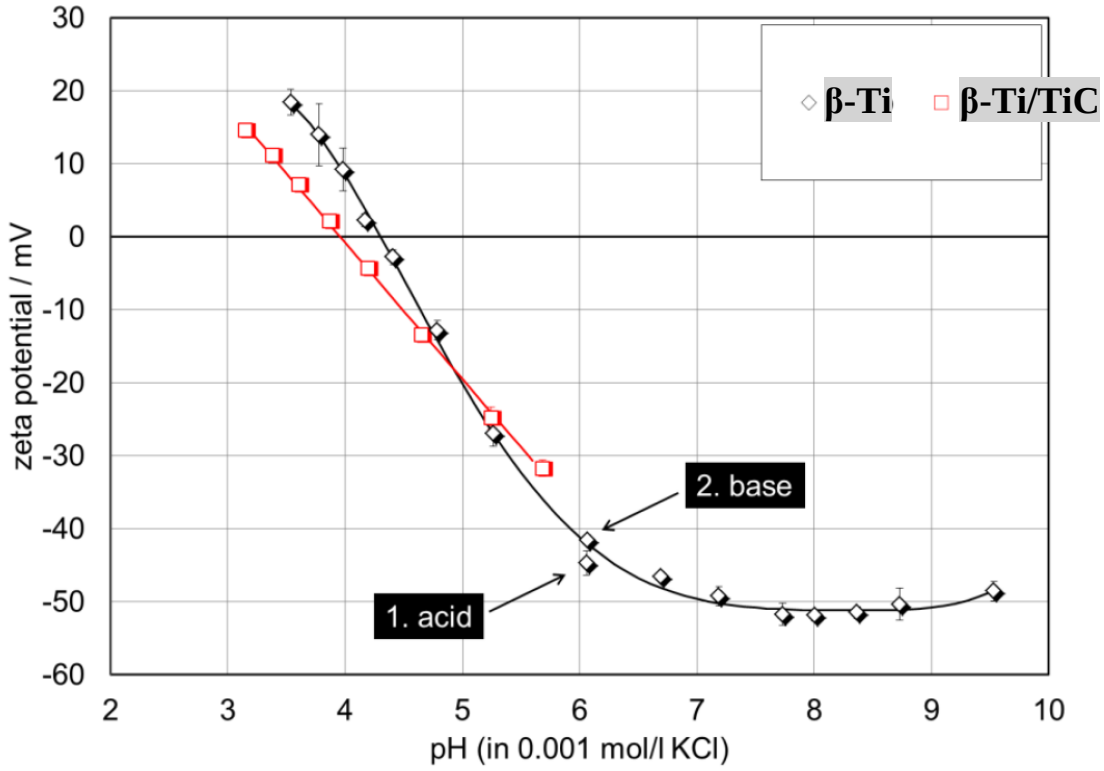

Figure 4.13. *pH dependence of the zeta potential for β-Ti and β-Ti/TiC samples from which the isoelectric point of 4.0 for β-Ti/TiC and 4.3 for β-Ti was determined. The starting values of the zeta potential for individual titration of β-Ti sample with acid and base are also indicated on the graph.*

Zeta potential measurements at different pH were also performed in order to determine the isoelectric point (IEP). The IEP is the pH at which the zeta potential and the total charge density become zero. Figure 4.13 shows the dependence of the zeta potential on the pH in the range of pH 3-9. From the graph, the isoelectric point (IEP) was determined. It is not dependent on the metal conductance and hence can be correctly calculated by the streaming potential measurements. For β-Ti samples, the IEP was determined at pH 4.3 and for β-Ti/TiC at pH 4.0. β-Ti samples at higher pH values (7-9) reach a plateau, which is likely to be linked with the amphoteric behaviour of a native oxide layer of β-Ti specimens. A study by Jirka *et al.* reported a similar value of the zeta potential for β-Ti at neutral pH, but a more acidic IEP at pH 3.4[182]. It can be correlated with the fact that several different oxides were formed on β-Ti. The IEP of β-Ti/TiC at pH 4 indicates an inert behaviour of the sample, which is good for biomaterial. The zeta potential of β-Ti/TiC samples was measured for the first time in this study; hence reference data are not available. However, the reported, almost linear dependence of the zeta potential on the pH was also found for a diamond-like carbon coating on a silicon oxide substrate[183].

The evaluation in this Section of the corrosion resistance, mechanical properties and zeta potential of α- and β-titanium substrates with a TiC coating showed a slight improvement of corrosion resistance, a comparable Young's modulus and hardness, and inert behaviour of β-Ti/TiC samples. Hence, the next step is to evaluate the biocompatibility of these samples.

4.3.3. Biocompatibility tests of TiC coatings

4.3.3.1. Techniques for biological investigations

α-Ti/TiC and β-Ti/TiC samples were produced in Chapter 4 with dimensions of 10x10 mm^2. Details regarding the samples can be found in Section 4.2. As the reference materials, only α-Ti substrates and not β-Ti were used due to the limited availability of the β-Ti substrates at the time of the experiments. The same cell culture and procedure as in Chapter 3 were used. A detailed description is presented in Section 3.2. In order to obtain a comprehensive picture of cell behaviour on Ti-based samples, the following parameters were chosen to be examined: metabolic activity; cell morphology and attachment; cell survival and mineralization. The techniques used to obtain this information are listed in Table 4.4.

Table 4.4. *Summary of cell culture techniques used to analyse cell behaviour on Ti-based alloys and the resulting information that is obtained while using each method.*

Technique	Information
Live/Dead kit	Number of cells survived
AlamarBlue	Metabolic activity and proliferation
OsteoImage	Hydroxyapatite Nodules

Live/dead assay

LIVE/DEAD viability/cytotoxicity kit for mammalian cells (Invitrogen, Molecular Probes, Cat. No. L3224) was used to determine the number of cells seeded on Ti-based samples that survived after day 1 and 3. fHobs were incubated in a solution with two fluorescent probes for 5 - 10 min at 37 °C in a humidified air atmosphere containing 5 %

of CO_2. One probe determines the number of live cells (calcine AM producing green fluorescence) while the other identifies dead cells (ethidium homodimer-1 emitting red fluorescence). Afterwards, cells were imaged using a Leica DMRXA2 fluorescence microscope with Retiga colour camera and Image Capture Pro software.

Metabolic activity

Metabolic activity was investigated using AlamarBlue® assay (AbDSerotec). The assessment was performed following the manufacturer's protocol as described in Section 3.3 using the fluorescence plate reader FLUOstar Optima (BMG Labtech, Offenburg, Germany).

Matrix mineralization

Osteogenic medium was added from day 16 with the purpose of evaluating the mineralization. The osteogenic media consisted of DMEM-low glucose medium supplemented with 10 % (v/v) foetal bone serum (FBS), 1 % (v/v) penicillin-streptomycin (10.000 units/mL penicillin and 10 mg/mL streptomycin), and 30 μg/mL of vitamin C plus 200nM hydrocortisone and 2mM β-glycerophosphate. For mineralization assessment, OsteoImage™ Mineralization Assay (Lonza, Walkersville, USA) was used according to the manufacturer's protocol. The working principle of this assay is the binding of fluorescent staining reagent to the hydroxyapatite deposited by the bone cells. At the 14th day in the culture medium, fHob cells were fixed with 4 % formaldehyde in PBS for 15 min at room temperature and stained with the staining reagent (1:100 in staining reagent dilution buffer) for 30 min at room temperature, protected from light. Samples were washed with the washing buffer, mounted with Fluoroshield antifade mountant containing 4', 6-diamidino- 2- phenylindole (DAPI) (Vector Laboratories) to stain cell nuclei, and imaged using a Leica DMRXA2 fluorescence microscope.

4.3.3.2. Cell culture studies of Ti/TiC samples

Live/dead assessment

A live/dead assay was used to see how many dead, and live cells are in the sample. Figure 4.14 shows fluorescence images of fHob's cells stained with live/dead assay attached to the Ti/TiC samples and α-Ti after 24 and 48 hours after seeding. A high number of live cells (stained green) and very low number of dead cells (stained red) was observed for all samples. The cell density slightly increased between 24 and 72 hours. This increase confirms a good viability of fHob's cells on both α-Ti/TiC and β- Ti/TiC samples.

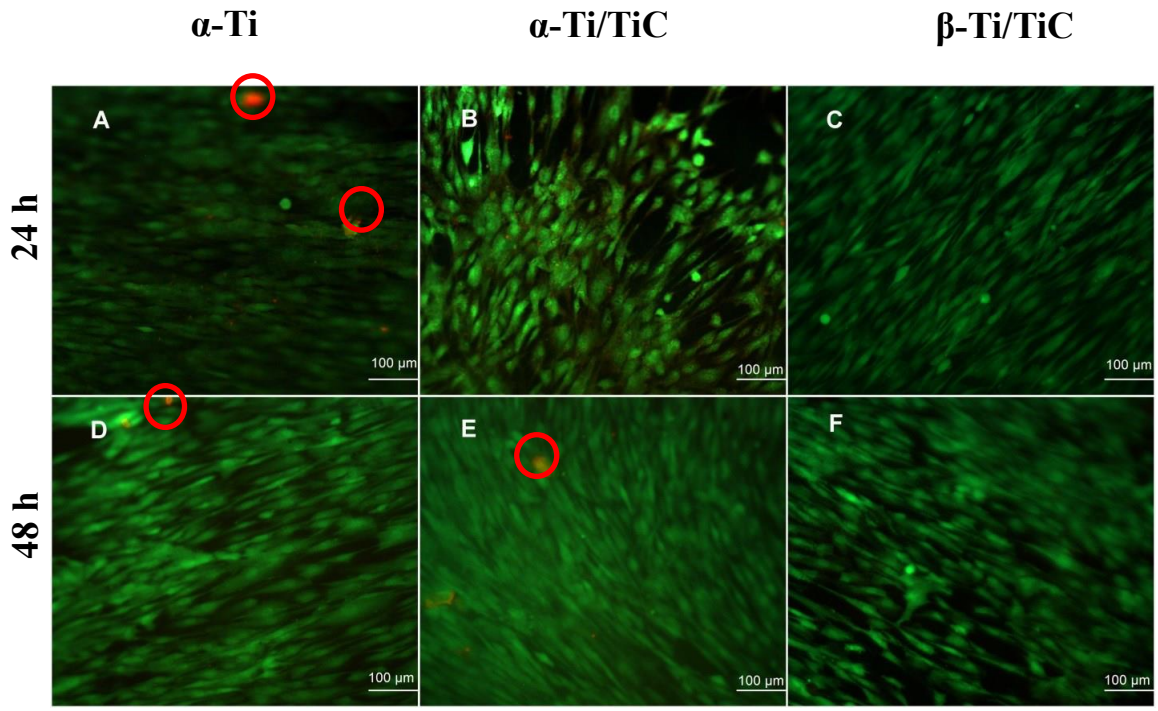

Figure 4.14. *Typical fluorescence micrographs illustrating the viability of fHob's cells after 24h and 48h days of culture on α-Ti, α-Ti/TiC, and β-Ti/TiC. Live cells are shown in green and dead cells are circled in red.*

Metabolic activity

For all the samples culture, the medium was changed and collected on day 1, 3, 6, 9, 12, 14, 16, 21, 25, and 29. The collected medium was assessed using alamarBlue assay to define the metabolic activity and cell proliferation.

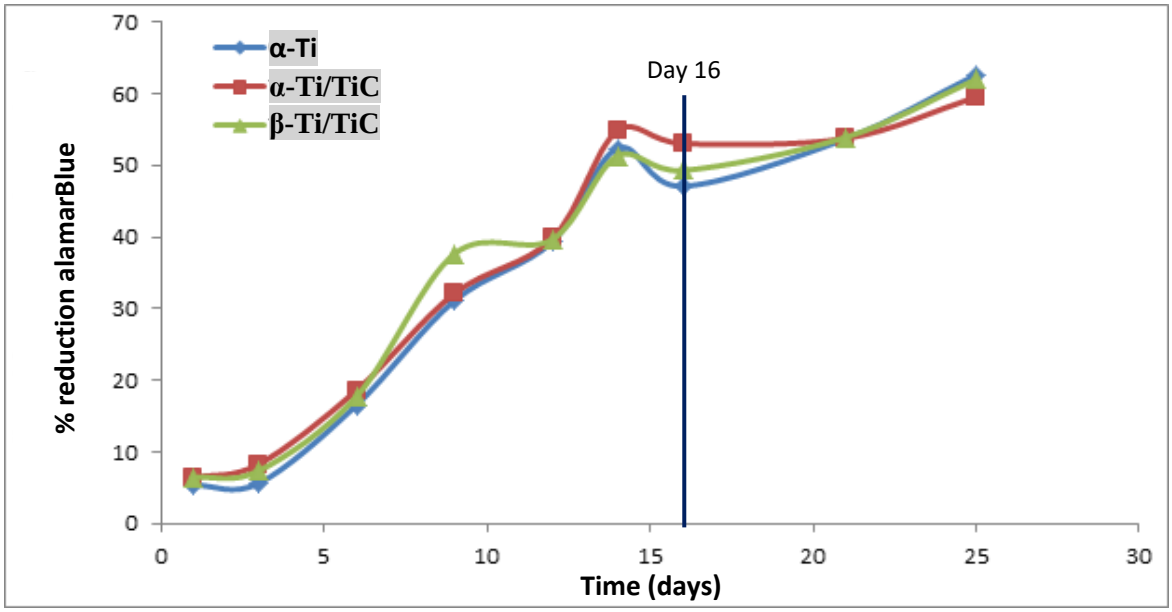

Figure 4.15. *Metabolic activity of fHob's seeded onto Ti-based materials at different time point up to 25 days; (up to day 16-normal growth medium, for day 16-25 with an addition of osteogenic media). Data are shown as mean ± SD at different time points, n=3.*

In Figure 4.15 the relation between the reduction of alamarBlue and the time of culturing, which corresponds to the typical cell culture behaviour is presented. It consists of the initial lag phase during 24 - 72 hours, log growth phase and the decrease of metabolic activity. The awaited reduction of metabolic activity in the graph is not present due to the addition of osteogenic medium on day 16, and hence, the metabolic activity is higher than expected. During the studies, no significant difference between non-treated Ti samples and the one with TiC coating was observed. Therefore, it is possible to conclude that there is no adverse effect of TiC on the metabolic activity of fHob's cultures.

Osteoblasts mineralization

Since the osteoblast cells were successfully grown on Ti/TiC samples, more detailed examination of the cells' activity was performed. Deposition of apatite mineral is an important characteristic of osteoblast growth since it is an indicator of osteoblast differentiation. Osteoblast differentiation was detected by staining on day 25 with an OsteoImage™ Mineralization kit. For the first 15 days, fHob's were cultured without the addition of an osteogenic medium and from day 16 an osteogenic medium containing hydrocortisone and β-glycerophosphate was added.

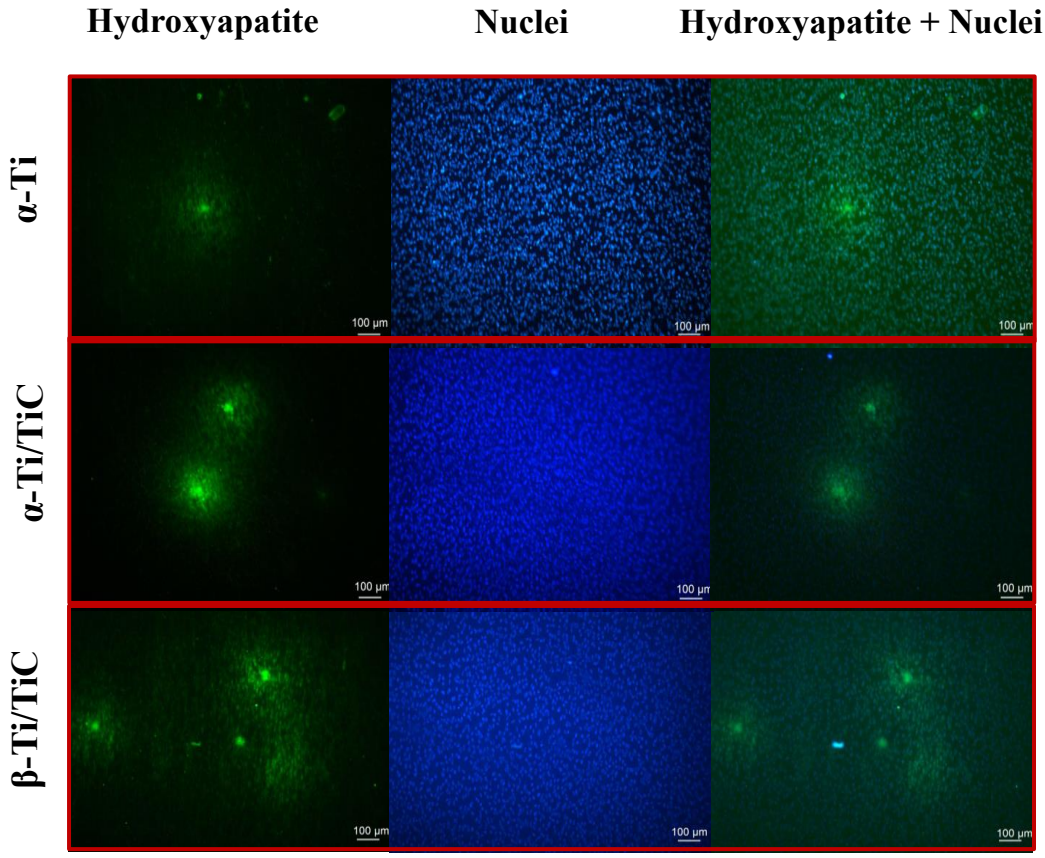

Figure 4.16. *Images of osteoblast mineralization when in contact with α-Ti; α-Ti/TiC; β-Ti/TiC; hydroxyapatite mineral is shown in green and cell nuclei in blue. The final column of images is a composition of the two colours.*

In summary, cell culture studies performed on Ti/TiC samples showed good cell attachment with a high number of viable cells and very low number of dead cells. The typical metabolic activity of osteoblast cells and slightly increased mineralization was also observed.

4.4. Conclusions

In this Chapter, the deposition of a TiC layer on the substrates was shown to be a promising method to improve the properties of the Ti-based implant material. The characterisation of a TiC layer synthesized with simple atmospheric pressure CVD techniques was performed. In the literature, the magnetron sputtering technique is most commonly used for TiC deposition[174,175]. However, in this Chapter, it was shown that it is possible to grow TiC layers on both α-Ti and β-Ti substrates with the more simple CVD method, which has advantages of being quicker, cheaper and easier to scale up compared to magnetron sputtering and other methods mentioned in Section 4.1. The TiC layer forms a strong connection with the titanium substrate, improving the implant-substrate adhesion by reducing implant loosening, which is currently a significant problem in orthopaedics[184,1]. Up until now only the synthesis of a TiC layer on α-Ti and α+β-Ti substrates were performed[51,185]. Since β-Ti possess a number of advantages for its use as an implant material, such as lower Young's modulus, the absence of toxic elements, *etc.*, the growth TiC on β-Ti samples is a significant step forward towards better titanium implants. It is important to mention that an equally thick layer of TiC formed on Ti alloys with different compositions (α-, β-). This indicates that the synthesis process can be extrapolated to any Ti-based alloy, which has a benefit for any future commercial use.

The evaluation of Ti-based samples covered with a TiC layer showed good corrosion and mechanical properties. No significant increase in Young's moduli and similar hardness values were observed for Ti/TiC samples. For β-Ti/TiC samples, improved corrosion resistance in comparison with bare β-Ti has been reported. The zeta potential was determined for β-Ti and β-Ti/TiC samples and is negative for both samples at neutral pH. Additionally, the isoelectric points of β-Ti and β-Ti/TiC, respectively, were identified

from the zeta potential titration to be at pH 4.3 and 4.0 respectively and revealed the inert behaviour of the β-Ti/TiC samples.

Biological studies using foetal osteoblast cells were performed on Ti/TiC samples and showed good cell response. Good short term attachment after 24 hours, identifying a high number of viable cells and a very small number of dead cells was observed, using the Live/Dead kit. The long-term behaviour of the cells, up to 29 days, was also good. The metabolic activity of the osteoblasts on Ti/TiC samples showed typical behaviour for a biocompatible implant material. It showed the initial increase of activity during 24-74 hours, further moderate increase and the decrease of metabolic activity up to day 16 when the osteogenic medium to measure the mineralization was added, and then increased activity again. The mineralization on titanium samples with a TiC layer slightly increased in comparison to titanium without the layer. Other studies did not report improved mineralization, but better surface stability and improved osseointegration through the improved bone growth were observed[50]. Additionally, a definite increase in osteoblast growth rate and differentiation, and a better and stronger anchorage of the cells to the coated substrates has been reported[185]. However in the studies presented in this Chapter, only a good biocompatibility of Ti/TiC samples can be concluded, similarly to the study by K. Balázsi *et al*[175].

Chapter 5. CNTs growth on various Ti-based substrates without additional transition metal catalysts

5.1. Background

A traditional method for the CVD carbon nanotubes growth involves the presence of transition metal catalysts such as Fe, Co, and Ni. The MWCNTs investigated in Chapters 2 and 3, were grown on titanium substrates with a Fe-based catalyst. The toxicity of CNTs is currently still under debate, and one of the possible reasons for their toxicity is the presence of transition metals catalyst particles in the nanotube itself, which could be released in human tissue[1,2]. Chapter 3 showed a poor biocompatibility of β-Ti/MWCNTs and MWCNTs themselves, and the metal catalyst could be a potential cause. Therefore, it is important to investigate whether CNTs can be grown without an additional transition metal catalyst. If such CNT growth is possible, the suspected, catalyst-associated toxicity and resulting poor biocompatibility might be eliminated or, at least, be lowered to a certain extent.

The growth of CNTs on a titanium substrate without an external catalyst has been the subject of numerous studies. Several researchers have reported the catalytic activity of titanium for CNTs growth[186,79,128]. All experiments were performed on commercially pure α-Ti. No substrates with other elemental compositions were investigated. As mentioned in Chapter 1, β-Ti alloys have a number of advantages for biomedical use such as low Young's modulus; excellent mechanical properties; and the absence of the toxic elements.

Therefore, it is important to look at the possibility of non-catalytic CNTs growth not only on pure (α-) titanium but also on β-Ti alloys.

While the mechanism of MWCNTs growth on titanium substrates using metal catalyst was discussed in Chapter 2, removing the catalyst from the reaction will certainly have some implications on the synthesis parameters. A number of factors has a strong influence on CNT growth: (a) the type of catalyst, (b) the kind of substrate (support material), (c) the type of precursor to generate carbons, and (d) synthesis conditions (temperature, gas additives, duration of the reaction). In order to achieve MWCNTs growth on titanium substrates without an additional metal catalyst, it is necessary to take into account all these factors.

(a) The choice of an appropriate catalyst is critical for achieving CNTs growth. Recently, a number of alternatives to the traditional transition metal catalysts for CNTs formation was discovered, which can be divided into two main groups. The first group includes non-transition metals such as Pt; Pd; Mn; Mo; Cr; Sn; Au; Mg; Al, the biocompatibility of which is not still proven and some toxic effects have been reported[187,188]. The second group contains so-called metal-free catalysts, including metal oxides and carbides, which are of particular interest in this Chapter. Widely-used metal-free catalysts are ceramics such as SiC and Al_2O_3. CNTs were first grown from SiC back in 1997[189]. Later, porous Al_2O_3 also proved to initiate CNTs formation[4,5]. Si, Ge[78], and nanodiamond[192] nanoparticles have also been reported to act as a catalyst. Additionally, various oxides were found to possess catalytic activity. Amongst these are metal oxides, which do not exhibit catalytic activity in the pure metal form (e.g. ZnO_2 [8,9], MgO [194], $SrTiO_3$ [129]), and non-metallic oxides (e.g. SiO_2 [195–199]). Oxygen is considered to play a crucial role in the CNTs formation, however, whether it is a catalyst itself remains a question[75]. SiO_2 is the most widely reported non-metal catalyst for the CNTs growth. Nevertheless,

investigations have suggested that CNTs are instead growing from SiC [91,186,200], which might be formed from SiO_2 under carbo-thermal reduction[201]. It is challenging to grow CNTs with titanium as a catalyst, since it is a poor catalyst due to the number of various titanium carbides formed and a strong Ti-C bond. However, oxygen was reported to weaken the Ti-C bond, and this might be a reason why recent publications indicated that the Ti and TiO_2 layer might be able to act as a catalyst for CNTs formation[77,128]. It was suggested from X-ray Photoelectron Spectroscopy measurements that TiO_2 nanoparticles are responsible for the CNTs growth, and that by varying the size of the TiO_2 nanoparticles it is possible to control the diameter distribution of CNTs. TiO_2 nanoparticles can be produced either by a sol-gel method or by sputtering of metallic Ti onto the Si wafer, which results in its further oxidation[79]. Taking into account the information presented above, all CNTs syntheses in this Chapter were performed without an additional metal catalyst, so that the possibility of titanium acting as a catalyst itself could be investigated.

(b) For the successful growth of CNTs not only the choice of the catalyst but also the substrate (support material) should be considered. There is a number of aspects, which should be considered while choosing a substrate: (i) the *composition* of a substrate (the elements of which the substrate consists) and (ii) the *form* of a substrate (bulk, powder, etc.). (iii) The *surface* of the substrate is also important, including the surface finish, roughness, etc. No previous studies have examined the influence of all these factors together on the growth of CNTs.

(i) Since different forms of titanium substrates can be used for CNTs growth, the first step in this Chapter was to define the optimal substrates for nanotubes growth. S. Sirivisoot *et al*. reported the growth of CNTs on anodized pure α-Ti without additional transition metal catalyst[67]. However, the paper does not contain substantial evidence that any CNTs were

grown. Hence, it is indeed doubtful that CNTs were formed on anodized Ti without catalyst, as claimed by the authors. More discussion regarding the validity of this study can be found in Section 5.3.1.1.

(ii) TiO_2 nanoparticles are another form of titanium that was reported to initiate CNTs growth[77]. Hence, in order to verify all previous claims of CNTs growth on various titanium substrates, in this Chapter bulk, anodized and titanium powder substrates were chosen, which will be described in Section 5.2.2. The results of CNTs growth on these different forms of titanium substrates are summarized in Section 5.2.3.1.

(iii) The surface of titanium substrates is also important for CNTs formation. Therefore, the next step was to find an appropriate surface modification for CNTs growth. In order to initiate CNTs growth without an additional metal catalyst, it is necessary to create reaction sites on the surface of titanium. Therefore, a great deal of attention is focused on surface modification of titanium surfaces to initiate the MWCNTs formation and make titanium act as a catalyst. It is necessary to pay attention to surface morphology and texture properties of the substrates, in particular, its surface roughness. The influence of surface roughness on CNTs growth was observed on stainless steel (SS) substrates without additional catalyst. With a roughness of 60 nm, mainly CNTs were formed, while, on the surfaces with higher roughness, CNFs formation was observed[202]. V. Khavrus *et al.* illustrated the influence of surface roughness of Al foils on the alignment and adhesion of CNTs[203].

There is a number of methods available to alter the surface roughness of the material, which include: mechanical scratching, mechanical polishing, acid treatment, Piranha solution treatment, *etc.* In the work of J. Sun *et al.*, it was shown that mechanical scratching of metals helped to form reaction sites leading to CNTs formation[129].

Mechanical polishing is another widely used method to alter the surface roughness[202]. Acid treatment including HF treatment[67] and sulphuric acid (H_2SO_4)[203] are also commonly used methods. HF or HF/HNO_3 treatment of Ti is also used to modify the surface roughness for better cell adhesion[26,27]. Hence, it can be also used to improve CNTs growth. Additionally, Piranha solution etching of Ti alloys, in particular, CP Ti[205], Ti-6Al-4V[206] and recently Ti-45Nb[207] was reported. Mechanical scratching, mechanical polishing, HF, and Piranha solution treatment methods were used in this Chapter to initiate the CNTs growth on titanium substrates. The influence of these techniques on titanium substrates is discussed in Sections 5.3.1.2 and 5.3.1.3.

(c) An appropriate carbon precursor for CNTs syntheses should be also chosen. The structure of the carbon precursor influences the morphology of the CNTs growth. Linear hydrocarbons such as methane and acetylene usually produce straight hollow CNTs. Meanwhile, cyclic hydrocarbons, such as toluene and benzene, produce relatively curved CNTs with tube walls often bridged inside[76, 208]. In this Chapter, in order to achieve CNTs growth without an additional metal catalyst two different precursors: methane and acetylene were used. Experiments using these precursors are presented in Section 5.3.

(d) Besides the substrate, catalyst and precursor, there is still a number of parameters that influence the CVD syntheses, which are vital to achieve CNTs growth without additional catalyst. Main parameters include temperature, additives (e.g. oxygen, hydrogen); and reaction time. It is essential to find an optimal temperature for the CVD synthesis. If the temperature is too low, the carbon precursor will not fully dehydrogenate, and if the temperature is too high, the precursor can self-dissociate in the gas phase and forms amorphous carbon and other compounds instead of CNTs. A reduction with hydrogen or oxidation with oxygen or water can influence the chemical state of the catalyst particle, and it can improve or prevent CNTs formation. In this Chapter, in order to identify the

optimal parameters for CNTs growth on titanium substrates, the syntheses with different reaction temperature, annealing and reaction time were performed. These findings are presented in Section 5.3.1.3.

Interestingly, the growth conditions applied in this Chapter revealed the growth of new titanium nanostructures. These nanostructures had some resemblance to the CNTs and hence they have been investigated in further detail to determine whether there is potential for improving the titanium implants. Toluene, methane, and acetylene were used as precursors for the growth of new nanostructures. Additionally, the influence of the reaction time, temperature, and annealing on the growth of titanium nanostructures is also discussed. The results are presented in Section 5.3.

5.2. Experimental Details

5.2.1. Experimental parameters

The growth of CNTs on titanium substrates, discussed in this Chapter, was performed using an atmospheric pressure CVD technique. The set up was identical to the one used and described in Chapter 2. Three different precursors were used for CVD syntheses and their structural formulas are presented in Figure 5.1.

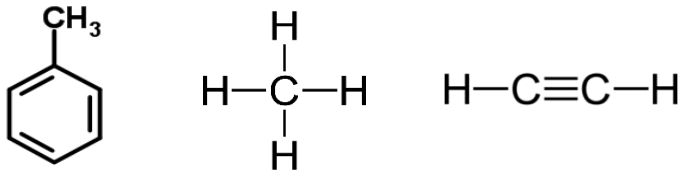

Toluene Methane Acetylene

Figure 5.1. *Structural formulas of carbon precursors: toluene, methane, and acetylene used for CNTs syntheses in Chapter 5.*

CVD experiments with a methane precursor were performed in an argon (Ar) atmosphere with a flow of 250 sccm. When the furnace reached the reaction temperature, 50 sccm of hydrogen (H_2) gas was introduced in addition to the Ar to reduce the amount of oxygen in the system and anneal the sample. A standard annealing time was 30 min. Afterwards, 50 sccm of methane was introduced for 15 min in addition to the Ar and H_2 gasses. Then the hydrogen and methane supplies were closed, and the furnace was cooled down under 250 sccm of Ar. Different reaction temperatures from 650 to 850 °C were used.

During the experiments with acetylene as a carbon precursor, the same heating, annealing and cooling procedures were followed, only 50 sccm of acetylene was used instead of

methane. Reaction times were 10, 15 and 20 min, and a wide temperature window between 645 and 900 °C was chosen.

For the experiments with toluene as a precursor, again Ar was used as a carrier gas, but with a flow of 200 sccm. As soon as the desired temperature was achieved, the Ar flow was increased up to 2000 sccm, and a toluene aerosol was introduced. Reaction times were 10 and 15 min, and two different reaction temperatures were used, 700 and 800 °C.

5.2.2. Substrates used for CNTs growth

CVD experiments were performed on the different titanium substrates summarized in Table 5.1:

1) Bulk substrates: commercially pure CP Ti foil (Alfa Aesar, 99.5 %) as a α-form and TiNb rod (ATI WahChang, Ti-45Nb wt. %) as a β-form;
2) Anodized substrates: anodized CP Ti;
3) Powder substrates: titanium dioxide (TiO_2) nanoparticles.

Table 5.1. *Substrates for CNTs growth without an additional metal catalyst.*

Code	**Substrate**	**Type of alloy**
α-Ti	CP Ti foil	Alpha
β-Ti	Ti-45Nb rod	Beta
TiO_2 NP	TiO_2 nanoparticles	Alpha
Anodized α-Ti	Anodized CP Ti foil	Alpha

Bulk α-Ti and β-Ti substrates were prepared in 10 mm^2 squares with the thickness of 0.25 and 0.5 mm respectively. α-Ti substrates were cut with a stainless steel cutter. β-Ti was cut with an electrical discharge machine (EDM) at the KU Leuven, Belgium (see description in Section 2.2) and cleaned by sonication with acetone and deionized water.

Anodized α-Ti substrates were produced by our collaborator Somayeh Abdi at IFW, Dresden (Germany) using 1M $(NH_4)_2SO_4$ and 0.25M NH_4F electrolyte at a potential of 20 V for 3 hours.

Bulk substrates underwent various surface modifications: mechanical scratching, mechanical polishing, acid treatment (HF), and Piranha solution treatment. Mechanical scratching was performed with a diamond pen. For mechanical polishing, SiC paper was used. 40 % and 10 % HF treatment were carried out on titanium substrates for 10 sec. For the etching of titanium substrates with Piranha solution, different ratios of its components, H_2SO_4 and H_2O_2, can be used. It was found that a 3:1 ratio was most efficient in obtaining a clean, smooth and hydrophilic layer on α-Ti in comparison with other ratios (1:3; 1:2; 1:1; 2:1; 4:1) [209]. Therefore, a 3 H_2SO_4 (98 %): 1 H_2O_2 (30 %) solution was used for the treatment of both α-Ti and β-Ti substrates.

5.2.3. Techniques for sample analysis

MWCNTs and other nanostructures grown during the CVD synthesis were investigated using a scanning electron microscope (SEM). Energy-Dispersive X-ray Spectroscopy (EDX) was used to identify the elemental composition of synthesized nanostructures and its distribution over the sample to evaluate the purity of substrates. The equipment used for both techniques is described in Section 2.2.3.

The X-ray Diffraction (XRD) technique was used to provide the necessary structural information about the arrangement of atoms in the crystals of nanostructures synthesized in this thesis. Measurements were performed by Dr. Phil Holdway, Oxford Materials Characterisation Services, Oxford, UK, using a Bruker D5000 XRD.

X-ray Photoelectron Spectroscopy (XPS) was used to identify and quantify the overall chemical composition of the Ti-based substrates, as well as to detect any impurities of the substrates and their concentrations. Additionally, the influence of Piranha treatment on the elemental composition of the Ti-based substrates was investigated by XPS. All XPS measurements presented in this thesis were performed by Dr. Alison Crossley, Oxford Materials Characterisation Services, Oxford, UK.

Contact angle measurements were performed to measure the wettability of different titanium substrates. Importantly, wettability was identified for Ti-based substrates after various surface treatments to monitor the changes of surface properties and understand how it influences further CNTs growth on those substrates. Dynamic contact angles of pure water were measured using a Rame´-Hart Inc. Goniometer and imaging software RHI2001 at the Department of Physical and Theoretical Chemistry, University of Oxford.

5.3. Results and discussion

5.3.1. MWCNTs growth without additional metal catalyst

This Section summarizes the results of MWCNTs grown without additional metal catalysts on titanium substrates, on a variety of substrates and under a range of reaction conditions. Section 5.3.1.1 presents results of the CVD syntheses on various titanium substrates to identify the most promising substrate for MWCNTs growth. Section 5.3.1.2 shows results of the CVD syntheses on the most promising substrates from 5.3.1.1, *i.e.* bulk α– and β-Ti, now treated with different surface modifications to induce better MWCNTs formation. Section 5.3.1.3 presents CNT syntheses on those substrates, now treated with the most successful surface modification from 5.3.3.2, *i.e.*, with Piranha solution, to investigate the improved MWCNTs growth.

5.3.1.1. Preliminary syntheses to define the optimal substrates for MWCNTs growth

In this Section bulk α-Ti, bulk β-Ti, anodized α-Ti, and TiO_2 nanoparticles (NP) were used as substrates in order to identify which form of titanium has the most potential for non-catalytic CNTs growth.

Bulk titanium substrates

In Chapter 2, MWCNTs with additional catalyst were successfully grown on bulk α-Ti and β-Ti substrates. Therefore, those substrates were the starting point for the investigations of non-catalytic MWCNTs growth.

α-Ti bulk substrates

A typical SEM micrograph showing the surface of the α-Ti substrate is shown in Figure 5.2a. EDX analysis (Figure 5.2b) of this sample was performed confirming the presence of titanium. No other elements, which could have been introduced while cutting the substrates with stainless steel cutter, were detected.

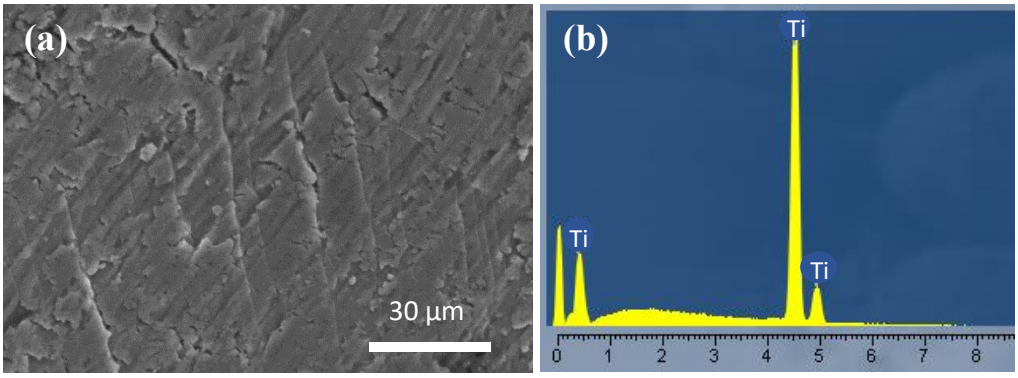

Figure 5.2. *(a) Representative SEM micrograph showing the surface of the bulk α-Ti substrate and (b) EDX spectrum indicating the presence of titanium.*

After CVD synthesis with a methane precursor at 800 °C, the formation of MWCNTs was revealed (Figure 5.3). Nanotubes were chaotically distributed across the sample. Unfortunately, MWCNTs growth under those conditions was not reproducible.

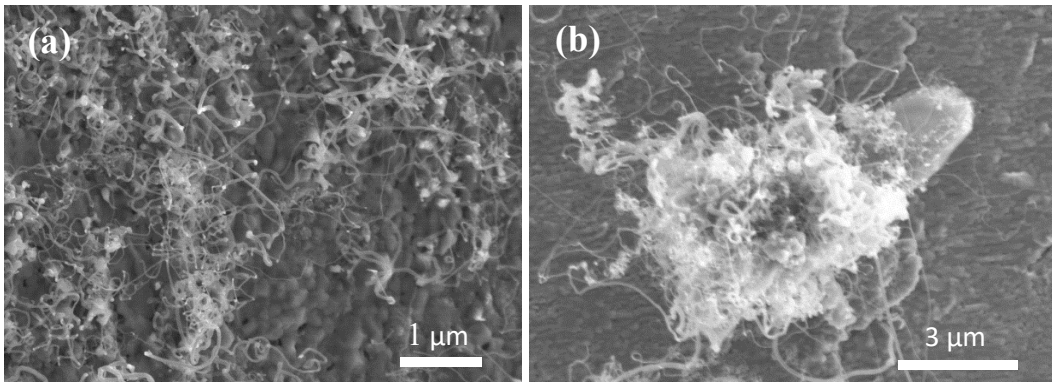

Figure 5.3. *SEM micrographs of MWCNTs synthesized by CVD technique with methane precursor on α-Ti substrates at 800 °C.*

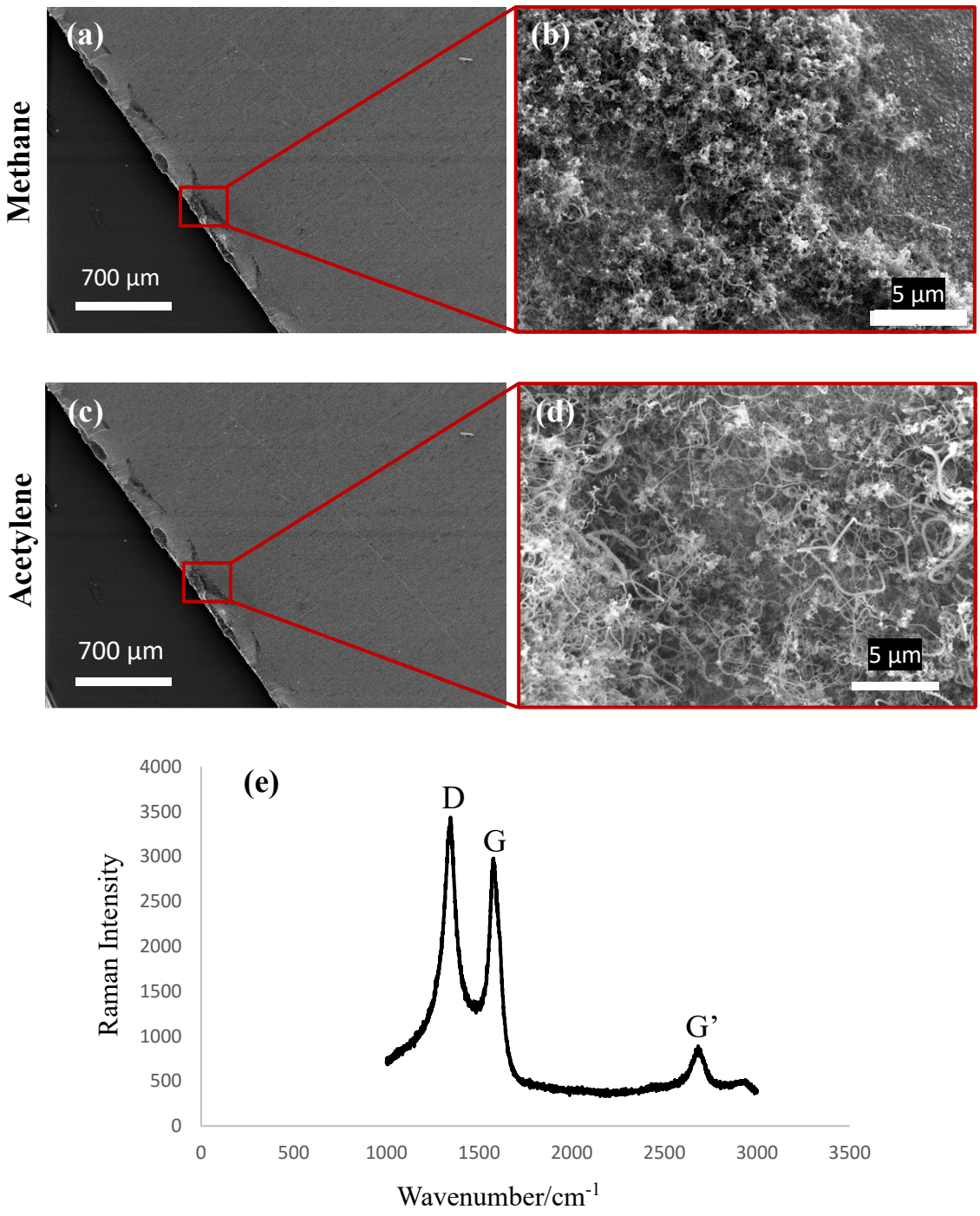

Figure 5.4. *SEM micrographs of non-treated bulk α-Ti substrates after the CVD syntheses: (a), (b) with methane precursor at 700 °C showing the localisation of MWCNTs in the valleys on the substrate edges; (c), (d) with acetylene precursor at 645 °C showing MWCNTs agglomerations at the edges of the substrates. (e) Representative Raman spectrum of the structures grown with acetylene, indicative of MWCNTs.*

Nevertheless, under the same conditions but at a lower temperature of 700 °C, MWCNTs growth was achieved (Figure 5.4a, b). The main aggregation of carbon nanotubes was visibly localized in the valleys of the sample, as shown in Figure 5.4a, which were formed by cutting the sample. On the main surface of the titanium, almost no MWCNTs were formed. These findings indicate that although MWCNTs growth on α-Ti is possible, it is necessary to find the optimum conditions to make it reproducible and homogeneous across the sample.

In order to induce better carbon nanotube formation, the use of a more reactive precursor such as acetylene was investigated. At 645 °C MWCNTs were detected in the valleys on the edges of the substrate, very similar to the results from the experiments with methane. No significant MWCNTs formation on the other parts of the sample was observed (Figure 5.4c).

The reason CNTs growth was not achieved on the principal surface of the α-Ti substrates can be explained by the reduced catalytic activity of titanium. The molecules of the precursor absorb strongly on the surface, but the reaction sites become saturated with carbon, and the Ti-C bond does not break to release the nanotube[130]. Additionally, titanium does possess sufficient carbon solubility and forms various carbides. The carbon precipitation happens only after all the carbides are formed. Thus, the process of nanotube formation is significantly slower and requires a higher concentration of carbon. Looking at the binary phase diagrams of carbon and typical CNTs catalysts (Fe, Co, Ni) shown in Figure 5.5, it was found that carbon solubility is achieved at ~ 1 at. %, meanwhile from the Ti-C diagram (Figure 5.6) it is clear that TiC saturation is achieved at ~ 50 at. %, and only then a carbon nanotube formation is possible[210].

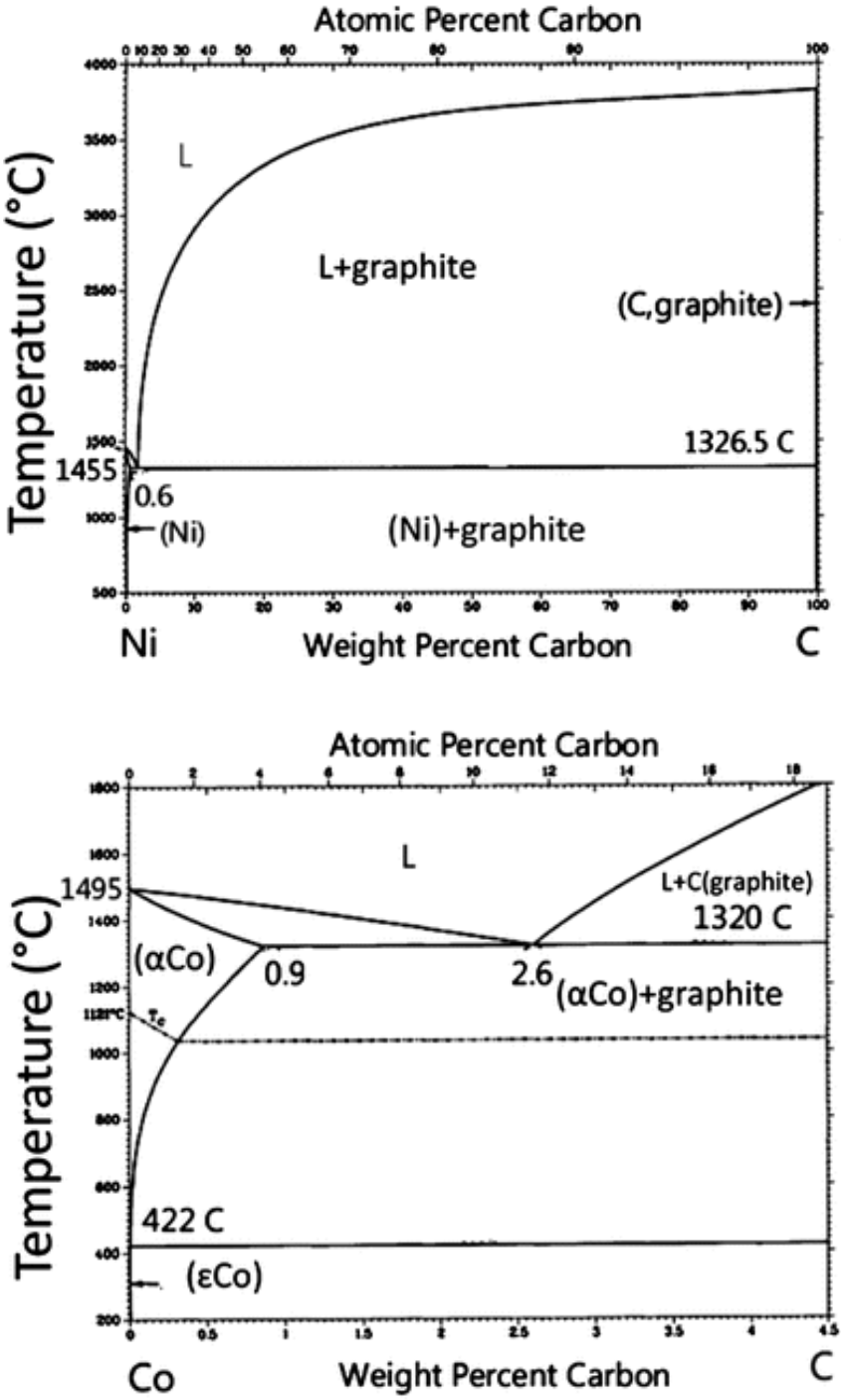

Figure 5.5. *Nickel–carbon and cobalt–carbon binary phase diagrams, which show that carbon solubility is achieved at ~ 1 at. % for all the catalysts*[210].

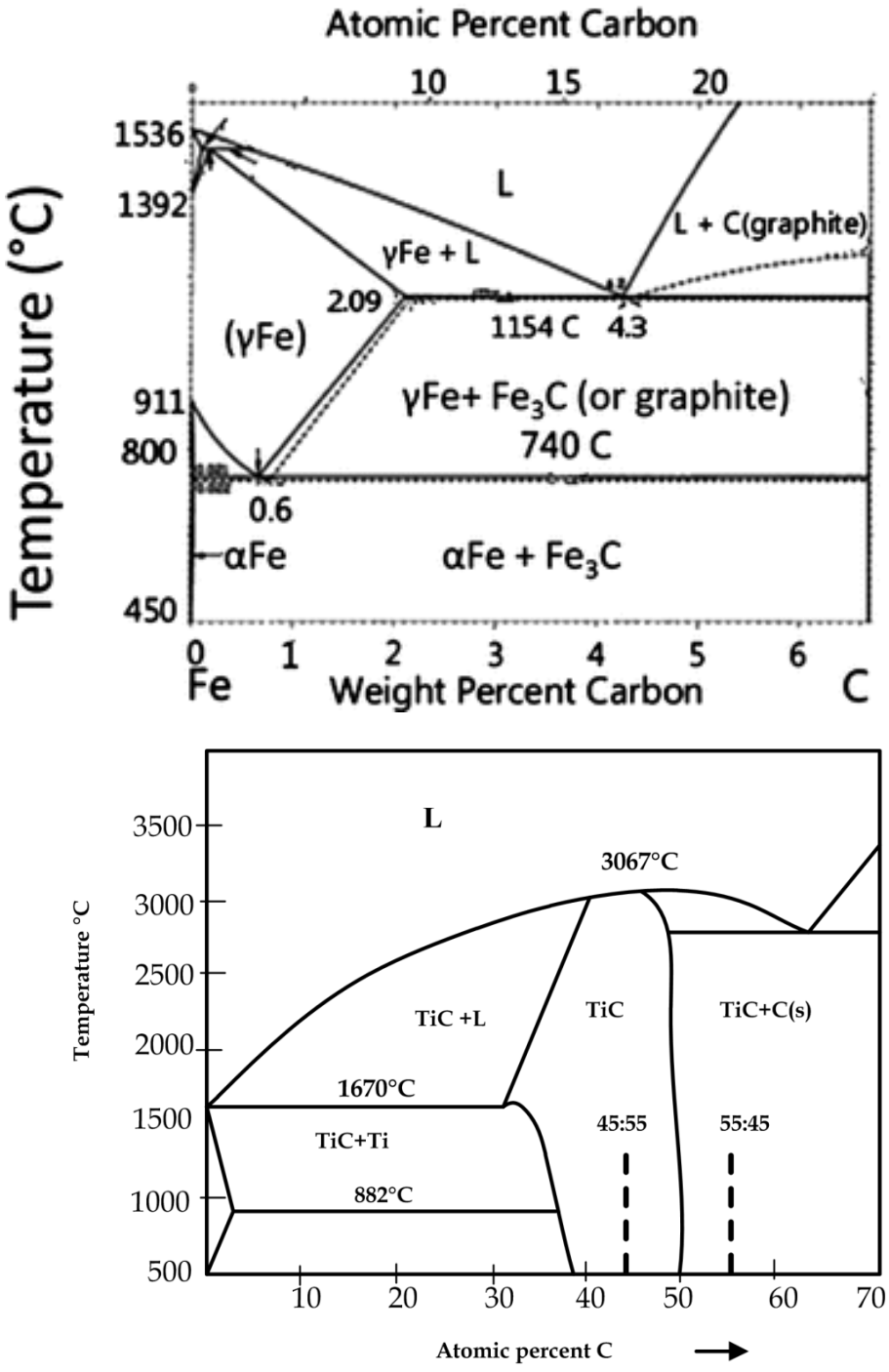

Figure 5.6. *Iron–carbon binary phase diagram, which show that carbon solubility is achieved at ~ 1 at. % for all the catalysts*[210]*. Titanium–carbon binary phase diagram, which shows that the carbon solubility is achieved at ~ 50 at. %*

β-Ti bulk substrates

β-Ti substrates were prepared using EDM from a Ti-45Nb rod with the elemental composition identified by the XRD measurements presented in Table 5.2.

Table 5.2. *XRF results of as produced Ti-45Nb bulk alloy performed by ATI WahChang, Huntsville, USA.*

Nominal compos.	Nb	O	N	Fe	Cr	Mn	Mg	Si	Na	Na	Ti
Ti-45Nb	44.94	0.095	0.007	<0.03	<0.01	<0.01	<0.01	<0.1	<0.01	<0.01	Balance

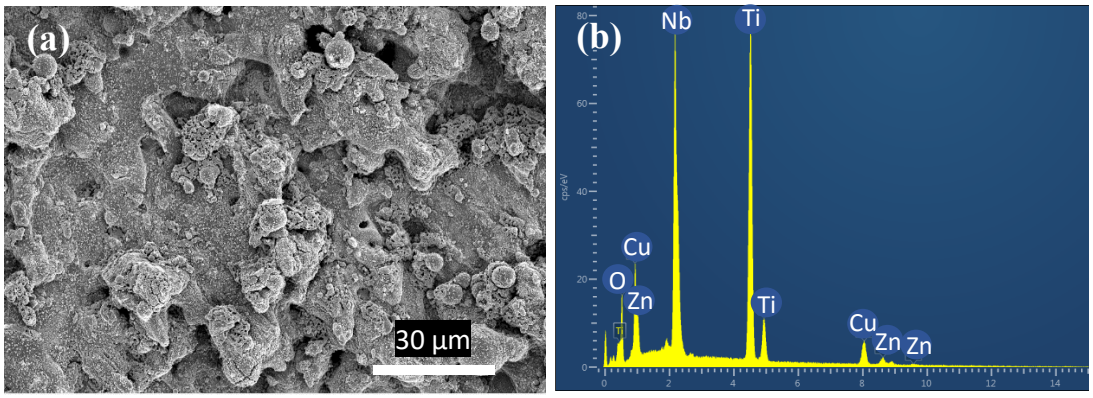

Figure 5.7. *Representative (a) SEM micrograph, and (b) EDX spectrum of bulk β-Ti substrate cut with EDM machine, showing the rough finish of the substrate and the presence of Ti and Nb as the elements of β-Ti and Cu and Zn elements as contaminations, which occurred during the cut.*

EDM automatically and quickly cuts substrates into squares, however, as shown in Figure 5.7a, it gives a non-homogenous, rough finish with some contaminations, since according to the EDX analysis (Figure 5.7b), Zn and Cu impurities are present. They came from the Cu-Zn electrode of the electrical discharged machine (EDM) machine. Traditionally, Zn and Cu are considered to be poor catalysts for CNTs growth, since they do not dissolve

carbon well and do not dissociate the hydrocarbons easily[130]. Nevertheless, they can influence the CNTs formation as some catalytic activity of Cu and ZnO_2 has been reported. Hence, the possibility of the influence of Zn and Cu will be investigated later in this Chapter.

No MWCNTs formation was observed on the main surface of non-surface-treated β-Ti substrates. In contrast to α-Ti, β-Ti substrates do not have trenches on the edges. Nevertheless, some MWCNTs growth on the very edges, similarly to the α-Ti substrates, was observed (Figure 5.8). Such growth indicates that the edges of titanium substrates favour the MWCNTs formation.

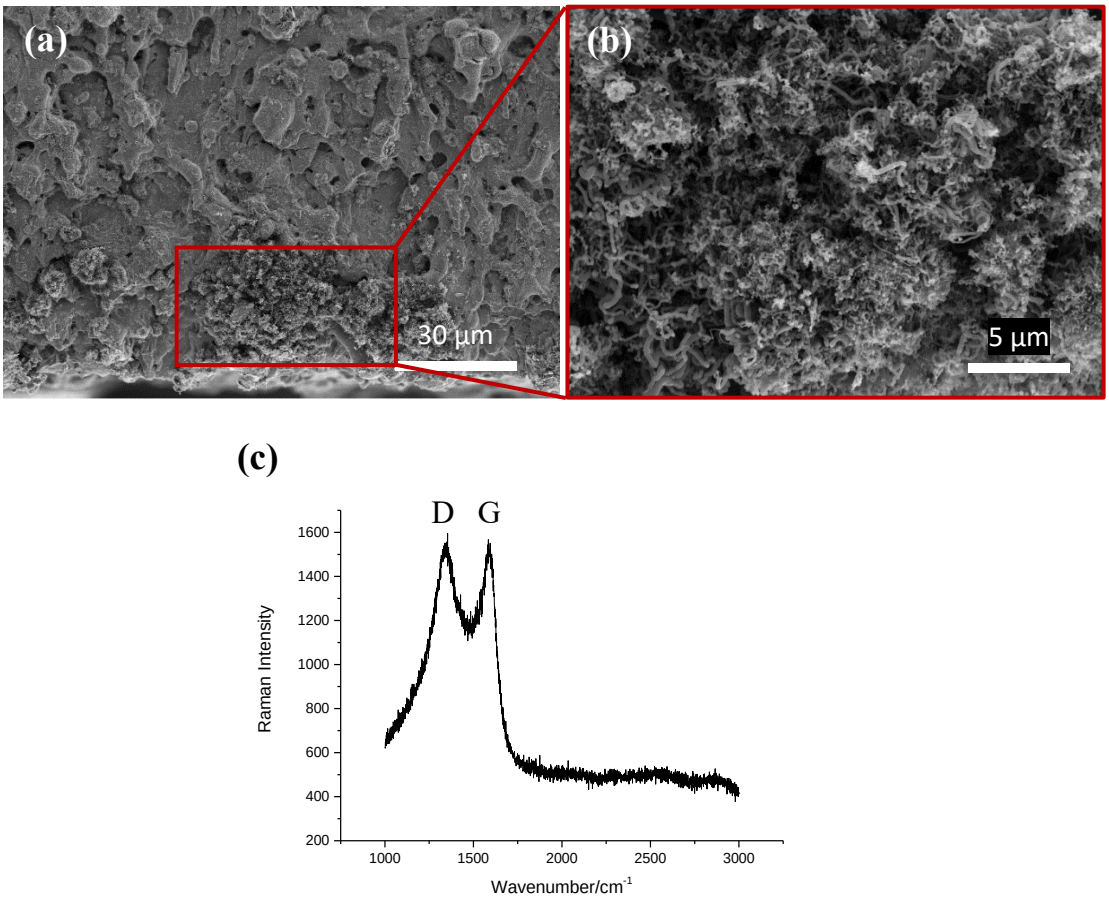

Figure 5.8. *SEM micrographs of non-treated bulk β-Ti substrates after the CVD syntheses with acetylene precursor showing (a), (b) MWCNTs formation on the edges of β-Ti cut with EDM; (c) representative Raman spectrum, indicative of the presence of MWCNTs on the β-Ti substrates.*

The results are indicative of the growth of MWCNTs on β-Ti, albeit only locally (on the sample's edges) and not on the whole surface of the bulk substrate. Possible reasons for such localized growth will be investigated further in this Chapter.

CVD growth of new titanium nanostructures

Alongside with the syntheses of MWCNTs, new titanium nanostructures were discovered during the CVD syntheses. These structures were observed during the experiments with all the used precursors: toluene, methane, and acetylene. Results of CVD syntheses with each precursor are presented in Appendix III.

Anodized α-Ti

Anodized α-Ti was chosen as a substrate for CNTs growth because of the presence of TiO_2 nanotubes, and earlier reported growth of CNTs on this substrate[67]. In this Chapter, it was investigated whether TiO_2 nanotubes on anodized α-Ti would promote CNTs growth in comparison with bulk substrates.

CVD experiments were performed under the same conditions as the experiments on bulk titanium, and no CNTs formation was observed. In Figure 5.9 it is visible that at 645 °C with an acetylene precursor, TiO_2 tubes start to be destroyed. At 700 °C with methane, TiO_2 tubes were partially destroyed in one part of the sample and entirely destroyed in the others. After the synthesis with methane precursor at 800 °C (Figure 5.10b), TiO_2 tubes were almost entirely destroyed. Therefore, it can be concluded that the temperature during the CVD process has a detrimental influence on the stability of TiO_2 tubes of anodized Ti, and, as a consequence, on the formation of CNT formation.

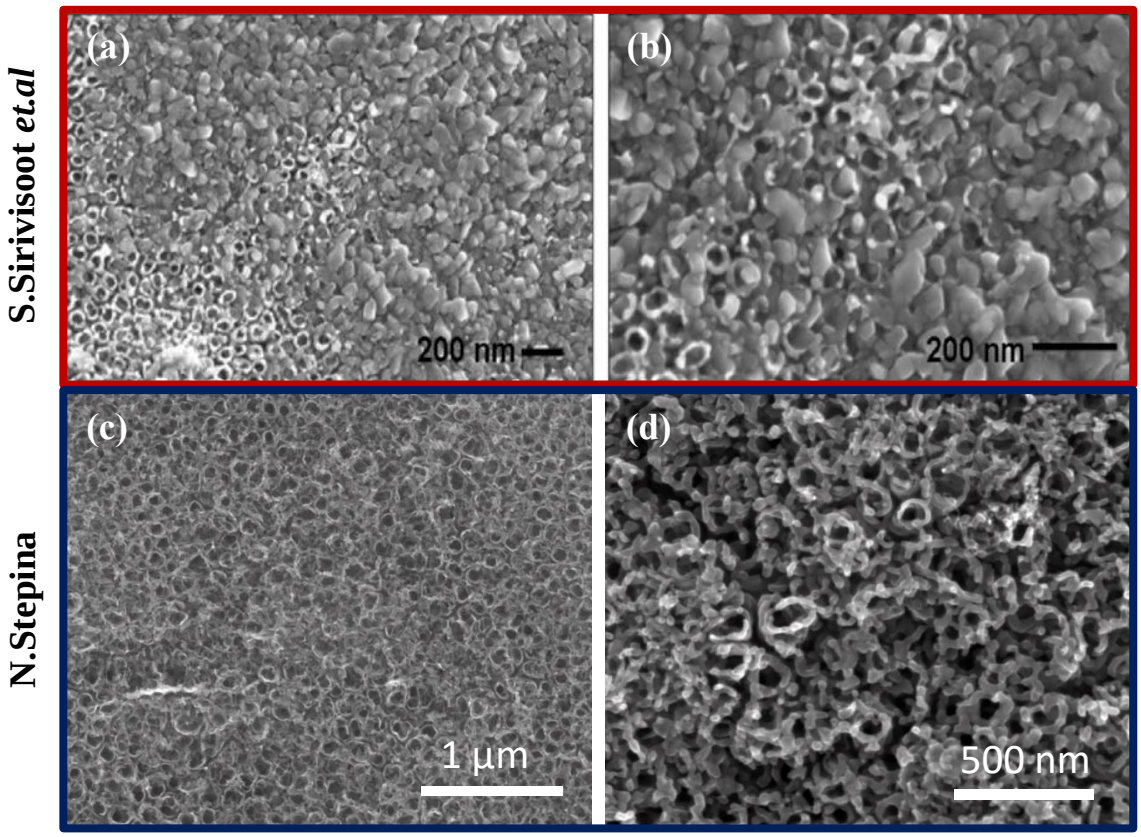

Figure 5.9. *SEM micrographs of lower (a) and higher (b) magnification showing anodized α-Ti after the CVD without additional catalyst reported by S. Sirivisoot et al.*[67]*. CNTs formation was reported by the authors, but cannot be determined from these micrographs. SEM micrographs of anodized α-Ti substrates performed in this Chapter before (c) and after (d) thermal treatment during the CVD at 645 °C. No CNTs are formed after, but the TiO_2 are partially destroyed.*

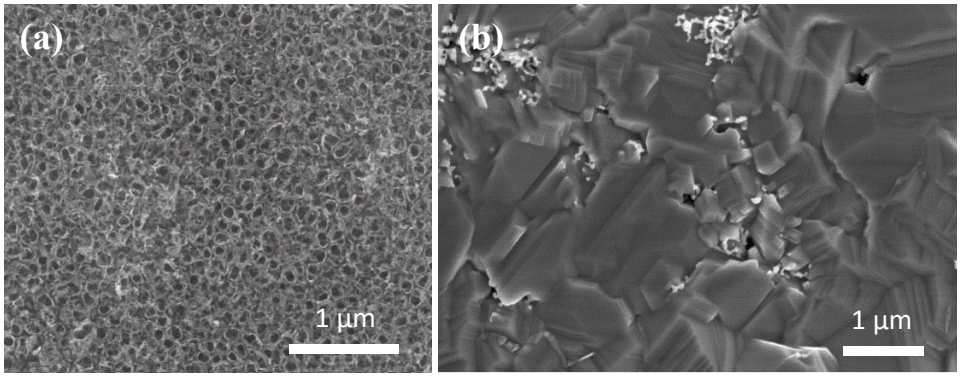

Figure 5.10. *SEM micrographs showing (a) the initial structure of anodized α-Ti, which reveals the formation of TiO_2 nanotubes all across the substrate; (b) anodized α-Ti after the CVD synthesis at 800 °C for 15 min with methane precursor showing destroyed TiO_2 nanotubes.*

TiO_2 nanoparticles

Titanium dioxide (TiO_2) nanoparticles have been reported to initiate the growth of CNTs[77]. Hence, TiO_2 nanoparticles were another substrate candidate for investigation. The conditions for the CVD experiments were set to be identical as for the syntheses on α-Ti and anodized α-Ti (800 °C and 700 °C, for 15 min). Interestingly, after these syntheses, the presence of CNTs could not be detected (Figure 5.11).

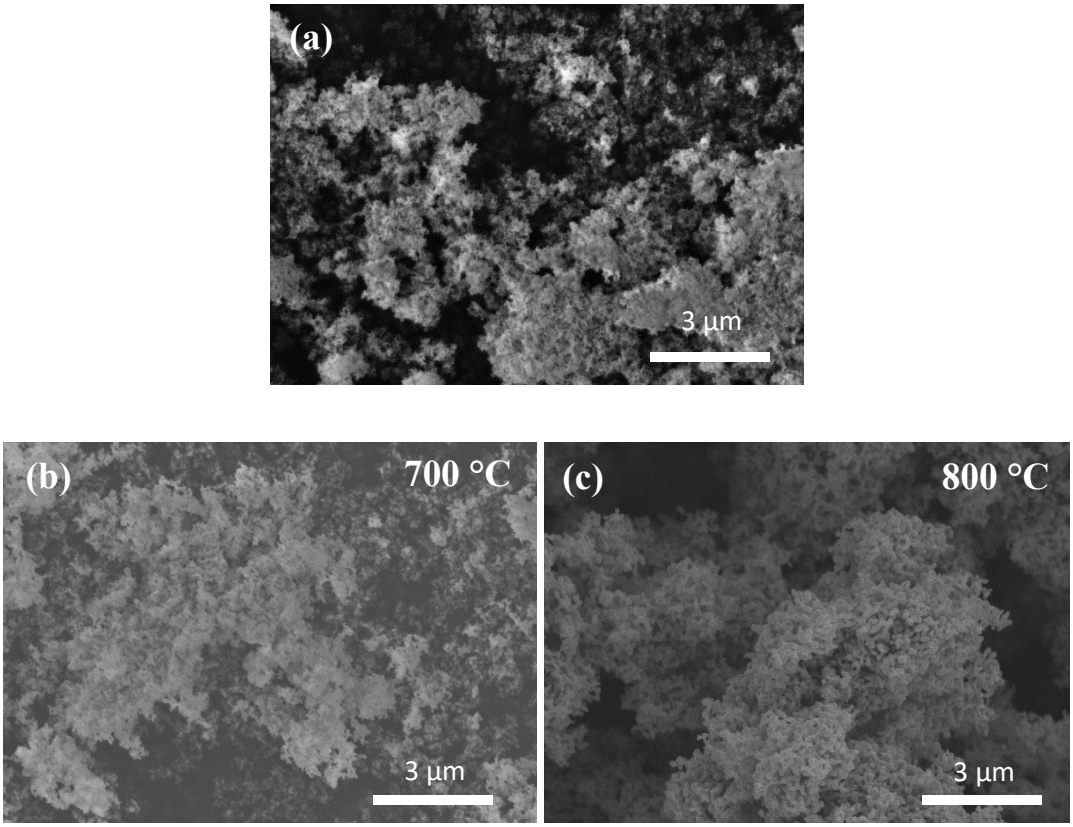

Figure 5.11. *SEM micrographs of TiO_2 nanoparticles (a) before CVD; after CVD synthesis (b) at 645 °C with an acetylene precursor; (c) at 700 °C with a methane precursor; (d) at 800 °C with a methane precursor.*

Although during the CVD experiments on TiO_2 nanoparticles no CNTs were grown, the influence of temperature on the synthesis was observed. The increase of the temperature of the CVD synthesis leads to a slight aggregation of the TiO_2 nanoparticles, and hence to the increase of the particle size. At 700 °C with methane as precursor, a slight

aggregation of nanoparticles was observed (Figure 5.11b), while Figure 5.11c showed much stronger aggregation of TiO_2 at 800 °C. The influence of the temperature on TiO_2 nanoparticles was also reported by G. C. Collazzo *et al.*[211] where an increase in the temperature lead to the aggregation of the nanoparticles.

In conclusion, by investigating various forms of titanium substrates, bulk titanium substrates were the only type of substrates which showed any carbon nanotube formation. Therefore, further attention was focused on bulk α-Ti and β-Ti substrates.

5.3.1.2. Syntheses trials to find an appropriate surface modification for MWCNTs growth on bulk Ti substrates

In the experiments in the previous section, MWCNTs growth was observed only on the edges of bulk α-Ti and β-Ti substrates. Therefore, further experiments were performed in order to understand the reason behind this localized MWCNTs growth, and how to achieve uniform, reproducible, and controllable non-catalytic MWCNTs growth on the whole surface of α-Ti and β-Ti substrates.

MWCNTs growth in the valleys on the edges of bulk α-Ti and β-Ti could be explained by two reasons: a) a difference in the surface roughness of the edges and the rest of the sample, since it is visible that the edges possess a different surface roughness to the rest of the surface of the substrates; b) the presence of contaminations on the edges. In order to explore these two possibilities, several methods for pre-synthesis substrate treatment were used. These include HF etching, mechanical polishing, and piranha solution etching methods, which eliminate contaminations and should create a homogeneous surface roughness of the substrates.

HF etching

It was revealed that α-Ti substrates etched quicker than β-Ti substrates, resulting from a more rapid reaction of the HF solution with Ti rather than with Nb, which is present in the β-Ti alloy. The schematic reactions of Ti and Nb with HF are presented in equation (1) and (2).

$$Ti + 3HF = TiF_3 + 3/2\ H_2 \qquad (1)$$

$$2Nb + 10HF = 2NbF_5 + 5H_2 \qquad (2)$$

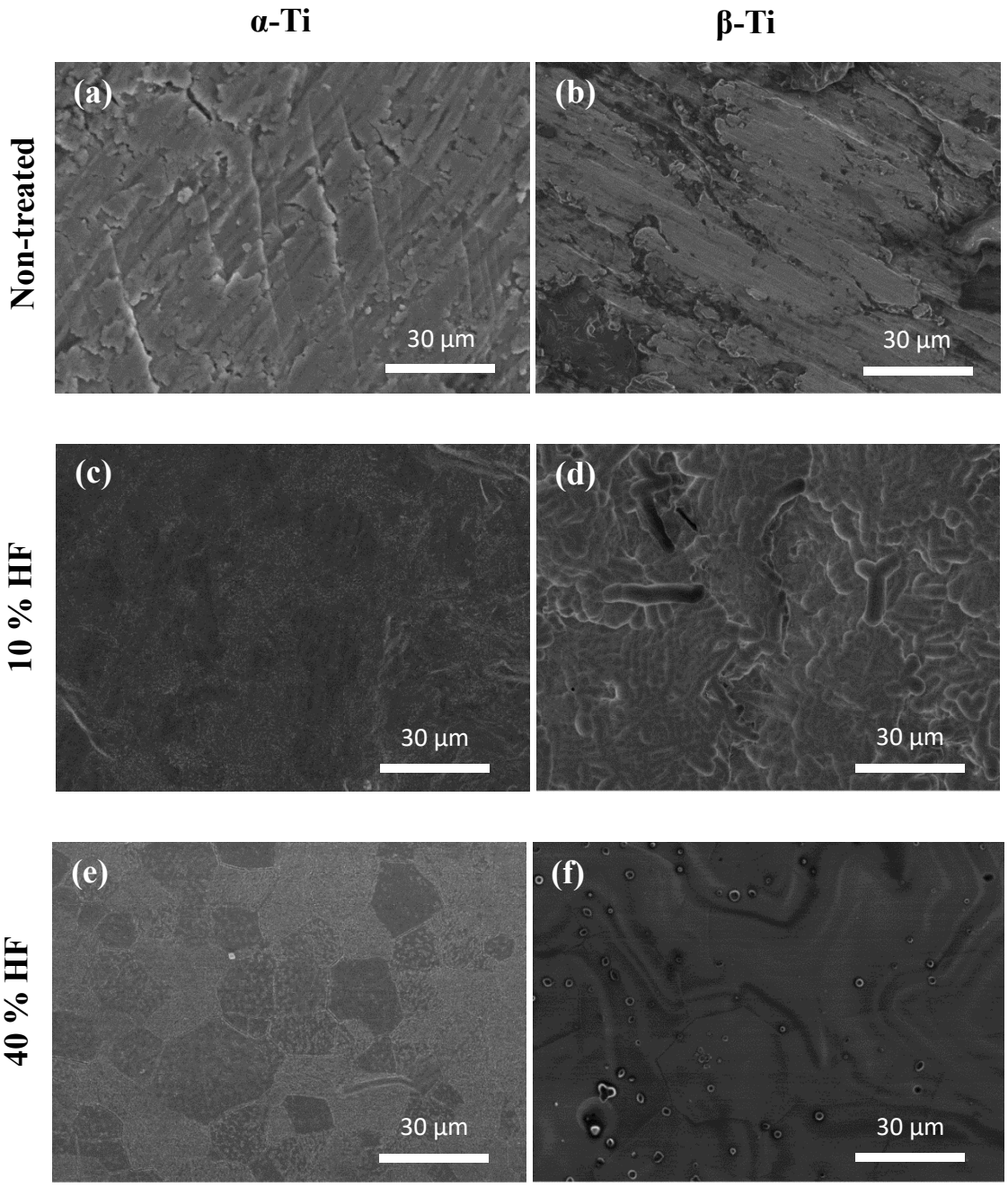

Figure 5.12. *Representative SEM micrographs showing the initial structure of non-treated (a) α-Ti; (b) β-Ti substrates; the changes in the structure of the samples after the Piranha treatment of (c) α-Ti treated with 10 % HF; (d) β-Ti treated with 10 % HF; (e) α-Ti treated with 40 % HF; (f) β-Ti treated with 40 % HF, revealing the appearance of the grain boundaries after the 40 % HF + Piranha treatment.*

A treatment of α-Ti and β-Ti substrates with 40 % HF revealed the grain boundaries as shown in Figures 5.12e, f. 10 % HF treatment also changed the surfaces of both titanium substrates (Figures 5.12c, d), however, no grain boundaries were observed since the treatment was less active than with 40 % HF. CVD syntheses on all the substrates treated with HF did not result in CNTs growth. This is likely to be due to the absence of reaction sites for the initiation of the CNTs growth.

Mechanical polishing

In order to see whether any MWCNTs growth is due to the layer that is formed by the cutting procedure, substrates were polished in order to remove this layer. No MWCNTs growth on polished α-Ti and β-Ti substrates was observed, indicating that polished titanium is not favourable for CNTs formation, and some surface roughness is needed for successful nanotube formation.

Piranha solution etching

By comparing different surface treatment of titanium performed in this Chapter (HF etching, mechanical polishing, Piranha etching), Piranha solution treatment was found to be the only method which fostered CNTs formation over all of the surface of both bulk-type Ti samples. Further experiments of CNTs growth on Piranha-treated titanium substrates are presented in the following subsection.

5.3.1.3. Investigation of CVD synthesis with acetylene on bulk titanium substrates treated with Piranha solution

CVD synthesis on Piranha-treated α-Ti and β-Ti substrates were performed using acetylene, since it was determined to be the most reactive precursor for CNTs growth.

Piranha solution treatment of bulk α-Ti substrates with acetylene precursor

During the CVD experiments performed on Piranha-treated α-Ti substrates, several different parameters were investigated, including the duration of the piranha treatment; the duration of the CVD experiment; and annealing with hydrogen.

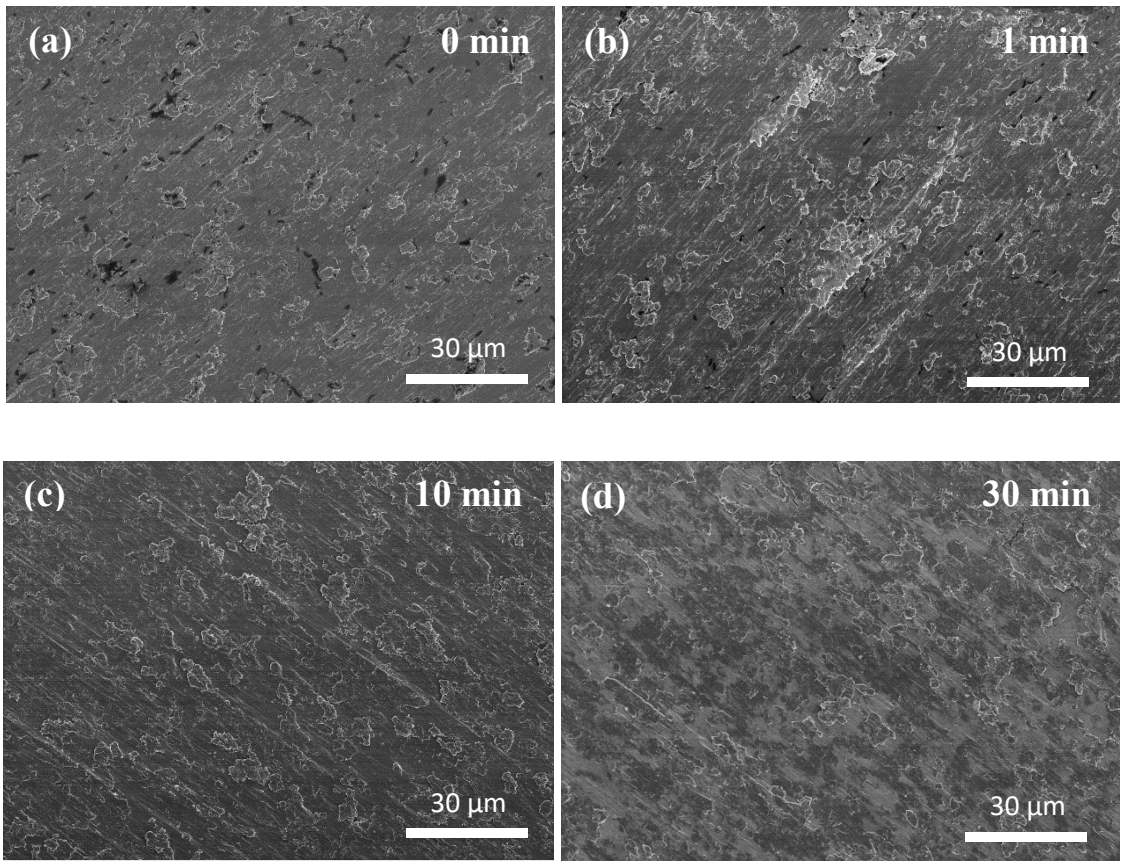

Figure 5.13. *SEM micrographs showing the surface of bulk α-Ti substrates (a) before; (b) after 1 min of Piranha treatment; (c) after 10 min of Piranha treatment; (d) after 30 min of Piranha treatment, revealing the disappearance of the contaminations after Piranha treatment.*

The first parameter under investigation was the duration of Piranha etching. Figure 5.13 presents SEM micrographs showing the surface of α-Ti treated with Piranha solution for different times. It is visible that the substrates have some initial contaminations, which are shown in black in Figure 5.13a. Already after 1 min of Piranha treatment (Figure 5.13b), much fewer contaminations were observed, and after 10 min and more (Figure 5.13c, d) no impurities remained. These experiments confirm that Piranha solution effectively cleans the surface of bulk titanium substrates.

Figures 5.14a, b, revealed the extensive growth of MWCNTs on α-Ti substrates treated with Piranha solution for 1 min, both on the edges and across the whole surface of the substrate. It suggests that, after Piranha solution treatment, the primary surface roughness of α-Ti substrate changed and became more similar to that of the edges, which previously showed the growth of nanotubes. By gradually increasing the time of Piranha treatment to 5, 10, and 30 min, MWCNTs growth became less intense and at 30 min reaction time, no MWCNTs growth was observed. A possible explanation of this observation will be given in this section. Raman spectra presented in Figure 5.14d were taken to determine any presence of MWCNTs on α-Ti substrates. The ratio of the intensities of the Raman D and G-bands $I_D/I_G = 0.58$, showing that MWCNTs grown on the α-Ti substrates after Piranha treatment are less defective than those on non-treated samples, as illustrated in Figure 5.4e. The growth of MWCNTs on Piranha-treated α-Ti substrates indicates that some changes in the surface properties of the titanium took place, because CNTs formation on non-treated substrates was previously only favourable on the edges, whereas after the Piranha treatment the rest of the substrate also became viable to initiate nanotube growth.

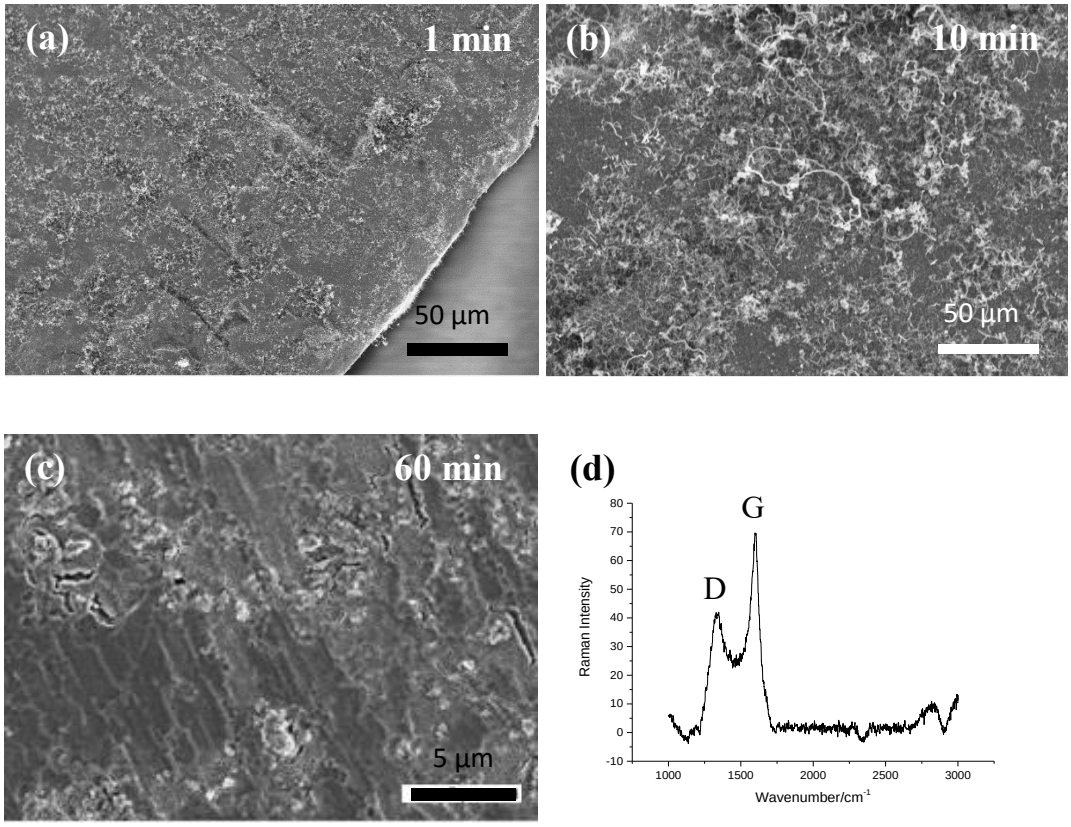

Figure 5.14. *SEM micrographs of bulk α-Ti substrates after the CVD synthesis with acetylene with different time of Piranha treatment: (a), (b) 1 min; (c) 60 min; (d) Raman spectra of MWCNTs synthesized on α-Ti treated with Piranha solution for 1 min.*

The second parameter under the investigation was the reaction time of the CVD experiments with acetylene. Syntheses during 10, 20 and 30 min were performed. At 10 min, no CNTs growth was observed, but after the CVD for 20 and 30 min, MWCNTs formation was revealed. Therefore, the minimum reaction time for nanotube formation was 20 min, which might be related to the fact that, before the nanotube formation starts, first a number of titanium carbides are formed, for which a significant amount of carbon is needed in the system. Ten minutes should be sufficient to form titanium carbides, but will not be long enough for the CNTs to form, while after 20 min also the growth of CNTs will have taken place.

The last investigated parameter was the influence of annealing in hydrogen. Substrates were annealed before the experiment for 0, 30, 60 and 90 min. No influence of annealing on MWCNTs formation was observed and hence this step can be eliminated for further experiments. The reason behind it might be that annealing processes already partially occurred during Piranha treatment (formation of hydrogen radicals).

To summarize the influence of the synthesis parameters, it can be concluded that MWCNTs growth without additional metal catalyst on bulk α-Ti is possible under the condition that substrates are treated with Piranha solution during for 1 to 30 min before using 20 min CVD reaction time.

The next step was to understand the mechanism of MWCNTs growth and what influences the improvement of the growth. There are two possible reasons for the MWCNTs growth: 1) changes in the surface properties, and 2) presence of contaminations, which are both investigated below.

1) Surface properties

It was observed that the surface roughness of α-Ti changes after the Piranha solution treatment. 3D images revealing the surface roughness of α-Ti substrates before and after the Piranha treatment are presented in Figure 5.15. It can be derived from the pictures that the Piranha-treated samples are rougher compared to non-treated substrates. Surface roughness values presented in Table 5.3 show the increase in surface roughness of 10 nm after the Piranha treatment. However, the roughness of the samples treated with Piranha for 1 and 30 min is very similar; interestingly, no CNTs growth is observed after 30 min. Therefore other factors should also be responsible for the promotion of CNTs growth.

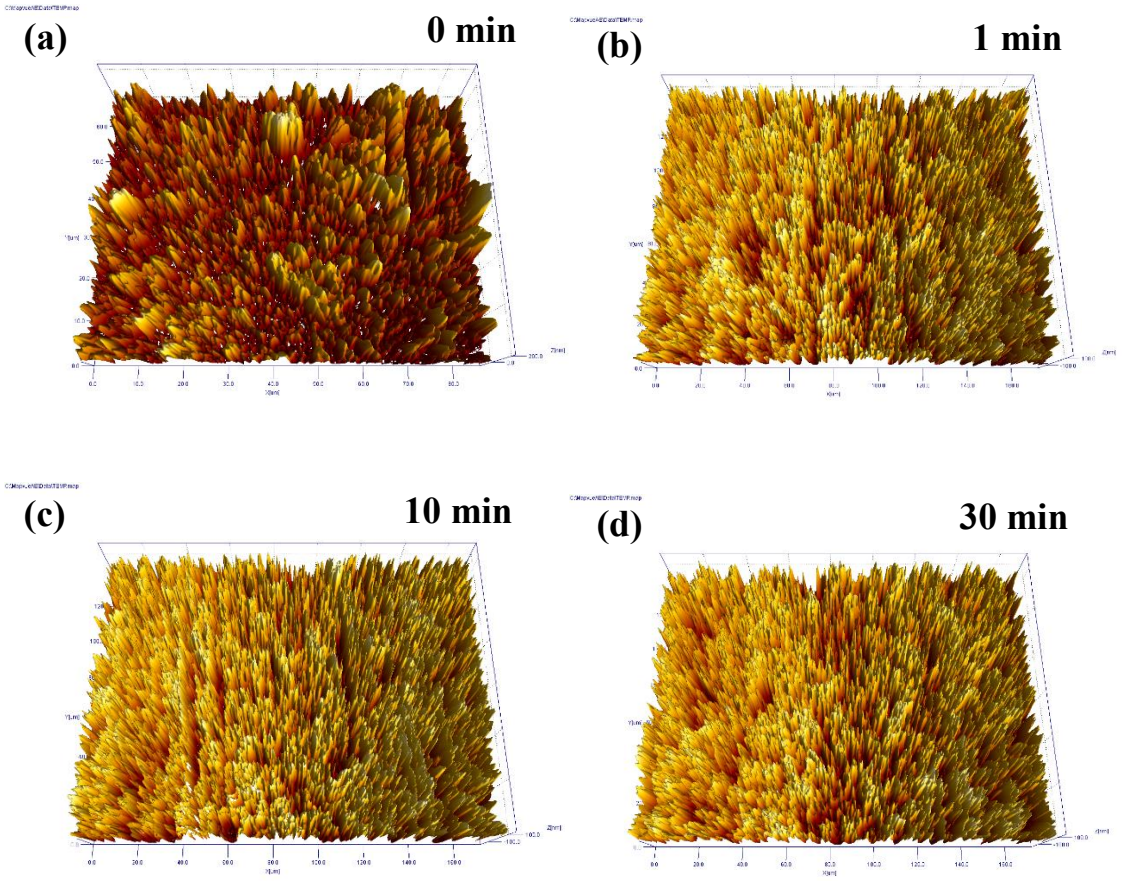

Figure 5.15. *3-D roughness profiles of bulk α-Ti substrates (a) before Piranha treatment; (b) after 1 min of Piranha treatment; (c) after 10 min of Piranha treatment; (d) after 30 min of Piranha treatment revealing the increase in the surface roughness for Piranha treated substrates.*

Table 5.3. *Values of the surface roughness of bulk α-Ti substrates treated with Piranha solution during a different time.*

Time of Piranha treatment	0 min	1 min	10 min	30 min
S_a of α-Ti substrates, nm	49.9	59.9	61.3	59.7

It should be taken into account that during the Piranha treatment, not only the cleaning and the changes in the surface roughness occurs, but that also the surface becomes more hydrophilic due to the -OH groups that appear on the surface. This might therefore also

have an influence on the MWCNTs growth. In order to evaluate the hydrophilic/hydrophobic nature of the substrates, contact angle measurements were performed. Figure 5.16 shows that the surface of α-Ti substrates became hydrophilic after the Piranha treatment. Already after 1 min in the Piranha solution, the surface switch from the hydrophobic with a contact angle of 101 to the hydrophilic with a twice smaller angle of 56 (Table 5.4). After the Piranha treatment for 10 and 30 min, the surface became even more hydrophilic, with contact angles of 43 and 33 respectively. Therefore, the wettability and adhesiveness of α-Ti substrates after the Piranha treatment switch from poor to good.

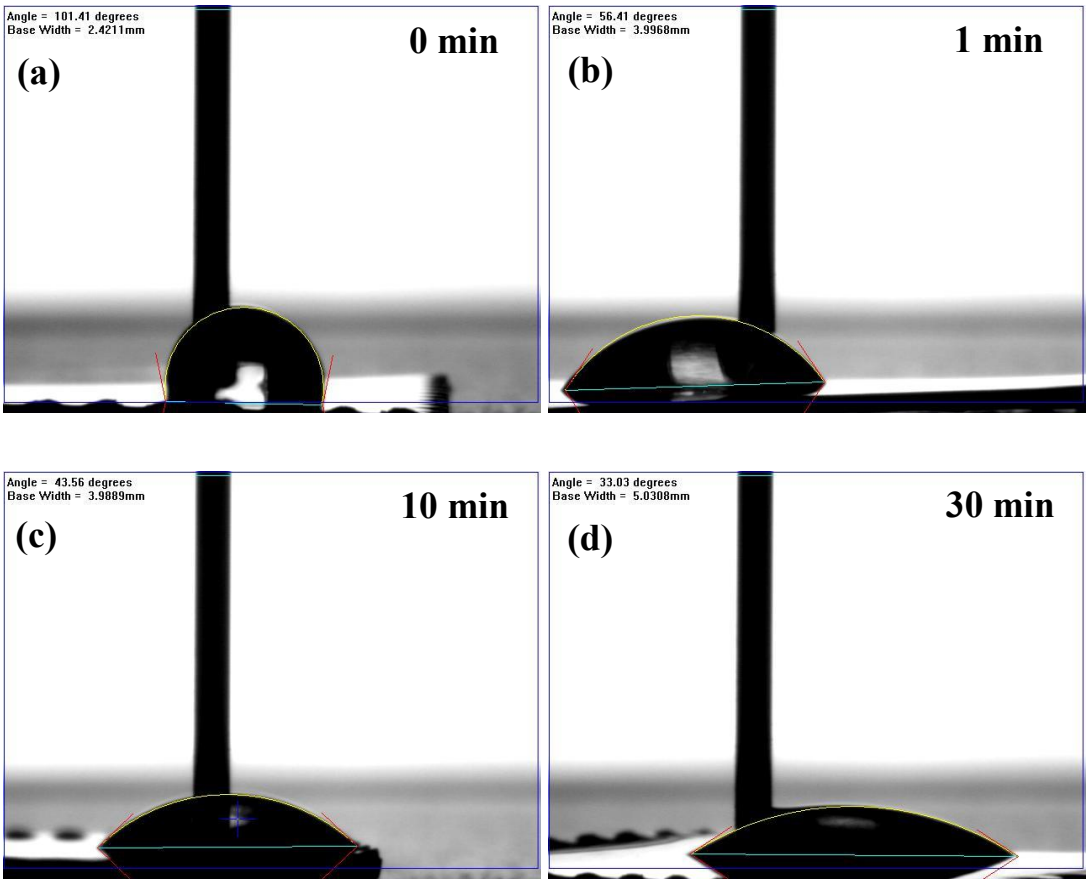

Figure 5.16. *Images of dynamic water contact angles on bulk α-Ti substrates treated with Piranha solution during the different time: (a) 0 min; (b) 1 min; (c) 10 min; (d) 30 min showing the decrease of the contact angle after the Piranha treatment.*

Table 5.4. *Values of dynamic water contact angle measured on non-treated and treated bulk α-Ti substrates with Piranha solution during a different time.*

Time of Piranha treatment	0 min	1 min	10 min	30 min
Contact angles values of α-Ti substrates, °	101	56	43	33

2) Contaminations

The presence of metal contaminations/additives is another parameter that could influence the CNTs growth. In order to see whether metallic impurities were present on the substrate, XPS measurements (Figure 5.17) of α-Ti substrates before and after piranha treatment were conducted. From Figure 5.17 it can be concluded that no metallic impurities were present on the substrates. After Piranha treatment, only the appearance of sulphur (S) was observed, which is likely to appear due to the Piranha solution itself (H_2SO_4: H_2O_2).

In conclusion, it was difficult to identify the direct influence of one single parameter on the CNTs formation on α-Ti substrates. Therefore, it is likely that the combination of the increased surface roughness and moderate hydrophilicity favours carbon nanotubes formation on bulk α-Ti substrates.

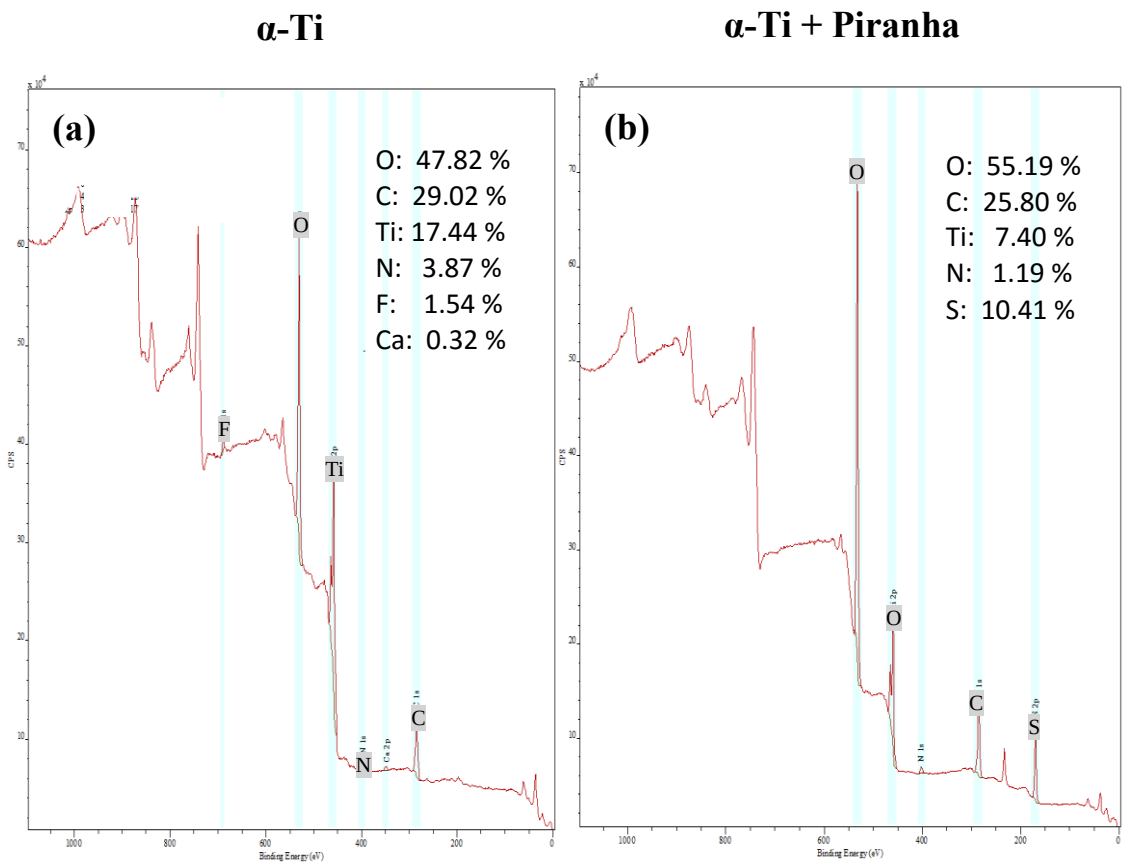

Figure 5.17. *XPS results of bulk α-Ti substrates (a) before and (b) after Piranha treatment showing the difference in the elemental composition between non-treated and Piranha treated samples.*

Piranha solution treatment of bulk β-Ti substrates with acetylene precursor

For the experiments on Piranha-treated β-Ti substrates, the same synthesis parameters as for α-Ti were investigated, including time duration of the Piranha treatment; the duration of the CVD experiment; and annealing with hydrogen. Looking at the SEM micrographs of β-Ti substrates presented in Figure 5.18, very small difference between non-treated and Piranha-treated substrates was observed. After the Piranha treatment the smaller-scale structure has disappeared and a wider-spaced structure has developed which indicates the generation of smoother surface.

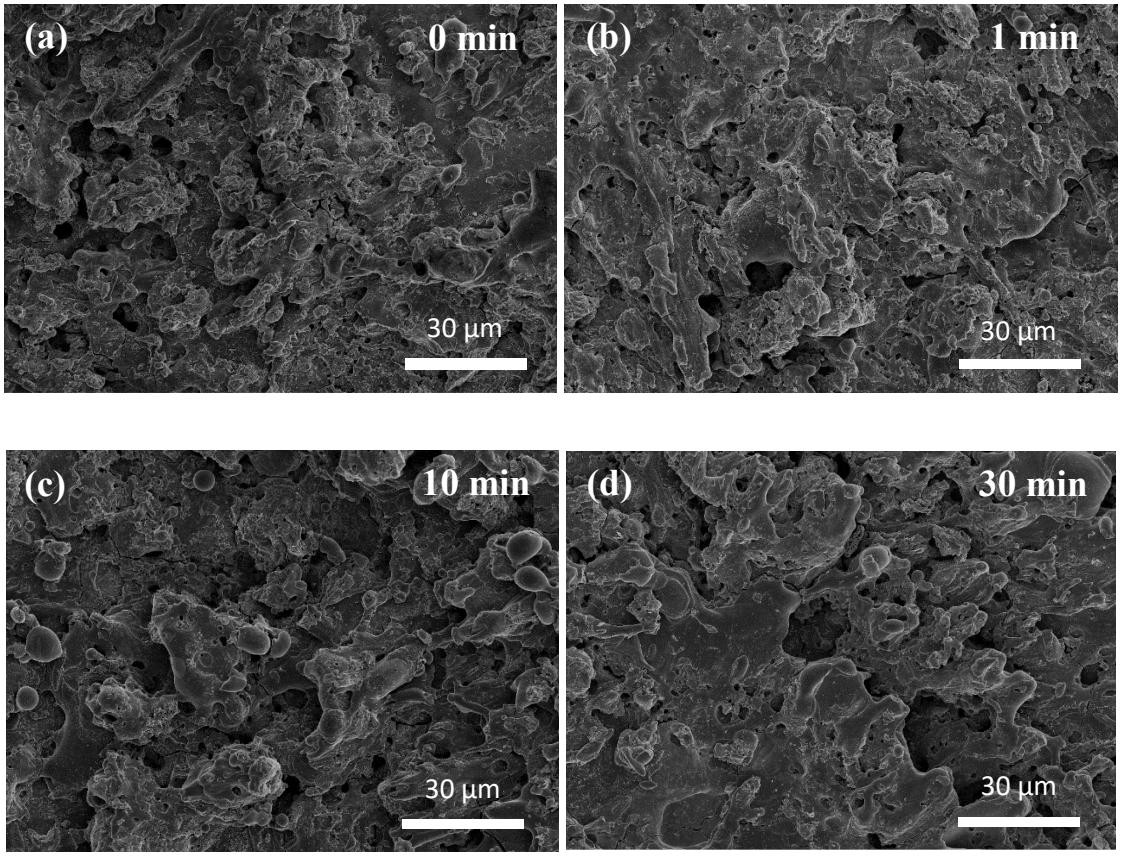

Figure 5.18. *SEM micrographs showing the surface of bulk β-Ti substrates (a) before Piranha treatment; (b) after 1 min of Piranha treatment; (c) after 10 min of Piranha treatment; (d) after 30 min of Piranha. No significant difference before and after treatment was observed for the substrates.*

All substrates were treated with Piranha solution during different time periods from 1 min to 3.5 hours, before synthesis. For β-Ti substrates after Piranha treatment for 1 min, MWCNTs deposition was observed all over the sample (Figure 5.19a, b). MWCNTs were not aligned and had different diameters. MWCNTs were also observed when the time of the Piranha treatment was increased to 5, 10, 30 and 60 min (Figure 5.19). Even after 3.5 hours, MWCNTs were still observed, although their deposition was very thin and mostly of a smaller diameter (Figure 5.19d). Hence, the longer the Piranha treatment, the thinner the MWCNTs layer is formed. According to the Raman spectrum presented in Figure

5.19e, the ratio of the intensities of the Raman D and G-bands (I_D/I_G) is approximately one, which indicates that MWCNTs grown on the β-Ti substrates are very defective.

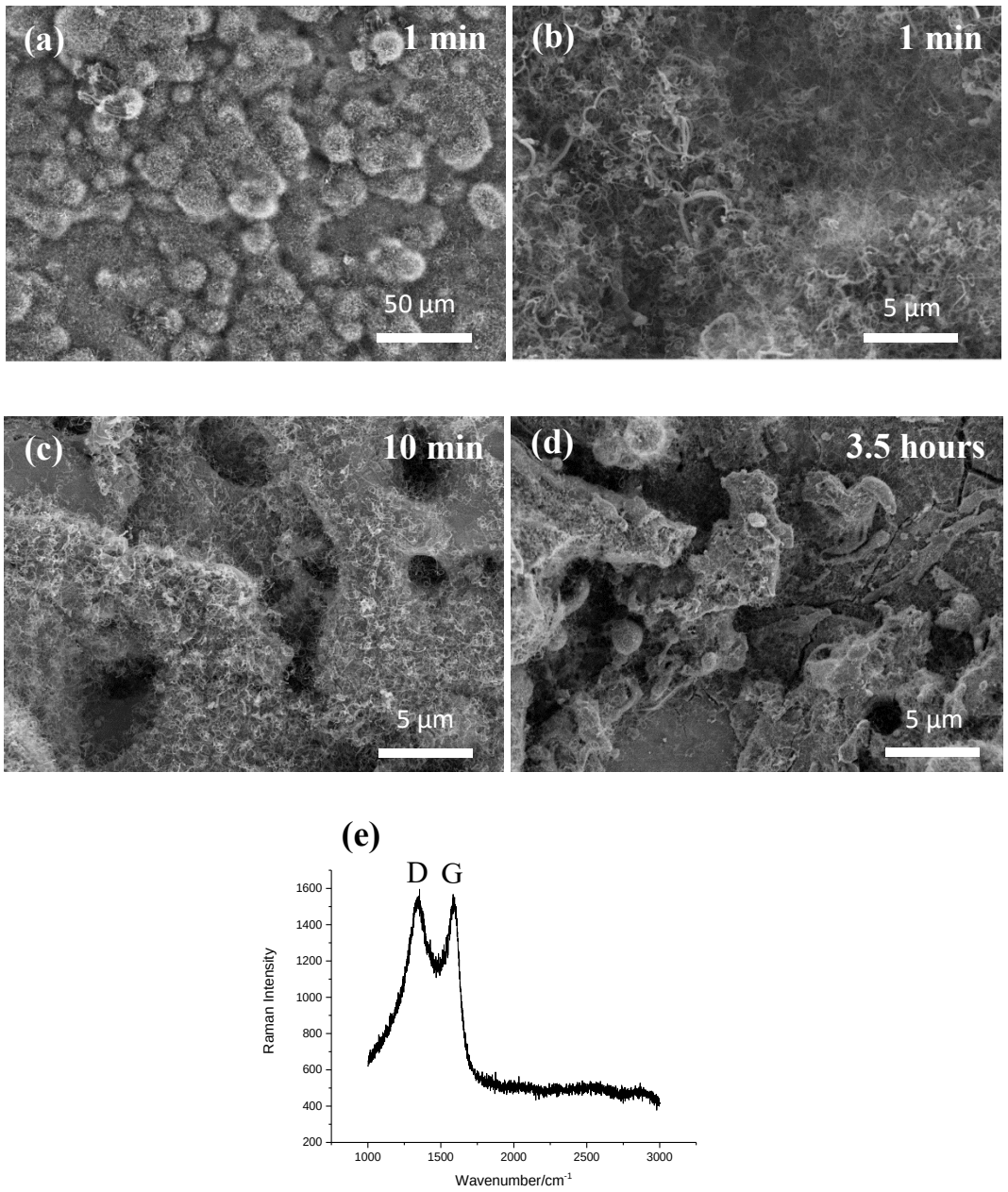

Figure 5.19. *SEM micrographs showing MWCNTs growth after the CVD synthesis with acetylene precursor on bulk β-Ti substrates treated with Piranha solution during (a),(b) 1 min; (c) 10 min; (d) 3.5 hours; (e) representative Raman spectrum of MWCNTs grown on β-Ti after 1 min Piranha treatment confirming the presence of (defective) MWCNTs on the sample.*

In contrast to the syntheses on α-Ti, the duration of the CVD experiment did not have any visible influence on the growth on β-Ti substrates. However, similar to the syntheses on α-Ti, annealing had no influence on MWCNTs formation on β-Ti substrates.

To understand the mechanism of MWCNTs growth on Piranha-treated β-Ti substrates, similarly to that on α-Ti substrates, the influence of surface properties and the presence of additional elements were investigated.

1) Surface properties

The surface roughness of β-Ti substrates was not possible to measure with the available equipment due to the high range of roughnesses and their inhomogeneity.

In order to evaluate the influence of surface hydrophilicity on the growth of CNTs, contact angle measurements on the β-Ti substrates were also performed. Representative images of dynamic water contact angle measurements with different durations of Piranha treatment are presented in Figure 5.20. Even though β-Ti substrates are very rough, without Piranha treatment they are already hydrophilic with a contact angle of 61 (Table 5.5), however, no CNTs growth was observed for those substrates. These findings indicate that the high surface roughness and hydrophilicity of the surface are not enough for CNTs formation on β-Ti. After 1 min of Piranha treatment, the surface becomes more hydrophilic, and this trend continues for 10 and 30 min treated substrates. The contact angle values after 10 min are the same for α-Ti and β-Ti. After 30 min treatment of β-Ti, the contact angle becomes lower than for α-Ti, with an angle of 22. Interestingly, CNTs on β-Ti are still growing on the substrates even after 30 min Piranha treatment, with an even smaller contact angle, while no CNTs growth was observed on α-Ti substrates with a contact angle of 33.

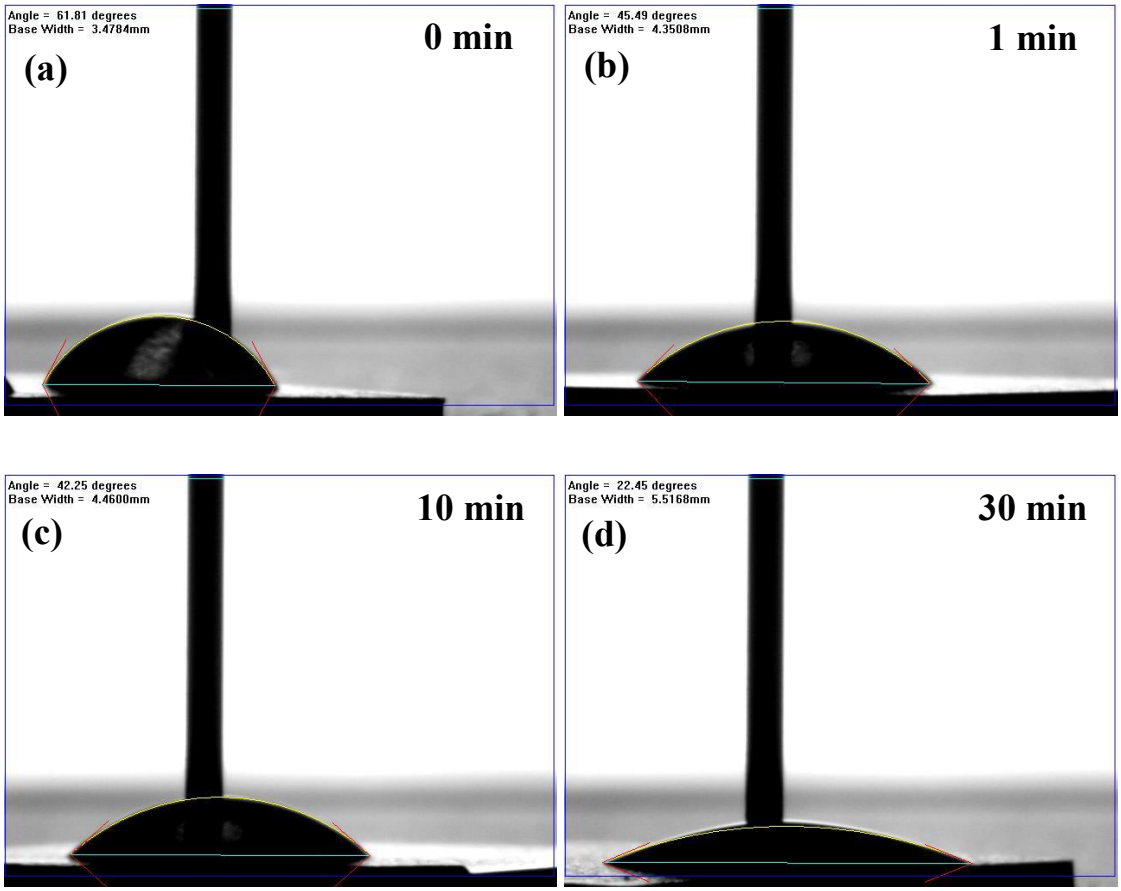

Figure 5.20. *Images of dynamic water contact angles on bulk β-Ti substrates with different time of Piranha solution treatment: (a) 0 min; (b) 1 min; (c) 10 min; (d) 30 min showing the decrease of the contact angle after Piranha treatment. Values are given in Table 5.5.*

Table 5.5. *Values of dynamic water contact angle measured on β-Ti substrates treated with different time of Piranha solution.*

Time of Piranha treatment	0 min	1 min	10 min	30 min
Contact angles values of β-Ti substrates, °	61	47	42	22

2) Contaminations

For the β-Ti substrates, which were cut using EDM, Zn and Cu contaminations from the EDM electrodes were identified by the EDX measurements presented in Figure 5.7b. Nevertheless, CNTs growth on the main surface of the substrates was only observed on Piranha-treated substrates, and therefore, it is important to understand in detail the changes caused by Piranha treatment on β-Ti substrates.

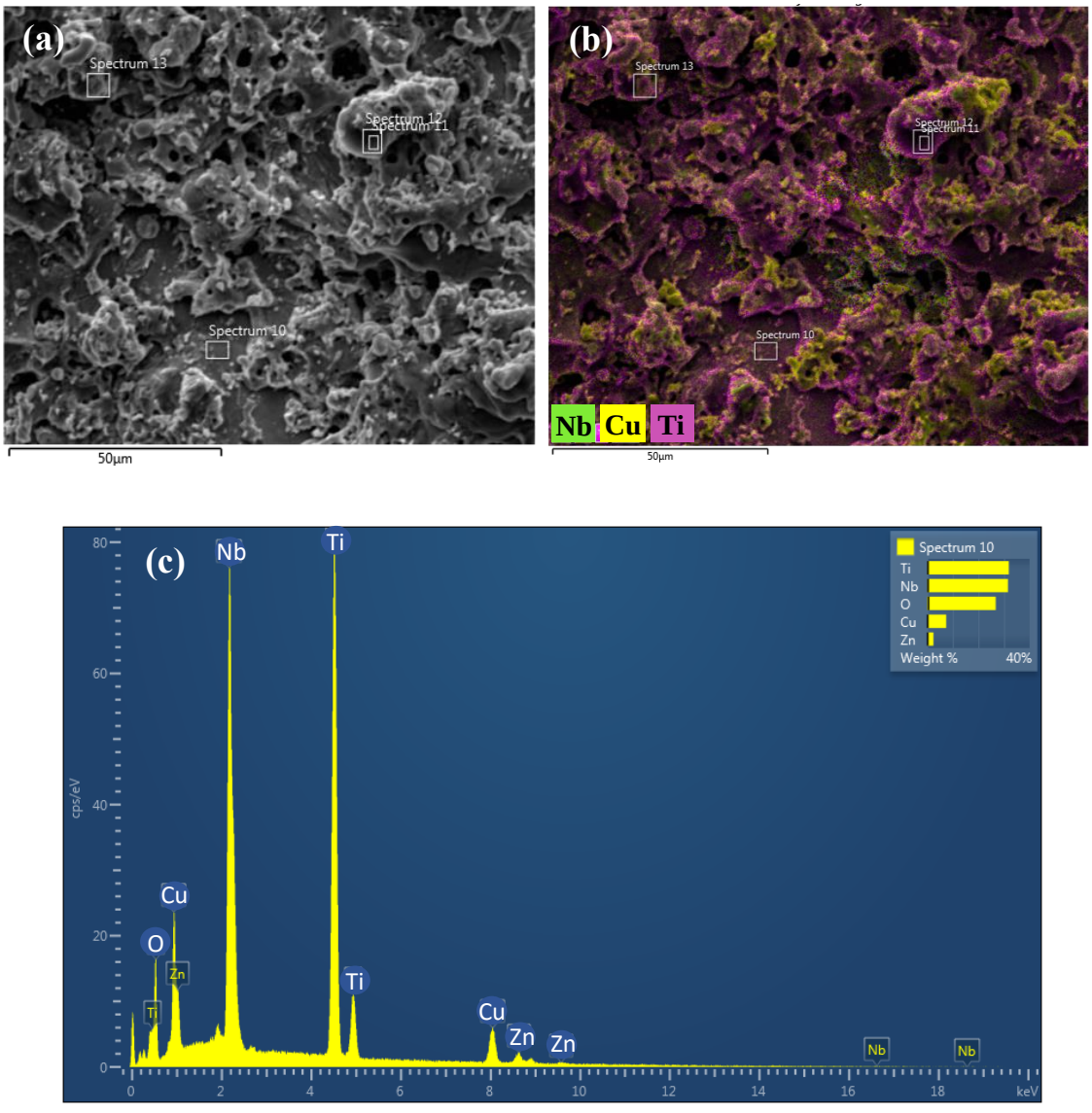

Figure 5.21. *(a) SEM micrograph and (b) EDX map showing the main elements present in bulk β-Ti substrates (cut with EDM). (c) EDX spectrum identifying Ti, Nb, O, Cu, and Zn as the main elements present in bulk β-Ti substrate.*

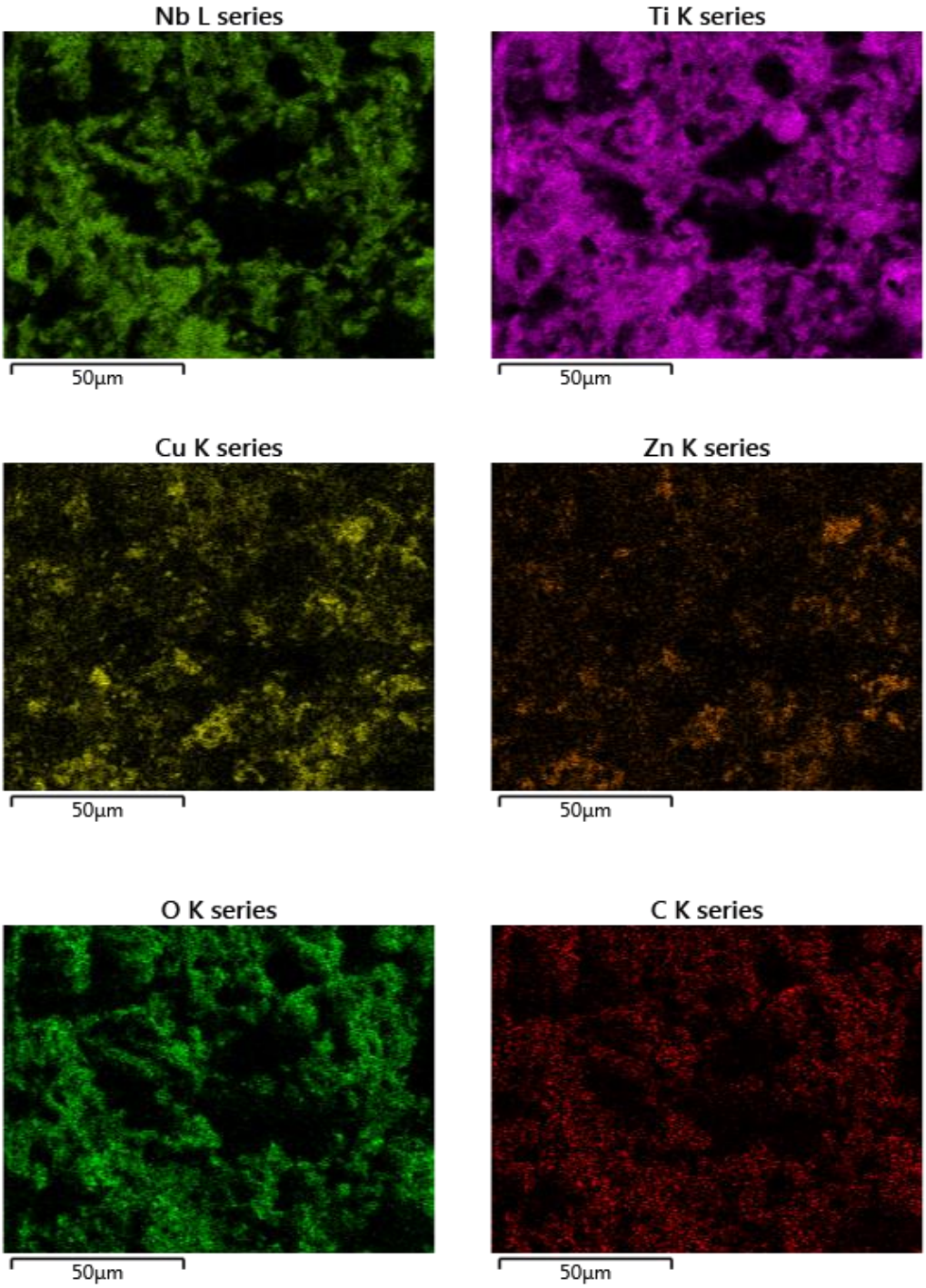

Figure 5.22. *EDX mapping of the (untreated) β-Ti substrate showing the deposition of each detected element across the substrate.*

It is important to discover the distribution of Zn and Cu across the sample, in order to be certain whether they are all over the sample or just localized on the edges, where some CNTs were observed. EDX mapping (Figure 5.21) in various parts of the sample was

performed to localize the presence of Zn and Cu. Figure 5.22 summarizes the elemental maps of all main elements. Elemental maps indicate that both Zn and Cu are deposited all over the substrate; however, it is hard to be sure about the exact deposition of the elements due to the high surface roughness of the samples.

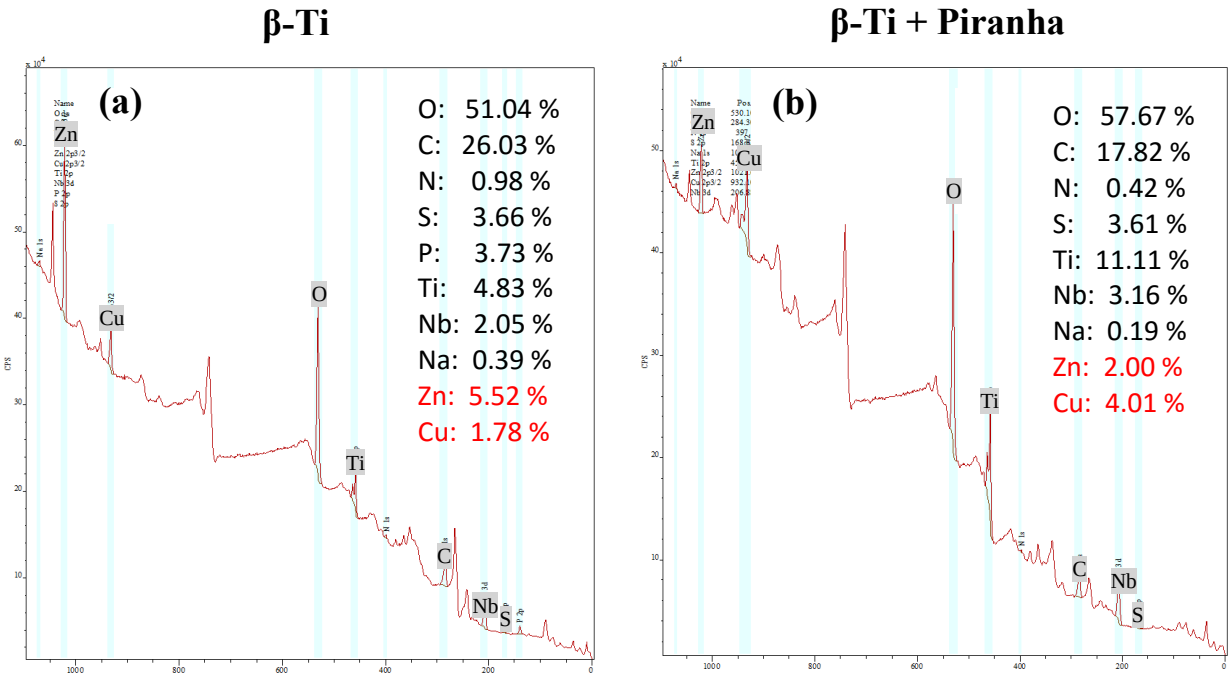

Figure 5.23. *XPS results of bulk β-Ti substrates (a) before and (b) after Piranha treatment revealing the presence of Ti and Nb as the component of the β-Ti, as well as C, Zn, Cu, and S in both spectrums and changes in the elemental composition.*

To identify the chemical composition and the percentage of each element on the surface layer, XPS measurements of β-Ti substrates were performed (Figure 5.23). The presence of Zn and Cu before and after Piranha treatment was confirmed. After Piranha treatment, the Zn content decreased, but the Cu content increased more than twice (from 1.78 % to 4.01 %) and the reason for this increase should be further investigated. It is possible that the increase of Cu is responsible for the CNTs growth, as SWCNTs formation from copper nanoparticles at was reported by D. Takagi *et al* [147]. The catalytic activity of Cu

is significantly lower than for a typical transition metal. Nevertheless, the combination of a Ti substrate with Cu additives seems to be beneficial for the CNTs growth.

The presence of Zn and Cu impurities in combination with Piranha treatment results in the successful synthesis of MWCNTs on β-Ti titanium substrates. It is likely that the increase in Cu content and the hydrophilicity of the surface promote the MWCNTs growth, but further investigations would be needed to confirm these speculations.

In general, it can be concluded that Piranha solution treatment of α- and β-Ti substrates results in the growth of MWCNTs, without the use of an additional transitional metal catalyst. For α-Ti substrates, an increased surface roughness and hydrophilic surface with a contact angle ≤ 56 is favourable for the formation of CNTs. For the successful synthesis of CNTs on β-Ti substrates, hydrophilic surfaces with similar contact angle values as for α-Ti were found to be favourable. Additionally, for β-Ti substrates, the slightly smoother surface morphology, and an increase of the Cu content after Piranha treatment seems to induce the nanotube formation.

5.4. Conclusions

This Chapter aimed to explore the possibility of CNTs growth on bulk Ti substrates without using an additional metal catalyst. The reason for such investigations was the bad osteoblast response on β-Ti substrates covered with CNTs grown with a Fe-based catalyst, even though the catalyst concentration was very low, as reported in Chapter 3. The growth of CNTs without typical transition metal catalysts is known to be challenging on different types of substrates, and on titanium in particular[130], which is not a typical substrate for nanotubes growth in general. Nevertheless, the growth of CNTs with titanium as a catalyst will be ideal for further biomedical application, since it is already proven to be biocompatible and is widely used as implant material. Ti can act as a catalyst for CNTs growth under certain conditions[128,77], as has been confirmed by the experiments described in this Chapter. Hence, the following conclusions can be drawn.

After having investigated various types of titanium-based substrates, bulk titanium was shown to be the best substrate for non-catalytic CNTs growth. On bulk Ti, localized CNTs growth was observed on the edges of the substrates. Experiments performed in this Chapter on anodized Ti with TiO_2 nanotubes, and TiO_2 nanoparticles did not result in any CNTs growth, even though it was reported in other studies[128,77,67]. Looking more precisely at the study by S. Sirivisoot *et al.*[67], the claimed CNTs growth on anodized Ti is not convincing since CNTs cannot be identified from the SEM micrograph presented in the paper, and moreover, no additional proof regarding the CNTs growth was given[67]. Moreover, the experiments presented in Section 5.3.1 showed that instead considerable breakage of TiO_2 nanotubes must have taken place, which was unfortunately mistaken for CNTs formation.

Among the three different precursors, methane gas, toluene aerosol, and acetylene gas, used for CVD growth of MWCNTs without additional metal catalyst, acetylene was found to be the most efficient precursor. This can be understood by the fact that acetylene is much less stable than methane and toluene, and its fG is already negative at 200 °C [212]. Acetylene was also used as a precursor for non-catalytic experiments by S. Sirivisoot *et al* [67].

Different types of substrate modifications were investigated, and Piranha solution was found to be most effective for the improvement of carbon nanotubes growth. MWCNTs were grown on both bulk α- and β-Ti substrates after their treatment with Piranha solution. No investigation of the influence of the Piranha treatment on MWCNTs has been reported until now. It can be concluded from the performed experiments, that the combination of changes in the surface roughness, improved hydrophilicity and elemental composition of the surface leads to the formation of MWCNTs. Nevertheless, further investigations should be conducted to understand precisely, and optimise the mechanism of MWCNTs formation and the role of each parameter separately.

Chapter 6. Summary and future work

6.1. Summary

The thesis describes a study of various modifications of orthopaedic Ti-based substrates using nanomaterials, and the evaluation of their biocompatibility with the aim to develop new, β-Ti/CNT composite implant materials. The nanostructures of choice were carbon nanotubes (CNTs) and titanium carbide (TiC). Both types of structures were synthesized using simple atmospheric pressure chemical vapour deposition (CVD) technique. The advantage of CVD synthesis is that its products can be grown directly on the substrate. This enables a good connection between titanium and, *e.g.*, CNTs, which is essential in order to prevent the implant from loosening. Cell culture studies with fetal human osteoblasts (fHobs) were performed on the newly created materials in order to evaluate their biocompatibility.

Chapter 2 presented the optimization of multi-wall CNTs (MWCNTs) growth on Ti-based substrates. MWCNTs were synthesized with very low concentration of Fe + Al nitrate catalyst in order to reduce possible toxic effects, an important aspect for future biological applications. Spin coating was found to be an efficient method for the deposition of the catalyst onto the titanium substrates of different type and shape including bulk alloys, thin films, and 3D porous scaffolds. Moreover, it allowed MWCNTs growth on both implants and scaffolds, which broadens their use as biomaterials. By investigating various Ti-based substrates, it was shown that the differences in the elemental composition have no significant influence on the MWCNTs formation. In contrast, the topography of the substrate was found to be an important factor that influenced MWCNTs growth. Therefore, catalyst-assisted CVD synthesis of

MWCNTs, as developed in Chapter 2, can be applied to a variety of Ti-based alloy materials with different composition and geometry.

Chapter 3 reported on the biological responses of Ti-alloy substrates from Chapter 2, on which two types of MWCNTs (entangled and aligned) had been synthesized, as discovered through cell culture studies. Good initial short-term activity was observed for β-Ti/MWCNTs samples, but long-term osteoblast activity was not detected. In order to understand whether the MWCNTs were the reason for the bad cell response, two types of isolated (*i.e.* without a Ti substrate) MWCNTs were studied, buckypaper (BP) and stand-alone carpets. For both types of MWCNTs samples a very low osteoblast activity was observed. A possible explanation is that the investigated MWCNTs were not purified (cleaned) or modified. Hence, the presence of a metal catalyst in the nanotube could have contributed to the bad cell response. The hydrophobicity of MWCNTs could also have played a role. In order to make MWCNTs hydrophilic they would need to be chemically modified with peptides, acids, polymers, *etc.* but then the connection between the substrate and nanotubes would not be very strong.

In Chapter 4 an alternative coating material, titanium carbide (TiC), was introduced on β-Ti, since the samples with MWCNTs did not exhibit a very good biocompatibility. The CVD technique could be used for the TiC synthesis. β-Ti/TiC samples showed good corrosion resistance and mechanical properties (*i.e.* Young's moduli, hardness) that are essential for the long-term performance of implant materials. Cell culture studies revealed good short term osteoblast activity after 24 hours with a very low number of dead cells. Good long-term function after 25 days with improved mineralization was also observed for Ti/TiC samples.

Chapter 5 showed the, first ever, successful non-catalytic CVD MWCNTs synthesis on Ti-based substrates. Non-catalytic MWCNTs growth is of great importance for the work described in this Thesis, since it eliminates the, potentially toxic, catalysts from the implant material, which could initiate the production of β-Ti/MWCNT composites with good biocompatibility. Bulk titanium substrates were found to be the best substrates for reproducible MWCNTs growth, and acetylene was the most efficient precursor. Piranha solution etching was essential in order to achieve a homogeneous carbon nanotube formation all over the sample, while for non-treated samples only localized MWCNTs growth was observed. No evidence of such influence of Piranha treatment has been reported before.

6.2. Future directions

Catalyst –assisted CNTs growth

It was shown in Chapter 2 that for β-Ti films no visible relationship between the catalyst concentration and MWCNTs coverage could be observed. This might be related to the topography of β-Ti films, but further experiments should be performed in order to confirm this assumption. Efforts to incorporate the established techniques in order to understand the aggregation of the catalyst faced difficulties, as was described in Section 2.3.1.3. Therefore, further investigations to establish the method to evaluate the exact mechanism of catalyst behaviour on Ti-based films should be conducted.

Spin coating was shown to be the most efficient method for catalyst deposition as a result of the fact that while rotating at a high speed, the catalyst solution is spreading very quickly due to the centrifugal force and evaporates at the same time, which gives rather uniform thin films on the substrate. Nevertheless, the experiments with different rotation speed and the amount of catalyst that will allow varying the thickness of the deposited catalyst were beyond the scope of this thesis. Future experiments should aim to investigate these parameters and their influence on catalyst deposition and CNTs formation.

CNTs growth on Ti-based porous scaffolds was reported for the first time in Chapter 2. However, the synthesis process itself needs to be optimised in order to avoid the structural damage (cracks), which was observed after the synthesis.

Non-catalytic CNTs growth

The discovery of successful, non-catalytic MWCNTs growth on Ti-based samples is of great importance for the improvement of orthopaedic implants. It can be concluded from the performed experiments, that the combination of changes in the surface roughness, improved hydrophilicity and elemental composition of the surface leads to the formation of MWCNTs. The next step should be a more detailed study of the mechanism of MWCNTs formation in order to clarify the reasons that trigger the nanotube growth and the role of each parameter separately. Afterwards, extensive cell culture studies will be necessary in order to evaluate the MWCNTs biocompatibility. The preliminary biocompatibility evaluations of the new β-Ti/MWCNTs material (grown without catalyst) should be performed using the same cell culture study protocol as the one developed in Chapter 3, in order to ascertain a fair comparison. The comparison of osteoblasts' response towards MWCNTs grown by catalyst-assisted CVD and non-catalytic CVD should give the answer whether the catalyst particles are the reason for the bad cell response reported in Chapter 3. If MWCNTs without catalyst particles are still not biocompatible, the next step will be to find out whether any impurities or defects in the nanotubes themselves are the reason. Therefore, a comparison of conventional, purified, and functionalized MWCNTs should be performed.

Bibliography

1. Geetha, M., Singh, a. K., Asokamani, R. & Gogia, a. K. Ti based biomaterials, the ultimate choice for orthopaedic implants – A review. *Prog. Mater. Sci.* **54,** 397–425 (2009).
2. Akesson, K. & Woolf, A. D. How to develop strategies for improving musculoskeletal health. *Best Pract. Res. Clin. Rheumatol.* **21,** 5–25 (2007).
3. Woolf, A. D. & Åkesson, K. Preventing fractures in elderly people. *BMJ Br. Med. J.* **327,** 89–95 (2003).
4. Kurtz, S. M. *et al.* Future clinical and economic impact of revision total hip and knee arthroplasty. *J. Bone Joint Surg. Am.* **89 Suppl 3,** 144–51 (2007).
5. Long, M. & Rack, H. J. Titanium alloys in total joint replacement--a materials science perspective. *Biomaterials* **19,** 1621–39 (1998).
6. Goodman, S. B., Yao, Z., Keeney, M. & Yang, F. The future of biologic coatings for orthopaedic implants. *Biomaterials* **34,** 3174–83 (2013).
7. Weiner, S. & Wagner, H. D. THE MATERIAL BONE: Structure-Mechanical Function Relations. *Annu. Rev. Mater. Sci.* **28,** 271–298 (1998).
8. *ASD Reports*. (Markets and Markets, 2013).
9. Applications, I. Titanium and its Alloys in Biomedical. *Encycl. Mater. Science Technol.* 9374–9381 (2001).
10. Niinomi, M. Mechanical biocompatibilities of titanium alloys for biomedical applications. *J. Mech. Behav. Biomed. Mater.* **1,** 30–42 (2008).
11. Minagar, S., Berndt, C. C., Wang, J., Ivanova, E. & Wen, C. A review of the application of anodization for the fabrication of nanotubes on metal implant surfaces. *Acta Biomater.* **8,** 2875–88 (2012).
12. Donachie M. *Titanium: A technical guide*. (ASM International, 2000).
13. C-H., K. P. Kuo P.pdf. *J. Electrochem. Soc.* **159,** 103–107 (2012).
14. Armendia, M. *et al.* Influence of Heat Treatment on the Machinability of Titanium Alloys. *Mater. Manuf. Process.* **27,** 457–461 (2012).
15. Niinomi, M. Recent research and development in titanium alloys for biomedical applications and healthcare goods. *Sci. Technol. Adv. Mater.* **4,** 445–454 (2003).
16. Yamamoto, A., Mishima, S., Maruyama, N. & Sumita, M. A new technique for direct measurement of the shear force necessary to detach a cell from a material. *Biomaterials* **19,** 871–879 (1998).
17. Zhi Lin Sun, Wataha, J. C. & Hanks, C. T. Effects of metal ions on osteoblast-like cell metabolism and differentiation. *J. Biomed. Mater. Res.* **34,** 29–37 (1997).
18. Matsuno, H., Yokoyama, a, Watari, F., Uo, M. & Kawasaki, T. Biocompatibility and osteogenesis of refractory metal implants, titanium, hafnium, niobium,

tantalum and rhenium. *Biomaterials* **22,** 1253–62 (2001).

19. Eisenbarth, E., Velten, D., Müller, M., Thull, R. & Breme, J. Biocompatibility of β-stabilizing elements of titanium alloys. *Biomaterials* **25,** 5705–5713 (2004).

20. Chi-Hsiun Kuo, P. *et al.* Effects of Surface Functionalization on the Nanostructure and Biomechanical Properties of Binary Titanium-Niobium Alloys. *J. Electrochem. Soc.* **159,** E103 (2012).

21. Elias, C. N., Lima, J. H. C., Valiev, R. & Meyers, M. A. Biomedical Applications of Titanium and its Alloys. 1–4 (2008).

22. Summer D.R, Turner T.M, Igloria R, Urban R.M, G. J. . Summer DR.pdf. *J. Biomech.* **31,** 909–17 (1998).

23. Niinomi, M. *et al.* Development of Low Rigidity .BETA.-type Titanium Alloy for Biomedical Applications. *Mater. Trans.* **43,** 2970–2977 (2002).

24. Li, Z. & Kawashita, M. Current progress in inorganic artificial biomaterials. *J. Artif. Organs* **14,** 163–70 (2011).

25. Sumner, D. R., Turner, T. M., Igloria, R., Urban, R. M. & Galante, J. O. Functional adaptation and ingrowth of bone vary as a function of hip implant stiffness. *J. Biomech.* **31,** 909–917 (1998).

26. Tsutsumi, H., Niinomi, M., Akahori, T., Takeuchi, T. & Katsura, S. Dental Precision Casting of Ti-29Nb-13Ta-4.6Zr Using Calcia Mold. *Mater. Trans.* **50,** 2057–2063 (2009).

27. Christenson, E. M. *et al.* Nanobiomaterial Applications in Orthopedics. 11–22 (2007). doi:10.1002/jor

28. Fukumoto, S. *et al.* Surface modification of titanium by nitrogen ion implantation. *Mater. Sci. Eng. A* **263,** 205–209 (1999).

29. Liu, X., Chu, P. K. & Ding, C. Surface modification of titanium, titanium alloys, and related materials for biomedical applications. *Mater. Sci. Eng. R Reports* **47,** 49–121 (2004).

30. Rani, V. V. D. *et al.* Osteointegration of titanium implant is sensitive to specific nanostructure morphology. *Acta Biomater.* **8,** 1976–89 (2012).

31. Variola, F. *et al.* Improving biocompatibility of implantable metals by nanoscale modification of surfaces: an overview of strategies, fabrication methods, and challenges. *Small* **5,** 996–1006 (2009).

32. Puckett, S. D., Taylor, E., Raimondo, T. & Webster, T. J. The relationship between the nanostructure of titanium surfaces and bacterial attachment. *Biomaterials* **31,** 706–13 (2010).

33. Iwasa, F. *et al.* Enhancement of osteoblast adhesion to UV-photofunctionalized titanium via an electrostatic mechanism. *Biomaterials* **31,** 2717–2727 (2010).

34. Webster, T. J., Ergun, C., Doremus, R. H., Siegel, R. W. & Bizios, R. Enhanced functions of osteoblasts on nanophase ceramics. *Biomaterials* **21,** 1803–1810 (2000).

35. Li, X. *et al.* Direct measurements of interactions between polypeptides and carbon nanotubes. *J. Phys. Chem. B* **110,** 12621–5 (2006).

36. Balasundaram, G. & Webster, T. J. A perspective on nanophase materials for orthopedic implant applications. *J. Mater. Chem.* **16,** 3737 (2006).

37. Webster, T. J. & Ejiofor, J. U. Increased osteoblast adhesion on nanophase metals: Ti, Ti6Al4V, and CoCrMo. *Biomaterials* **25,** 4731–9 (2004).

38. Ward, B. C. & Webster, T. J. The effect of nanotopography on calcium and phosphorus deposition on metallic materials in vitro. *Biomaterials* **27,** 3064–3074 (2006).

39. Divya Rani, V. V, Manzoor, K., Menon, D., Selvamurugan, N. & Nair, S. V. The design of novel nanostructures on titanium by solution chemistry for an improved osteoblast response. *Nanotechnology* **20,** 195101 (2009).

40. Durmus, N. G. & Webster, T. J. Nanostructured titanium: the ideal material for improving orthopedic implant efficacy? *Nanomedicine (Lond).* **7,** 791–3 (2012).

41. Divya Rani, V. V, Manzoor, K., Menon, D., Selvamurugan, N. & Nair, S. V. The design of novel nanostructures on titanium by solution chemistry for an improved osteoblast response. *Nanotechnology* **20,** 195101 (2009).

42. Portan, D., Papaefthymiou, K. & George, C. P. Manufacturing and characterization of TiO2 nanotubes on pure titanium surfaces for advanced biomedical applications. **73,** (2011).

43. Brammer, K. S., Frandsen, C. J. & Jin, S. TiO2 nanotubes for bone regeneration. *Trends Biotechnol.* **30,** 315–22 (2012).

44. Yang, W.-E. & Huang, H.-H. Improving the biocompatibility of titanium surface through formation of a TiO2 nano-mesh layer. *Thin Solid Films* **518,** 7545–7550 (2010).

45. Chang, P.-C. *et al.* Bone tissue engineering with novel rhBMP2-PLLA composite scaffolds. *J. Biomed. Mater. Res. A* **81,** 771–780 (2007).

46. Bauer, S. *et al.* Size selective behavior of mesenchymal stem cells on ZrO(2) and TiO(2) nanotube arrays. *Integr. Biol. (Camb).* **1,** 525–532 (2009).

47. Park, J. *et al.* TiO2 nanotube surfaces: 15 nm - an optimal length scale of surface topography for cell adhesion and differentiation. *Small* **5,** 666–671 (2009).

48. Brammer, K. S. *et al.* Improved bone-forming functionality on diameter-controlled TiO2 nanotube surface. *Acta Biomater.* **5,** 3215–3223 (2009).

49. Brammer, K. S. *et al.* Comparative cell behavior on carbon-coated TiO2 nanotube surfaces for osteoblasts vs. osteo-progenitor cells. *Acta Biomater.* **7,** 2697–2703 (2011).

50. Brama, M. *et al.* Effect of titanium carbide coating on the osseointegration response in vitro and in vivo. *Biomaterials* **28,** 595–608 (2007).

51. Sonoda, T., Watazu, A., Kato, K., Yamada, T. & Asahina, T. Deposition of Ti / C compositional gradient film onto superplastic Ti-alloy by magnetron sputtering. 1144–1146 (2004). doi:10.1002/sia.1861

52. Zhang, H. F., Cheng, Y. & Zheng, Y. F. Modification of biomedical NiTi shape memory alloy by TiC/Ti films using PIIID. *Surf. Coatings Technol.* **201,** 6857–6860 (2007).

53. Cheng, Y. & Zheng, Y. F. Characterization of TiN, TiC and TiCN coatings on Ti-50.6 at.% Ni alloy deposited by PIII and deposition technique. *Surf. Coatings Technol.* **201,** 4909–4912 (2007).

54. Zhao, Y. *et al.* Effects of Carbon and Nitrogen Plasma Immersion Ion Implantation on In vitro and In vivo Biocompatibility of Titanium Alloy. *ACS Appl. Mater. Interfaces* **5,** 1510–1516 (2013).

55. Price, R. L., Ellison, K., Haberstroh, K. M. & Webster, T. J. Nanometer surface roughness increases select osteoblast adhesion on carbon nanofiber compacts. *J. Biomed. Mater. Res. A* **70,** 129–138 (2004).

56. Elias, K. L., Price, R. L. & Webster, T. J. Enhanced functions of osteoblasts on nanometer diameter carbon fibers. *Biomaterials* **23,** 3279–87 (2002).

57. Iijima, S. Helical microtubules of graphitic carbon. *Nature* **354,** 56–58 (1991).

58. Wang, K. The use of titanium for medical applications in the USA. *Mater. Sci. Eng. A* **213,** 134–137 (1996).

59. Kim, S., Bosque, J., Meehan, J. P., Jamali, A. & Marder, R. Increase in outpatient knee arthroscopy in the United States: a comparison of National Surveys of Ambulatory Surgery, 1996 and 2006. *J. Bone Joint Surg. Am.* **93,** 994–1000 (2011).

60. Spear, R. L. & Cameron, R. E. Carbon nanotubes for orthopaedic implants. *Int. J. Mater. Form.* **1,** 127–133 (2008).

61. Liang, Y. T., Vijayan, B. K., Lyandres, O., Gray, K. A. & Hersam, M. C. Effect of Dimensionality on the Photocatalytic Behavior of Carbon − Titania Nanosheet Composites: Charge Transfer at Nanomaterial Interfaces. (2012).

62. Tang, H. *et al.* High dispersion and electrocatalytic properties of platinum on well-aligned carbon nanotube arrays. *Carbon N. Y.* **42,** 191–197 (2004).

63. Kurusu, F., Koide, S., Karube, I. & Gotoh, M. Electrocatalytic Activity of Bamboo-Structured Carbon Nanotubes Paste Electrode Toward Hydrogen Peroxide. *Anal. Lett.* **39,** 903–911 (2006).

64. Roy, S., Vedala, H. & Choi, W. Vertically aligned carbon nanotube probes for monitoring blood cholesterol. *Nanotechnology* **17,** S14–S18 (2006).

65. Padigi, S. K., Reddy, R. K. K. & Prasad, S. Carbon nanotube based aliphatic hydrocarbon sensor. *Biosens. Bioelectron.* **22,** 829–837 (2007).

66. Sirivisoot, S. & Webster, T. J. Multiwalled carbon nanotubes enhance electrochemical properties of titanium to determine in situ bone formation. *Nanotechnology* **19,** 295101 (2008).

67. Sirivisoot, S., Yao, C., Xiao, X., Sheldon, B. W. & Webster, T. J. Greater osteoblast functions on multiwalled carbon nanotubes grown from anodized nanotubular titanium for orthopedic applications. *Nanotechnology* **18,** 365102 (2007).

68. Lahiri, D., Ghosh, S. & Agarwal, A. Carbon nanotube reinforced hydroxyapatite composite for orthopedic application: A review. *Mater. Sci. Eng. C* **32,** 1727–1758 (2012).

69. Li, K.Sun, W.Dong, D. Z. Li.pdf. 1839–1844 (2007).

70. S. Facca, D.Lahiri, F. Fioretti, N. Messadep, D. Mainard, N. Benkirane-Jessel, A. A. Partners. *ACS Nano* **5,** 4790–4799 (2011).

71. Sato, S., Kawabata, A., Kondo, D., Nihei, M. & Awano, Y. Carbon nanotube growth from titanium-cobalt bimetallic particles as a catalyst. *Chem. Phys. Lett.* **402,** 149–154 (2005).

72. Prasek, J. *et al.* Methods for carbon nanotubes synthesis—review. *J. Mater. Chem.* **21,** 15872 (2011).

73. Sinnott, S. B. *et al.* Model of carbon nanotube growth through chemical vapor deposition. *Chem. Phys. Lett.* **315,** 25–30 (1999).

74. Xu, X., Huang, S., Hu, Y., Lu, J. & Yang, Z. Continuous synthesis of carbon nanotubes using a metal-free catalyst by CVD. *Mater. Chem. Phys.* **133,** 95–102 (2012).

75. Kumar, M. & Ando, Y. Chemical vapor deposition of carbon nanotubes: a review on growth mechanism and mass production. *J. Nanosci. Nanotechnol.* **10,** 3739–3758 (2010).

76. Nerushev, O. a., Dittmar, S., Morjan, R. E., Rohmund, F. & Campbell, E. E. B. Particle size dependence and model for iron-catalyzed growth of carbon nanotubes by thermal chemical vapor deposition. *J. Appl. Phys.* **93,** 4185–4190 (2003).

77. Cai, Q., Hu, Y., Liu, Y. & Huang, S. Growth of carbon nanotubes from titanium dioxide nanoparticles. *Appl. Surf. Sci.* **258,** 8019–8025 (2012).

78. Takagi, D., Homma, Y., Hibino, H., Suzuki, S. & Kobayashi, Y. Single-walled carbon nanotube growth from highly activated metal nanoparticles. *Nano Lett.* **6,** 2642–5 (2006).

79. Rümmeli, M. H. *et al.* Synthesis of carbon nanotubes with and without catalyst particles. *Nanoscale Res. Lett.* **6,** 303 (2011).

80. Esconjauregui, S., Whelan, C. M. & Maex, K. The reasons why metals catalyze the nucleation and growth of carbon nanotubes and other carbon nanomorphologies. *Carbon N. Y.* **47,** 659–669 (2009).

81. Aoki, N. *et al.* Carbon Nanotubes Deposited on Titanium Implant for Osteoblast Attachment. *J. Bionanoscience* **1,** 14–16 (2007).

82. Banhart, F. Interactions between metals and carbon nanotubes: at the interface between old and new materials. *Nanoscale* **1,** 201–13 (2009).

83. Zhang, Y., Franklin, N. W., Chen, R. J. & Dai, H. Metal coating on suspended carbon nanotubes and its implication to metal–tube interaction. *Chem. Phys. Lett.* **331,** 35–41 (2000).

84. Felten, A. *et al.* The role of oxygen at the interface between titanium and carbon nanotubes. *Chemphyschem* **10,** 1799–804 (2009).

85. Palmquist, A., Emanuelsson, L. & Sjövall, P. Chemical and structural analysis of the bone-implant interface by TOF-SIMS, SEM, FIB and TEM: Experimental study in animal. *Appl. Surf. Sci.* **258,** 6485–6494 (2012).

86. Jackson, P. & Attalla, M. I. N-Nitrosopiperazines form at high pH in post-combustion capture solutions containing piperazine: a low-energy collisional behaviour study. *Rapid Commun. Mass Spectrom.* **24,** 3567–3577 (2010).

87. Sjövall, P., Lausmaa, J. & Johansson, B. Mass spectrometric imaging of lipids in brain tissue. *Anal. Chem.* **76,** 4271–4278 (2004).

88. Zhao, B., Qi, H., Xu, D. & Zhang, Y. Effects of Amplitude on Carbon Nanotube Nanowelding. *Fullerenes, Nanotub. Carbon Nanostructures* **21,** 19–23 (2013).

89. Binnig, G. & Quate, C. F. Atomic Force Microscope. *Phys. Rev. Lett.* **56,** 930–933 (1986).

90. Lievonen, J. & Ahlskog, M. Lateral force microscopy of multiwalled carbon nanotubes. *Ultramicroscopy* **109,** 825–829 (2009).

91. Botti, S. *et al.* Carbon nanotubes grown by laser-annealing of SiC nano-particles. *Chem. Phys. Lett.* **400,** 264–267 (2004).

92. Kagan, V. E. *et al.* Carbon nanotubes degraded by neutrophil myeloperoxidase induce less pulmonary inflammation. *Nat. Nanotechnol.* **5,** 354–359 (2010).

93. Singh, R. *et al.* Tissue biodistribution and blood clearance rates of intravenously administered carbon nanotube radiotracers. *Proc. Natl. Acad. Sci. U. S. A.* **103,** 3357–3362 (2006).

94. Cherukuri, P., Bachilo, S. M., Litovsky, S. H. & Weisman, R. B. Near-infrared fluorescence microscopy of single-walled carbon nanotubes in phagocytic cells. *J. Am. Chem. Soc.* **126,** 15638–15639 (2004).

95. Cheng, C. *et al.* Toxicity and imaging of multi-walled carbon nanotubes in human macrophage cells. *Biomaterials* **30,** 4152–4160 (2009).

96. Smart, S. K., Cassady, a. I., Lu, G. Q. & Martin, D. J. The biocompatibility of carbon nanotubes. *Carbon N. Y.* **44,** 1034–1047 (2006).

97. Lobo, A. O. *et al.* Biocompatibility of multi-walled carbon nanotubes grown on titanium and silicon surfaces. *Mater. Sci. Eng. C* **28,** 532–538 (2008).

98. Price, R. L., Waid, M. C., Haberstroh, K. M. & Webster, T. J. Selective bone cell adhesion on formulations containing carbon nanofibers. *Biomaterials* **24,** 1877–1887 (2003).

99. Wörle-Knirsch, J. M., Pulskamp, K. & Krug, H. F. Oops they did it again! Carbon

nanotubes hoax scientists in viability assays. *Nano Lett.* **6,** 1261–1268 (2006).

100. Flahaut, E., Durrieu, M. C., Remy-Zolghadri, M., Bareille, R. & Baquey, C. Study of the cytotoxicity of CCVD carbon nanotubes. *J. Mater. Sci.* **41,** 2411–2416 (2006).

101. Chłopek, J. *et al.* In vitro studies of carbon nanotubes biocompatibility. *Carbon N. Y.* **44,** 1106–1111 (2006).

102. Webster, T. J., Waid, M. C., McKenzie, J. L., Price, R. L. & Ejiofor, J. U. Nano-biotechnology: carbon nanofibres as improved neural and orthopaedic implants. *Nanotechnology* **15,** 48–54 (2003).

103. Gabay, T., Jakobs, E., Ben-Jacob, E. & Hanein, Y. Engineered self-organization of neural networks using carbon nanotube clusters. *Phys. A Stat. Mech. its Appl.* **350,** 611–621 (2005).

104. Naguib, N. N. *et al.* Effect of carbon nanofibre structure on the binding of antibodies. *Nanotechnology* **16,** 567–571 (2005).

105. Correa-Duarte, M. a. *et al.* Fabrication and biocompatibility of carbon nanotube-based 3D networks as scaffolds for cell seeding and growth. *Nano Lett.* **4,** 2233–2236 (2004).

106. Zanello, L. P., Zhao, B., Hu, H. & Haddon, R. C. Bone cell proliferation on carbon nanotubes. *Nano Lett.* **6,** 562–7 (2006).

107. Brooks, R. Developing Cell Culture Systems for Testing Implant Materials. (2012).

108. Journet, C., Picher, M. & Jourdain, V. Carbon nanotube synthesis: from large-scale production to atom-by-atom growth. *Nanotechnology* **23,** 142001 (2012).

109. Vajtai, R., Wei, B. Q. & Ajayan, P. M. Controlled growth of carbon nanotubes. *Philos. Trans. A. Math. Phys. Eng. Sci.* **362,** 2143–60 (2004).

110. Meysami, S. S., Dillon, F., Koós, A. a., Aslam, Z. & Grobert, N. Aerosol-assisted chemical vapour deposition synthesis of multi-wall carbon nanotubes: I. Mapping the reactor. *Carbon N. Y.* **58,** 159–169 (2013).

111. Meysami, S. S., Snoek, L. C. & Grobert, N. Versatile in Situ Gas Analysis Apparatus for Nanomaterials Reactors. *Anal. Chem.* (2014). doi:10.1021/ac5022858

112. Saito, N. *et al.* Carbon nanotubes: biomaterial applications. *Chem. Soc. Rev.* **38,** 1897–903 (2009).

113. Liebau, M. *et al.* Carbon nanotubes in interconnect applications. *Microelectron. Eng.* **64,** 399–408 (2002).

114. Endo, M. Carbon Nanotube Research: Past and Future. *Jpn. J. Appl. Phys.* **51,** 040001 (2012).

115. Saito, N. *et al.* Carbon nanotubes: biomaterial applications. *Chem. Soc. Rev.* **38,** 1897–1903 (2009).

116. Wang, X. & Liu, Z. Carbon nanotubes in biology and medicine: An overview.

Chinese Sci. Bull. **57,** 167–180 (2011).

117. Wang W., Zhu Y., Liao S., L. J. *Carbon Nanotubes Reinforces Composites for Biomedical Application*.

118. Li, X., Fan, Y. & Watari, F. Current investigations into carbon nanotubes for biomedical application. *Biomed. Mater.* **5,** 22001 (2010).

119. Battigelli, A., Ménard-Moyon, C., Da Ros, T., Prato, M. & Bianco, A. Endowing carbon nanotubes with biological and biomedical properties by chemical modifications. *Adv. Drug Deliv. Rev.* **65,** 1899–1920 (2013).

120. Liu, Z., Robinson, J. T., Tabakman, S. M., Yang, K. & Dai, H. Carbon materials for drug delivery & cancer therapy. *Mater. Today* **14,** 316–323 (2011).

121. Bianco, A., Kostarelos, K., Partidos, C. D. & Prato, M. Biomedical applications of functionalised carbon nanotubes. *Chem. Commun. (Camb).* 571–7 (2005). doi:10.1039/b410943k

122. Newman, P., Minett, A., Ellis-Behnke, R. & Zreiqat, H. Carbon nanotubes: Their potential and pitfalls for bone tissue regeneration and engineering. *Nanomedicine Nanotechnology, Biol. Med.* **9,** 1139–1158 (2013).

123. Stevens, M. M. Biomaterials for bone tissue engineering. *Mater. Today* **11,** 18–25 (2008).

124. (Iso), I. O. for S. Online Browsing Platform (OBP). (2012).

125. Ward, B. C. & Webster, T. J. Increased functions of osteoblasts on nanophase metals. *Mater. Sci. Eng. C* **27,** 575–578 (2007).

126. Xia, L. *et al.* In vitro and in vivo studies of surface-structured implants for bone formation. *Int. J. Nanomedicine* **7,** 4873–81 (2012).

127. Sirivisoot, S. & Webster, T. J. In Situ Bone Growth Detection Using Carbon Nanotubes–Titanium Sensors. *Bionanoscience* **3,** 184–191 (2013).

128. Terada, M. *et al.* Multiwalled carbon nanotube coating on titanium. *Biomed. Mater. Eng.* **19,** 45–52 (2009).

129. Sun, J. *et al.* Controlled growth of Ni nanocrystals on SrTiO(3) and their application in the catalytic synthesis of carbon nanotubes. *Chem. Commun. (Camb).* **49,** 3748–50 (2013).

130. Robertson, J. Heterogeneous catalysis model of growth mechanisms of carbon nanotubes, graphene and silicon nanowires. *J. Mater. Chem.* **22,** 19858 (2012).

131. Shenderova, O. A., Zhirnov, V. V & Brenner, D. W. Carbon Nanostructures. **27,** 227–356 (2002).

132. Ummethala, R., Khavrus, V. O., Leonhardt, A., Büchner, B. & Eckert, J. A comparative study of various supported catalysts on the growth of aligned carbon nanotube forests on aluminum foils. *Chem. Vap. Depos.* **18,** 326–335 (2012).

133. Hahn, A., Fuhlrott, J., Loos, A. & Barcikowski, S. Cytotoxicity and ion release of alloy nanoparticles. *J. Nanopart. Res.* **14,** 1–10 (2012).

134. Kim, D. Y. *et al.* The density control of carbon nanotubes using spin-coated nanoparticle and its application to the electron emitter with triode structure. *Diam. Relat. Mater.* **14,** 2084–2088 (2005).

135. Ward, J. W., Wei, B. Q. & Ajayan, P. M. Substrate effects on the growth of carbon nanotubes by thermal decomposition of methane. *Chem. Phys. Lett.* **376,** 717–725 (2003).

136. Ortega-Cervantez, G., Rueda-Morales, G. & Ortiz-López, J. Catalytic CVD production of carbon nanotubes using ethanol. *Microelectronics J.* **36,** 495–498 (2005).

137. Makris, T. D., Giorgi, L., Giorgi, R., Lisi, N. & Salernitano, E. CNT growth on alumina supported nickel catalyst by thermal CVD. *Diam. Relat. Mater.* **14,** 815–819 (2005).

138. Xie, R. *et al.* Carbon nanotube growth for through silicon via application. *Nanotechnology* **24,** 125603 (2013).

139. Parthangal, P. M., Cavicchi, R. E. & Zachariah, M. R. A generic process of growing aligned carbon nanotube arrays on metals and metal alloys. *Nanotechnology* **18,** 185605 (2007).

140. Speirs, M., Van Humbeeck, J., Schrooten, J., Luyten, J. & Kruth, J. P. The effect of pore geometry on the mechanical properties of selective laser melted Ti-13Nb-13Zr scaffolds. *Procedia CIRP* **5,** 79–82 (2013).

141. Seah, C. M., Chai, S. P., Ichikawa, S. & Mohamed, A. R. Parametric study of methane catalytic CVD into single-walled carbon nanotubes using spin-coated iron nanoparticles. *Chem. Vap. Depos.* **19,** 53–60 (2013).

142. Chuang, C.-C., Liu, W.-L., Chen, W.-J. & Huang, J.-H. The role of Ti interlayer in carbon nanotube growth. *Surf. Coatings Technol.* **202,** 2121–2125 (2008).

143. Ma, L. *et al.* In-situ fabrication of CNT/TiO2 interpenetrating network film on nickel substrate by chemical vapour deposition and application in photoassisted water electrolysis. *Catal. Commun.* **21,** 27–31 (2012).

144. Bayer, B. C. *et al.* Support-Catalyst-Gas Interactions during Carbon Nanotube Growth on Metallic Ta Films. 4359–4369 (2011).

145. Voort, G. F. Vander. *Metallography, Principles and Practice*. *ASM International* (1984). doi:10.1017/CBO9781107415324.004

146. Vander Wal, R. L. & Hall, L. J. Carbon nanotube synthesis upon stainless steel meshes. *Carbon N. Y.* **41,** 659–672 (2003).

147. Takagi, D., Homma, Y., Hibino, H., Suzuki, S. & Kobayashi, Y. Single-Walled Carbon Nanotube Growth from Highly Activated Metal Nanoparticles. *Nano Lett.* **6,** 2642–2645 (2006).

148. N. Zulkapli, Mohd A. Azam, Nik Zubir, Nur A. Ithnin, N. R. A simple and room temperature sol-gel process for the fabrication of cobalt nanoparticles as an effective catalyst for carbon nanotube growth. *RSC Adv.* **5,** (2015).

149. Zulkapli, N. N. *et al.* Control of Cobalt Catalyst Thin Film Thickness by Varying Spin Speed in Spin Coating towards Carbon Nanotube Growth. *Applied Mechanics and Materials* **761,** 421–425 (2015).

150. Khavrus, V. O. *et al.* Application of Carbon Nanotubes Directly Grown on Aluminum Foils as Electric Double Layer Capacitor Electrodes. *Chem. Vap. Depos.* **18,** 53–60 (2012).

151. Levchenko, I. *et al.* Large Arrays and Networks of Carbon Nanotubes : Morphology Control by Process Parameters. (2013).

152. Khavrus, V. O. *et al.* On the potential of long carbon nanotube forest for sensing gases and vapors. *Phys. E Low-dimensional Syst. Nanostructures* **43,** 1199–1207 (2011).

153. Ion, R. *et al.* In vitro bio-functional performances of the novel superelastic beta-type Ti-23Nb-0.7Ta-2Zr-0.5N alloy. *Mater. Sci. Eng. C. Mater. Biol. Appl.* **35,** 411–9 (2014).

154. Vasilescu, E. *et al.* In vitro biocompatibility and corrosion resistance of a new implant titanium base alloy. *J. Mater. Sci. Mater. Med.* **21,** 1959–1968 (2010).

155. Rosalbino, F., Macciò, D., Giannoni, P., Quarto, R. & Saccone, a. Study of the in vitro corrosion behavior and biocompatibility of Zr-2.5Nb and Zr-1.5Nb-1Ta (at%) crystalline alloys. *J. Mater. Sci. Mater. Med.* **22,** 1293–302 (2011).

156. Abrishamchian, A., Hooshmand, T., Mohammadi, M. & Najafi, F. Preparation and characterization of multi-walled carbon nanotube/hydroxyapatite nanocomposite film dip coated on Ti-6Al-4V by sol-gel method for biomedical applications: an in vitro study. *Mater. Sci. Eng. C. Mater. Biol. Appl.* **33,** 2002–10 (2013).

157. Rajzer, I., Menaszek, E., Bacakova, L., Rom, M. & Blazewicz, M. In vitro and in vivo studies on biocompatibility of carbon fibres. *J. Mater. Sci. Mater. Med.* **21,** 2611–2622 (2010).

158. Malheiro, V. Ferromagnetic Fibre Networks for Magneto-Active Layers on Orthopaedic Implants by. (University of Cambridge, 2013).

159. Scientific, T. F. alamarBlue Cell Viability Assay Protocol. (2015).

160. LABTECH, B. Use of the FLUOstar OPTIMA Microplate Reader to Monitor Amyloid Formation. (2008).

161. Przekora, A. *et al.* Titanium coated with functionalized carbon nanotubes — A promising novel material for biomedical application as an implantable orthopaedic electronic device. *Mater. Sci. Eng. C* **45,** 287–296 (2014).

162. Cui, H.-F., Vashist, S. K., Al-Rubeaan, K., Luong, J. H. T. & Sheu, F.-S. Interfacing carbon nanotubes with living mammalian cells and cytotoxicity issues. *Chem. Res. Toxicol.* **23,** 1131–47 (2010).

163. Akiladevi, D. *et al.* Increased osteoblast adhesion on nanophase metals: Ti, Ti6Al4V, and CoCrMo. *Nanotechnology* **1,** 365102 (2009).

164. S. Bellucci, M. Chiaretti, A. Cucina, GA Carru, A. C. Multiwalled carbon nanotube buckypaper: toxicology and biological effects in vitro and in vivo. *Nanomedicine (Lond).* **4,** 531–40 (2009).

165. J Liu, AG Rinzler, H Dai, JH Hafner, RK Bradley, PJ Boul, A Lu, T Iverson, K Shelimov, CB Huffman, F Rodriguez-Macias, YS Shon, TR Lee, DT Colbert, R. S. Fullerene pipes. *Science* **280,** 1253–6 (1998).

166. Y A Kim, H Muramatsu, T Hayashi, M Endo, M Terrones, M S Dresselhaus. Fabrication of High-Purity, Double-Walled Carbon Nanotube Buckypaper. *Chem. Vap. Depos.* **12,** 327–330 (2006).

167. Meysami, S. S., Koós, A. a., Dillon, F. & Grobert, N. Aerosol-assisted chemical vapour deposition synthesis of multi-wall carbon nanotubes: II. An analytical study. *Carbon N. Y.* **58,** 151–158 (2013).

168. M Shim, N WS Kam, R J Chen, Y Li, H. D. M.pdf. *Nano Lett.* **2,** (2002).

169. M A Correa-Duarte, N Wagner, J Rojas-Chapana, C Morsczeck, M Thie, M Giesig. Fabrication and biocompatibilut of carbon nanobute-based 3D networks as scaffolds for cell seeding and growth. *Nano Lett.* **4,** 2233–6 (2004).

170. J. Young. Continuous Buckypaper Manufacturing Process: Process Investigation and Improvement. (2009).

171. Popat, K. C., Leoni, L., Grimes, C. a. & Desai, T. a. Influence of engineered titania nanotubular surfaces on bone cells. *Biomaterials* **28,** 3188–3197 (2007).

172. Reis, J., Capela-silva, F., Potes, J. & Fonseca, A. Carbon Nanotubes – Interactions with Biological Systems. **1991,** (2009).

173. Kornu, R., Maloney, W. J., Kelly, M. a. & Smith, R. L. Osteoblast adhesion to orthopaedic implant alloys: Effects of cell adhesion molecules and diamond-like carbon coating. *J. Orthop. Res.* **14,** 871–877 (1996).

174. Balázsi, K., Vandrovcová, M., Bačáková, L., Bertóti, I. & Balázsi, C. Development of biocompatible TiC / a : C nanocomposite barrier coating for dental implants. **24,** 101453 (2012).

175. Balázsi, K., Vandrovcová, M., Bačáková, L. & Balázsi, C. Structural and biocompatible characterization of TiC/a:C nanocomposite thin films. *Mater. Sci. Eng. C* **33,** 1671–1675 (2013).

176. A. Krajewski, A. Piancastell, R. M. Albumin adhesion on ceramics and correlation with their Z- potential,. *Biomaterials* **19,** 637–641 (1998).

177. Hynowska, A. *et al.* Novel Ti–Zr–Hf–Fe Nanostructured Alloy for Biomedical Applications. *Materials (Basel).* **6,** 4930–4945 (2013).

178. T. Luxbacher, R. K. SurPASS Measurement Report Zeta Potential of TiNb Alloys SurPASS Measurement Report Introduction. *Ant. Paar* 1–5 (2014).

179. Lincks, J. *et al.* Response of MG63 osteoblast-like cells to titanium and titanium alloy is dependent on surface roughness and composition. *Biomater. Silver Jubil. Compend.* **19,** 147–160 (2006).

180. Degasne, I. *et al.* Effects of roughness, fibronectin and vitronectin on attachment, spreading, and proliferation of human osteoblast-like cells (Saos-2) on titanium surfaces. *Calcif. Tissue Int.* **64,** 499–507 (1999).

181. Lorenzetti, M. *et al.* Improvement to the Corrosion Resistance of Ti-Based Implants Using Hydrothermally Synthesized Nanostructured Anatase Coatings. *Materials (Basel).* **7,** 180–194 (2014).

182. Jirka, I. *et al.* On the role of Nb-related sites of an oxidized β-TiNb alloy surface in its interaction with osteoblast-like MG-63 cells. *Mater. Sci. Eng. C* **33,** 1636–1645 (2013).

183. Jelínek, M. *et al.* Biocompatibility and sp3/sp2 ratio of laser created DLC films. *Mater. Sci. Eng. B Solid-State Mater. Adv. Technol.* **169,** 89–93 (2010).

184. Niinomi, M., Nakai, M. & Hieda, J. Development of new metallic alloys for biomedical applications. *Acta Biomater.* **8,** 3888–3903 (2012).

185. Longo, G. *et al.* Effect of titanium carbide coating by ion plating plasma-assisted deposition on osteoblast response: A chemical, morphological and gene expression investigation. *Surf. Coatings Technol.* **204,** 2605–2612 (2010).

186. Takagi, D., Hibino, H., Suzuki, S., Kobayashi, Y. & Homma, Y. Carbon nanotube growth from semiconductor nanoparticles. *Nano Lett.* **7,** 2272–2275 (2007).

187. Q. Chen, G. T. *Biomaterials: A Basic Introduction*. (CRS Press, 2015).

188. Keegan, G. M., Learmonth, I. D. & Case, C. P. Orthopaedic metals and their potential toxicity in the arthroplasty patient: A review of current knowledge and future strategies. *J. Bone Joint Surg. Br.* **89,** 567–573 (2007).

189. Dirk M. Guldi, N. M. Carbon Nanotubes and Related Structures. Synthesis, Characterization, Functionalization, and Applications. 1–562 (2010).

190. Schneider, J. J. *et al.* Catalyst free growth of a carbon nanotube-alumina composite structure. *Inorganica Chim. Acta* **361,** 1770–1778 (2008).

191. Bae, E. J. *et al.* Selective Growth of Carbon Nanotubes on Pre-patterned Porous Anodic Aluminum Oxide. *Adv. Mater.* **14,** 277–279 (2002).

192. Takagi, D., Kobayashi, Y. & Homma, Y. Carbon nanotube growth from diamond. *J. Am. Chem. Soc.* **131,** 6922–6923 (2009).

193. Gao, F., Zhang, L. & Huang, S. Zinc oxide catalyzed growth of single-walled carbon nanotubes. *Appl. Surf. Sci.* **256,** 2323–2326 (2010).

194. Rümmeli, M. H. *et al.* Direct low-temperature nanographene cvd synthesis over a dielectric insulator. *ACS Nano* **4,** 4206–4210 (2010).

195. Huang, S., Cai, Q., Chen, J., Qian, Y. & Zhang, L. Metal-Catalyst-Free Growth of Single-Walled Carbon Nanotubes on Substrates. 2094–2095 (2009).

196. Page, A. J., Chandrakumar, K. R. S., Irle, S. & Morokuma, K. SWNT nucleation from carbon-coated SiO2 nanoparticles via a vapor-solid-solid mechanism. *J. Am. Chem. Soc.* **133,** 621–628 (2011).

197. Liu, H., Takagi, D., Chiashi, S. & Homma, Y. The growth of single-walled carbon nanotubes on a silica substrate without using a metal catalyst. *Carbon N. Y.* **48,** 114–122 (2010).

198. Bachmatiuk, A. *et al.* Hydrogen-induced self-assembly of helical carbon nanostructures from ethanol over SiO2 catalysts. *J. Appl. Phys.* **109,** (2011).

199. Liu, B. *et al.* Metal-catalyst-free growth of single-walled carbon nanotubes. *J. Am. Chem. Soc.* **131,** 2082–3 (2009).

200. Botti, S. *et al.* Catalyst-free growth of carbon nanotubes by laser-annealing of amorphous SiC films. *Chem. Phys. Lett.* **396,** 1–5 (2004).

201. Lincks, J. *et al.* Response of MG63 osteoblast-like cells to titanium and titanium alloy is dependent on surface roughness and composition. *Biomaterials* **19,** 2219–2232 (1998).

202. Hashempour, M., Vicenzo, A., Zhao, F. & Bestetti, M. Direct growth of MWCNTs on 316 stainless steel by chemical vapor deposition: Effect of surface nano-features on CNT growth and structure. *Carbon N. Y.* **63,** 330–347 (2013).

203. Khavrus, V. O. *et al.* Application of Carbon Nanotubes Directly Grown on Aluminum Foils as Electric Double Layer Capacitor Electrodes. *Chem. Vap. Depos.* **18,** 53–60 (2012).

204. Bagno, A. & Di Bello, C. Surface treatments and roughness properties of Ti-based biomaterials. *J. Mater. Sci. Mater. Med.* **15,** 935–49 (2004).

205. Yi, J. H. *et al.* Characterization of a bioactive nanotextured surface created by controlled chemical oxidation of titanium. *Surf. Sci.* **600,** 4613–4621 (2006).

206. Variola, F. *et al.* Tailoring the surface properties of Ti6Al4V by controlled chemical oxidation. *Biomaterials* **29,** 1285–1298 (2008).

207. Gostin, P. F. *et al.* Surface treatment, corrosion behavior, and apatite-forming ability of ti-45Nb implant alloy. *J. Biomed. Mater. Res. - Part B Appl. Biomater.* **101 B,** 269–278 (2013).

208. Morjan, R. E. *et al.* Growth of carbon nanotubes from C 60. *Appl. Phys. A Mater. Sci. Process.* **78,** 253–261 (2004).

209. Gu, Q. Self Assembly for Surface Functionalization to improve Biocompatibilities in Ti-based implants and Enzyme immobilization in Biofuel cells. *PhD Thesis* (2010).

210. Mattevi, C., Kim, H., Chhowalla, M. A review of chemical vapour deposition of graphene on copper, *Journal of Materials Chemistry.* **21,** 3324–3334 (2011).

211. Collazzo, G. C., Jahn, S. L. & Foletto, E. L. Temperature and reaction time effects on the structural properties of titanium dioxide nanopowders obtained via the hydrothermal method. *Brazilian J. Chem. Eng.* **28,** 265–272 (2011).

212. Xiao, L. *et al.* Flexible, stretchable, transparent carbon nanotube thin film loudspeakers. *Nano Lett.* **8,** 4539–4545 (2008).

Appendix I

Influence of elemental composition on MWCNTs growth

In order to investigate whether the elemental ratio of Ti-based films influences the nanotube formation, TiHf films with different Hf content were prepared including Ti85Hf15, Ti80Hf20, and Ti70Hf30. For all the films very similar MWCNTs patterns were observed in all the samples (Figure 1). Thus, no significant difference of elemental ratio on MWCNTs growth for TiHf films was observed.

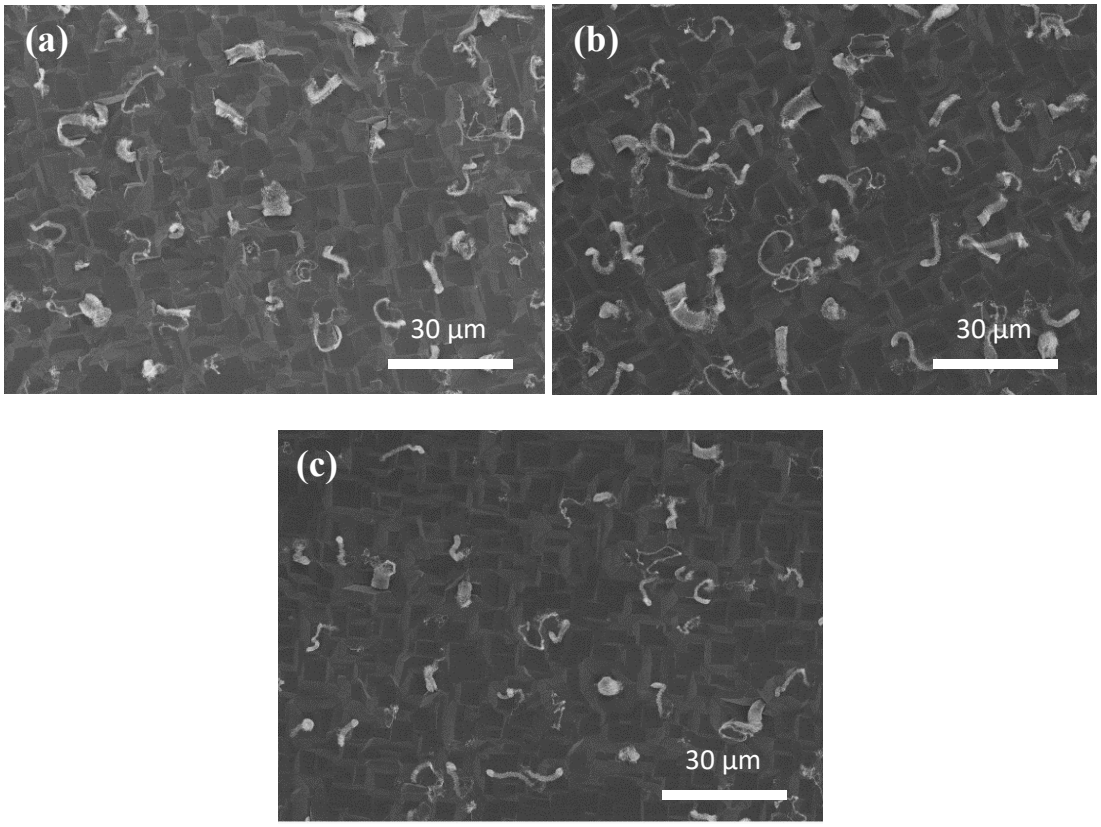

Figure 1. *Representative SEM micrographs of MWCNTs pattern growth with 0.0005M Fe+Al nitrate catalyst during 10 min CVD synthesis on TiHf films with different elemental ratio: (a) Ti85Hf15; (b) Ti80Hf20; and (c) Ti70Hf30 revealing very similar MWCNTs formation of all the films.*

Appendix II

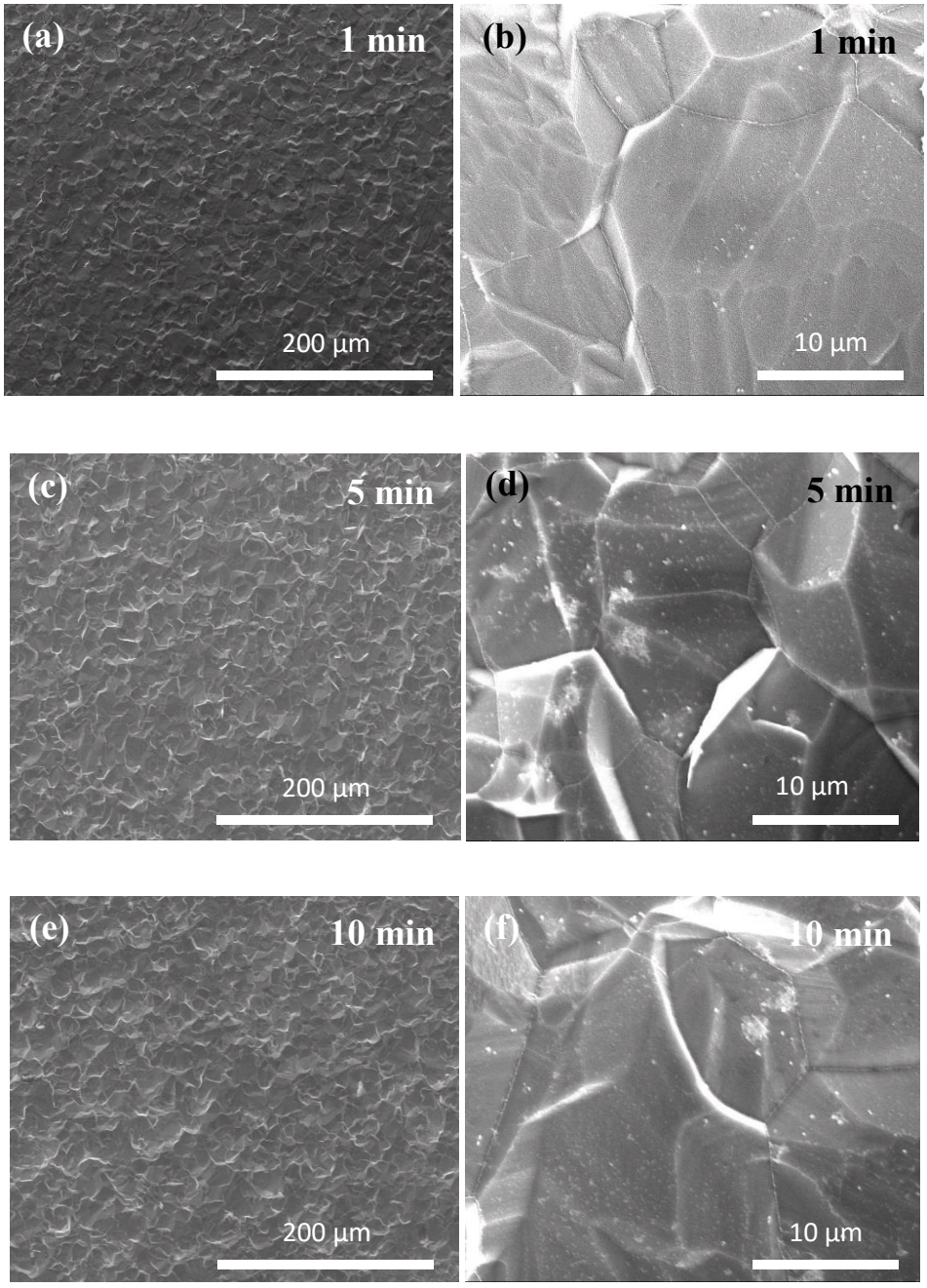

Figure 2. *SEM micrographs of higher and lower magnification showing the structure of α-Ti substrates after 8 % HF treatment for 1, 5, and 10 min showing the appearance of grain boundaries, which are very similar for all the substrates. No influence of the time of HF treatment was observed.*

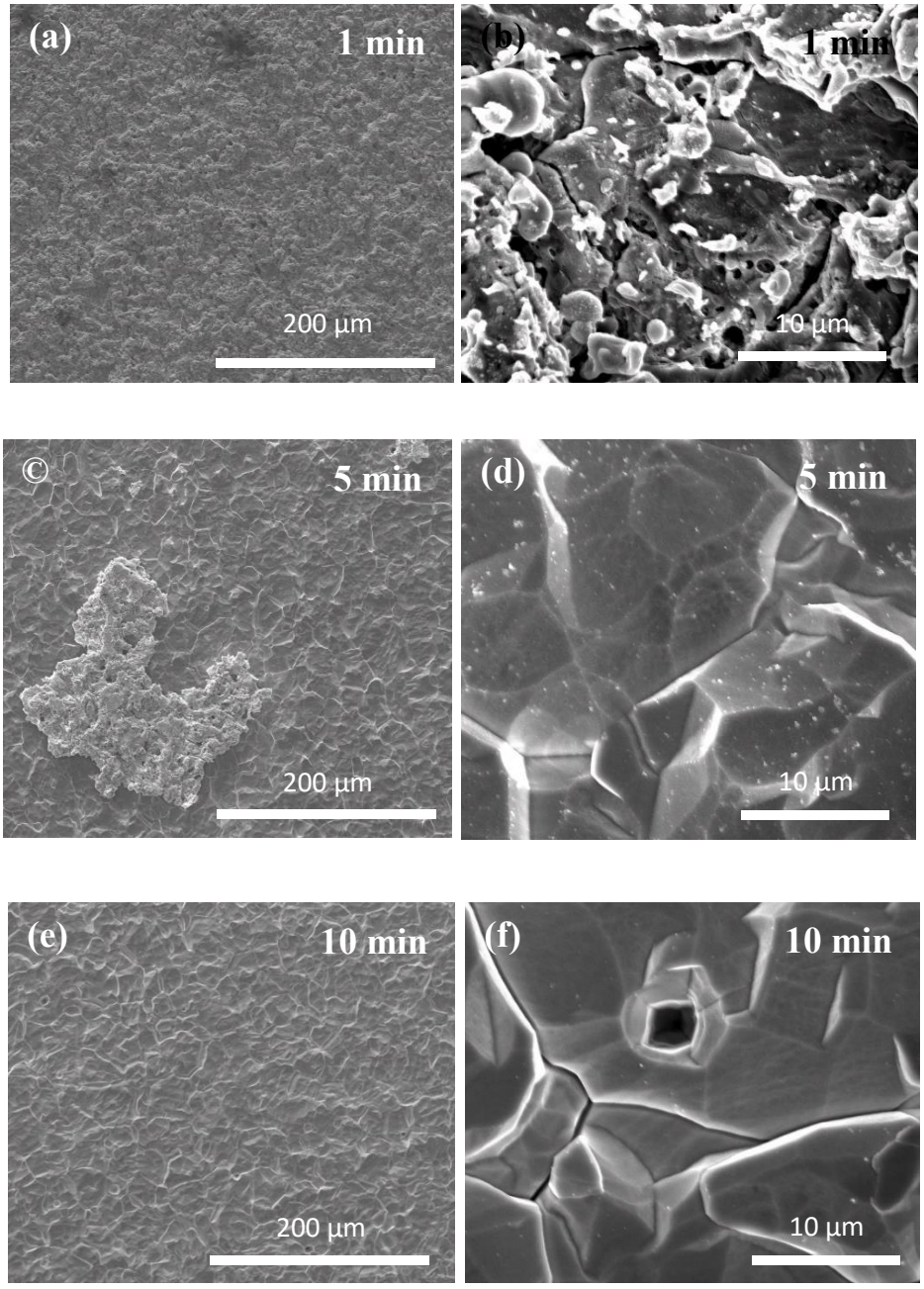

Figure 3. *SEM micrographs of higher and lower magnification showing the structure of β-Ti substrates after 8 % HF treatment for 1, 5, and 10 min. After the treatment for 5 min and more grain boundaries of substrates appear, while after 10 min treatment cracks and individual flaws also appear.*

The influence of different time of HF (8 %) treatment on α- and β-Ti substrates has been also investigated. In Figure 2 the structure of α-Ti substrates after HF treatment for 1, 5 and 10 min is shown. Looking at the grain boundaries of α-Ti substrates after the treatment no influence of the reaction time has been observed. However, for β-Ti substrates, after the 10 min treatment cracks and individual flaws also appear.

CVD experiments on 8 % HF treated titanium substrates with Fe + Al nitrate catalyst revealed MWCNTs formation on in the cavities of substrates that appeared due to the HF treatment. However, no homogeneous distribution of carbon nanotubes was achieved on any HF-treated substrates (Figure 4). Therefore, other surface modification method should be used.

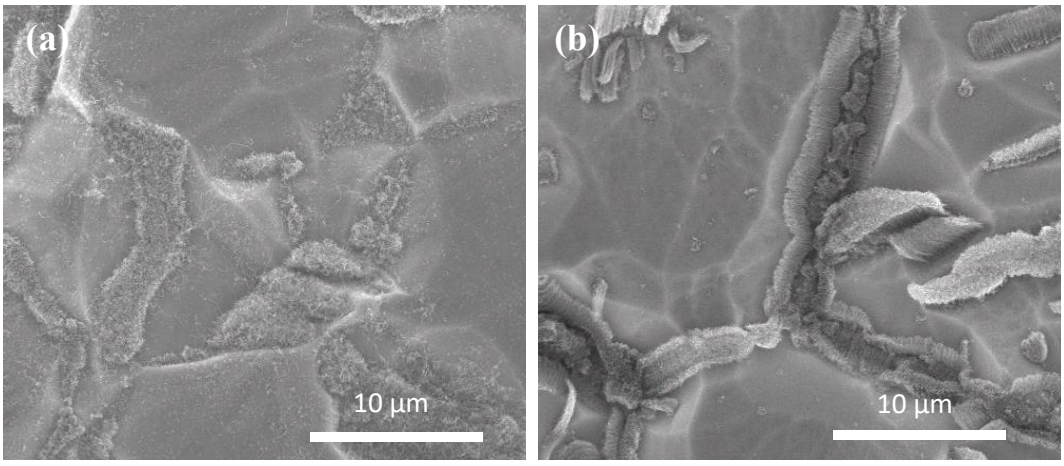

Figure 4. *SEM micrographs showing a non-homogeneous distribution of MWCNTs grown with Fe +Al nitrate catalyst on HF-treated (a) α-Ti and (b) β-Ti substrates.*

Appendix III

CVD growth of new titanium nanostructures

Alongside with the syntheses of MWCNTs, new titanium nanostructures were discovered during the CVD syntheses. These structures were observed during the experiments with all the used precursors: toluene, methane, and acetylene. Results of CVD syntheses with each precursor are presented further in this Section.

CVD experiments with toluene precursor

CVD syntheses with toluene precursor revealed the formation of new structures not reported before. Figure 5a shows a representative SEM images of these structures, which grow all over the substrate. At low magnification, synthesized structures can resemble CNTs, however, at higher magnification they look like a bunch of nails pointing from one spot (Figure 5b).

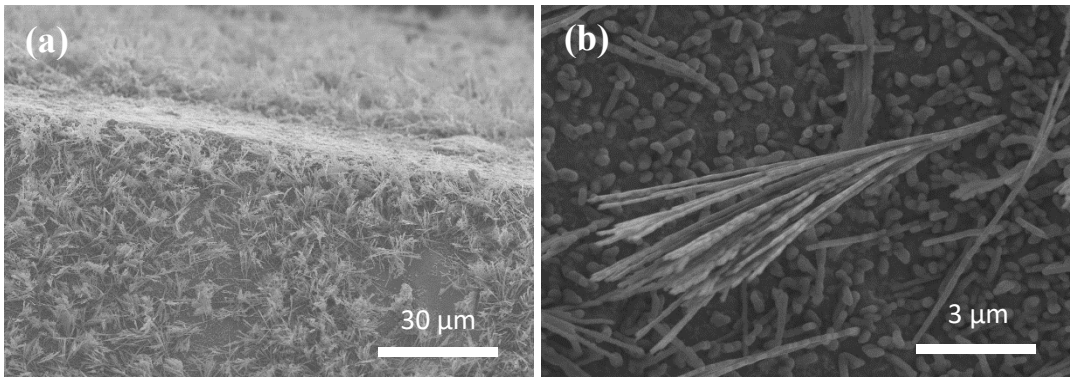

Figure 5. *SEM micrographs of α-Ti substrates of (a) higher and (b) lower magnification after the CVD synthesis with toluene at 800 °C and 15 min reaction time showing the formation of new titanium nanostructures across the sample and its structure.*

It was observed that by activating the surface of Ti substrates with a diamond pen, titanium structures become more frequent than for the non-activated substrates. The influence of the reaction time and temperature on the formation of titanium structures was

also detected. At 800 °C after 10 and 15 min reaction time, titanium structures were fully developed as shown in Figure 5. However, under the same conditions but at 700 °C, the difference between the structures formed after 10 and 15 min was detected. After 10 min, only the beginning stage of those structures was observed (Figure 6a), while, after 15 min, titanium structures were fully developed even though the nails were assembled with each other (Figure 6b).

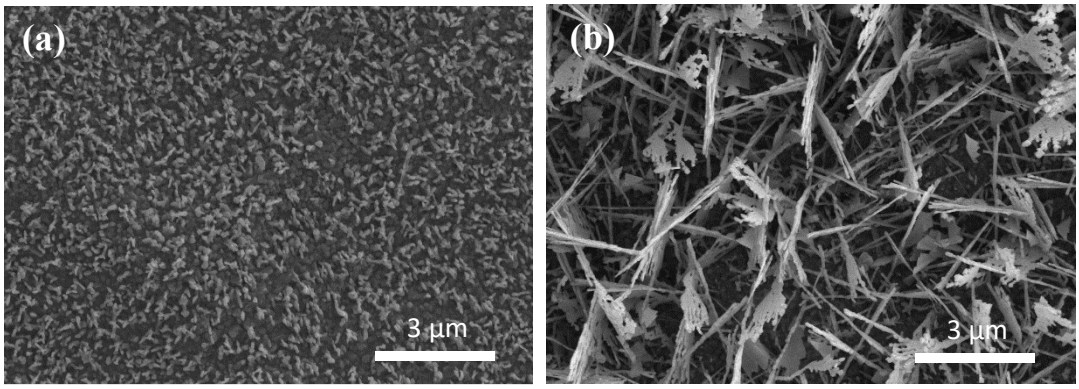

Figure 6. *SEM micrographs of α-Ti substrates after the CVD syntheses with toluene: (a) at 700 °C and 10 min reaction time showing the beginning stage of titanium nanostructures formation; (b) at 700 °C and 15 min reaction time showing fully formed titanium nanostructures.*

To identify the chemical structure of the structures, XRD measurements, presented in Figure 7 were conducted. According to the XRD, the main phase is titanium nitride (TiN) with smaller amounts of titanium oxide (TiO_2) and carbide nitrate (TiCN).

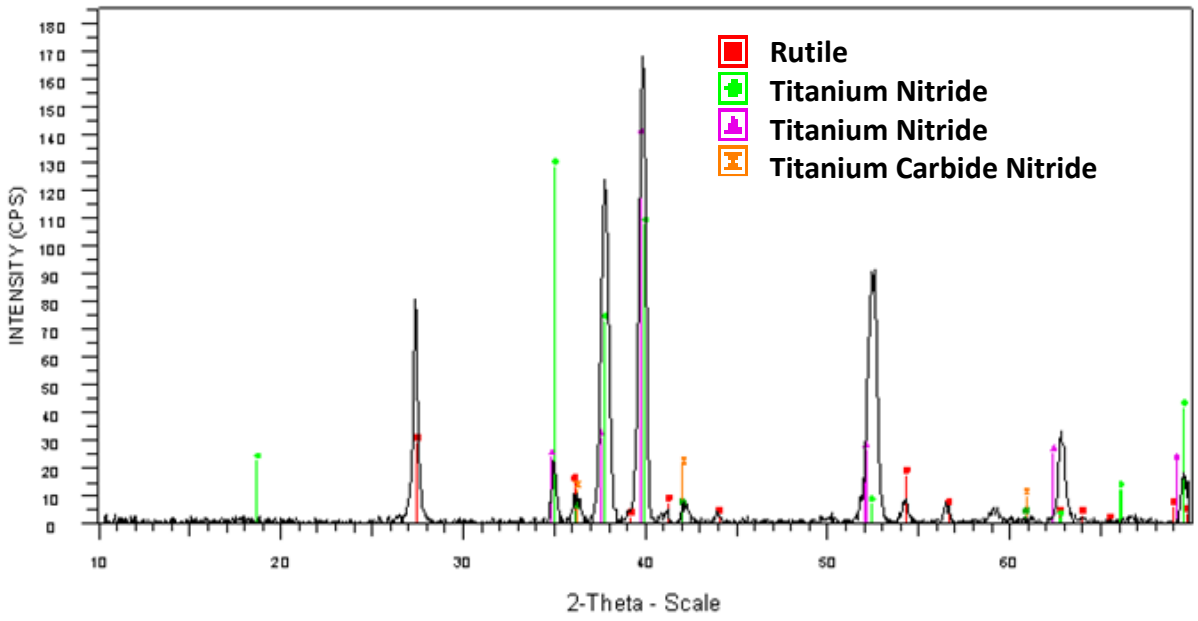

Figure 7. *XRD graph of titanium structures grown by the CVD with toluene on an α-Ti substrate indicating titanium nitride, titanium oxide (rutile) and titanium carbide nitride as the main components.*

To understand the mechanism of titanium structures formation we looked into the carbothermal formation of titanium nitride (TiN) from TiO_2. It is a known process, which can be summarized by the following equation:

$$TiO_2 + 2C + ½\ N_{2\,(g)} = TiN + 2\ CO_{\,(g)}$$

However, in reality, the whole process is more complicated. While looking at the phase diagrams, it was suggested that the formation of TiN goes through the formation of various titanium oxides. The combination of the excess of carbon and high temperature leads to the formation of TiC. Therefore, it is possible to assume that during the CVD syntheses with toluene, TiN is formed similarly as during the carbothermal treatment from the TiO_2 layer, which is present on α-Ti. When Ti substrates are scratched with a diamond pen, it is possible that a TiO_2 layer is formed more rapidly, and hence, more nanostructures are generated. Meanwhile, titanium carbide nitride is formed due to the excess amount of carbon, which is released from toluene (C_6H_5-CH_3), which contains

seven carbon atoms. Residual TiO_2 was detected in the rutile form, instead of its more favourable for biomedical application, anatase[1]. Therefore, the newly synthesized titanium nanostructures are not particularly attractive for the biological application. Nevertheless, further work will have to show whether there are other possible applications for these structures.

CVD experiments with methane precursor

New structures were also observed during the CVD synthesis with a methane precursor. Figure 8 presents SEM micrographs, revealing the formation of new titanium structures on both α-Ti and β-Ti substrates in the temperature window of 800 - 700 °C. These structures look like a chaotic batch of nails deposited all over the surface of the substrate.

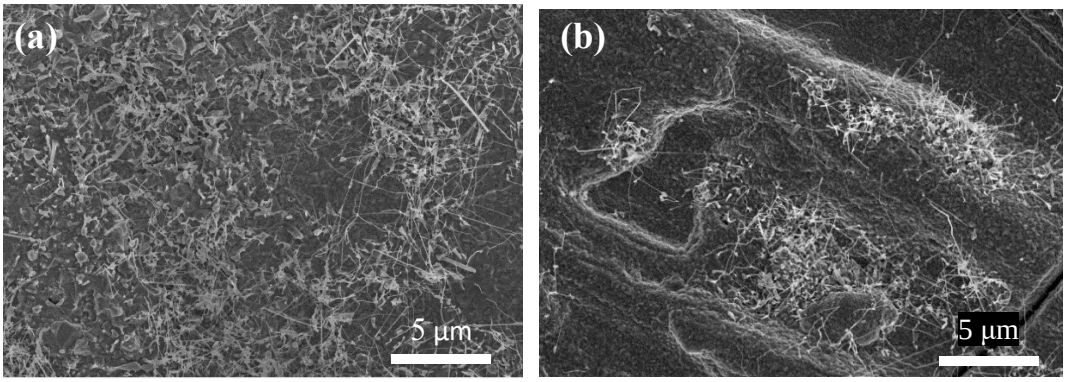

Figure 8. *SEM micrographs showing titanium nanostructures synthesized by the CVD technique with methane at 800 °C for 15 min reaction time on: (a), α-Ti; (b) β-Ti substrates.*

[1.] He, J. et al. (2008) The anatase phase of nanotopography titania plays an important role on osteoblast cell morphology and proliferation. J. Mater. Sci. Mater. Med. 19, 3465–3472

The morphology of the nanostructures is similar to the one grown with toluene; however, they are not originating from one point. According to the XRD, the main phase was titanium nitride with a few titanium oxides (mainly rutile) (Figure 9). It is estimated that those structures are formed according to a similar mechanism, which was predicted above for the experiments with toluene.

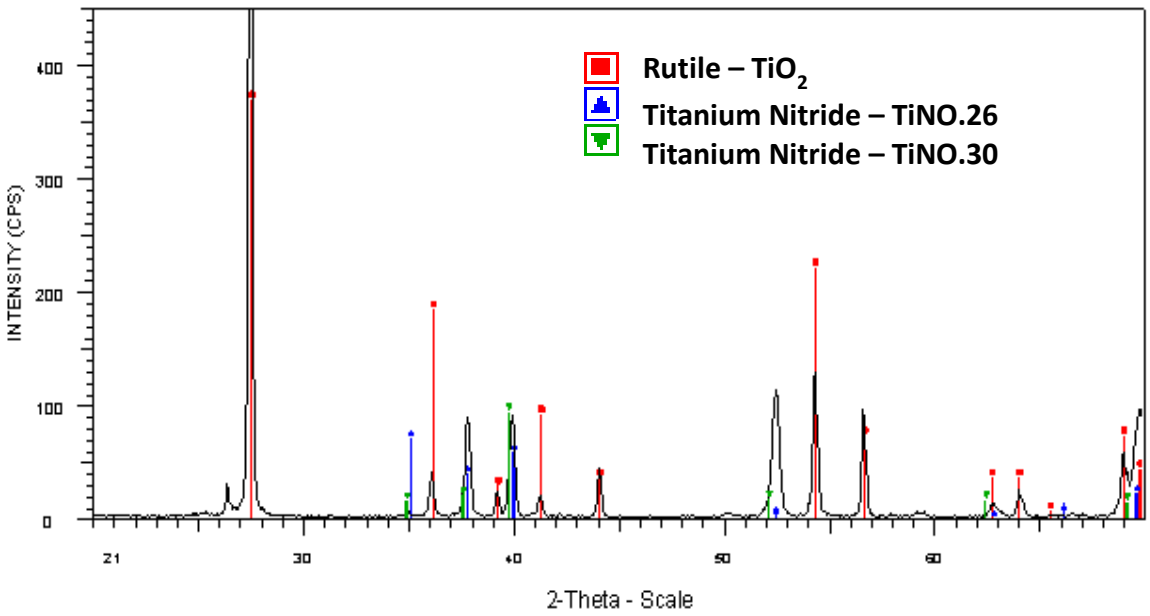

Figure 9. *XRD spectrum of Ti nanostructures synthesized by the CVD technique with methane precursor on α-Ti substrate indicating titanium oxide (rutile) and titanium nitrides as the main components.*

The reported titanium nanostructures were a reproducible product of CVD syntheses. Hence, they were investigated in greater details. Focus ion beam (FIB) microscope was used to look at the cross-section of titanium nanostructures. In Figure 10 it can be distinguished from the layer of titanium, TiO_2, and titanium nanostructures. It is visible that titanium nanostructures are grown from a TiO_2 layer and are well connected with a substrate, which is essential for the transfer of the curtain properties of the nanostructures to the whole composite.

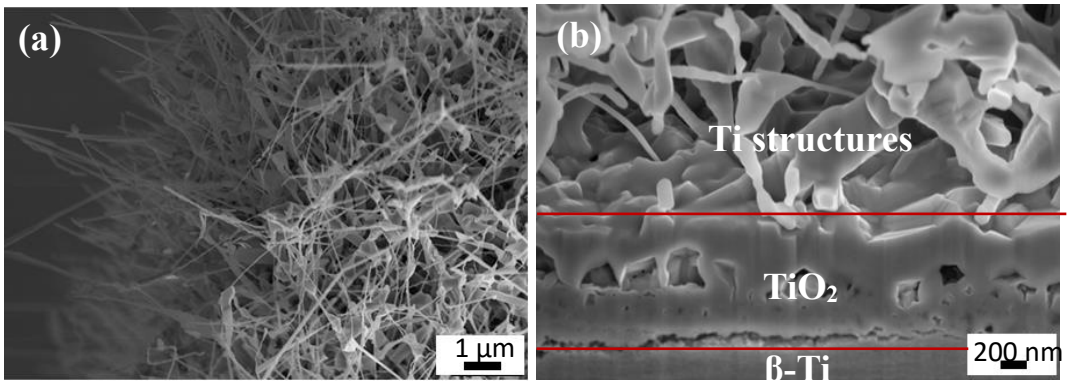

Figure 10. *(a) SEM micrograph and (b) FIB cross-section of Ti nanostructures synthesized by the CVD technique with methane at 800 °C during 15 min on β-Ti substrate indicating the three regions: Ti structures, TiO_2 layer and β-Ti itself.*

CVD experiments with acetylene precursor

Titanium nanostructures were also observed after experiments with an acetylene precursor in the temperature range of 700 – 900 °C. They were chaotically distributed through the sample.

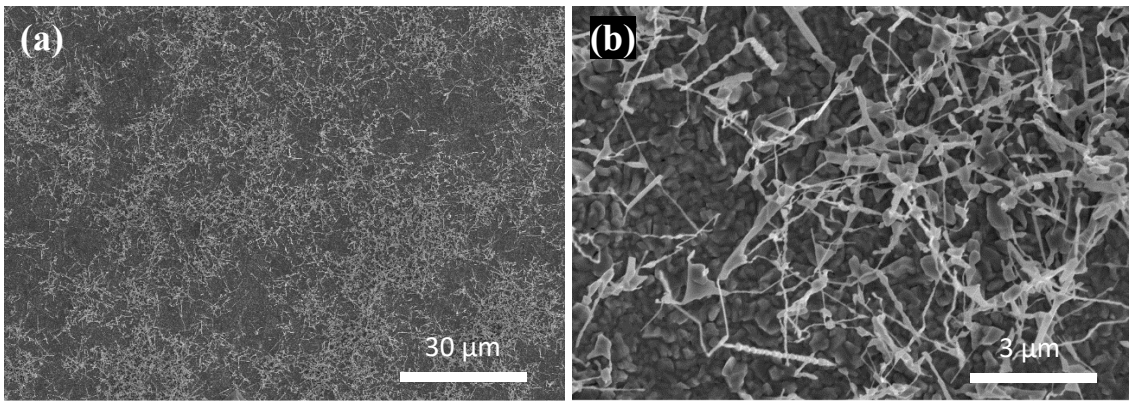

Figure 11. *SEM micrographs of higher and lower magnifications of titanium nanostructures grown on α-Ti with an acetylene precursor at high temperatures 700 – 900 °C, after annealing in hydrogen.*

According to the SEM micrographs (Figure 11) the morphology of synthesized structures is very similar to that formed with a methane precursor. However, the chemical composition is different. The main phases identified by the XRD measurements (Figure

12) are titanium nitride and carbide. There may also be some oxides, but this is hard to confirm.

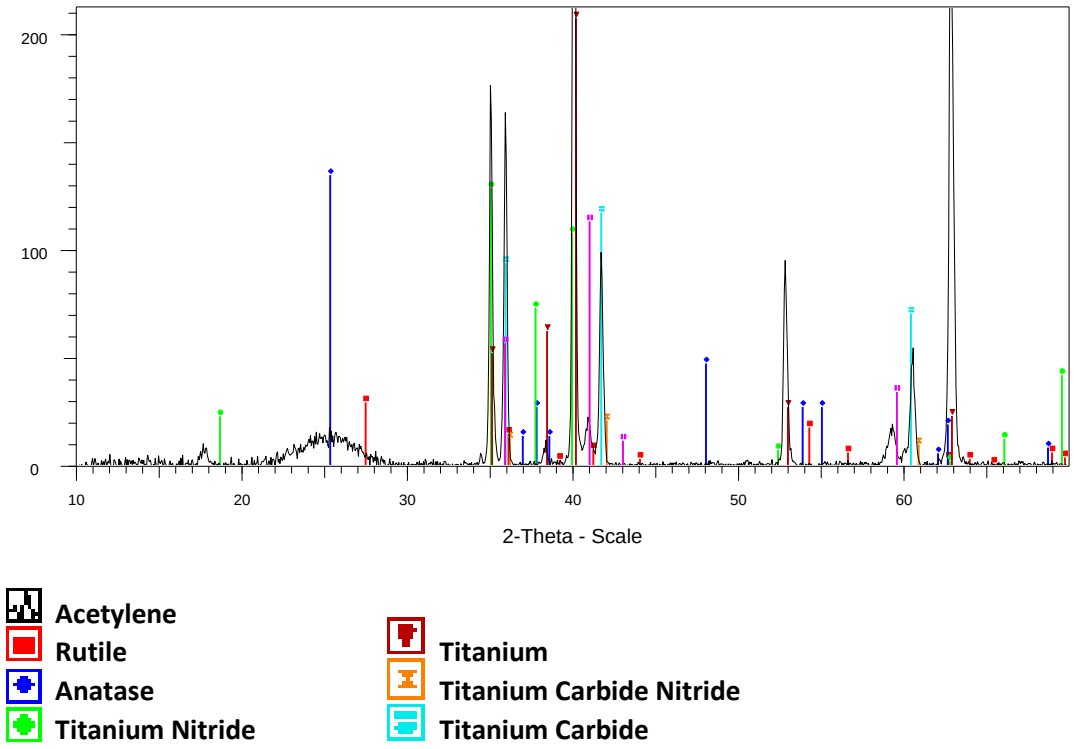

Figure 12. *XRD graph of Ti structures synthesized by the CVD with acetylene precursor on α-Ti substrate indicating titanium oxide (rutile) and titanium carbide as the main components.*

Interestingly, the influence of annealing with hydrogen on the formation of Ti nanostructures was observed. No Ti structures were found without annealing in hydrogen; therefore, it is an essential step in the synthesis of Ti structures. Moreover, for the experiments on α-Ti foil without annealing and at different reaction temperatures, various structures were formed. For synthesizes at 900 °C, the whole substrate was covered with spherical particles, which resemble bubbles (Figure 13). EDX measurements revealed a high peak of C and a slight peak of Ti and O, which might indicate the presence of the amorphous carbon (Figure 14a).

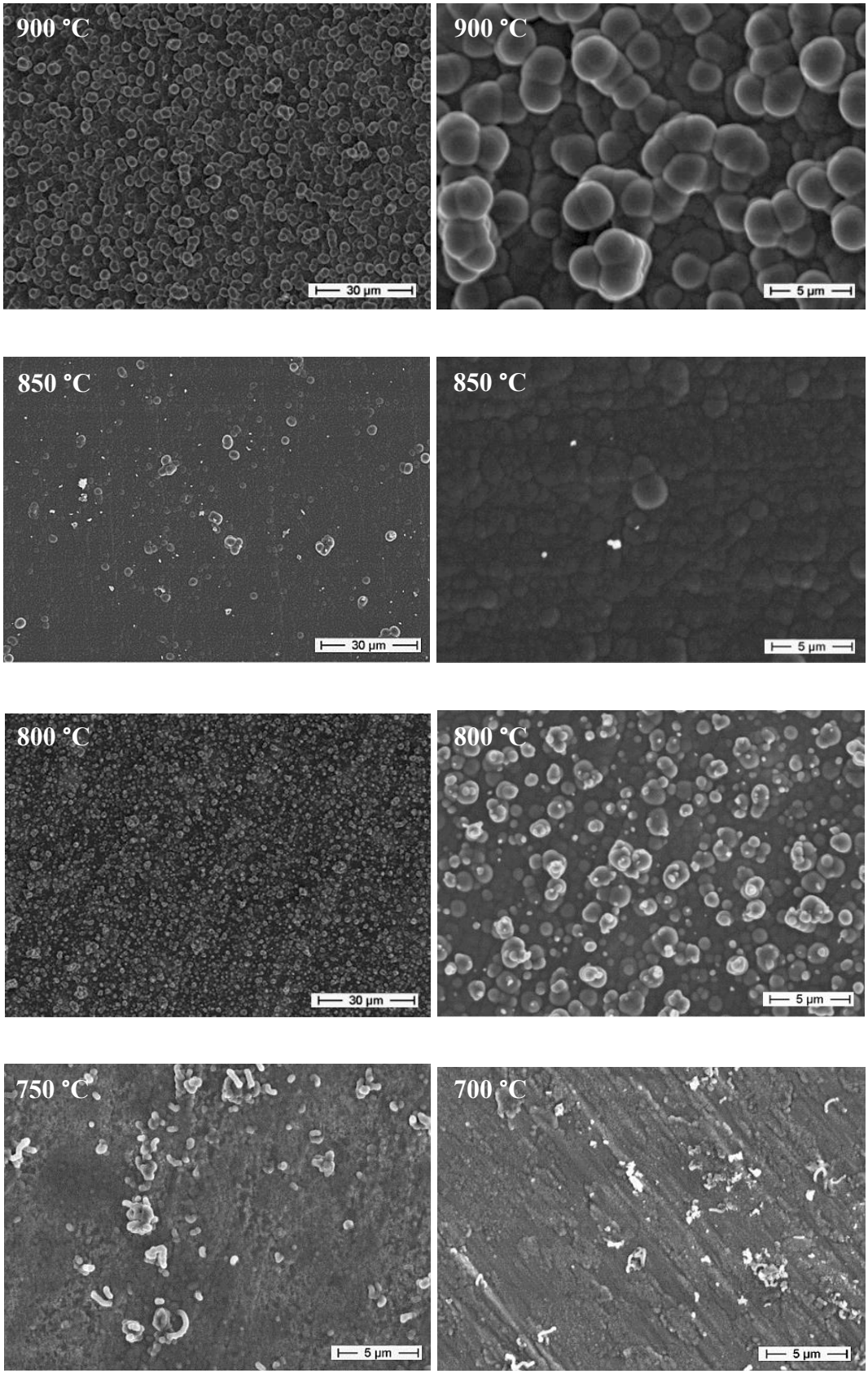

Figure 13. *SEM micrographs of α-Ti substrates after CVD syntheses with acetylene precursor without annealing, showing the different structures formed at various temperatures from 700 to*

900 °C. At lower temperatures (700 – 800 °C) titanium, containing structures were formed, while at higher temperatures (850, 900 °C) mainly carbon containing bubble-looking structures were formed.

At 850 °C, similar structures were observed, even though, they were not as pronounced as those formed at 900 °C. Lowering the temperature to 800 °C resulted in bubbles of a smaller size. However, at 750 and 700 °C no bubble structures were observed. Instead, we can see the beginner stage of Ti nanostructures formation. EDX spectrum is also different for the samples synthesized at different temperatures (Figure 14). Together with a pronounced C peak, the strong presence of Ti was observed, which is correlated with a fact that most parts of titanium substrate were not covered in structures. At 750 and 700 °C, no bubble-like structure was observed.

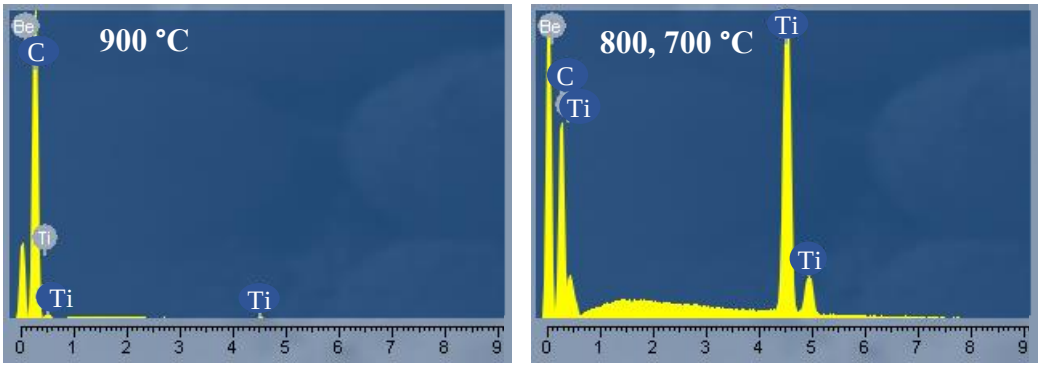

Figure 14. *EDX graphs of Ti substrates after CVD synthesis with acetylene precursor without annealing at different temperatures revealing the peak of titanium at 900 °C and peaks of titanium and carbon at 800 and 700 °C.*